# Active tectonic study in northeast Iran: contribution of the Kopeh Dagh and Binalud mountains to the accommodation of the Arabia-Eurasia convergence

Esmaeil Shabanian

# UNIVERSITE PAUL CEZANNE AIX-MARSEILLE III

**Centre Européen de Recherche et d'Enseignement en Géosciences de l'Environnement**

N° attribué par la bibliothèque: 2009AIX30027

## Active tectonic study in northeast Iran: contribution of the Kopeh Dagh and Binalud mountains to the accommodation of the Arabia-Eurasia convergence

Tectonique active du Nord-est de l'Iran et accommodation de la convergence entre l'Arabie et l'Eurasie: contribution des chaînes du Kopeh Dagh et du Binalud

## T H E S E

Pour obtenir le grade de

DOCTEUR DE L'UNIVERSITE Paul CEZANNE

Faculté des Sciences et Techniques

*Discipline*: Géosciences de l'Environnement

Présentée et soutenue publiquement par

**Esmaeil SHABANIAN**

Le 15 Juillet 2009 au CEREGE

*Les Directeurs de thèse*

***Olivier BELLIER et Mohammad R. ABBASSI***

*Ecole Doctorale :* ***Sciences de l'Environnement***

**J U R Y**

| | |
|---|---|
| Pr. Bertrand MEYER, Université Pierre et Marie Curie - Paris VI | Rapporteur |
| Dr. Jean-François RITZ, Université de Montpellier II | Rapporteur |
| Pr. Olivier BELLIER, CEREGE/Université Paul Cézanne | Directeur |
| Dr. Mohammad R. ABBASSI, IIEES, Iran | Codirecteur |
| Dr. Lionel L. SIAME, CEREGE/Université Paul Cézanne | Codirecteur |
| Pr. Jacques ANGELIER, Observatoire de Villefranche-sur-Mer | Examinateur |
| Dr. Khaled HESSAMI AZAR, IIEES, Iran | Examinateur |
| Dr. Denis HATZFELD, LGIT, Grenoble | Membre invité |
| Dr. Abdollah SAÏDI, RIES/Service Géologique de l'Iran | Membre invité |

ANNEE: 2009

# UNIVERSITE PAUL CEZANNE AIX-MARSEILLE III

**Centre Européen de Recherche et d'Enseignement en Géosciences de l'Environnement**

N° attribué par la bibliothèque: 2009AIX30027

## Active tectonic study in northeast Iran: contribution of the Kopeh Dagh and Binalud mountains to the accommodation of the Arabia-Eurasia convergence

Tectonique active du Nord-est de l'Iran et accommodation de la convergence entre l'Arabie et l'Eurasie: contribution des chaînes du Kopeh Dagh et du Binalud

## T H E S E

Pour obtenir le grade de

DOCTEUR DE L'UNIVERSITE Paul CEZANNE

Faculté des Sciences et Techniques

*Discipline*: Géosciences de l'Environnement

Présentée et soutenue publiquement par

**Esmaeil SHABANIAN**

Le 15 Juillet 2009 au CEREGE

*Les Directeurs de thèse*

***Olivier BELLIER et Mohammad R. ABBASSI***

*Ecole Doctorale :* ***Sciences de l'Environnement***

**J U R Y**

| | |
|---|---|
| Pr. Bertrand MEYER, Université Pierre et Marie Curie - Paris VI | Rapporteur |
| Dr. Jean-François RITZ, Université de Montpellier II | Rapporteur |
| Pr. Olivier BELLIER, CEREGE/Université Paul Cézanne | Directeur |
| Dr. Mohammad R. ABBASSI, IIEES, Iran | Codirecteur |
| Dr. Lionel L. SIAME, CEREGE/Université Paul Cézanne | Codirecteur |
| Pr. Jacques ANGELIER, Observatoire de Villefranche-sur-Mer | Examinateur |
| Dr. Khaled HESSAMI AZAR, IIEES, Iran | Examinateur |
| Dr. Denis HATZFELD, LGIT, Grenoble | Membre invité |
| Dr. Abdollah SAÏDI, RIES/Service Géologique de l'Iran | Membre invité |

ANNEE: 2009

## *Résumé*

Ce travail de thèse a été effectué afin de comprendre les processus de déformation active dans le NE de l'Iran, constitué des chaines de montagnes du Kopeh Dagh et du Binalud. Cet objectif a été poursuivi en combinant plusieurs approches : géologie structurale et tectonique, morpho-tectonique, géomorphologie quantitative et plusieurs méthodes de datation (datation radiométrique par $^{40}Ar/^{39}Ar$ et nucléides cosmogéniques produits *in situ*). Ce travail porte sur trois secteurs clefs du NE de l'Iran : le Kopeh Dagh, le Binalud et la Zone de Transfert de Meshkan. Cette étude a permis d'établir les premières estimations de vitesse sur l'ensemble du système de failles dans le Kopeh Dagh. La vitesse de déplacement horizontal dextre sur l'ensemble du système est de 9±2 mm/an. Cette vitesse peut être décomposée en deux vecteurs de déplacement du Kopeh Dagh Occidental par rapport à l'Eurasie stable, de l'ordre de 8 mm/an et 4 mm/an, vers le Nord et l'Ouest, respectivement. De l'ordre de 25% de la déformation décrochante du Kopeh Dagh est transférée vers le Sud, vers le Binalud, grâce à une série de structures tectoniques définissant un domaine de déformation complexe: la Zone de Transfert de Meshkan.

Sur les deux versants du Massif du Binalud, nous avons déterminé des vitesses de déplacements horizontaux de 3.6±1.2 mm/an et 1.6±0.1 mm/an, le long de zones de failles affectant les versants méridionaux et septentrionaux du Massif, respectivement. Ces vitesses permettent de calculer un taux de déplacement dextre long-terme et total d'environ 5 mm/an. Il correspond à un mouvement vers le Nord d'environ 4.5 mm/an et un mouvement vers l'Ouest de l'ordre de 2 mm/an, de l'Iran Central, à l'Ouest, par rapport au Kopeh Dagh Oriental, à l'Est. Les analyses cinématiques réalisées pendant ce travail indiquent que la convergence est accommodée par des décrochements et des chevauchements le long de structures d'orientations différentes. Cet assemblage structural est impliqué dans un champ de contraintes actuel mécaniquement compatible et homogène. L'homogénéité des états de contraintes déterminés n'est pas en faveur d'un partitionnement complet entre les failles décrochantes / inverses. Les différents types de mouvements observés sur les failles ne résultent que de l'orientation des failles par rapport au champ de contraintes à l'échelle régionale. L'ensemble de ces observations permettent de proposer un modèle tectonique cohérant qui explique la cinématique et la déformation active du NE de l'Iran.



***Mots clés:*** *Morpho-tectonique; états de contraintes; déformation crustale; nucléides cosmogéniques produits in situ.*

**Active tectonic study in northeast Iran: contribution of the Kopeh Dagh and Binalud mountains to the accommodation of the Arabia-Eurasia convergence**

## Abstract

This study focuses on the Plio-Quaternary faulting in northeast Iran including the Kopeh Dagh and Allah Dagh-Binalud mountains. A combined approach of detailed geological mapping, morphotectonic and fault kinematic analyses, as well as radiometric ($^{40}Ar/^{39}Ar$) and *in situ*-produced exposure dating ($^{36}Cl$ and $^{10}Be$) allowed us to characterize the active tectonic configuration of the northeastern Arabia-Eurasia collision zone. Along the Kopeh Dagh fault systems, a total strike-slip rate of 9±2 mm/yr is estimated. This is resolved to northward and westward slip rates of ~8 and ~4 mm/yr, respectively, for the western Kopeh Dagh relative to Eurasia. This strike-slip deformation is partly (~25 per cent) transferred southward through the "new-defined" Meshkan transfer zone. At the southwestern and northeastern sides of the Binalud, slip rates of 3.6±1.2 and 1.6±0.1 mm/yr are estimated, respectively. Our geologically determined long-term slip rates for both strike-slip (~4 mm/yr) and reverse (~2.4 mm/yr) components of faulting account for about 5 mm/yr of total slip rate at both sides of the range. This is resolved to a northward motion rate of ~4.5 mm/yr, and a rate of ~2 mm/yr for the westward motion of Central Iran relative to the eastern Kopeh Dagh. Quaternary stress analyses indicates that the different fault motions, from pure dip-slip to pure strike-slip, are only due to the fault orientations with respect to the far-field stress pattern, not due to partitioning. Altogether, these new data allow proposing a new tectonic configuration in which central Iran and the western Kopeh Dagh are translated northwestward relative to Eurasia due to intracontinental strike-slip faulting localized on distinct fault systems with unlike slip rates.

***Discipline*:** Géosciences de l'Environnement

***Keywords**: Morphotectonics; stress state; continental deformation; in situ-produced exposure dating.*

**C**entre **E**uropéen de **R**echerche et d'**E**nseignement en **G**éosciences de l'**E**nvironnement
Université Paul Cézanne Aix-Marseille III

## *Avant-propos*

Cette thèse fait partie du programme franco-iranien de coopération scientifique sur le risque sismique en Iran, excellemment dirigé par Denis Hatzfeld (LGIT- CNRS UJF) et Mohsen Ashtiani (IIEES). Cette étude a eu le soutien du Ministère des Affaires Etrangères, du INSU–CNRS (PNRN et Diety), du Ministère de la Recherche (ACI-FNS), du côté français et de l'IIEES, du côté iranien. Les images SPOT ont été acquises grâce au soutien du programme ISIS (CNES).

J'ai bénéficié d'une année de bourse (BGF, MAE), par l'intermédiaire du SCAC (Ambassade de France en Iran), ainsi que d'une subvention du MAE (ACI « Cotutelle »). Je remercie pour leurs soutiens Mrs Blanchy, Duhamel et Grimaud, ainsi que Mme Mirbaha pour son aide (SCAC, Ambassade de France en Iran).

## *Remerciements*

Quant j'étais petit j'ai toujours pensé être un berger pour rester a coté des montagnes! Un jour, j'avais dix ans, en regardant la télé, j'ai vu des gens qui examinaient les roches, en jouant avec les appareils bizarres et de grandes cartes dans leurs mains, pour découvrir ce qui était caché a l'intérieur de la terre !!! Ça a changé ma manière de regarder les montagnes. Aujourd'hui, je suis ravie de comprendre partiellement l'alphabet des montagnes. Et bien, ça vient d'une longue histoire!

Je veux ici remercier chaleureusement Olivier Bellier, mon directeur de thèse, qui hormis notre amitiés qui dure depuis 10 ans déjà, il a joué de nombreux autres rôles au cours de ces cinq années de thèse. Tout d'abord, j'ai été toujours étonné de sa confiance en moi! Il m'a appris à rester patient dans les débats scientifiques, ce qui n'a pas toujours été facile pour lui… notamment pour corriger mon caractère brutal! A coté de son rôle inestimable du point de vue scientifique, il a fait tout ce qu'il a pu pour que je reste au calme et que je travaille sereinement. En plus, il a partagé avec nous la joie d'être dans sa famille et d'être accueillis par Cathy, Mathieu et petite Amélie; ce ci restera d'inoubliables souvenirs pour nous!

Mohammad Reza Abbassi (qu'on appelle « Docteur »), le co-directeur de ma thèse, il a changé m'a philosophie de la vie. Dès notre connaissance depuis 1995 il m'a soutenu comme un grand frère, un professeur voire même un ange gardien. Je lui voue une reconnaissance éternelle.

Lionel et Fai, ont toujours été à nos côtés pour ne pas nous sentir amers et seuls. Lionel Siame a également codirigé ma thèse. Il a su m'écouter et guider au cours de cette thèse. Il m'a accompagné pas à pas dès les premiers mots anglais que j'ai écrit; Je n'oublie pas le premier manuscrit qu'il m'a corrigé. Il m'a appris comment se « débrouiller » dans les moments difficiles et même à s'amuser des moments agréables du monde scientifique.

Je remercie Bertrand Meyer et Jean-François Ritz qui ont accepté de rapporter sur ma thèse, ainsi que Jacques Angelier qui a Présidé le Jury. Merci aussi aux autres membres du Jury: Khaled Hessami Azar, Denis Hatzfeld et Abdollah Saïdi, qui ont accepté de juger mon travail.

Merci a Lucilla Benedetti, un peu pour son apprentissage concernant le $^{36}Cl$, et beaucoup pour avoir écouté mes idées, pour m'avoir encouragé, pour sa sympathie, etc. Merci à Jean-Jacques Cochemé, qui a généreusement passé du temps avec moi et m'a appris « des choses » sur les dômes volcaniques. Merci à Régis Braucher et

Didier Bourles, pour qui j'ai beaucoup d'estimes, ils m'ont aidé et donné de précieux conseils sur les datations $^{10}$Be, et ils m'ont encouragé dans mon travail jusqu'à la fin de cette thèse. Merci à Laëtitia Leanni, pour sa patience et son sourire « caché » ! Sans elle j'étais handicape face aux bouteilles HF et HCl du labo $^{10}$Be, aux moments de la préparation chimique des échantillons. Daniel Borschneck est remercié pour m'expliquer les principes de la diffraction des rayons X (DRX), et pour analyser généreusement mes échantillons volcaniques.

Quotidiennement au CEREGE, j'ai eu un grand plaisir à bénéficier de l'aide d'autres personnes: Cyril Blanpain, mon magicien d'informatique qui m'a fait confiance et qui a toujours utilisé tous les moyens pour m'aider efficacement. Brigitte Crubezy, pour qui j'ai beaucoup d'estime et de respect. Elle m'a aidé à chaque moment « du coin de » sa bibliothèque; Isabelle Hammad; Myrthysse Joanides, Michèle Decobert, Philippe Dussouillez et Jule Fleury, leurs aides et leurs amitiés m'ont été inestimables. Patricia Brissaud qui a suivi les démarches administratives de ma dernière mission pendant un an et demi; ses efforts ont enfin aboutis!

J'ai eu le plaisir de partager le bureau 259 avec la petite Christine, Julie, Grégoire et même « les passagers de l'été » qui sont venu s'installer à coté de moi pour analyser les échantillons aux labos $^{10}$Be ou $^{36}$Cl. Irène Schimmelpfennig, ma sœur allemande, chaque jour en face de moi, avec son sourire et sa gentillesse appréciables. Elle a été une véritable conseillère scientifique et culturelle. Si elle parcourt le chemin entre l'aéroport de Marignane et le CEREGE les yeux fermés, c'est grâce à moi!!! Fabienne, la nouvelle princesse de notre bureau, avec sa gentillesse et son regard sympathique qui toujours t'encourage.

Yassaman, Morteza, Leila, plus que mes amis, ma famille. Avec Yassaman j'ai partagé les moments agréables comme difficiles de la recherche, à l'IIEES ainsi qu'au CEREGE. Morteza, sans qui j'aurais été déprimé dans les conditions extrêmement difficiles de ma fin de thèse, ainsi que Leila qui a investi tout ce qu'elle a pu pour nous, pensant toujours à notre avenir. Au cours des deux dernières années de la thèse, ces trois méchants amis ont partagé notre vie quotidienne, et nous ont soutenus pour qu'on reste en France et pour que je puisse finir ma thèse en toute tranquillité.

Jacques-louis de Beaulieu, il nous regarde toujours comme un père avec une sagesse et une gentillesse infinies. Avec Françoise, ils nous ont accueillis dans un coin chaleureux de leur maison. Mes amis Majid, Stefan, Bita et tous les autres amis dont je ne me rappelle pas les noms sont remerciés.

Mohsen, qui n'est pas seulement le meilleur chauffeur de mon pays, c'est également un excellent compagnon de terrain en voiture comme à pied!

Azam, depuis notre mariage m'a accompagnée dans les moments parfois insupportables, et forts heureusement le plus souvent agréables de la vie. Elle a sacrifié sa réussite pour que je puisse réaliser mon rêve d'enfance et devenir « Géologue ». Merci d'avoir supporté mes discussions scientifiques, mes fatigues après le travail intensif, et surtout merci pour Soheil, le soleil de notre vie.

En fin à toute ma famille, je veux exprimer ma profonde affection, et surtout à nos parents qui ont toujours cru en nous et qui ont su nous aider dans les moments difficiles. Je voudrais dédier ce manuscrit à mon père qui a quitté la vie en souhaitant mon succès scientifique.

# *Contents*

## CHAPTER II



## CHAPTER III

# *Introduction*

This dissertation focuses on active tectonics in northeast Iran comprised of the Kopeh Dagh and Allah Dagh-Binalud mountain ranges (Fig. 1). The Iranian plateau is deformed between the converging Arabian and Eurasian plates. Their convergence is principally taken up by the active Makran subduction zone to the South, in addition to shortening and strike-slip faulting accommodated by crustal structures, which are non-uniformly distributed in several continental deformation domains such as the Zagros, Alborz and Kopeh Dagh mountain ranges (Fig 1). The present-day tectonic features are the result of a long and complicated story since the closure of the paleo-Tethysian basins (*Stöcklin*, 1968).

The Arabia-Eurasia convergence is accommodated differently in western and eastern Iran. The present-day GPS-derived rate of the northward motion of Arabia with respect to Eurasia is estimated to be on the order of 22±2 mm/yr at Bahrain longitude, south of the Persian Gulf (*Sella et al*., 2002; *McClusky et al*., 2003; *Vernant et al*., 2004; *Reilinger et al*., 2006). At the southern boundary of the Iranian plateau, the active Makran subduction zone is accommodating a significant portion of the convergence at a rate of 13-19 mm/yr (*Vernant et al*., 2004). The western and southwestern sides of the Iranian plateau are marked by the Zagros Mountains, which are accommodating the total shortening between central Iran and Arabia at a present-day rate of 5 to 9 mm/yr (*Hessami et al*., 2006) by involving active folding and thrust faulting parallel to the belt accompanied by strike-slip faulting parallel or oblique

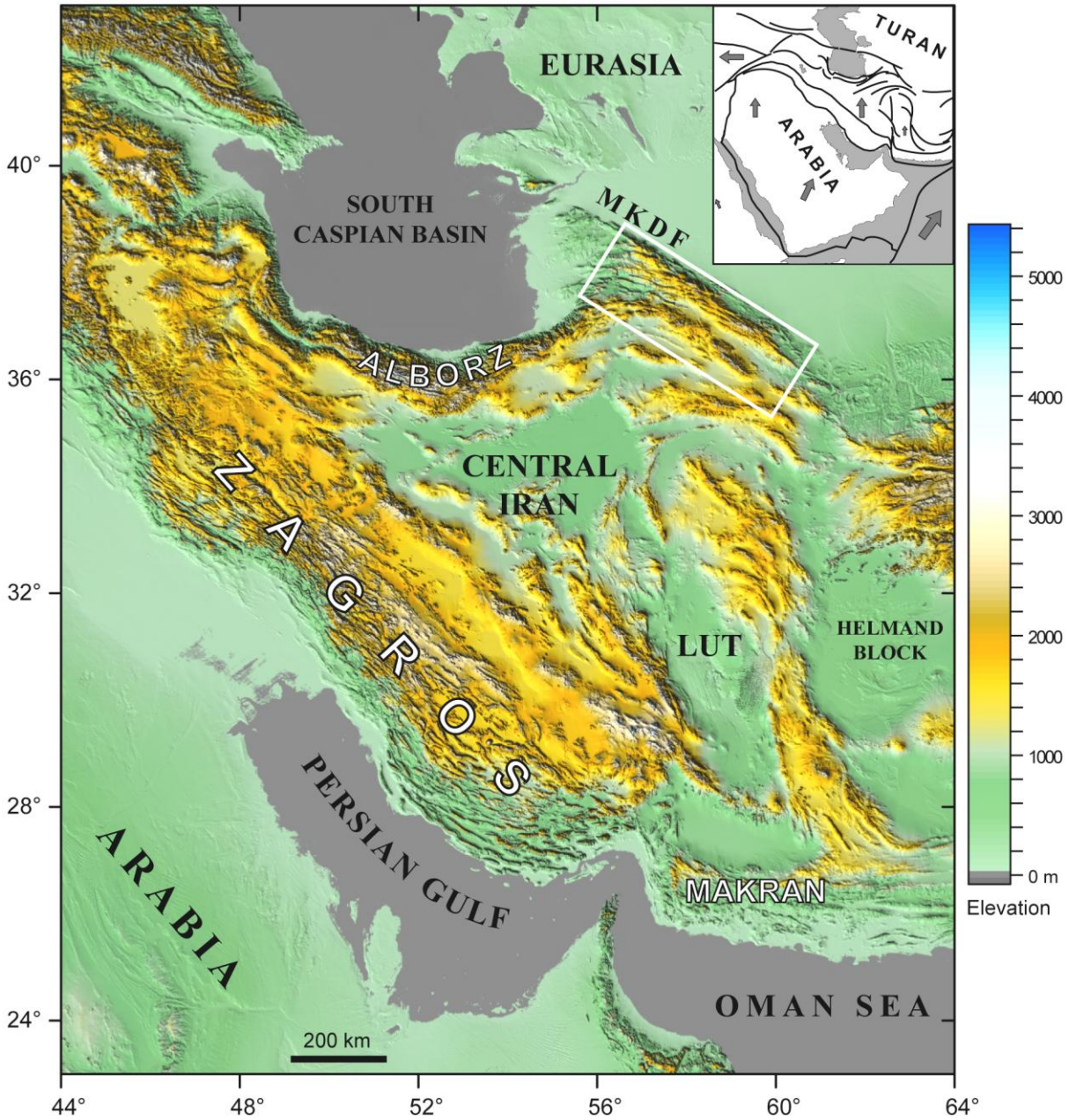


Figure 1. Shaded relief image of the Iranian plateau (GTOPO30 digital topographic data) showing its general morphology together with the main tectono-structural divisions. The white rectangle marks the area of study. The inset on the upper right shows the location in the Arabia-Eurasia collision framework. Gray arrows represent Arabia-Eurasia plate motions after *Reilinger et al.* (2006).

to the belt. Along the eastern side of the Iranian plateau, the northward motion between Iran and Eurasia is taken up by intracontinental right-lateral shear on N-trending strike-slip faults (*Tirrul et al*., 1983; *Meyer and Le Dortz*, 2007), at a rate of 7±2 mm/yr (*Vernant et al*., 2004; *Tavakoli*, 2007). Farther north, the Main Kopeh Dagh Fault system (MKDF) marks part of the northeast boundary of the Arabia-Eurasia collision. This 350 km-long fault corresponds to the intraplate boundary between Iran and Turan platform accommodating their relative motion at

a rate of 3 to 8 mm/yr (*Trifonov*, 1978; *Reilinger et al*., 2006). As a consequence, deformation domains to the North (Alborz, Kopeh Dagh, and Binalud ranges) should take up the residual deformation none absorbed by the southern deformation zones. In this context, the northeast Iran plays a key role in accommodating or transferring the deforming between central Iranian blocks and the Turan platform.

During the last decade, several studies carried out in the Zagros (*e.g*., *Authemayou et al*. 2006, 2009; *Bayer et al*. 2006; *Regard et al*. 2004, 2005; *Talebian and Jackson* 2004; *Walpersdorf et al*. 2006; *Yamini-Fard et al*. 2007; *Navabpour*, 2009), Alborz (*e.g*., *Axen et al*. 2001; *Jackson et al*. 2002; *Masson et al*. 2006; *Ritz et al*. 2006), and central Iran (*e.g*., *Meyer and Le Dortz*, 2007) have produced a better understanding of active deformation in these zones. Conversely, such detailed studies are less common in northeast Iran, where tectono-stratigraphic evolution of the Kopeh Dagh and Binalud mountains has been investigated by *Afshar Harb* (1979) and *Alavi* (1992), respectively. Late Cenozoic faulting as well as the accommodation mode of deformations was discussed by *Tchalenko* (1975), *Lyberis and Manby* (1999), *Jackson et al*. (2002), *Hollingsworth et al*. (2006, 2008).

At the scale of plate tectonics, the deformation of continental lithosphere seems to be distributed over zones up to a few hundred kilometers wide with the relatively aseismic blocks on both sides. This general character of actively deforming continental domains has led geo-scientists to propose two idealized end-member kinematic models. On one hand, it has been suggested that actively deforming regions are comprised of blocks or microplates. Most of the deformation occurs along major block bounding faults, with minor faulting but little internal deformation of the blocks themselves (*Avouac and Tapponnier*, 1993; *Peltzer and Saucier*, 1996; *Replumaz and Tapponnier*, 2003; *Ryerson et al*., 2006, *Thatcher*, 2007, and references therein). On the other hand, deformation is uniformly distributed and continents can be treated as a continuously deforming viscous medium, governed by the fluid-like solid-state flow of a viscous material (*England and McKenzie*, 1982; *Vilotte et al*., 1982; *McKenzie and Jackson*, 1983; *England and Molnar*, 1997; *Flesch et al*., 2001). In this scheme, faults play a minor role and slip in the brittle upper crust occurs on many faults with comparable slip rates. The strengths and limitations of each model have been widely discussed in review papers (*Molnar*, 1988; *England and Jackson*, 1989; *Gordon and Stein*, 1992; *Thatcher*, 1995; *Thatcher*, 2003, and references therein). However, there are perhaps a general agreement that the major unresolved issue is not which of the two extreme models is unconditionally correct, but how the observed deformation can be most usefully and simply

described and which intermediate case is most appropriate (*e.g*., *Molnar*, 1988; *Thatcher*, 1995).

Interestingly, NE Iran and specially the Kopeh Dagh (Fig. 1) were always referred as a key region to demonstrate the geological reliability of the continuous deformation model (*McKenzie and Jackson*, 1983, 1986; *Jackson and McKenzie*, 1984). On the basis of existing data provided by short-term instrumental seismicity and regional geological maps, active deformation in northeast Iran has always been described by predominant active thrust faulting parallel to the strike of isolated deforming zones (*i.e*., the Kopeh Dagh and Allah Dagh-Binalud mountains) without significant strike-slip faulting (*e.g*., *Berberian and Yeats*, 1999; *Hollingsworth et al*., 2008; *Jackson and McKenzie*, 1984). According to this model, unstable geometry of strike-slip faults combined with the thrusting, oblique to the boundaries of the deforming zone will require faults to rotate about a vertical axis until they become parallel to the zone boundary (*McKenzie and Jackson*, 1983, 1986; *Jackson and McKenzie*, 1984; *Jackson et al*., 2002). In this interpretation, kilometric strike-slip cumulative offsets along the NNW-trending faults within the Kopeh Dagh (*Tchalenko*, 1975; *Afshar Harb*, 1979) is described by continuum deformation processes, in which strike-slip faulting results from systematic block rotations around vertical axes (*e.g*., *Hollingsworth et al*., 2006, 2008). However, in the absence of detailed Quaternary fault maps and sufficiently well-constrained data about active faulting, it was difficult to demonstrate the ability of any kinematics model to describe active deformation in NE Iran. In any case, the absence of precise quantitative measures of regional continental deformation has been the chief obstacle in determining which model is able to describe the kinematics of deformation in actively deforming zones (*Thatcher*, 1995). Quantitative data, particularly offset amounts and slip rates on major faults hold the key to constrain these models. In this context, the study of the Quaternary faulting yields the most precise average velocities of slip on faults (*e.g*., *Molnar*, 1988; *Thatcher*, 1995; *Replumaz and Tapponnier*, 2003; *Nyst and Thatcher*, 2004).

Indeed, despite all the efforts made by previous workers to shed light on active tectonics in northeast Iran, this region still suffers from a lack of detailed structural and kinematics data and should be considered as a concealed segment in the geodynamic puzzle of the Arabia-Eurasia collision. This matter is made worse by the facts that northeast Iran is the second populated region and one of the most seismically active deformation domains in the country that has experienced at least nine large earthquakes ($M \geq 7$) during the last six centuries (*Tchalenko*, 1975; *Ambraseys and Melville*, 1982; *Berberian and Yeats*, 1999, 2001).

Within this general context, one simple but fundamental question still needs an answer: how is taken up the deformation in northeast Iran? To deal with this question, the following main objectives need to be achieved:

(1) To provide a detailed structural pattern of active faults for which a precise 2-D fault geometry, structural relationships and possible interactions between major faults can be described.

(2) To estimate rate of active deformation by determining geologic and geomorphic Quaternary slip rates along the recognized major faults.

(3) To characterize the states of stress responsible for Plio-Quaternary deformations in order to better understand the active faulting kinematics.

(4) To analyze the distribution pattern of deformation allowing describing the kinematics of active deformation.

Those main objectives have been pursued thanks to a combination of multidisciplinary approaches (structural geology, tectonic geomorphology, and dating methods) based on the following rationale. In this study, identification and characterization of active faults rely first on the analysis of remote sensing data such as satellite imagery (Landsat ETM+ and SPOT5) and digital elevation models (Space Radar Topographic Mission), complemented with fieldwork surveys, in order to map the fault systems from the fault zone (~100 km) to the fault segment (~10 km) scales, as well as to localize the sites of interest that deserve detailed investigations. From this morpho-structural analysis, fault traces were determined and their activity was highlighted by the displaced Quaternary geomorphic markers (volcanic domes, fluvial terraces, alluvial fans, and river networks). Once identified, fault zones were replaced in their seismotectonic contexts by comparing for example their segmentation with the seismicity distribution (both instrumental and historical) or the fault kinematics (determined by the analysis of either fault slip vectors or offsets cumulated by geomorphic markers), and with the focal solution mechanisms. On several sites of interest, the detail analysis of geological features (fold axes, geological strata) and geomorphic markers affected by the fault activity allowed determining the displacements cumulated over time scales ranging from 5 millions of years to several thousands of years. When needed, the vertical and horizontal components of displacement were measured thanks to a high-resolution topography produced by differential kinematic GPS technique. The fault slip rates, integrated over the Holocene and the Pleistocene, were determined by the combination of the displacement measurements with the dating of the offset geomorphic markers. The dating methods depended on the nature

of the material constituting the offset markers and on the envisaged time scales (radiometric Ar/Ar dating and surface exposure dating using cosmogenic $^{10}$Be and $^{36}$Cl).

This manuscript is organized around four chapters that examine the active tectonics and fault kinematics in northeast Iran. Chapter 1 is dealing with Quaternary slip rates along the northeastern boundary of the Arabia-Eurasia collision zone (Kopeh Dagh Mountains, Northeast Iran). Chapter 2 aims at discussing a new tectonic configuration in NE Iran based on active strike-slip faulting between the Kopeh Dagh and Binalud Mountains. Chapter 3 presents and discusses the Late Quaternary fault slip rates on both sides of the Binalud Mountains. Chapter 4 investigates the Plio-Quaternary states of stress in the Kopeh Dagh and Allah Dagh-Binalud mountain ranges Altogether, the data and interpretations presented in those different chapters allows proposing a new geodynamic model that significantly clarifies the active tectonics of this complicated region.

- Chapter 1 – Quaternary slip rates along the northeastern boundary of the Arabia-Eurasia collision zone (Kopeh Dagh Mountains, Northeast Iran).
- Chapter 2 – New tectonic configuration in NE Iran: active strike-slip faulting between the Kopeh Dagh and Binalud Mountains.
- Chapter 3 – Late Quaternary fault slip rates on both sides of the Binalud Mountains (NE Iran).
- Chapter 4 – Plio-Quaternary stress states in NE Iran: Kopeh Dagh and Allah Dagh-Binalud mountain ranges.

This work was funded by the INSU-CNRS (France) and the International Institute of Earthquake Engineering and Seismology (IIEES, Iran), and permanently carried out at CEREGE – University of Aix – Marseille III. Funding was provided by the Dyeti and PNRN programs (INSU-CNRS), and ACI FNS program (French Ministry of Research), within the above mentioned co-operative agreement. SPOT images were provided thanks to the ISIS program (©CNES 2004 to 2007, distribution SPOT images S.A.).

**References**

Afshar Harb, A. (1979), The stratigraphy, tectonics and petroleum geology of the Kopet Dagh region, northeastern Iran, Ph.D. thesis, Petroleum Geology Section, Royal School of Mines, Imperial College of Science and Technology, London.

Alavi, M. (1992), Thrust tectonics of the Binalood region, NE Iran, *Tectonics, 11*(2), 360-370.

Ambraseys, N., and C. Melville (1982), *A History of Persian Earthquakes*, Cambridge University Press, Cambridge, UK.

Authemayou, C., Chardon, D., Bellier, O., Malekzade, Z., Shabanian, E., and Abbassi, M. (2006), Late Cenozoic partitioning of oblique plate convergence in the Zagros fold-and-thrust belt (Iran), *Tectonics, 25*, TC3002, doi:10.1029/2005TCOO1860.

Authemayou, C., Bellier, O., Chardon, D., Benedetti, L., Malekzade, Z., Claude, C., Angeletti, B., Shabanian, E., and Abbassi, M. R. (2009), Quaternary slip-rates of the Kazerun and the Main Recent Faults: active strike-slip partitioning in the Zagros fold-and-thrust belt, *Geophys. J. Int., 178*, 524-540, doi: 10.1111/j.1365-246X.2009.04191.x.

Avouac, J.-P., and P. Tapponnier (1993), Kinematic model of active deformation in central Asia, *Geophys. Res. Lett., 20*, 895-898.

Axen, G. J., Lam, P. S., Grove, M., Stockli, D. F., and Hassanzadeh J. (2001), Exhumation of the west-central Alborz Mountains, Iran, Caspian subsidence, and collision-related tectonics, *Geology, 29*(6), 559–562.

Bayer, R., Chéry, J., Tatar, M., Vernant, Ph., Abbassi, M., Masson, F., Nilforoushan, F., Doerflinger, E., Regard, V., and Bellier, O. (2006), Active deformation in Zagros-Makran transition zone inferred from GPS measurements, *Geophys. J. Int., 165*(1), 373–381. doi:10.1111/j.1365-246X.2006.02879.x.

Berberian, M., and Yeats, R. (1999), Patterns of historical earthquake rupture in the Iranian Plateau, *Bull. Seism. Soc. Am., 89*, 120–139.

Berberian, M., and Yeats, R. (2001), Contribution of archaeological data to studies of earthquake history in the Iranian Plateau, *J. Structural Geology, 23*, 563-584.

England, P. C., and J. A. Jackson (1989), Active deformation of the continents, *Annu. Rev. Earth Planet. Sci., 17*, 197-226

England, P., and D. McKenzie (1982), A thin viscous sheet for continental deformation, *Geophys. J.R. Astron. Soc., 70*, 295-321.

England, P., and P. Molnar (1997), Active deformation of Asia: From kinematics to dynamics, *Science, 278*, 647-650.

Flesch, L. M., A. J. Haines, and W. E. Holt (2001), Dynamics of the India-Eurasia collision zone, *J. Geophys. Res., 106*, 16,435-16,460.

Gordon, R. G., and S. Stein (1992), Global tectonics and space geodesy, *Science, 256*, 333-342.

Hessami, K., Nilforoushan, F., and Talbot, C. (2006), Active deformation within the Zagros Mountains deduced from GPS measurements, *J. Geol. Soc. Lond., 163*, 143–148.

Hollingsworth, J., Jackson, J., Walker, R., Gheitanchi, M. R., and Bolourchi, M. J. (2006), Strike-slip faulting, rotation and along-strike elongation in the Kopeh Dagh Mountains, NE Iran, *Geophys. J. Int., 166*, 1161-1177, doi:10.1111/j.1365-246X.2006.02983.x.

Hollingsworth, J., Jackson, J., Walker, R., and Nazari, H. (2008), Extrusion tectonics and subduction in the eastern South Caspian region since 10 Ma, *Geology*, *36*(10), 763–766, doi:10.1130/G25008A.1.

Jackson, J. A., Haines, A. J., and Holt, W. E. (1995), The accommodation of Arabia–Eurasia plate convergence in Iran, *J. geophys. Res., 100*, 15,205-15,219.

Jackson, J., and McKenzie, D. (1984), Active tectonics of the Alpine-Himalayan Belt between western Turkey and Pakistan, *Geophys. J. R. astr. Soc., 77*(1), 185-264.

Jackson, J., Priestley, K., Allen, M., and Berberian, M. (2002), Active tectonics of the South Caspian Basin, *Geophys. J. Int., 148*, 214–245.

Lyberis, N., and Manby, G. (1999), Oblique to orthogonal convergence across the Turan block in the post-Miocene, *Am. Assoc. Petrol. Geol. Bull., 83*(7), 1135-1160.

Masson, F., Djamour, Y., Vangorp, S., Chéry, J., Tavakoli, F., Tatar M., and Nankali, H., (2006), Extension in NW Iran inferred from GPS enlightens the behavior of the south Caspian basin, *Earth Planet. Sci. Lett., 252*, 180–188.

McClusky, S., Reilinger, R., Mahmoud, S., Ben Sari, D,. and Tealeb, A. (2003), GPS constraints on Africa (Nubia) and Arabia plate motions, *Geophys. J. Int., 155*(1), 126–138, doi:10.1046/j.1365-246X.2003.02023.x.

McKenzie, D., and Jackson, J. (1983), The relationship between strain rates, crustal thickening, paleomagnetism, finite strain, and fault movements within a deforming zone, *Earth planet. Sci. Lett., 65*, 182-202.

McKenzie, D., and Jackson, J. (1986), A block model of distributed deformation by faulting, *J. Geol. Soc. London, 143*, 349-353.

Meyer, B., and Le Dortz, K. (2007), Strike-slip kinematics in Central and Eastern Iran: Estimating fault slip-rates averaged over the Holocene, *Tectonics, 26*, TC5009, doi:10.1029/2006TC002073.

Molnar, P. (1988), Continental tectonics in the aftermath of plate tectonics, *Nature*, *335*, 131-137.

Navabpour, P. (2009), Brittle tectonics and palaeostress reconstructions in the Zagros: passive palaeo-margin and continental collision, Ph.D. thesis, University of Nice – Sophia Antipolis, France.

Nyst, M., and W. Thatcher (2004), New constraints on the active tectonic deformation of the Aegean, *J. Geophys. Res.*, *109*, B11406, doi:10.1029/2003JB002830.

Peltzer, G., and F. Saucier (1996), Present-day kinematics of Asia derived from geologic fault rates, *J. Geophys. Res.*, *101*, 27,943-27,956.

Regard, V., Bellier, O., Thomas, J.-C., Abbassi, M. R., Mercier, J., Shabanian, E., Feghhi, K., and Soleymani, S. (2004), The accommodation of Arabia-Eurasia convergence in the Zagros-Makran transfer zone, SE Iran: a transition between collision and subduction through a young deforming system, *Tectonics*, *23*, TC4007, doi:10.1029/2003TC001599.

Regard, V., Bellier, O., Thomas, J.-C., Bourlès, D., Bonnet, S., Abbassi, M. R., Braucher, R., Mercier, J., Shabanian, E., Soleymani, S., and Feghhi, K. (2005), Cumulative right-lateral fault slip rate across the Zagros–Makran transfer zone: role of the Minab–Zendan fault system in accommodating Arabia–Eurasia convergence in southeast Iran, *Geophys. J. Int.*, *162*, 177–203, doi:10.1111/j.1365-246X.2005.02558.x.

Reilinger, R., et al. (2006), GPS constraints on continental deformation in the Africa-Arabia-Eurasia continental collision zone and implications for the dynamics of plate interactions, *J. Geophys. Res.*, *111*, B05411, doi:10.1029/2005JB004051.

Replumaz, A., and P. Tapponnier (2003), Reconstruction of the deformed collision zone between India and Asia by backward motion of lithospheric blocks, *J. Geophys. Res.*, *108*(B6), 2285, doi:10.1029/2001JB000661.

Ritz, J.-F., Nazari, H., Ghassemi, A., Salamati, R., Shafei, A., Solaymani, S. and Vernant, P., (2006), Active transtension inside central Alborz: A new insight into northern Iran–southern Caspian geodynamics, *Geology*, *34*(6), 477–480. doi:10.1130/G22319.1.

Sella, G. F., Dixon, T. H., and Mao, A. (2002), REVEL: A model for recent plate velocities from space Geodesy, *J. Geophys. Res.*, *107*(B4), 2081, doi:10.1029/2000JB000033.

Stöcklin, J., 1968. Structural history and tectonics of Iran: A review, *Am. Assoc. Petr. Geol. Bull.*, *52*(7), 1229–1258.

Talebian, M. and Jackson, J. (2004), A reappraisal of earthquake focal mechanisms and active shortening in the Zagros mountains of Iran, *Geophys. J. Int.*, *156*(3), 506–526.

Tavakoli, F. (2007), Present-day kinematics of the Zagros and east of Iran faults, Ph.D. thesis, University of Joseph Fourier, France, Grenoble.

Tchalenko, J. S. (1975), Seismicity and structure of the Kopet Dagh (Iran, USSR), *Phil. Trans. R. Soc. Lond., Series A, 278* (1275), 1–28.

Tirrul, R., Bell, I. R., Griffis, R. J., and Camp, V. E. (1983), The Sistan suture zone of eastern Iran, *Geol. Soc. Am. Bull., 94*, 134 – 150.

Trifonov, V., (1978), Late Quaternary tectonic movements of western and central Asia, *Geol. Soc. Am. Bull., 89*, 1059-1072.

Vernant, P., et al. (2004), Present-day crustal deformation and plate kinematics in the Middle East constrained by GPS measurements in Iran and northern Oman, *Geophys. J. Int., 157*(1), 381–398, doi:10.1111/j.1365-246X.2004.02222.x.

Walpersdorf, A., Hatzfeld, D., Nankali, H., Tavakoli, F., Nilforoushan, F., Tatar, M., Vernant, P., Chéry, J. and Masson, F. (2006), Difference in the GPS deformation pattern of North and Central Zagros (Iran), *Geophys. J. Int., 167*(3), 1077-1088. doi:10.1111/j.1365-246X.2006.03147.x.

Yamini-Fard, F., Hatzfeld, D., Farahbod, A.M., Paul, A. and Mokhtari, M. (2007), The diffuse transition between the Zagros continental collision and the Makran oceanic subduction (Iran): microearthquake seismicity and crustal structure, *Geophys. J. Int., 170*(1), 182–194.

# *Chapter I*

This chapter is focused on active tectonics in the Kopeh Dagh Mountains, which corresponds to the main deformation domain in northeast Iran. The Kopeh Dagh range is bounded by the Main Kopeh Dagh Fault system accommodating the relative motion between Iran and Turan platform. This intraplate strike-slip deformation is principally transferred southeastward to the post-Miocene Bakharden-Quchan Fault System dissecting the Central Kopeh Dagh. Nevertheless, geological knowledge of the rate and kinematics of this deformation is largely insufficient. Our morphotectonic investigations are conducted along the Bakharden-Quchan Fault System to constrain the long-term slip rates, to fill the huge gap of time between geological and geodetic data sets. After a review of the geological setting and structural framework of the Kopeh Dagh Mountains, we present the active faulting evidence along the fault system. Then, we analyzed post-folding brittle deformation and the obtained fault slip rates together, in order to characterize active deformation pattern. Finally we estimate inception of the strike-slip faulting in the range.

# Quaternary slip rates along the northeastern boundary of the Arabia-Eurasia collision zone (Kopeh Dagh Mountains, Northeast Iran)*

Esmaeil Shabanian[a], Lionel Siame[a], Olivier Bellier[a], Lucilla Benedetti[a], Mohammad R. Abbassi[b]

[a] CEREGE - UMR CNRS, Université Aix-Marseille, IRD, Collège de France, Europôle de l'Arbois, BP 80, 13545 Aix-en-Provence Cedex 4, France

[b] International Institute of Earthquake Engineering and Seismology, BP 19395-3913 Tehran, Iran

## Abstract

The Kopeh Dagh is accommodating a large portion of the northward motion of Central Iran with respect to Eurasia, involving a major right-lateral strike-slip fault system (Bakharden-Quchan). This fault system corresponds to the north-eastern boundary of the Arabia-Eurasia collision, and can be considered as a lithospheric-scale tectonic feature. We present a well-constrained estimation of late Quaternary slip rates along two major strike-slip faults (the Baghan and Quchan faults) in this fault system, using *in situ*-produced $^{36}$Cl nuclide to date two offset alluvial fan surfaces. Combining detailed satellite image and digital topographic data analyses complemented with geomorphic field work allows quantifying the cumulative offset values of 940±100 and 360±50 m of the fan surfaces along the Baghan and Quchan faults, respectively. A total of 12 carbonate boulders from the fan surfaces were collected and dated. This yields minimum age of two episodes of fan abandonment at 280±16 (Baghan fault) and 83±4 ka (Quchan fault). Age estimates and measured offsets of the fans are consistent with respective maximum long-term fault slip rates of 2.8±1.0 and 4.3±0.6 mm/yr for the Baghan and Quchan faults over the Middle-Late Pleistocene. Applying the slip rates to cumulative post-folding offsets along the Baghan and Quchan faults indicates that strike-slip motion within the Kopeh Dagh may have started ~4 Ma. This constrains the timing of a major tectonic reorganization in the Kopeh Dagh, previously recorded through Arabia-Eurasia collision between 3 and 7 Ma. At the regional scale, the sum of total cumulative strike-slip offsets is about 35-40 km which implies a total maximum slip rate of about 9±2 mm/yr in the Central-Eastern Kopeh Dagh. This is resolved to average northward and westward slip rates of ~8 and ~4 mm/yr, respectively, for the Western Kopeh Dagh with respect to Eurasia. Our results also suggests that the localized strike-slip faulting in the Central Kopeh Dagh can be considered as an intercontinental movement between north-east Iran and Eurasia, accommodating about 80% of northward motion of Central Iran with respect to Eurasia.

*Keywords: Seismicity and tectonics; Continental neotectonics; Continental tectonics: strike-slip and transform; Tectonics and landscape evolution.*

---

*Shabanian* et al. (*2009), Geophys. J. Int., 178, 1055-1077, doi: 10.1111/j.1365-246X.2009.04183.x.*

## 1. Introduction

Tectonic deformations in Iran result from the Arabia-Eurasia convergence. This convergence took place by crustal shortening and strike-slip faulting in different intracontinental deformation zones, such as the Zagros, Alborz and Kopeh Dagh mountain ranges, and the active subduction zone of the Makran. The Kopeh Dagh range (Fig. 1) corresponds to the main deformation zone at the north-eastern boundary of the Arabia-Eurasia collision. During the last decade, several studies carried out in the Zagros (*e.g., Authemayou et al.,* 2005; *Authemayou et al.,* 2006; *Bayer et al.,* 2006; *Regard et al.,* 2004; *Regard et al.,* 2005; *Talebian and Jackson* 2004; *Walpersdorf et al.,* 2006; *Yamini-Fard et al.,* 2007) and Alborz (*e.g., Axen et al.,* 2001; *Jackson et al.,* 2002; *Masson et al.,* 2006; *Ritz et al.,* 2006), have produced a better understanding of active deformation in these zones; such detailed studies are less common in the Kopeh Dagh (*e.g., Hollingsworth et al.,* 2006; *Masson et al.,* 2007; *Tavakoli,* 2007).

The northward motion of Arabia with respect to Eurasia is accommodated at a rate of 22±2 mm/yr at the longitude of Bahrain (*McClusky et al.,* 2003; *Reilinger et al.,* 2006; *Sella et al.,* 2002; *Vernant et al.,* 2004). According to the available geodetic data, this northward motion should be accommodated in north-eastern Iran (mainly in the Kopeh Dagh Mountains) at a rate ranging from 4 to 10 mm/yr (*Masson et al.,* 2007; *Reilinger et al.,* 2006; *Tavakoli,* 2007; *Vernant et al.,* 2004), given angular relationships between block motions and major structures (Fig. 1).

The Kopeh Dagh Mountains form a NW-SE active belt separating Central Iran from Eurasia (Turan platform) (Fig. 1). This mountain range accommodates a significant part of the Arabia-Eurasia convergence not absorbed by the Makran subduction (*Vernant et al.,* 2004), involving thrust faulting, left-lateral strike-slip (on minor faults) in the Western, and right-lateral strike-slip in the Central-Eastern Kopeh Dagh (*Afshar Harb, 1979*; *Jackson and McKenzie,* 1984) mainly accommodated along a large intracontinental fault system.

In the Kopeh Dagh, the fault slip rates have been estimated using approaches spanning very different time scales: the short-term (a few years) from geodetic analysis (*Masson et al.,* 2007; *Tavakoli,* 2007; *Vernant et al.,* 2004), and the long-term (~5 Myr), using geological data (*Afshar Harb,* 1979; *Lyberis et al.,* 1998; *Lyberis and Manby,* 1999). Geodetic measurements give access to short-term, almost instantaneous rates that include both inter- and post-seismic deformation (*Tapponnier et al.,* 2001). Such short-term rates are integrated over the last several years, and long-term geological slip rates do not necessarily need to be

identical, especially if strain build-up varies through the seismic cycle and on larger time scales (*e.g.*, *Dixon et al.*, 2003; *Friedrich et al.*, 2003). Despite the geodynamical constraints brought by the previous studies, those may integrate different tectonic regimes and consequently variations of the slip rates. Detailed geomorphic data on fault activity is thus essential to better constrain the slip rates over the last several tens- to hundreds-of-thousands of years along the Arabia-Eurasia collision boundary in north-eastern Iran, to fill the huge gap of time between geological and geodetic data sets.

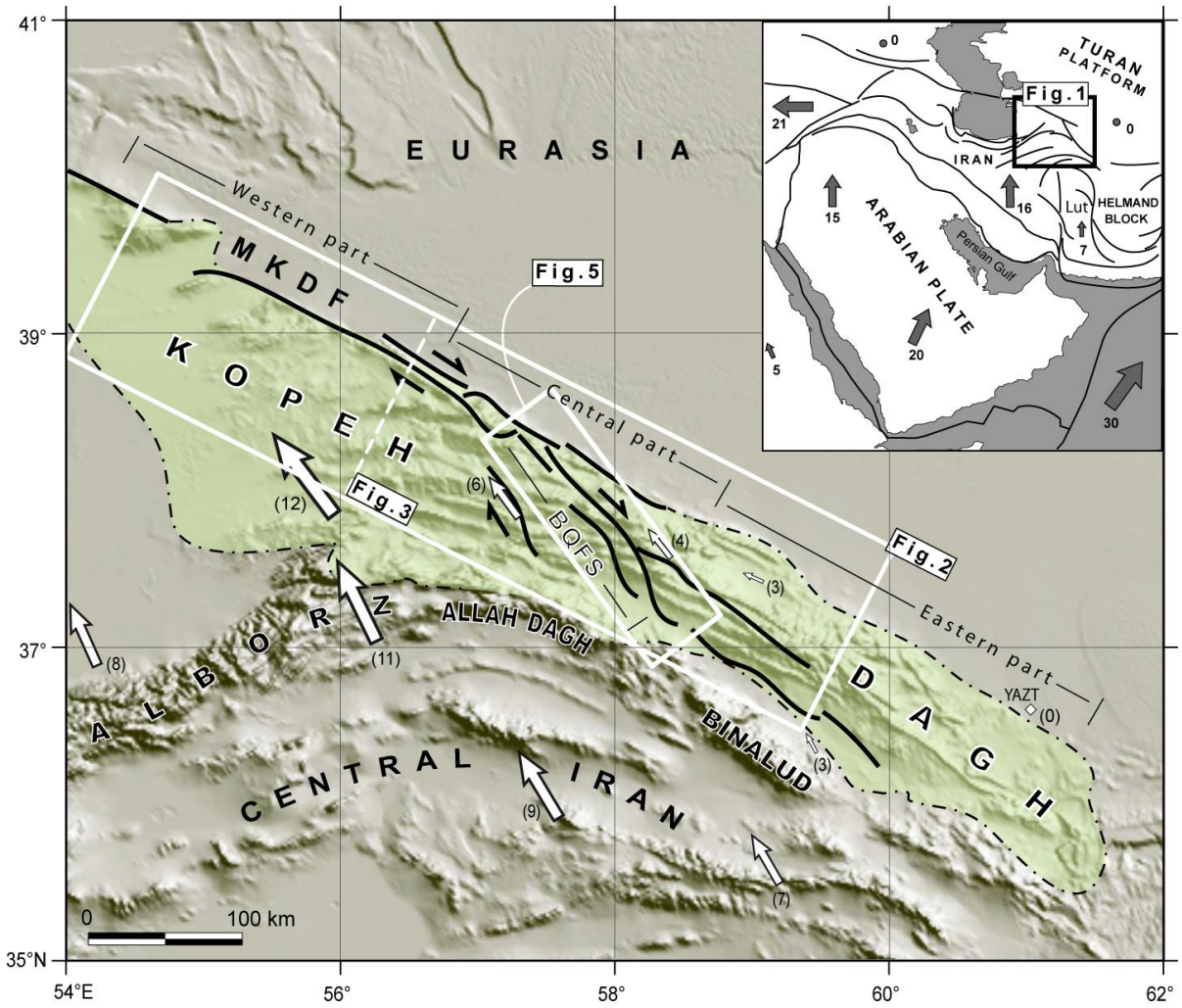


Figure 1. GTOPO30 image of northeastern Iran showing divisions of the Kopeh Dagh Mountains, the location of Bakharden – Quchan Fault System (BQFS) as well as other mountain ranges and structural units mentioned in the text. Right-lateral shear between Central Iran and Eurasia is taken up on the Main Kopeh Dagh Fault (MKDF), accommodated through the Kopeh Dagh on the BQFS (black-half arrows). White arrows and associated numbers are GPS horizontal velocities in a Eurasia-fixed reference frame in millimeters per year (*Tavakoli,* 2007). The inset with the box on the upper right shows the location in the Arabia-Eurasia collision. Gray arrows and associated numbers represent Arabia-Eurasia plate velocities. Rates are in millimeters per year (*Reilinger et al.,* 2006).

This paper presents the first well-constrained estimation of Late Quaternary slip rates in the Kopeh Dagh Mountains, combining *in situ*-produced $^{36}Cl$ exposure dating, detailed satellite image (Landsat and SPOT) analyses, and geomorphic field surveys. After a review of the geological setting and structural framework of the Kopeh Dagh Mountains, we present the active faulting evidence along the main fault system (Bakharden-Quchan Fault) within this mountain belt. Then, we describe the morpho-tectonic investigations conducted along two major strike-slip fault segments (Baghan and Quchan faults), allowing us determining individual Quaternary fault slip rates on the order of several millimeters per year. Our results imply that the Kopeh Dagh region has accommodated the deformation due to the collision between Arabia and Eurasia at a rate of roughly 9±2 mm/yr, suggesting that the Bakharden-Quchan Fault System can be considered as an intercontinental boundary between Iranian micro-plate and Eurasia, accommodating about 80% of northward motion of Central Iran with respect to Eurasia. Moreover, analyzing post-folding brittle deformation combined with the obtained fault slip rates leads to our estimate that the strike-slip faulting within the Kopeh Dagh Mountains began roughly 4 Ma ago.

## 2. Geological setting and structural framework

The Kopeh Dagh range forms a 600 km-long and up to 200 km-wide mountain belt between the Eurasian plate (Turan platform) to the North and the Iranian block to the South (Fig. 1). It includes 10-17 km-thick, Mesozoic and Tertiary sediments, which were folded during the Oligo-Miocene orogenic movements (*Afshar Harb*, 1979; *Lyberis and Manby*, 1999; *Stöcklin*, 1968). The emergence of the Kopeh Dagh has been diachronous, getting younger from the eastern toward the western part of the mountain range (*Afshar Harb*, 1979; *Lyberis and Manby*, 1999). Folding of the Mesozoic-Tertiary sedimentary rocks after the Miocene period indicates the closure of the Kopeh Dagh basin, and emplacement of the Kopeh Dagh Mountains as a consequence of the northward motion of the Arabian shield towards Eurasia (*Afshar Harb*, 1979; *Lyberis et al.*, 1998; *Lyberis and Manby*, 1999). Kopeh Dagh deformation accommodates part of the convergence between the Turan platform to the North and the Lut-Central Iran blocks to the South.

In the North-West, the Kopeh Dagh range is bounded by the Main Kopeh Dagh Fault zone (MKDF) which has been named either *the Main Fault Zone* (*Tchalenko*, 1975), *the main Kopeh-Dagh fault* (*Trifonov*, 1978), or *the Ashgabat fault* (*Lyberis and Manby*, 1999). This 350 km-long fault corresponds to a fundamental, inherited basement structure (*Amurskiy*,

1971; *Maggi et al.*, 2000) forming the NE margin of the Kopeh Dagh as the boundary between Iran and Turan platform, and is considered as a seismically active structure (*Trifonov*, 1978). The width of the MKDF ranges from ~6 km, northeast of Kizyl-Arvat, to ~20 km southwest of Bakharden, where it is intersected by the post-Miocene Bakharden-Quchan Fault System (BQFS) (Figs 1 and 2). This particular region has been suggested as the south-eastern limit of the clear surface expression of the MKDF (*Hollingsworth et al.*, 2006).

The BQFS is constituted by active NNW-trending, right-lateral strike-slip fault segments dissecting the Central-Eastern part of the Kopeh Dagh range (Fig. 1). This fault system extends between the MKDF to the North, and the Binalud range, which can be regarded as the northern margin of Central Iran to the South. The BQFS is the surface expression of basement faults with a considerable cumulative lateral displacement at the surface (*Afshar Harb*, 1979; *Amurskiy*, 1971; *Tchalenko*, 1975). The lack of basement steps (gravity survey - *Amurskiy*, 1971) along these faults suggests also a predominance of lateral movements at depth. Combining the results of recent geodetic and geodynamic studies (*Masson et al.*, 2007; *Reilinger et al.*, 2006; *Tavakoli*, 2007; *Vernant et al.*, 2004) as well as seismicity distribution, with large cumulative geomorphic (this study) and geologic feature offsets (*e.g.*, *Afshar Harb*, 1979; *Afshar Harb et al.*, 1987) observed along the BQFS, strongly implies that the BQFS can be interpreted as a continuation of the eastern Iran boundary, allowing Central Iran to move northward with respect to Afghanistan, as a part of Eurasia (*Jackson and McKenzie*, 1984; *Vernant et al.*, 2004).

## 3. Active faulting along the Bakharden-Quchan Fault System (BQFS)

The BQFS is composed of 10 major, roughly parallel, NNW-trending faults or fault zones with individual segment lengths ranging from 40 to 140 km, corresponding to a 45 km-wide band of transpressive deformation (Figs 1 and 2). . Most of the fault segments were mapped on regional scale geological maps (*Afshar Harb*, 1982; *Afshar Harb et al.*, 1980; *Afshar Harb et al.*, 1987; *Huber*, 1977). Both on digital topography and satellite imagery, their parallel and straight surface traces indicate an array of nearly vertical faults (Fig. 2).

In the northwest, the BQFS bends into the MKDF without clear evidence of crosscutting relationships, which indicates the merging of the both fault systems (Fig. 2). Along the southern limit of the BQFS, the fault zone expression is not conspicuous but it may terminate in the Kashafrud-Atrak Valley between the Kopeh Dagh and Binalud mountain ranges (*Hollingsworth et al.*, 2006).

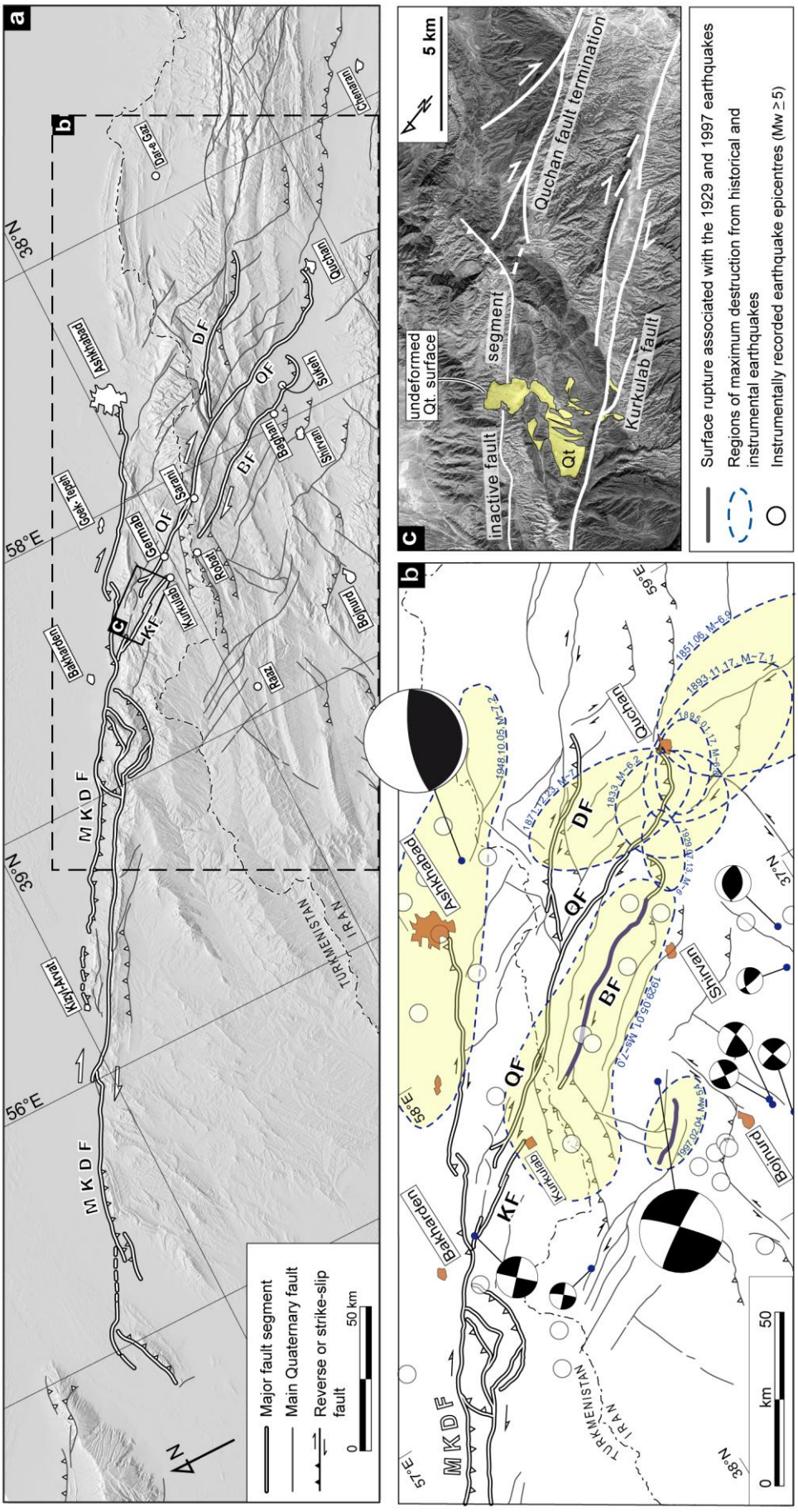
a
b
c
N.38°
N.39°
56°E
58°E
MKDF
DF
QF
BF
KF
Garmab
Kkyr-Aarai
Ashkhabad
Gaok-Tepeh
Bakharden
Quchan
Shirvan
Bojnurd
Chenaran
Dara-e Gaz
Sis
Rabat
Kkrmuied
Raz
TURKMENISTAN
IRAN
Major fault segment
Main Quaternary fault
Reverse or strike-slip fault
0
50 km
5 km
undeformed Qt. surface
inactive fault
segment
Qt
Quchan fault termination
Kurkulab fault
Surface rupture associated with the 1929 and 1997 earthquakes
Regions of maximum destruction from historical and instrumental earthquakes
Instrumentally recorded earthquake epicentres (Mw ≥ 5)
57°E
59°E
37°N
km
50

In this study, analyses of satellite images combined with digital topographic SRTM data and direct field observations allowed us to investigate active faulting along the BQFS. Two different resolutions of satellite images (Landsat ETM+ and SPOT5 with pixel size of 14 and 5 m, respectively) were used for regional mapping. The entire fault system is mapped in detail with special attention to the relay zones and intersection points between different fault segments. This allows distinguishing, on a geometric and geomorphic basis, fault segments representative of the dominant structural pattern. Fig. 2 presents all the recognized Quaternary fault segments with a length longer than 10 km. Among the 10 individual main Quaternary faults and fault zones in the BQFS, the Baghan Fault and the Kurkulab-Quchan Fault zone (KQF) are considered as the two principal structures. The next two sections provide a set of short-term (~$10^2$ yr) and long-term (~$10^6$ yr) evidence to consider the KQF and the Baghan Fault as the major active structures in the Kopeh Dagh Mountains.

### 3.1. Instrumental and historical seismicity in the Kopeh Dagh Mountains

A long and detailed historical record of earthquakes in north-east Iran spans over the last nine hundred years (*Ambraseys and Melville*, 1982; *Berberian and Yeats*, 1999; *Berberian and Yeats*, 2001; *Tchalenko*, 1975). Along the BQFS, the relationship between seismicity and fault segments has already been discussed by *Tchalenko* (1975) and *Ambraseys and Melville* (1982), and recently re-evaluated by *Hollingsworth et al.* (2006) for modern large earthquakes in the western part of the region. Since the 19$^{th}$ century, the Kopeh Dagh region has experienced at least 12 large earthquakes with magnitudes ranging from 6.5 to 7.5, and almost all of those seismic events occurred in the vicinity of the BQFS (Fig. 2). In this context, the Baghan and Quchan faults are responsible for at least 6 of these large earthquakes

Figure 2. (a) Detailed Quaternary fault map of the Central-Eastern Kopeh Dagh and the Main Kopeh Dagh Fault system, including recognized Quaternary faults with a length longer than 10 km (prepared in this study). Two rectangles marked by b and c are the region of Figs 2b and c. Abbreviations are as follows: MKDF, Main Kopeh Dagh Fault; KF, Kurkulab Fault; QF, Quchan Fault; BF, Baghan Fault; DF, Dorbadam Fault. (b) Historical and instrumental seismicity of the Kopeh Dagh. Focal mechanisms are mainly taken from the Harvard catalogue (http://www.globalcmt.org/CMTsearch.html) and *McKenzie* (1972). Epicenters are from the NEIC catalogue (http://neic.usgs.gov/neis/epic/epic_global.html). The regions of maximum destruction are mainly based on *Tchalenko* (1975) and *Ambraseys & Melville* (1982), with one of the 4th February 1997 Garmkhan earthquake from *Hollingsworth et al.* (2007). Thick-black lines are surface ruptures associated with the 1929 Baghan (*Tchalenko*, 1975) and 1997 Garmkhan (*Hollingsworth et al.*, 2007) earthquakes. (c) LANDSAT image of the Kurkulab-Quchan relay fault zone; the Quaternary trace of the Quchan segment terminates as it splits into a horse-tail structure.

(Baghan earthquake: 1929; Quchan earthquakes: 1851(?), 1871-72, 1893, 1895 – *Ambraseys and Melville*, 1982; *Tchalenko*, 1975). When considering the macroseismic regions associated to these historical earthquakes, the band of maximum destruction appears to follow the trends of the Quchan and Baghan faults. There is no evidence for such seismicity along the other structures in this zone. This supports the major role of the Quchan and Baghan faults within seismogenic behavior of the Central-Eastern Kopeh Dagh.

### 3.2. Distribution of cumulative geological offsets in the Kopeh Dagh Mountains

To understand and quantify the contribution of the BQFS to the accommodation of the Quaternary deformation at a regional scale, distribution of post-folding brittle deformation in the Kopeh Dagh was carefully examined using satellite imagery, SRTM data and field observations (Fig. 3). This analyzes allowed us investigating detailed morphologies, total offset measurements, as well as the structural linkage between the different fault segments. At the regional scale, there is no geomorphic or geological evidence for a significant vertical component along the major strike-slip faults over the whole BQFS. This is in agreement with a predominance of lateral movements at depth (*Amurskiy*, 1971), as well as focal mechanism data (Fig. 2). In addition, according to our field observations, a fault rake (slip-vector on fault plane) ranging from 0 to 10 degrees (Fig. 4) can be considered as a characteristic value for strike-slip motions in the Kopeh Dagh. Taking this characteristic fault rake into account, a maximum vertical displacement on each fault segment might not exceed by 11% the associated lateral displacement. According to these observations, cumulative post-folding horizontal displacements can be measured directly on satellite images, thanks to parallel fold axes and well-stratified geological formations offset by strike-slip faults. The cumulative displacements measured along the BQFS segments range from 100 m to 18 km. Those measurements are presented as displacement isolines at a regional scale (Fig. 3), allowing us distinguishing the structural importance of each individual fault segment in the region. The North-eastern part of the region is occupied by the Turan platform where there is no deformation (Fig. 3). The largest portions of strike-slip movements are localized on the MKDF and the BQFS. Among the investigated faults, the KQF and the Baghan Fault are the most important ones, exhibiting maximum cumulative displacements of ~15 and ~10 km, respectively (*Afshar Harb*, 1979; *Afshar Harb et al.*, 1987; *Hollingsworth et al.*, 2006). As a result, the combined observations of large post-folding offsets and occurrence of major destructive earthquakes during the last three centuries, suggest that the KQF and the Baghan

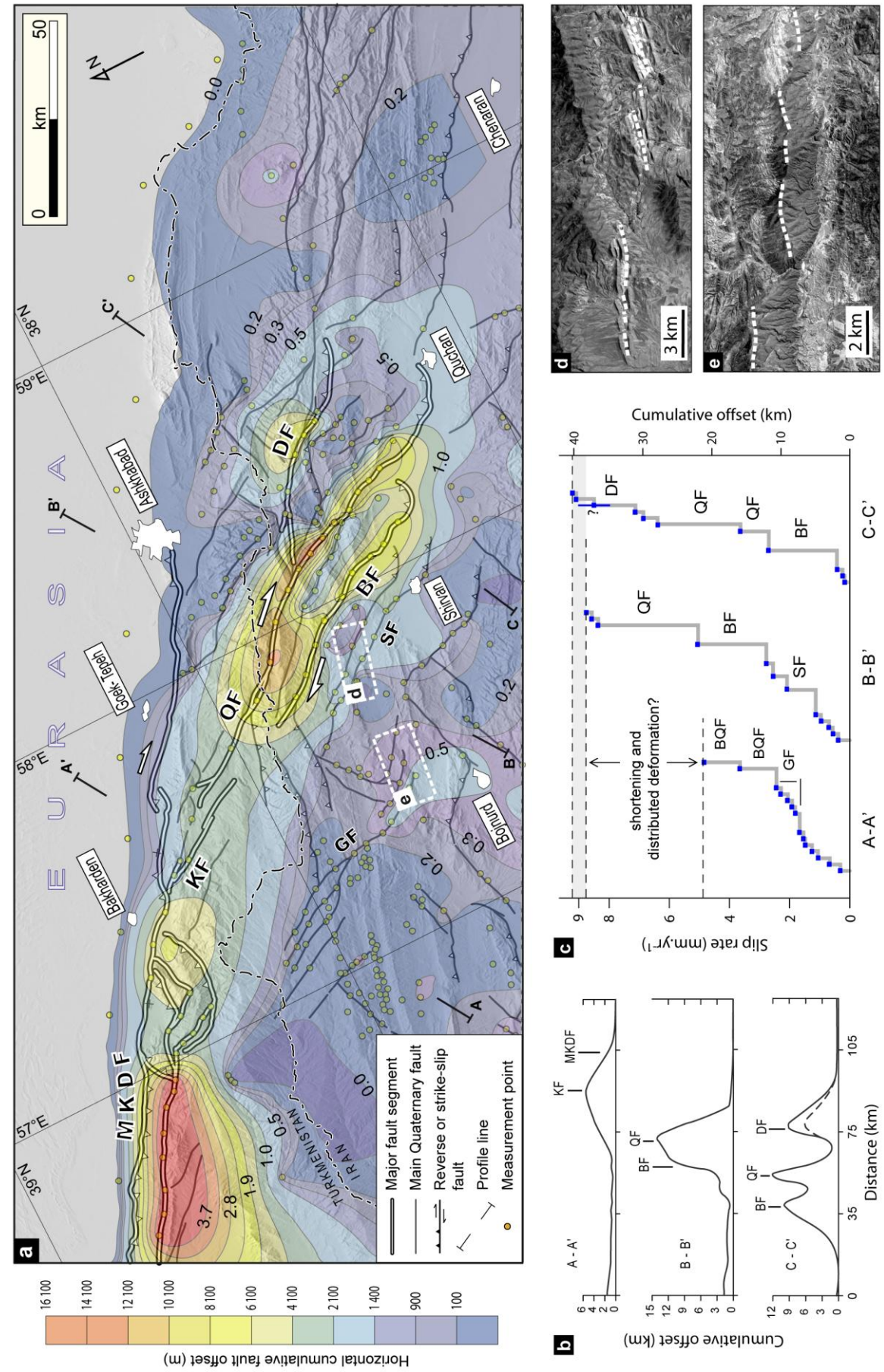
a
EURASIA
MKDF
KF
QF
DF
BF
SF
GF
Bakharden
Ashkhabad
Gaudk Tepeh
Chenaran
Quchan
Shirvan
Bojnurd
TURKMENISTAN
IRAN
Major fault segment
Main Quaternary fault
Reverse or strike-slip fault
Profile line
Measurement point
Horizontal cumulative fault offset (m)
b
A - A'
B - B'
C - C'
Cumulative offset (km)
Distance (km)
c
Slip rate (mm.yr⁻¹)
Cumulative offset (km)
shortening and distributed deformation?
A-A'
B-B'
C-C'
d
3 km
e
2 km

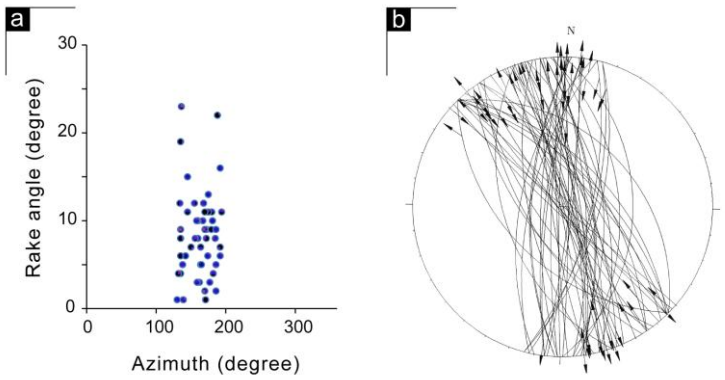


Figure 4. Fault plane data indicating a characteristic rake value ranging from 1 to 10° for strike-slip faults within the Kopeh Dagh Mountains. (a) Fault rake angle versus fault azimuth. (b) Stereographic projection of the fault data including fault striations.

Fault can be considered as the major strike-slip faults and consequently the main seismogenic sources in the Kopeh Dagh Mountains.

### 3.3. The Kurkulab–Quchan Fault zone

The longest fault zone in the BQFS system is constituted by two major fault segments which connect the MKDF to the northern limit of the Binalud fault system (Fig. 2). This fault zone was previously considered to be the Quchan Fault (*Hollingsworth et al.*, 2006). However, even if the Quchan Fault connects to the MKDF, there is no direct Quaternary structural linkage between these two fault zones. On the basis of our observations, we propose the name of Kurkulab-Quchan fault zone (KQF) for this complex structure.

The Quchan Fault is the longest segment of the KQF, which is the largest strike-slip fault zone in the BQFS. The Quchan Fault extends from the city of Quchan in the southeast to 24 km north of Germab village in the northwest (Fig. 2). As characteristic features, displaced geomorphic markers such as alluvial fans, beheaded drainages and offset active stream beds, indicate Quaternary activity along much of its length. More to the north, the Quaternary trace

---

Figure 3. (a) Regional distribution of cumulative strike-slip offsets (filled contours) and their equivalent long-term slip rates (numbered contours) in the Kopeh Dagh Mountains. Slip rates are expressed in millimeters per year. GF, Gholaman Fault zone; SF, Shirvan Fault; other abbreviations as the caption of Figure 2. (b) Profiles along which distribution pattern of the cumulative geological offsets is presented through the Kopeh Dagh Mountains. Location of profiles is marked on Fig. 3a. It should be noted that the cumulative offset on the DF (<10 km) is undifferentiated sum of right-lateral displacement (the probable dotted line: ~6 km) and apparent offset due to oblique thrust faulting with respect to fold axes. (c) Total slip rates for paths A-A', B-B', and C-C' shown in Fig. 3a. (d) And (e) SPOT5 image of the southern part of the GF and SF, respectively, two examples for cumulative geological offsets analyzed in this study.

of the fault terminates as it splits into a horsetail structure (Fig. 2). The ancient trace of the main fault is conspicuous on satellite image and digital topography, and runs northward about 2 km beyond this area, where it is covered by an uplifted Quaternary terrace that is not affected by the fault trace (Fig. 2c). On the basis of our observations, the northern termination of the Quchan Fault is a relay zone between two major fault segments of the BQFS. The Kurkulab Fault runs between the relay zone and the MKDF continuing the BQFS to the North, turning obliquely into the MKDF (Fig. 2). Hereafter, we pay a special attention to the structural and geomorphic characteristics of the Quchan Fault.

### 3.4. The Quchan Fault

Although Quchan Fault can be mapped continuously from Quchan up to 134 km northwards and the northern termination can be clearly delineated, the southern limit is less clear. However, subtle geomorphic evidences indicating its thrust-bend termination in the Atrak Valley (Fig. 5) have been described near the city of Quchan by *Hollingsworth et al.* (2006). The Quchan Fault obliquely cuts the Oligo-Miocene folds of the Kopeh Dagh with a maximum right-lateral offsets of ~15 km in the folded bedrock (Fig. 5). The strike of the fault segment does not varies much, except southeast of Sarani village, where the Quchan Fault rotates anti-clockwise by ~27° along a 25 km-long restraining bend (Fig. 5). This particular area is characterized by rotation and dragging in both morphological and structural features, and probably represents an old short-cut zone between two distinct fault segments.

In the case of the Quchan Fault, aside from fault tip terminations, the main prominent structural complexities are the intersection points of the main fault with other faults traces. The Owghaz and Bey-Bahreh faults are two parallel, strike-slip faults with a maximum length of roughly 50 km, which intersect the Quchan Fault (Fig. 5). These faults displace the bedrock in clear right-lateral offsets (of about 2 km) east and west of the main structure. Due to this structural arrangement, maximum offset of the major fault corresponds to the sum of total offsets along the three faults within the intersection zone (Fig. 5).

In this area of the Kopeh Dagh, several rivers flow across the Quchan Fault. The river courses follow synclinal axes parallel to the belt, and incise through growing anticlines (Fig. 5). Assuming that those rivers initiated during the same period of time, they can be used to compare contemporaneous offsets along the fault traces. A maximum cumulative, right-lateral offset of about 10 km can be measured on the Southern and Central parts of the Quchan Fault, while this value decreases northward to roughly 5 km, near of Germab (Fig. 5).

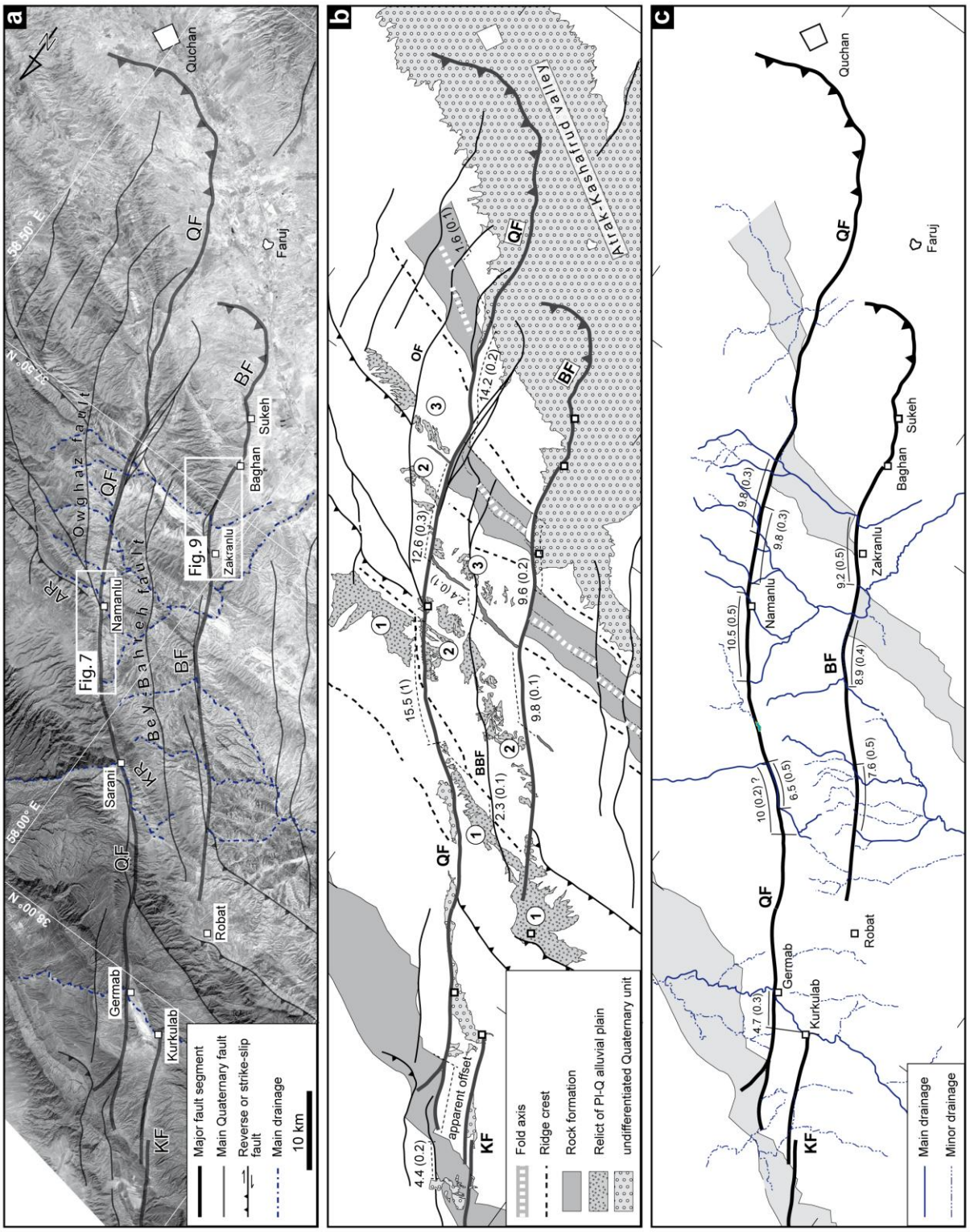


Figure 5. (a) LANDSAT image of the BQFS indicating detailed 2D-geometry of the Quchan and Baghan faults and their associated right-lateral offsets in the folded bedrock as well as un-deformed linear markers such as anticline axes and ridge crests. AR, Agh-Kamar Ridge; KR, Konjukhor Ridge. (b) Morphotectonic map of the BQFS based on Fig. 5a. The values of cumulative geological offsets are presented as numbers with their associated uncertainties in parenthesis. Corresponding relict alluvial plains have been marked by the same numbers (1 to 3) beside the faults. (c) Cumulative geomorphic offsets on the BQFS. The offset values are expressed in kilometers.

This observation is in agreement with a northward termination of the Quchan Fault in the relay zone, where the fault trace is covered by a non-deformed Quaternary terrace (section 3.3).

### 3.5. The Baghan Fault

With a length of 80 km, the Baghan Fault runs northwest between Sukeh village on the northern bank of the Kashafrud Valley, and Robat village at the border between Iran and Turkmenistan (Fig. 5). The Baghan Fault trends exactly parallel to the Quchan Fault as a single fault segment, so the perpendicular distance between the two faults (an average of ~11 km) is constant along strike (Fig. 5). This common geometry probably indicates a structural inheritance in the basement and/or a rheological effect of different geological formations affected by the faults.

The Baghan Fault is responsible for the 1929 Baghan earthquake (Ms ~7) that was associated with a 50 km-long coseismic ground rupture (*Ambraseys and Melville*, 1982; *Tchalenko*, 1975; *Tchalenko et al.*, 1974). *Tchalenko* (1975) described a SE-facing fault scarp, visible from place to place as a 2 m-high, rounded topographical step (or 1 m according to *Ambraseys and Melville*, 1982). Comparing total length of the Baghan Fault (80 km) with this 50 km-long coseismic ground rupture (Fig. 2), indicates that only 60% of the whole length of the fault may have been reactivated during the 1929 Baghan earthquake. The Baghan Fault is characterized by kilometric geological displacements to metric geomorphologic offsets that can be observed both on satellite images and in the field (*e.g.*, *Afshar Harb*, 1979; *Tchalenko*, 1975). Among those features, the river network that flows north across the Baghan Fault is right-laterally displaced by a maximum of 9 km (Fig. 5).

## 4. Morpho-tectonic investigations

### 4.1. Methodologies

#### 4.1.1. Geomorphic mapping and site selection

At the site scale, analyses of SPOT5 images combined with aerial photographs, and direct field observations were used to quantify geomorphic offsets along the recognized active fault segments. Among several possibilities, we selected two key sites offering several advantages for understanding the displacement history of the Quchan and Baghan faults: (1) Maximum total offset on a single fault strand, (2) well-preserved alluvial fans offset by the fault, providing readily datable markers and constrained fault offset values, and (3) small

catchment basins close to the alluvial fans to minimize inheritance of *in situ*-produced cosmogenic $^{36}$Cl in our samples. The first studied site is located close to Namanlu village (Fig. 5), on an alluvial fan which is offset by the Quchan Fault (Fig. 7). At this particular location, we also surveyed several thousand topographic data points (~86000 x,y,z points) using Leica 530 post-processing kinematic (PPK) GPS, to provide a large-scale digital elevation model of the fan surface. The second site is a large alluvial fan located close to Zakranlu village (Fig. 5), and affected by the Baghan Fault.

### 4.1.2. Sampling and estimating surface exposure ages

On the two offset fan surfaces, both the geomorphic setting and the surface characteristics were carefully considered in selecting boulders to be sampled. For both the Namanlu and Zakranlu surfaces, limestone boulders (>50 cm) embedded on their surfaces were sampled avoiding angular, visibly broken and non-rooted boulders. Considering exponential drop off *in situ*-produced $^{36}$Cl concentrations with respect to sampling depth, spalled boulder surfaces were avoided, and samples were collected from the upper 1-8 cm on top of boulders. Additionally, there is no evidence that the boulders might have been moved and /or buried before their exposition at the present surface. Most of the sampled boulders are characterized by carbonate collars (*e.g., McFadden et al.,* 1998) covering the bottom of the boulders (Fig. 6), supporting that the sampled boulders were embedded at the fan surfaces for relatively long span of time. In fact, carbonate collars are relatively abundant in pavements associated with alluvial fans of various ages formed on limestone-rich alluvium. Overland flows and locally extensive surface erosion by sheet flow (*Wells et al.,* 1985, *Wells et al.,* 1987; *McDonald*, 1994) would likely limit or preclude carbonate collar formation. In addition, any sub-aerially exposition of carbonate collars should also dissolve such precipitates quickly (*McFadden et al.,* 1998). In other words, the formation of these carbonate collars implies a long-term stability of the fan surface, and a long residence of the boulders at the surface. According to *McFadden* et al. (1998), in areas currently favorable to vesicular horizon (Av) formation, this horizon (and its associated collars) must have formed at times before the Holocene during similarly arid conditions.

For all the sampled sites, the shielding by the surrounding topography, snow cover, and sample geometry are found to be of negligible impact on the surface production rates. The watersheds identified to be the source areas of the sampled alluvial fans are rather short and steep catchments, implying short transport times and little along-stream storage. This particular geomorphic situation allows minimizing inheritance of *in situ*-produced

cosmogenic $^{36}$Cl in our samples. For the Namanlu alluvial fan, the sampled surfaces are located away from recent incision rills, and show a relatively fresh morphology (Fig. 6). For the Zakranlu (Honameh) alluvial fan(s), the region today is under traditional dry-farming cultivation but these activities had little effects on the initial morphology of the fan surface (Fig. 6).

Considering that, on such abandoned surfaces, erosion cannot be expected to be uniform, either temporally or spatially (*e.g.,* Fig. 6), erosional effects on the boulder exposure ages were minimized by carefully analyzing the geomorphic setting and the surface characteristics of the alluvial fans. In this context, the most preserved parts of the fan surfaces were selected for sampling (Fig. 6). Preserved morphology of the selected parts of the fan surfaces indicates a trivial influence of erosion on these sampled parts. Although we suspect that little erosion of the surfaces may have occurred, any erosion would render our ages as minima. That is, the actual exposure ages of the surface may be older than the cosmogenic ages we report herein. In the following discussions, all of our exposure ages are minima, even though we think that the true abandonment ages may be close to the sample ages (due to the absence of surface runoff and lateral transport). We note however, in the following discussion that because our cosmogenic ages provide minimum abandonment ages (and initiation of offset) of the fan surfaces, that all the slip rates we discuss below should be considered maximum rates.

To date the sampled boulders, we used the *in situ*-produced $^{36}$Cl cosmogenic exposure dating method. The systematic of *in situ*-production of cosmogenic nuclides is described within the review paper by *Gosse and Phillips* (2001). One can also refer to *Stone et al.* (1996), *Stone et al.* (1998) and *Schimmelpfennig et al.* (2008) for *in situ*-produced $^{36}$Cl specifically. The treatment of the samples, such as grinding, leaching and chemical extraction of chlorine by precipitation of silver chloride, was performed following the methodology described by *Stone et al.* (1996). The $^{36}$Cl and chloride concentrations in the carbonate were determined for all samples by isotope dilution accelerator mass spectrometry (AMS) at the Lawrence Livermore National Laboratory's CAMS. Blank was two orders of magnitude lower than the samples and replicates were within less than 5%.

Chlorine-36 has multiple production pathways, which include spallation reactions (Ca, K, Ti, and Fe), capture of low-energy epithermal and thermal neutrons ($^{35}$Cl), and direct capture of slow negative muons ($^{40}$Ca and $^{39}$K). Moreover, the radiogenic $^{36}$Cl must be evaluated by measuring uranium and thorium concentrations in the target mineral (*Stone et al.*, 1998; *Bierman et al.*, 1995; *Gosse and Phillips*, 2001; *Schimmelpfennig et al.*, 2009). It is

therefore important to know precisely the chemical composition of the target mineral to determine the rate of production (see hereafter), and thus correctly interpret the measured $^{36}Cl$ concentrations. Major elemental composition of rock samples was determined by ICP-OES technique. The boulder ages were calculated using the Ca concentrations in the dissolved part of the samples (target fraction) according to *Schimmelpfennig et al.* (2008). The production rates proposed by *Stone et al.* (1998) were found more appropriate with respect to other production rates measured in whole-rock content (*e.g., Phillips et al.,* 1996). Indeed, *Stone et al*. (2008) production rates were calibrated using calcium-rich mineral separates in which the spallation production mechanism from calcium is dominant. The rates were corrected for elevation and latitude using the correction factors from *Stone* (2000). To illustrate cosmogenic-derived minimum exposure age data and their associated uncertainties, we used the sum of the Gaussian probability distributions (*e.g., Deino and Potts* 1992), already used by different authors for dating purposes (*e.g.*, *Daëron et al.*, 2004; *Lowell,* 1995), according to (*e.g.*, *Taylor*, 1997):

$$p_{sum}(t) = \sum_i e^{-(t-a_i)^2/2\sigma_i^2} / \sigma_i\sqrt{2\pi}$$

where $t$ is time, $a_i$ is the exposure age of sample $i$ and ($2\sigma_i$) is the reported error. A probability value less than 0.05 indicates that there is a significant amount of non analytical error in the data set, and that one or more samples are outliers. In such a case, cumulative frequency plots are generally bimodal in shape, with the secondary peak identifying outliers.

### 4.2. Morpho-tectonic investigations along the Quchan Fault

Along its whole length, the Quchan Fault offsets geomorphic landforms such as Quaternary alluvial fans, fluvial plains and drainage channels at different observation scales (Figs 5 and 7). The Quchan Fault exhibits a convincing right-lateral offset of ~15 km marked by a linear mountain ridge, made up of Cretaceous limestone. Located close to the junction of the Quchan and Owghaz faults (Fig. 5), this offset corresponds to the maximum observed post-folding displacement along the Quchan Fault trace. In this area, a ~16 km-long, west-facing fault scarp was caused by dragging and stretching of the limestone ridge parallel to the fault, separating the Agh-Kamar and Konjukhor ridges in eastern and western fault blocks, respectively (Fig. 5). The fault scarp prepared a suitable condition to form several post-offset talus and alluvial fans which have been cut during the Late Quaternary fault activity. Among these Quaternary landforms, the Namanlu alluvial fan is one of the best geomorphic features

providing favorable conditions for both surface exposure dating and measurements of cumulative displacements (Fig. 7). Crossing the Namanlu fan, the fault is characterized by a relatively narrow, 110 to 150 m-wide fault zone. The Namanlu fan is comprised of a single fan surface and there is no evidence for post-offset successive depositions onto the fan surface. These observations suggest that no aggradation episode has occurred since the fan surface was abandoned. Therefore, considering the fan location, narrowness of the fault zone and relatively well-preserved fan surface, the Namanlu fan provides an excellent opportunity to estimate the late Quaternary slip rate of the Quchan Fault.

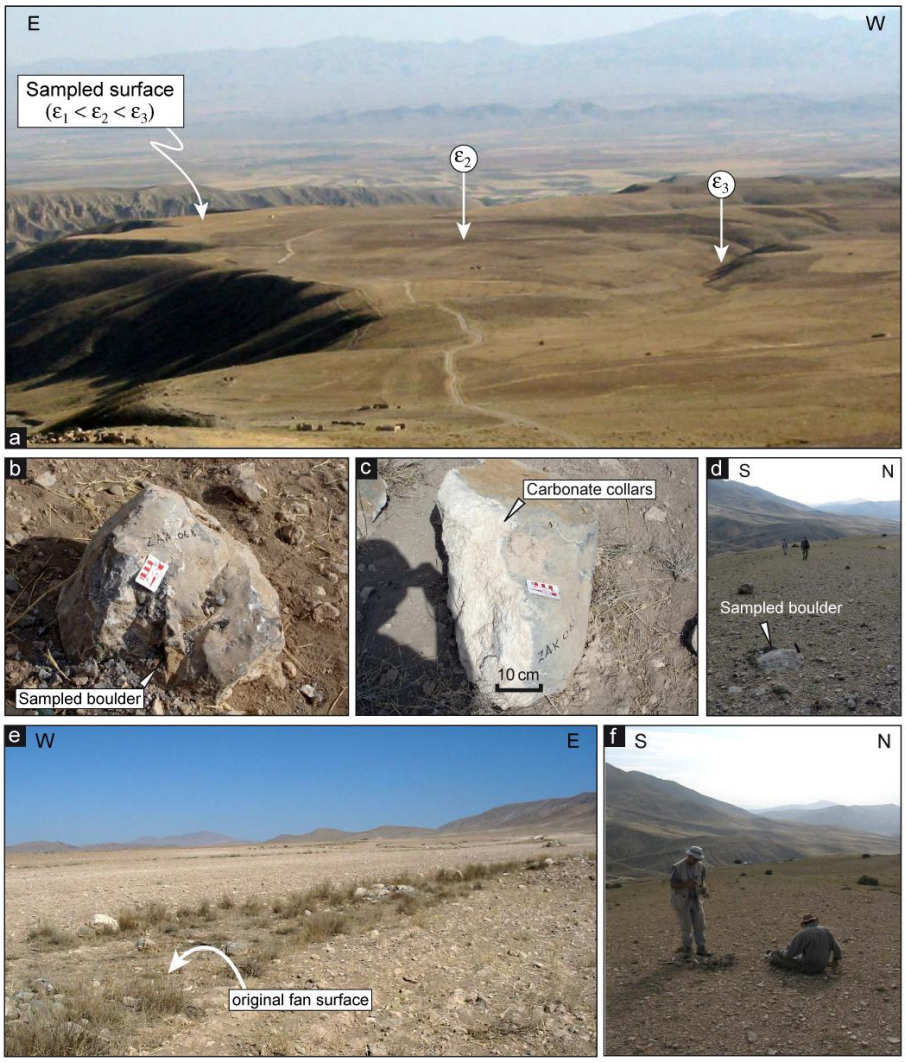


Figure 6. (a) General view of the Zakranlu fan surface, taken from the fan apex, showing non-uniform erosion ($\varepsilon$ – whatever the involved mechanism) on the different parts of the fan surface. The most preserved part of the surface was sampled. (b) Typical carbonate boulder sampled on the Zakranlu fan surface. (c) An example of characteristic carbonate collars on the embedded parts of the sampled boulders. This boulder was exhumed by the field team after sampling in order to demonstrate the degree of carbonate collar development typical of the samples embedded in the fan surface. (d) And (f) General view of the relatively well-preserved sampled part of the Namanlu fan surface. (e) Insignificant effect of traditional dry-farming cultivation on the initial morphology of the Zakranlu fan surface (darker part of the surface).

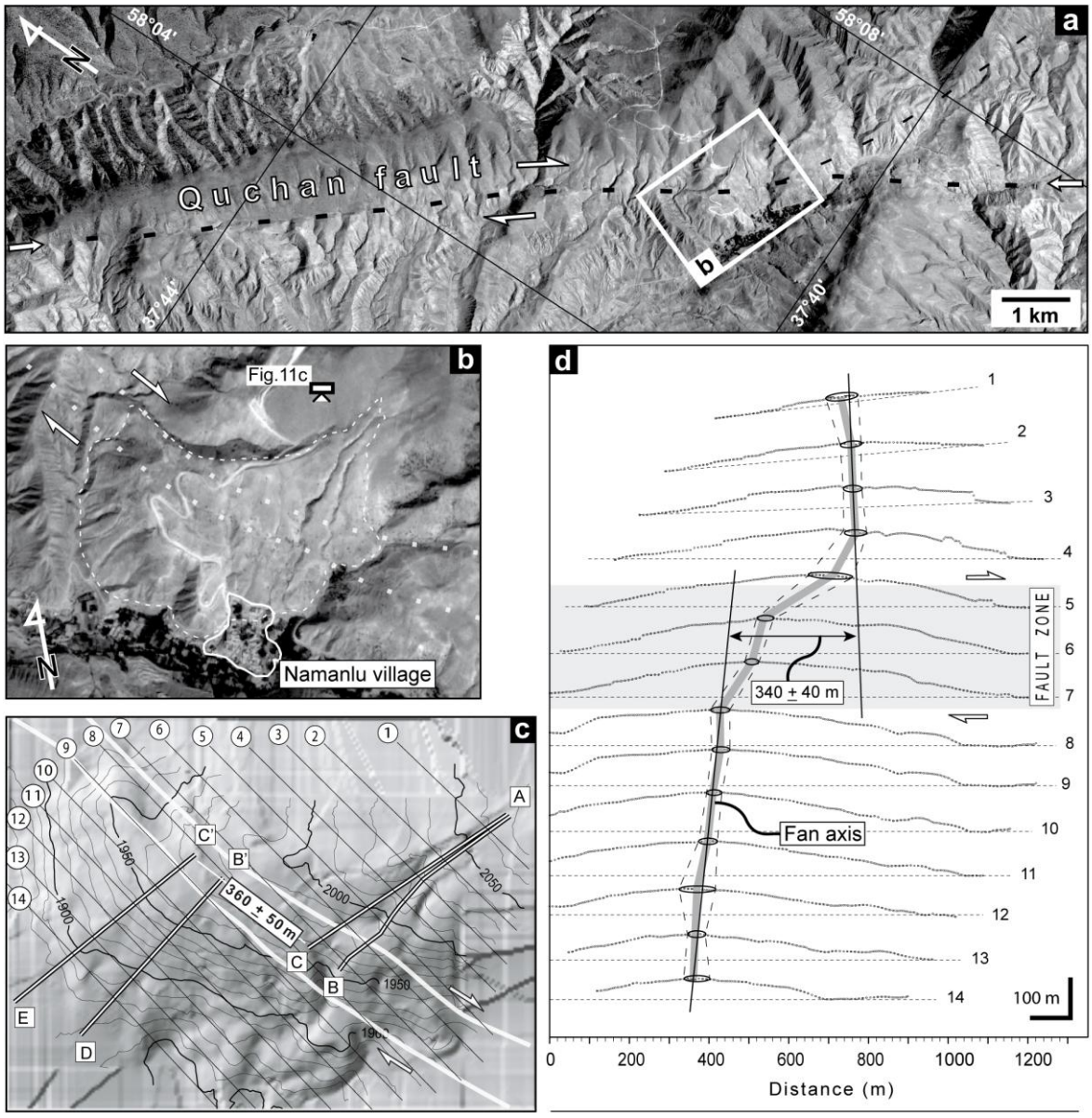


Figure 7. (a) And (b) SPOT5 image of the Namanlu alluvial fan at two different scales. The Namanlu fan has been deformed along the Quchan Fault (dotted lines in Fig. 7b). (c) Differential GPS-derived DEM of the fan (constituted by 85663 x, y, z points). Numbered lines indicate transverse topographic profiles used to reconstruct the initial shape of the fan axis. Double lines are the location of longitudinal profiles plotted in Fig. 8b, respecting the restored offset value of 360±50 m. (d) Accurate position of the Namanlu fan axis, reconstructed analyzing fourteen topographic profiles across the fan. The reconstruction of initial fan axis indicates a cumulative right-lateral offset of 340±40 m along the Quchan Fault.

### 4.2.1. Cumulative offset recorded by the Namanlu fan

The Namanlu fan border is strongly incised by drainages, and several landslides distributed around the edge of the fan have modified its initial shape (Figs 7 and 8). Within this context, the present-day fan shape does not permit to accurately measure the actual fault offset. To measure the cumulative horizontal offset recorded by the Namanlu fan, we used two different methods. The first method consists of aligning the deformed axial trace of the

fan on both sides of the fault to reconstruct the initial fan axis. The second method compares different centers of concentric topographic contour lines on the fan surface in order to locate the initial apex point. To apply the first method, several transverse topographic profiles were used to reconstruct the initial shape of the fan axis (Fig. 7). Along such profiles, the fan surface envelope forms an upward, convex curve where its highest part corresponds to the fan axis. However, in regions of active tectonics, this classic shape can be tilted or deformed due to both vertical and horizontal displacements. In such cases, regardless symmetry of the profiles, areas of maximum amplitude (in comparison with the initial base) represent the axis area (Fig. 7). Plotting on the fan surface the identified axial areas, results in illustrating the cumulative deformation of the fan axis, caused by lateral fault motions. On the Namanlu fan, thanks to the high-resolution topographic survey, fourteen topographic profiles, with horizontal intervals of about 80 m, were analyzed across the fan to determine the exact position of the fan axis (Fig. 7). The reconstruction of initial fan axis represents a cumulative right-lateral offset of 340±40 m along the Quchan Fault. The uncertainty accounts for the average length of the planar part of the fan axis area along each topographic profile.

To apply the second method, one can also make the assumption that topographic contour lines are concentric arcs having their curvature centers located at the fan apex. Fitting alluvial fan contours with circular arcs; one can thus reconstruct the fan radii and thus determine the location of the fan apex at the time of deposition (*e.g.*, *Keller et al*., 2000 and references herein). Due to this geometry, lateral offsets appear as different centers which are aligned parallel to the fault, while, tilting or vertical offsets can be identified as different centers shifted across the fault, respecting angle of tilting and fault dip. Using this method, the fan toe contours project back to a different centre than that of present-day fan head contours (Fig. 8), which is considered as representative of the horizontal displacement accumulated by the Namanlu fan. This fan shape reconstruction yields to a right-lateral offset of 380±20 m for the toe with respect to the apex of the Namanlu fan (Fig. 8). Both approaches yield similar values that permit to calculate a mean cumulative right-lateral offset of 360±50 m on the Quchan Fault.

As mentioned above, observed offsets along the Quchan Fault are mainly horizontal. However, a minor vertical component offset has been observed along the fault. Cumulative vertical offsets coeval with horizontal offsets are usually more complicated to estimate using displaced geomorphic markers. For obliquely offset alluvial fans (due to oblique-slip fault motions), it is necessary to restore the cumulative lateral offset of the fan before making longitudinal profiles on the fan surface. Vertical offset of the fan is then represented by the

difference in elevation between two corresponding surfaces on both sides of the fault. To do so, we used the previously described horizontal offset of the Namanlu alluvial fan to reconstruct the initial fan shape, and then, we produced two longitudinal profiles along and parallel to the actual fan axis, revealing a 48±2 m-high, NE-facing vertical offset (Fig. 8).

In summary, the Namanlu alluvial fan has been displaced right-laterally by 360±50 m and vertically by 48±2 m, *i.e.*, the horizontal component is ~7 times higher than the vertical one. This ratio of estimated horizontal and vertical displacements implies a rake (slip-vector) value of 8±1°SE on a vertical fault plane.

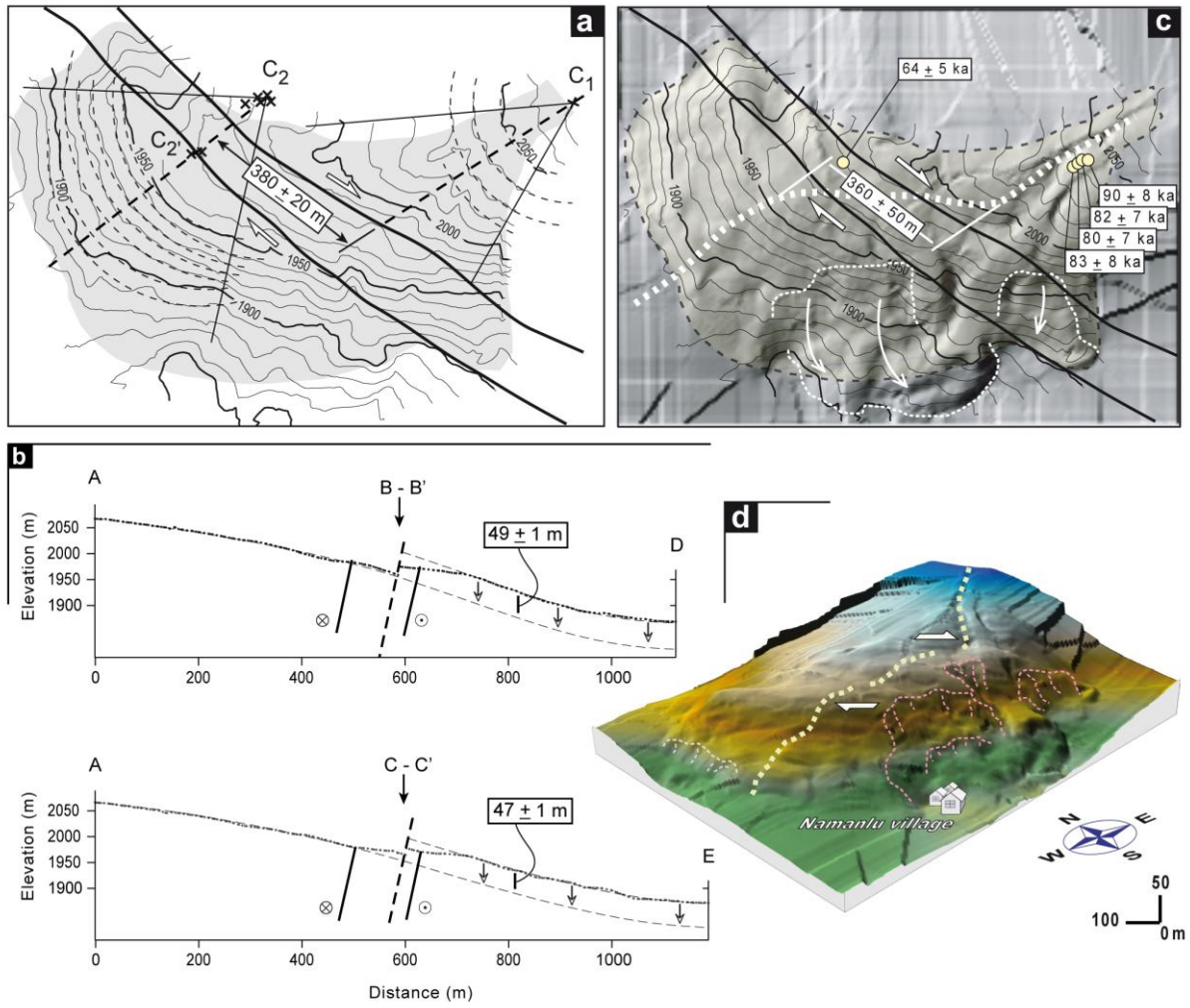


Figure 8. (a) Geometric analysis of the Namanlu fan using the concentric-contour lines method (*Keller et al.*, 2000) indicates a right-lateral offset of 380±20 m along the Quchan Fault. (b) Topographic profiles along the fan axis exhibiting a vertical offset of 48±2 m on the Namanlu fan surface. (c) Superimposed DGPS-derived topographic and shaded relief maps of the fan indicating general morphology of the fan, reconstructed fan axis (thick, white dashed line), and landslides (thin, white dashed line) distributed around the edge of the fan. Sampling location and associated *in situ*-produced $^{36}Cl$ ages are shown in this figure. (d) 3D-view of the Namanlu fan.

### 4.3. Morpho-tectonic investigations along the Baghan Fault

Along the Baghan Fault, the most common geomorphic feature offsets are provided by drainage systems such as river beds and terraces which are clearly displaced by the fault. A set of spectacular geomorphologic features can be observed in the Honameh region (Fig. 9), between the deserted village of Zakranlu and Baghan village along the southern half of the fault trace, where several alluvial fan systems and the major Karganeh River have been involved in the Quaternary history of the Baghan Fault.

In the Honameh region (Fig. 9), a sharp contrast between the piedmont and the mountain range developed due to large right-lateral offsets along the Baghan Fault. This west-facing, 600 m-high strike-slip fault scarp is incised by a transverse drainage system running to the west (Fig. 9). These drainages are displaced or beheaded by the Baghan Fault, showing systematic lateral offset ranging from about 4 m, for the recent gullies, to 10 km for the main drainages.

Reconstructions of Mid-to Late-Pleistocene alluvial fans developed in the outlet of drainages offset by the Baghan Fault can be use to restore dextral offset along this fault. Analyses of SPOT5 images combined with direct field observations allow identifying at least three main abandoned alluvial fan surfaces overlaying older Early Quaternary fanglomerates sourced from the main river (Fig. 9). The Q3 unit corresponds to alluvial fan surfaces which are essentially more incised, but not more elevated than the two other surface generations. The Q2 unit is an intermediate fan generation which is inset in/or partially covers the Q3 unit, and exhibits preserved fan shapes. The Q1 unit corresponds to the youngest, abandoned alluvial fan surfaces, that can be observed at the toe of the two other fan generations or covering the Q3 unit south and north of the Karganeh River, respectively. Between these three alluvial fan units, the intermediate and oldest ones are right-laterally offset several hundred meters (roughly 550 and 950 m, respectively) from their feeding drainage basin situated in the other side of the Baghan Fault. They are now completely disconnected from the basins (Fig. 9). We focused our study on the Q3 fan surfaces which are associated with a cumulative horizontal offset of up to 1 km along the Baghan Fault (Fig. 11).

South of the Karganeh River, there are at least six Q3 alluvial fan systems. Four of them have been separated from their corresponding drainage basins by right-lateral motions along the Baghan Fault. North of the Karganeh River, the Zakranlu fan is the only one belonging to the Q3 unit that is offset by the Baghan Fault (Figs 9 and 10). This characteristic avoids misinterpretation of the fault offset that may arise from uncertainty in geomorphic correlation

of the fan bodies and their possible associated basins. In addition, the Zakranlu alluvial fan represents the largest and best preserved Q3 fan having approximately held its initial geometric form (Figs 9 and 10). Consequently, it is well-suited for constraining a cumulative, post Q3 abandonment, right-lateral offset along the Baghan Fault.

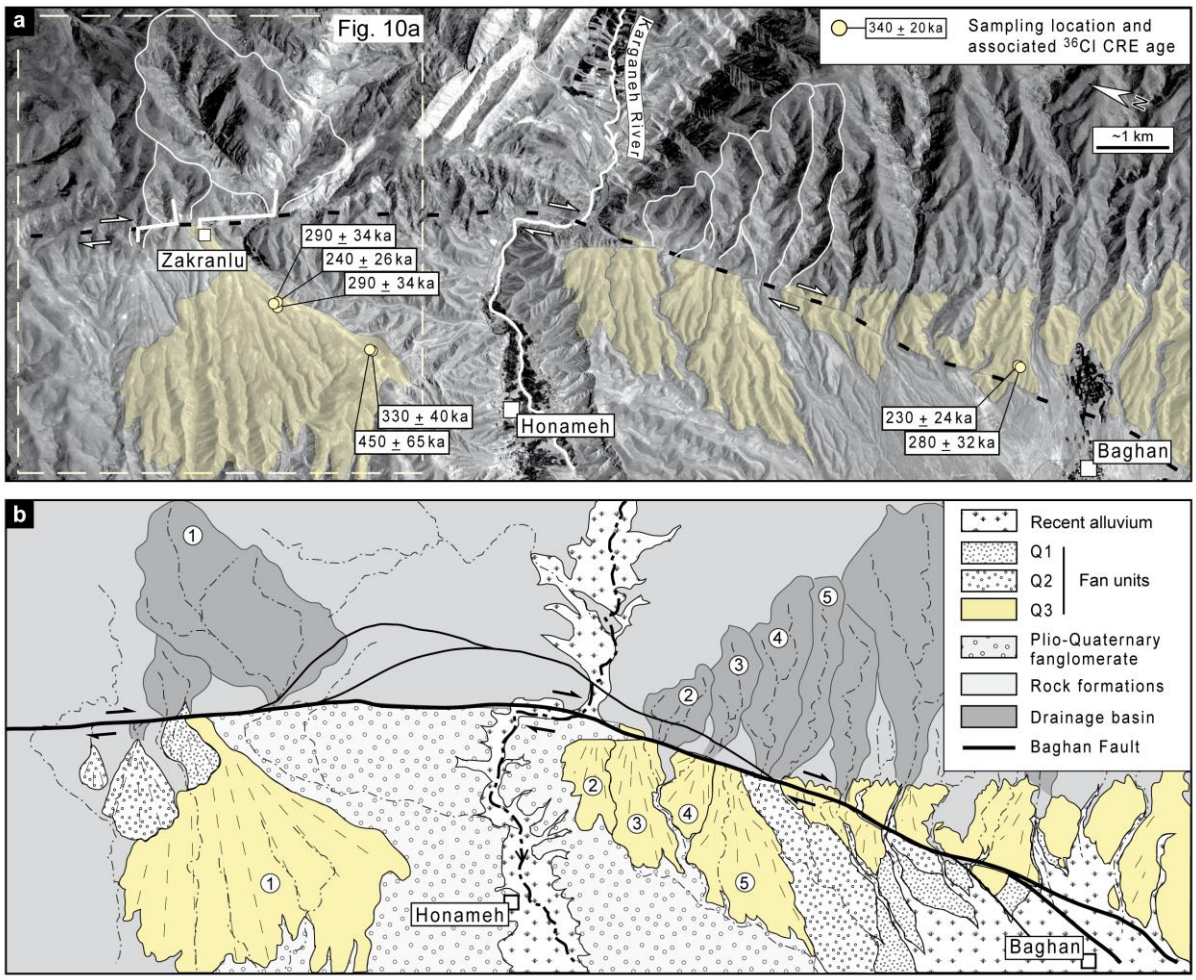


Figure 9. (a) SPOT5 image of the Honameh region including the Zakranlu alluvial fan (within dashed rectangle), Karganeh River and other geomorphic features offset along the Baghan Fault. Sharp mountain front in this region is due to cumulative right-lateral offsets along the Baghan Fault. (b) Morphotectonic map of the Honameh region based on SPOT5 image (above) and field observations. At least three abandoned alluvial fan surfaces have been offset along the Baghan Fault. Five fans (marked by numbers in circle) belonging to the Q3 unit are presently disconnected from their original feeding basins.

### 4.3.1. Offset of the Zakranlu alluvial fan

Fig. 9 presents a morphotectonic map of the Honameh region based on SPOT5 satellite image and field observations. To measure the cumulative offset recorded by the Zakranlu alluvial fan, its eroded apex must be reconstructed. To do so, two different methods were applied: a geomorphic method, in which the former fan shape can be reconstructed using the remaining fan shape and its convergence slope-lines (Fig. 10); and the concentric topographic

contour method described in section 4.2.1. To complete the geomorphic method, we assumed that the three different fan generations, observed in the Zakranlu area, were developed in the same physical conditions such as piedmont slope, tectonic regime and fault mechanism. It is noteworthy that whatever the age and the size, all these fans have a similar geometric shape, denoting a common factor controlling their evolution (Figs 9 and 10). This assumption allows considering that the observed shape is a characteristic of the alluvial fans in the studied region, regardless of size and age. This leads to reconstruct the initial form of the Zakranlu fan indicating that the apex is right-laterally offset by 930±50 m with respect to its former associated basin outlet along the Baghan Fault (Figs 10 and 11).

Applying the analysis of concentric topographic contours, we obtained an offset value of 960±90 m that is close to the value derived from the geomorphic method but with a larger uncertainty. In fact, larger uncertainty in the geometric method is due to the sum of technical resolution of SRTM elevation data and geometric uncertainty in the location of the fan axis. However, the consistency between the results suggests reliability of the offset value regardless of the methods. Considering the two determined values, a mean cumulative right-lateral offset value of 940±100 m can be calculated for the Baghan Fault since emplacement and abandonment of the Zakranlu alluvial fan.

### 4.3.2. Consistency of contemporaneity of Q3 fan surface offsets

To verify the reliability of the Zakranlu offset, we examined spatial consistency of the observed fault offsets affecting Q3 surfaces in the Honameh region (Fig. 10). Applying all along the fault trace the horizontal offset of 940±100 m measured for the Zakranlu fan, allows a convincing restoration of the simultaneous Late Quaternary landforms such as the Karganeh River (Fig. 10). To allow this reconstruction, we assumed the same age for both the Karganeh valley in this part of its length, main drainages and all of the four displaced Q3 alluvial fans located south of the Karganeh River. In addition, random and irregular distances between the fan apexes or the basin outlets imply few possibilities to reconstruct the initial arrangement of the fan systems (Figs 9 and 10).

Another way to verify the consistency of the measured cumulative lateral offset along the Baghan Fault is to restore separately lateral offset of each individual geomorphic element, using two topographic profiles parallel to the fault trace (Fig. 10d). The profiles were chosen to be as close as possible to the fault trace, to decrease uncertainties caused by the cosine effect of non-perpendicular objects with respect to the fault trace. Among the main geomorphic landforms (Fig. 10c), 6 elements out of 10 are aligned after 1050±90 m of lateral

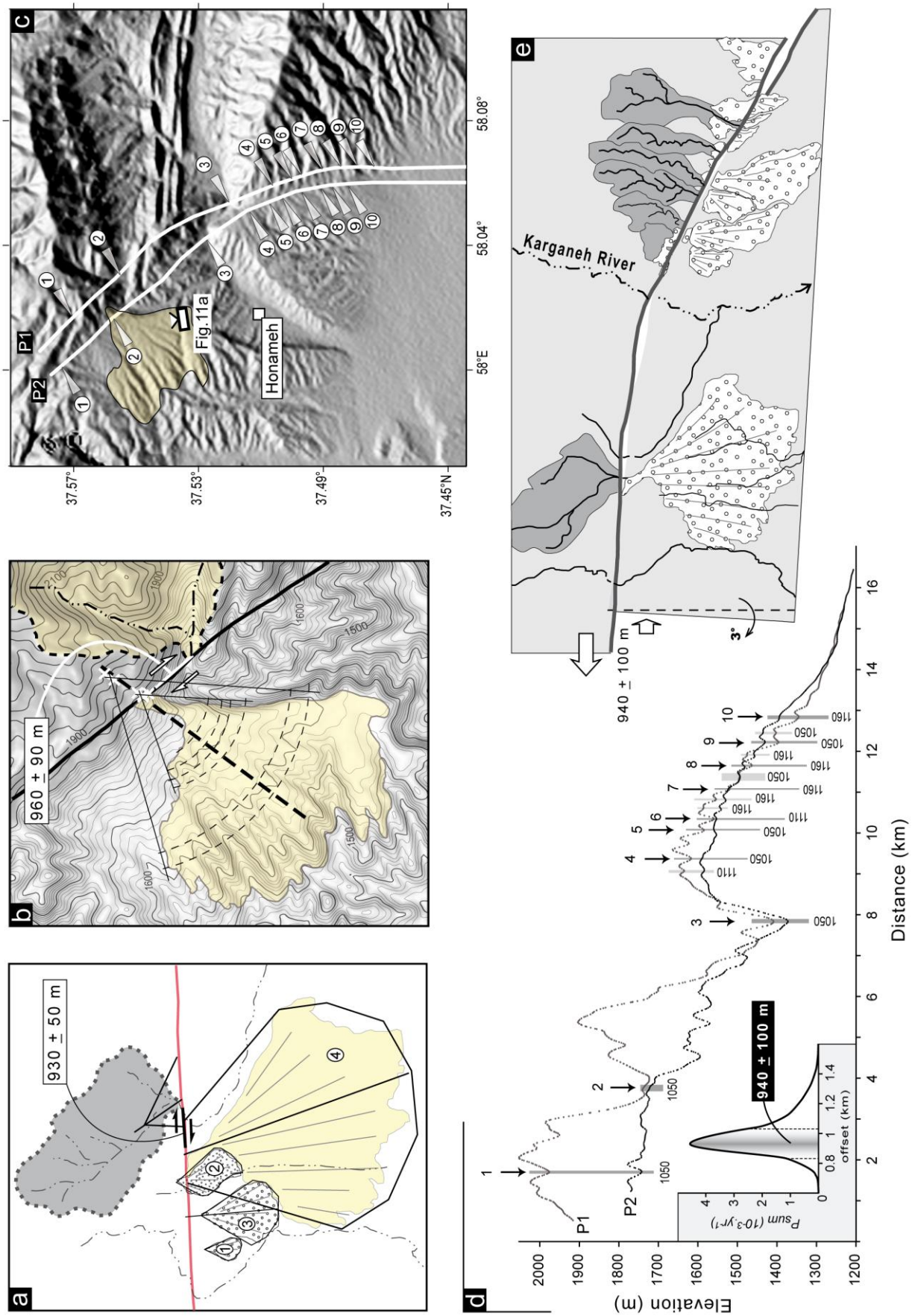
a
930 ± 50 m
b
960 ± 90 m
c
P1
P2
Fig.11a
Honameh
37.57°
37.53°
37.49°
37.45°N
58°E
58.04°
58.08°
e
Karganeh River
940 ± 100 m
3°
d
Elevation (m)
Distance (km)
P1
P2
940 ± 100 m
offset (km)
Psum (10-3.yr-1)

back-slip along the Baghan Fault. Comparing the obtained values from both geomorphic and topographic methods indicates a good consistency of the right-lateral offset value of 940±100 m, representative of the Baghan Fault cumulative offset since the emplacement of Q3.

### 4.4. Dating of the studied offset alluvial fans

On the Namanlu fan surface, six boulders were analyzed, among which one of them was not dated at the final state (AMS measurement). These carbonate boulders embedded in the fan surface were collected from the most preserved parts of the alluvial fan surface (Figs 8 and 11). Four samples out of six were collected from the proximal part and the two others from the middle part of the fan, between two fault strands (Fig. 8). Within collected boulders, measured *in situ*-produced cosmogenic $^{36}$Cl concentrations allow calculating minimum boulder exposure ages ranging between 64±6 and 90±8 kyr (Table 1, Fig. 8). For the Namanlu surface samples, the sum of the Gaussian age probability distributions ($P_{sum}$) shows a relatively sharp-peaked distribution (Fig. 12), which corresponds to a small value of $\sigma$ (*e.g.*, *Taylor,* 1997). The minimum exposure age of the sample from the surface between the two fault strands (NAM-9) is only slightly smaller than the weighted-mean age of the boulders. This difference is indicated as a slight step-like peak in the left part of the curve (Fig. 12). Since the Namanlu fan is completely isolated and there is no evidence of successive depositions onto the fan surface, the younger exposure age of NAM-9, with respect to the principal age peak, can be interpreted as an outlier resulting from post-abandonment exhumation of the boulder within the fault zone. When considered all together (but NAM-9), the surface samples collected on the Namanlu fan surface yield a weighted-mean $^{36}$Cl minimum exposure age of 83±4 kyr (Table 1, Fig. 12). This weighted-mean $^{36}$Cl minimum

Figure 10. Applied methods to quantify cumulative offset of the Zakranlu fan: (a) Assuming that the three different fan generations in the Zakranlu fan area were developed in the same physical conditions; the initial shape of the fan was reconstructed. (b) Determining the displaced fan apex using the geometric method. (c) Shaded relief map of the Honameh region based on SRTM digital topographic data. White lines are the paths of two topographic profiles parallel to the Baghan Fault, plotted in Fig. 10d. Corresponding geomorphic features beside the fault trace are marked by numbers. (d) Reconstruction of morphotectonic features along the Baghan Fault. Numbered arrows correspond to the feature numbers in Fig. 10c. Corresponding offset value for each individually reconstructed feature is expressed in meters below the curves. Inset indicates the Normal probability sum of the cumulative offsets representing a constrained offset value of 940±100 m. (e) Preferred reconstruction of Q3 surfaces and other contemporaneous offset features restoring the offset value of 940±100 m.

exposure age is calculated assuming that there has been no significant erosion acting on the fan surface since its abandonment.

In the Honameh region, we dated a total of 7 samples of carbonate boulders embedded in a series of displaced Q3 fan surfaces (Fig. 9). Among those samples, five were collected from two well-preserved parts of the Zakranlu alluvial fan surface (Fig. 6). The analyzed samples from the Zakranlu fan yield minimum exposure ages ranging from 288±34 to 448±65 kyr. Among the sampled boulders, 6 among 7 yielded minimum exposure ages ranging from 288±34 to 326±40 kyr. One sample is significantly older (448±65 kyr). To interpret this age distribution, one can consider that the oldest sample is an outlier, indicating a previous exposure episode in the source area (inheritance). If it is so, the weighted-mean minimum $^{36}$Cl exposure age of 280±16 kyr is the closest evaluation of the actual abandonment age. On the other hand, since erosional processes acting on the fan surface may be responsible for exhumation of the boulders from deeper positions within the alluvial material, the oldest age (448±65 kyr) may be the closest to the actual age of abandonment, which is the more conservative estimation that can be done considering the dataset.

We already discussed about the regional reliability of the offset recorded by the Zakranlu alluvial fan, examining spatial consistency of the observed fault offsets recorded by other Q3 fans. To verify temporal consistency of these offsets, two other samples were collected from another Q3 fan surface approximately 9 km in the south of the Zakranlu fan (Fig. 9). Those yield minimum $^{36}$Cl exposure ages of 232±24 and 283±32 kyr, strengthening our confidence for an isochronous abandonment age for the regional Q3 surface (Fig. 9).

In the lack of direct erosional features (*i.e.*, even young gullies and/or differential erosion) on the sampled parts of the fan surfaces (section 4.1.2), sensitivity of the surface exposure ages to erosion can be distinguished from the boulder age distribution patterns. In other words, soil erosion (whatever the involved mechanism) produces a distribution of apparent ages between the actual surface age and some younger age limit. The width of the distribution being proportional to the surface age and the actual age, being close to the maximum of the distribution (*Phillips et al.,* 1997; *Wells et al.,* 1995; *Zreda et al.,* 1994).

Considering this suggestion as a guide in interpreting the age distributions observed on the offset fan surfaces, the relatively well-clustered exposure age distributions of both the Namanlu and Zakranlu boulders imply small erosion depths on the fan surfaces. In such a case, the weighted-mean boulder exposure ages of 83±4 kyr and 280±16 kyr can be interpreted as the best estimate (±10% - *Bierman*, 1994) of the true abandonment age for the

Namanlu and Zakranlu alluvial fan surfaces, respectively. However, the accuracy of the calculated ages depends on future improvement of $^{36}$Cl production rates calibration.

### 4.5. Long-term slip rates along the BQFS

In this study, slip rate evaluations are based on three main assumptions: 1) there has been no erosion of the sampled surfaces since their abandonment, 2) the fault slip rates remained constant since formation of the offset Quaternary markers, and 3) the main traces of the Baghan and Quchan faults are assumed to have accumulated all of the horizontal strain at studied sites. Accepting these assumptions, the accuracy of our slip rates relies on the geomorphic relevance, and analytical accuracy of the obtained minimum $^{36}$Cl exposure ages respect to the cumulative fault offsets.

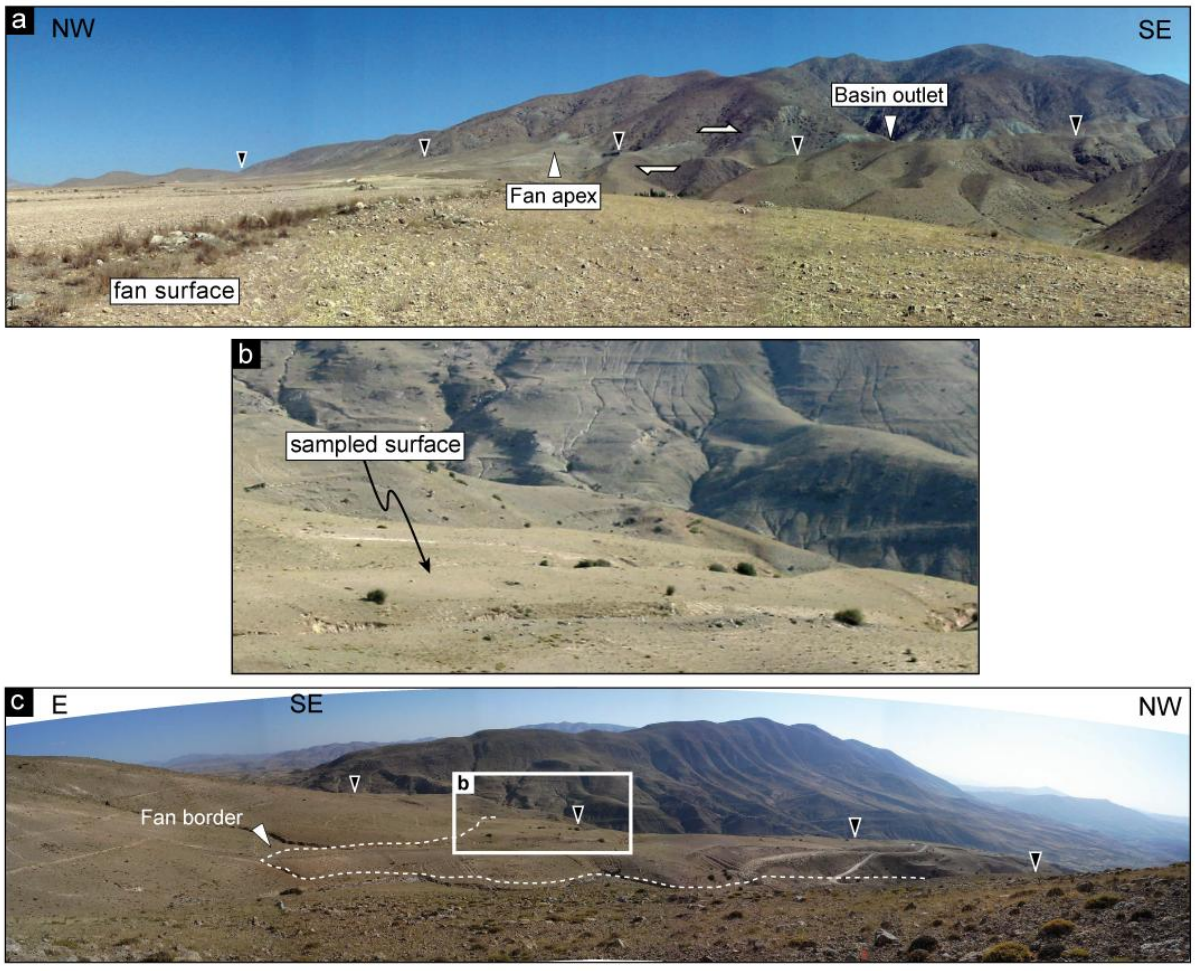


Figure 11. (a) Panoramic view of the Zakranlu fan and its catchment basin, taken from a distance of ~2 km, the photography location was marked on Fig. 10c. (b) The most preserved part of the Namanlu fan surface selected to be sampled; the frame of this view was marked on Fig. 11c, (c) Panoramic view of the proximal part of the Namanlu fan surface, taken from a distance of ~1 km marked on Fig. 7b. Its distal part is hidden behind the Baghan fault scarp. Black triangles on (a) and (c) indicate the trace of the Baghan and Quchan faults, respectively.

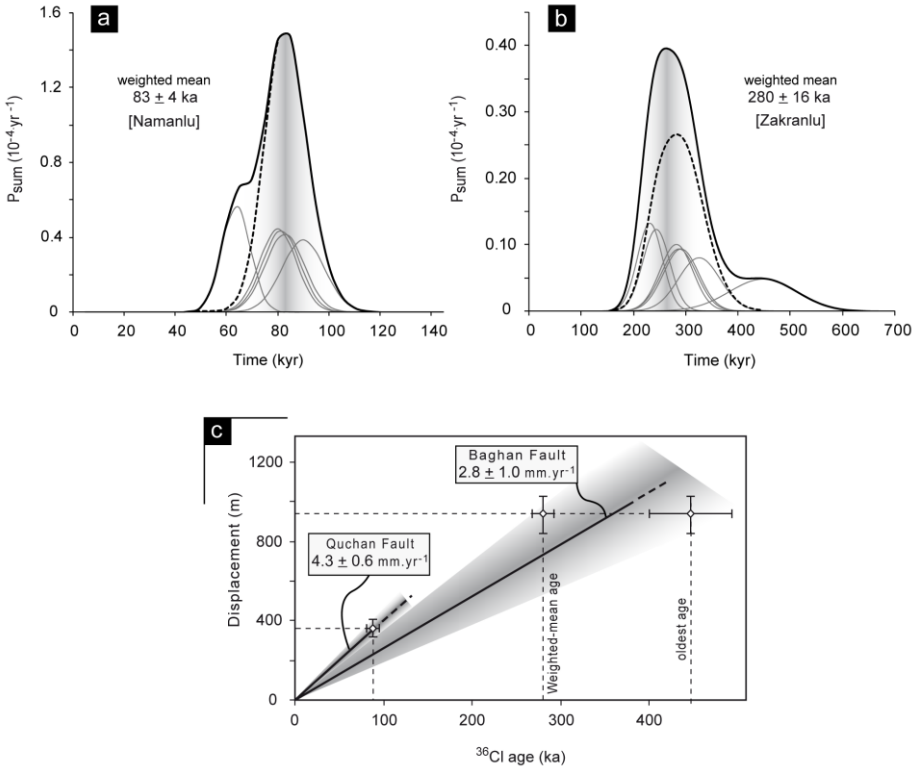


Figure 12. *In situ*-produced $^{36}$Cl exposure ages of samples collected on the Namanlu (a), and Zakranlu (b) fan surfaces. Black curves are age probability sum, and gray curves represent the age probability for each individual sample. The age probability sum without outlier sample ages is presented by dotted-curves. (c) Calculated slip rates along the Quchan and Baghan faults during late Quaternary.

At the Namanlu fan, the Quchan Fault runs through the fan body, and there is no evidence of post-offset deposition on any parts of the fan surface. In this case, we may conclude that the Namanlu fan surface was abandoned at minimum 83±4 kyr and subsequently offset by 360±50 m, yielding a maximum long-term slip rate of 4.3±0.6 mm/yr for the Quchan Fault (Fig. 12).

The Zakranlu alluvial fan has been separated from its feeding watershed due to a right-lateral cumulative displacement of 940±100 m along the Baghan Fault. Since the age of abandonment of the Zakranlu surface is comprised between the weighted-mean minimum $^{36}$Cl exposure age of 280±16 kyr and minimum exposure age of 448±65 kyr (the oldest sample in the dataset), yields a Late Quaternary slip rate of 2.8±1.0 mm/yr for the Baghan Fault (Fig. 12).

## 5. Discussion and conclusion

Combining high resolution satellite images, SRTM digital topographic data and field observations, the entire fault system of Central-East Kopeh Dagh was mapped in detail (Fig. 2). Thus, we determined a precise 2D-geometry of the fault system and its individual

fault segments. Analyzing cumulative post-folding geological offsets (ranging from 100 m to 18 km in 337 different sites) on the different fault segments, we examined the gradient changes in the distribution of strike-slip deformation over the Central-East Kopeh Dagh (Fig. 3). Regardless of possible continuous deformation (see section 5.2), a large portion (30±2 km) of the total deformation (35-40 km) is accommodated on a localized fault system (BQFS) dissecting the Central Kopeh Dagh (Fig. 3). Within this regional fault system, the Quchan and Baghan faults are the most important ones, exhibiting maximum cumulative displacements of 15.5±0.5 and 9.8±0.2 km, respectively (Fig. 5). The rest of this strike-slip deformation is taken up by the other strike-slip faults spread within this part of the Kopeh Dagh (Fig. 3).

Table 1. Sample characteristics and exposure ages

| Sample | Latitude (°N) | Altitude (m) | Thickness (cm) | Ca/(g rock) (%) | Chlorine (ppm) | $^{36}$Cl [atoms (g rock)$^{-1}$] | $^{36}$Cl production rate [atoms (g rock)$^{-1}$ yr$^{-1}$] | Age (kyr) |
|---|---|---|---|---|---|---|---|---|
| BAG16 | 37,47 | 1337 | 5 | 33,6 | 159,8 | 12445351±150058 | 59,9 | 283±32 |
| BAG17 | 37,47 | 1337 | 3 | 32,6 | 164,4 | 11783860±269762 | 65,5 | 232±24 |
| NAM1 | 37,68 | 2084 | 5 | 36,2 | 86,8 | 6721881±110768 | 88,9 | 83±8 |
| NAM2 | 37,68 | 2084 | 3 | 35,4 | 122,3 | 7110103±95266 | 87,2 | 90±8 |
| NAM3 | 37,68 | 2083 | 5 | 33,8 | 161,3 | 7114060±148307 | 95,4 | 82±7 |
| NAM4 | 37,68 | 2080 | 7 | 36,3 | 121,9 | 6789294±103179 | 92,5 | 80±7 |
| NAM9 | 37,68 | 1989 | 12 | 34,1 | 70,6 | 4667172±69984 | 78,4 | 64±6 |
| ZAK17 | 37,54 | 1600 | 7 | 34,8 | 81,3 | 14601738±175272 | 63,6 | 326±40 |
| ZAK18 | 37,54 | 1601 | 2 | 34,8 | 88,7 | 17819540±198713 | 63,7 | 448±65 |
| ZAK19 | 37,55 | 1659 | 6 | 34,9 | 62,3 | 14262743±158884 | 67,1 | 292±34 |
| ZAK20 | 37,55 | 1659 | 7 | 34,8 | 105,4 | 13837007±221580 | 74,1 | 244±26 |
| ZAK22 | 37,55 | 1658 | 11 | 35,6 | 63,7 | 13405045±153424 | 63,7 | 288±34 |

Elemental composition (%)

| | Water | Al2O3 | CaO | Fe2O3 | K2O | MgO | MnO | Na2O | P2O5 | SiO2 | TiO2 | Th | U |
|---|---|---|---|---|---|---|---|---|---|---|---|---|---|
| BAG16 | 0,12 | 0,90 | 52,89 | 0,25 | 0,05 | 0,76 | 0,02 | 0,01 | 0,04 | 1,52 | 0,03 | <3 | <2 |
| BAG17 | 0,00 | 1,38 | 52,54 | 0,37 | 0,09 | 1,02 | 0,02 | 0,00 | 0,03 | 1,89 | 0,04 | <3 | <2 |
| NAM1 | 0,08 | 1,01 | 54,01 | 0,13 | 0,02 | 0,58 | 0,00 | 0,01 | 0,01 | 1,82 | 0,03 | <3 | <2 |
| NAM2 | 0,16 | 1,08 | 53,30 | 0,22 | 0,04 | 0,55 | 0,00 | 0,01 | 0,02 | 2,34 | 0,04 | <3 | <2 |
| NAM3 | 0,08 | 1,08 | 55,75 | 0,14 | 0,03 | 0,63 | 0,01 | 0,01 | 0,02 | 2,42 | 0,03 | <3 | <2 |
| NAM4 | 0,12 | 1,11 | 53,89 | 0,18 | 0,04 | 0,68 | 0,00 | 0,01 | 0,03 | 2,45 | 0,04 | <3 | <2 |
| NAM9 | 0,04 | 1,25 | 55,01 | 0,14 | 0,07 | 0,69 | 0,01 | 0,03 | 0,01 | 2,29 | 0,04 | <3 | <2 |
| ZAK17 | 0,08 | 0,96 | 55,80 | 0,18 | 0,05 | 0,72 | 0,00 | 0,01 | 0,00 | 1,62 | 0,03 | <3 | <2 |
| ZAK18 | 0,08 | 1,17 | 53,72 | 0,25 | 0,04 | 0,77 | 0,01 | 0,00 | 0,01 | 1,64 | 0,04 | <3 | <2 |
| ZAK19 | 0,00 | 1,04 | 55,12 | 0,21 | 0,05 | 0,84 | 0,01 | 0,00 | 0,02 | 1,28 | 0,04 | <3 | <2 |
| ZAK20 | 0,00 | 1,02 | 54,66 | 0,25 | 0,04 | 1,00 | 0,01 | 0,04 | 0,01 | 2,51 | 0,03 | <3 | <2 |
| ZAK22 | 0,12 | 0,95 | 55,36 | 0,26 | 0,02 | 0,60 | 0,01 | 0,00 | 0,00 | 0,79 | 0,03 | <3 | <2 |

*In situ*-produced $^{36}$Cl concentrations and CRE ages of samples from the two alluvial fans, offset by the Baghan and Quchan faults. Measurements of $^{36}$Cl concentrations were undertaken at the Livermore National Laboratory's CAMS. The production rates are those of *Stone et al.* (1998), corrected for elevation and latitude using the correction factors from *Stone* (2000). Assuming no inheritance and no erosion, $^{36}$Cl cosmogenic concentrations are interpreted to give a minimum surface exposure age.

Combined quantitative geomorphic and geometric analysis, as well as *in situ*-produced cosmogenic $^{36}Cl$ dating of two regionally distinct alluvial fan surfaces yield the first direct and well-constrained geological estimate of the Late Quaternary slip rates on the Quchan and Baghan faults, bearing the caveat in mind that the slip rates we discuss herein are maximum. The oldest geomorphologically-preserved alluvial fan shows a cumulative offset of 940±100 m postdating its abandonment (between 280±16 kyr and 450±65 kyr), yielding a maximum slip rate of 2.8±1.0 mm/yr for the Baghan Fault. The younger alluvial fan shows a cumulative offset of 360±50 m postdating its abandonment at minimum 83±4 kyr, yielding a maximum slip rate of 4.3±0.6 mm/yr for the Quchan Fault.

### 5.1. Initiation of the strike-slip motions in the Kopeh Dagh

Applying the calculated Late Quaternary slip rates to maximum post-folding cumulative geological offsets along the Baghan and Quchan faults, and assuming that the slip rates have been constant during the life of the fault; one can estimate onset of strike-slip motion on those faults. For the Quchan Fault, considering a maximum cumulative offset of 15.5±0.5 km (Fig. 5) and a maximum-possible slip-rate of 4.3±0.6 mm/yr yields a maximum inception age of 3.6±0.6 Ma for the initiation of strike-slip motion. In the same way, the results obtained for the Baghan Fault yield a maximum inception age of 3.5±1.3 Ma. It is worth noting that the slip rates have been determined independently for both faults (using deformed geomorphic markers of different ages), which strengthen the confidence one can have about the reliability of the proposed date for the beginning of the strike-slip motion along the Baghan and Quchan faults.

From the local geomorphic point of view, our detailed mapping provides evidences that both Plio- fold axes and Quaternary alluvial plains are offset about the same amount of right-lateral cumulative displacements along the Baghan and Quchan faults (Fig. 5). This strongly supports the idea that the strike-slip motion should be started no earlier than the Pliocene. From the regional plate kinematics perspective, our estimated age for inception of strike-slip motions on both faults is in good agreement with (1) the stratigraphic-derived value of 4 Ma for the beginning of strike-slip faulting in the Kopeh Dagh (*Afshar Harb*, 1979), (2) the timing of widespread reorganization of tectonic deformation in the Middle East at roughly 5 Ma (*Axen et al.*, 2001; *Hempton*, 1987; *Westaway*, 1994), which is emphasized by the present-day distribution of active faulting within the Arabia-Eurasia collision margin at 3-5 Ma (*Allen et al.*, 2004; *Authemayou et al.*, 2006; *Bozkurt*, 2001; *Copley and Jackson*, 2006; *Koçyigit et al.*, 2001; *Regard et al.*, 2004; *Talebian and Jackson*, 2002; *Walker and Jackson*,

2004), and a possible change in the rotation of the plates bordering the Dead Sea fault in the early to late Pliocene (*Livnat et al.*, 1987; *Ron et al.*, 1984).

The time and duration of tectonic reorganization in the Arabia-Eurasia collision zone are suggested to be diachronous (*i.e.*, *Allen et al.*, 2004), but the apparent age differences might also arise either from age uncertainties due to the lack of direct dating of corresponding tectonic events, or because of confusing and ambiguous cause-and–effect relationships between the events, *i.e.*, the relationships between the South Caspian Basin subsidence/subduction and rapid exhumation of the west-central Alborz (see *Allen et al.*, 2002; *Allen et al.*, 2004; *Axen et al.*, 2001; *Devlin et al.*, 1999; *Jackson et al.*, 2002). In the present study, different geomorphic and geological arguments accompanied with *in situ*-produced cosmogenic $^{36}$Cl dating allow us to constrain the age of this tectonic reorganization in the Central Eastern Kopeh Dagh at ~4°Ma.

### 5.2. Integrating our data-derived results within preexisting models

The main results of our study are (1) the well-constrained Late Quaternary slip rates on the Quchan and Baghan faults, and (2) the initiation of strike-slip motion along these faults that can be considered as the time of a major tectonic reorganization in the Central Eastern Kopeh Dagh. The minimum bound of our slip rate bracketing is close to the revised average geological slip rate of ~6 mm/yr estimated for the Quchan and Baghan faults (*Afshar Harb*, 1979), assuming that the post-folding total displacement along these faults (~25 km, *Afshar Harb et al.*, 1987) occurred over the last 4 Ma. Conversely, our results are not in agreement with the model-derived estimate of *Hollingsworth et al*. (2006) that proposes the respective slip rates of ~1.5 and ~1 mm/yr for the Quchan and Baghan faults during the last 10 Ma.

To calculate these slip rates, *Hollingsworth et al*. (2006) assumed that the maximum offsets achieved in 10 Ma, a time span calculated dividing 70 km of total deformation (10 km for N–S shortening before the onset of strike-slip faulting plus 60 km for post-folding N–S motion) by the present-day GPS-derived rate of 7 mm/yr for northward motion of Central Iran with respect to Eurasia. Accepting the proposed value of 10 Ma for the initiation of strike-slip faulting (*Hollingsworth et al.*, 2006), it comes into conflict with its pre-strike-slip nature, *i.e.*, 10 km of N–S shortening before the onset of strike-slip faulting. Therefore, this overestimated age for the initiation of strike-slip faulting (10 Ma) yields at best underestimated fault slip rates.

The model proposed by *Hollingsworth et al*. (2006) is based on anticlockwise rigid block rotation around a vertical axis, allowing across-strike shortening and along-strike elongation in the Kopeh Dagh Mountains. However, the application of this model need (1) that all the involved faults, which define lateral limits of the rotating blocks (*i.e.*, the Baghan, Quchan, and Dorbadam faults), should be cutting across the deforming zone, (2) that blocks with the same width should represent the same rotation angle, and consequently the same apparent strike-slip displacement, and (3) that the displacement gradient has to be constant along length of the faults regardless the distance from fault terminations. To the contrary, the data set, provided in this study, indicates that the strike-slip brittle deformation is heterogeneously distributed on several fault segments within the Central-Eastern Kopeh Dagh (Fig. 3), and not homogenously localized on three faults cutting across the range, which strongly favors a simple strike-slip faulting mechanism that moves the western Kopeh Dagh northwards relative to the east.

### 5.3. Distribution of slip rates in the Kopeh Dagh

Based on the distribution of cumulative displacements along the different fault segments mapped within the BQFS (see section 3.2), one can infer the regional distribution of fault slip rates. To regionally propagate the results obtained for the Quchan and Baghan faults, it must be assumed that the initiation of all strike-slip faults in the Kopeh Dagh is contemporaneous (at ~4 Ma). If this assumption is correct, then differences in measured cumulative geological offsets should reflect long-term fault slip rate differences on individual fault segments. Fig. 3 shows the regional distribution of cumulative displacements and consequent maximum long-term slip rates derived from the above assumption. This figure illustrates how the deformation is mainly localized along the BQFS in which, the Baghan and Quchan faults have the highest slip rates. At the regional scale, one can also budget the sum of total cumulative offsets across the Kopeh Dagh at about 35-40 km. In fact, this sum is accommodated along at least eleven distinct fault segments, making it different from the proposed value by *Hollingsworth et al* (2006) for only three faults. We note that, because slip rates for the Baghan and Quchan faults are maximum rates, it is more reliable considering the upper bound of the inception age estimate (3.5-5.1 Ma) to calculate the total slip rate of strike-slip faulting in the Kopeh Dagh. Applying the deduced time span of 4.3±0.8 Myr for accumulation of the offsets, this bracketed value implies a total slip rate of about 9±2 mm/yr (Fig. 3) to be distributed over all the right-lateral strike-slip faults in the Central Eastern Kopeh Dagh. Consequently, this total slip rate has to be accommodated on the northeastern boundary of the Arabia-Eurasia collision

zone. According to these results, in northeast Iran, a large part of the northward motion between Central Iran and Eurasia (30±2 km) seems to be accommodated along the BQFS as strike-slip deformation, which indicates that the BQFS can be considered as an intercontinental boundary between Iranian micro-plate and Eurasia, accommodating about 80 per cent of northward motion of Central Iran with respect to Eurasia.

It is noteworthy that no evidence of deep-seated active thrust faulting is observed in the central part of the Kopeh Dagh. Moreover, the internal deformation of the blocks between strike-slip faults seems to be low, as evidenced by non-deformed linear markers such as anticline axes and ridge crests (Fig. 5). In addition, thanks to high resolution satellite imagery and well-stratified formations, geological cumulative offsets from 100 m up to 18 km are taken into account in our measurements, which make our estimate reliable with respect to the total geological deformation in this part of the Kopeh Dagh. Therefore, the total slip rate of 9±2 $mmyr^{-1}$ is comparable with the maximum bound of geodetic/geodynamic-derived rate of 8-10 mm/yr proposed for the northward motion between Central Iran and Eurasia (*Reilinger et al.,* 2006; *Vernant et al.,* 2004), and close to the total GPS rate of 9±2 mm/yr for strike-slip motion in the Kopeh Dagh (*Tavakoli*, 2007). Though, long-term geological slip rates do not necessarily need to be identical to such short-term rates integrated over the last several years.

Resolving the total strike-slip displacement value of 35-40 km on a regional average structural orientation representative of the BQFS (azimuth: N28°W, dip: 75°NE, rake: 10°) deduced from direct field observations and satellite image mapping, total ~34 km northward and ~16 km westward displacements can be derived for Central and Western Kopeh Dagh with respect to Eurasia. If one accepts these calculated values as representative for the total deformation of this part of the Kopeh Dagh, they imply an averaged northward slip rate of roughly 8 mm/yr, and an averaged westward slip rate of about 4 mm/yr. Recent GPS measurements in the Kopeh Dagh (*Tavakoli*, 2007) evaluated a total northward motion rate of about 8±2 mm/yr at the longitude of ~56°E, and a rate of 5±2 mm/yr between the Western and Eastern Kopeh Dagh toward the South Caspian Basin, accommodated by right-lateral slip on the MKDF and by left-lateral slip on the Shahrud fault system (at the southern boundary of the Western Kopeh Dagh, west of ~56°E). This consistency between our geological and geomorphic estimates and GPS rates indicates that regardless some probable errors in both measurements, they may have be representative of the total deformation in the Central-Eastern Kopeh Dagh since emplacement of the present-day tectonic configuration at ~4 Ma.

**Acknowledgements**

This work was funded by the INSU-CNRS (France) and the International Institute of Earthquake Engineering and Seismology (IIEES, Iran), supervised by D. Hatzfeld and M.G. Ashtiani. Funding was provided by the Dyeti and PNRN programs (INSU-CNRS), and ACI FNS program (French Ministry of Research), within the above mentioned co-operative agreement. SPOT images were provided thanks to the ISIS program (©CNES 2004 to 2007, distribution SPOT images S.A.). E. Shabanian benefits of a Foreign Affair Ministry (Ministère des Affaires Etrangères) grant through French Embassy in Iran, and a complement support through the "Cotutelle de thèse" program (ACI du Ministère des Affaires Etrangères). We thank V. Grimault, Ch. Duhamel and the staff of the SCAC of the French Embassy in Tehran, for their support. We greatly acknowledge R. Finkel at CAMS-LLNL (Lawrence Livermore National Laboratory), who performed the $^{36}$Cl measurements. We are grateful to two anonymous reviewers for constructive reviews. We thank D. Bourlès, R. Braucher, D. Hatzfeld, I. Schimmelpfennig and M. Djamali for fruitful discussions and help during the course of this work. The General governments of Khorassan-e Razavi and Shomali provinces have efficiently helped us during three years. Mohsen Zolfaqary with his careful driving provided excellent assistance in the field. We thank J. Crider for comments and English language corrections.

**References**

Afshar Harb, A., 1979. The stratigraphy, tectonics and petroleum geology of the Kopet Dagh region, northeastern Iran, PhD thesis, Petroleum Geology Section, Royal School of Mines, Imperial College of Science and Technology, London.

Afshar Harb, A., 1982. Geological quadrangle map of Iran no. K3 (Darreh Gaz sheet), scale 1:250 000, Geological Survey of Iran.

Afshar Harb, A., Bolourchi, M., and Mehr Parto, M., 1987. Geological quadrangle map of Iran no. J5 (Bojnurd sheet), scale 1:250 000, Geological Survey of Iran.

Afshar Harb, A., Soheili, B.M., and Valeh, C.N., 1980. Geological quadrangle map of Iran no. I3 (Kuh-e Kurkhud sheet), scale 1:250 000, Geological Survey of Iran.

Allen, M., Jackson, J., and Walker, R., 2004. Late Cenozoic reorganization of the Arabia-Eurasia collision and the comparison of short-term and long-term deformation rates, *Tectonics, 23*, TC2008. doi:10.1029/2003TC00153.

Allen, M.B., Blanc, E.J.-P., Walker, R., Jackson, J., Talebian, M., and Ghassemi, M.R., 2006. Contrasting styles of convergence in the Arabia-Eurasia collision: Why escape tectonics does not occur in Iran, in Postcollisional tectonics and magmatism in the Mediterranean region and Asia, pp. 579–589, ed. Dilek, Y., and Pavlides, S., *Geol. Soc. Am. Special Paper, 409*. doi:10.1130/2006.2409(26).

Allen, M.B., Jones, S., Ismail-Zadeh, A., Simmons, M., and Anderson, L., 2002. Onset of subduction as the cause of rapid Pliocene-Quaternary subsidence in the South Caspian Basin, *Geology*, *30*(9), 775-778. doi:10.1130/0091-7613(2002)030<0775.

Ambraseys, N., and Melville, C., 1982. A History of Persian Earthquakes, Cambridge University Press, Cambridge, UK.

Amurskiy, G.I., 1971. The deep structure of the Kopetdagh, *Geotectonics, 1*, 34-40. (Engl. Transl.).

Authemayou, C., Bellier, O., Chardon, D., Malekzade, Z., and Abbassi, M., 2005. Role of the Kazerun fault system in active deformation of the Zagros fold and-thrust belt (Iran), *C. R. Geosci., 337*, 539–545.

Authemayou, C., Chardon, D., Bellier, O., Malekzade, Z., Shabanian, E., and Abbassi, M., 2006. Late Cenozoic partitioning of oblique plate convergence in the Zagros fold-and-thrust belt (Iran), *Tectonics, 25*, TC3002. doi:10.1029/2005TCOO1860.

Axen, G.J., Lam, P.S., Grove, M., Stockli, D.F., and Hassanzadeh, J., 2001. Exhumation of the west-central Alborz Mountains, Iran, Caspian subsidence, and collision-related tectonics, *Geology*, *29*(6), 559–562.

Bayer, R., Chéry, J., Tatar, M., Vernant, Ph., Abbassi, M., Masson, F., Nilforoushan, F., Doerflinger, E., Regard, V., and Bellier, O., 2006. Active deformation in Zagros-Makran transition zone inferred from GPS measurements, *Geophys. J. Int.*, *165*(1), 373–381. doi:10.1111/j.1365-246X.2006.02879.x.

Berberian, M., and Yeats, R., 1999. Patterns of historical earthquake rupture in the Iranian Plateau, *Bull. Seism. Soc. Am.*, *89*, 120–139.

Berberian, M., and Yeats, R., 2001. Contribution of archaeological data to studies of earthquake history in the Iranian Plateau, *J. Str. Geol.*, *23*, 563-584.

Bierman, P.R., 1994. Using *in situ* produced cosmogenic isotopes to estimate rates of landscape evolution: A review from the geomorphic perspective, *J. GEOPHYS. RES.*, *99*(B7), 13885-13896.

Bierman, P.R., Gillespie, A.R., Caffee, M.W., and Elmore, D., 1995. Estimating erosion rates and exposure ages with $^{36}$Cl produced by neutron activation, *Geochimica Cosmochimica Acta, 59*, 3779–3798.

Bozkurt, E., 2001. Neotectonics of Turkey – A synthesis, *Geodinamica Acta, 14*(1), 3-30. doi:10.1016/S0985-3111(01)01066-X.

Copley, A., and Jackson, J., 2006. Active tectonics of the Turkish-Iranian Plateau, *Tectonics, 25*, TC6006. doi:10.1029/2005TC001906.

Daëron, M., Benedetti, L., Tapponnier, P., Sursock, A., and Finkel, R.C., 2004. Constraints on the post ~25-ka slip rate of the Yammoûneh fault (Lebanon) using in situ cosmogenic $^{36}$Cl dating of offset limestone-clast fans, *Earth Planet. Sci. Lett.*, *227*, 105-119.

Deino, A. and Potts, R., 1992. Age-probability spectra from examination of single-crystal $^{40}$Ar/$^{39}$Ar dating results: Examples from Olorgesailie, Southern Kenya Rift, *Quaternary International*, *13/14*, 47-53.

Devlin, W., Cogswell, J., Gaskins, G., Isaksen, G., Pitcher, D., Puls, D., Stanley, K., and Wall, G., 1999. South Caspian Basin: Young, cool, and full of promise, *GSA Today, 9*(7), 1-9.

Dixon, T.H, Norabuena, E., and Hotaling, L., 2003. Paleoseismology and Global Positioning System: Earthquake cycle effects and geodetic versus geologic fault slip rates in the Eastern California shear zone, *Geology, 31*, 55-58.

Friedrich, A.M., Wernicke, B.P., Niemi, N.A., Bennett, R.A., and Davis J.L., 2003. Comparison of geodetic and geologic data from the Wasatch region, Utah, and implications for the spectral character of Earth deformation at periods of 10 to 10 million years, *J. Geophys. Res., 108*(B4), 2199. doi:10.1029/2001JB000682.

Gosse, J.C., and Phillips, F.M., 2001. Terrestrial in situ cosmogenic nuclides: theory and application, *Quat. Sci. Rev., 20*, 1475-1560.

Hempton, M R., 1987. Constraints on Arabian plate motion and extensional history of the Red Sea, *Tectonics, 6*(6), 687-705. doi:10.1029/TC006i006p00687.

Hollingsworth, J., Jackson, J., Alarcón, J.E., Bommer, J.J., and Bolourchi, M.J., 2007. The 4th February 1997 Bojnurd (Garmkhan) earthquake in NE Iran: field, teleseismic, and strong-motion evidence for rupture directivity effects on a strike-slip fault, *Journal of Earthquake Engineering, 11*, 193–214.

Hollingsworth, J., Jackson, J., Walker, R., Gheitanchi, M.R., and Bolourchi, M.J., 2006. Strike-slip faulting, rotation and along-strike elongation in the Kopeh Dagh Mountains, NE Iran, *Geophys. J. Int., 166*, 1161-1177. doi:10.1111/j.1365-246X.2006.02983.x.

Huber, H., 1977. Geological map of Iran Sheet no. 3, North East Iran, scale: 1:1 000 000, National Iranian Oil Company.

Jackson, J., and McKenzie, D., 1984. Active tectonics of the Alpine-Himalayan Belt between western Turkey and Pakistan, *Geophys. J. R. astr. Soc., 77*(1), 185-264.

Jackson, J., Priestley, K., Allen, M., and Berberian, M., 2002. Active tectonics of the South Caspian Basin, *Geophys. J. Int., 148*, 214–245.

Keller, E.A., Seaver, D.B., Laduzinsky, D.L., Johnson, D.L., and Ku, T.L., 2000. Tectonic geomorphology of active folding over buried reverse faults: San Emigdio Mountain front, southern San Joaquin Valley, California, *Geol. Soc. Am. Bull., 112*(1), 86–97.

Koçyigit, A., Yilmaz, A., Adamia, S., and Kuloshvili, S., 2001. Neotectonics of East Anatolian Plateau (Turkey) and Lesser Caucasus: implication for transition from thrusting to strike-slip faulting, *Geodinamica Acta, 14*(1), 177-195. doi:10.1016/S0985-3111(00)01064-0.

Livnat, A., Lifshitz, A., and Flexer, A., 1987. The tectonic style of the southern Arava Rift margins, Israel: alternating stress fields in wrench-rifting processes, *Tectonophysics, 141*(1-3), 151-168. doi:10.1016/0040-1951(87)90182-X.

Lowell, T.V., 1995. The application of radiocarbon age estimates to the dating of glacial sequences: an example from the Miami sublobe, Ohio, USA, *Quaternary Science Reviews, 14*, 85– 99.

Lyberis, N., and Manby, G., 1999. Oblique to orthogonal convergence across the Turan block in the post-Miocene, *Am. Assoc. Petrol. Geol. Bull., 83*(7), 1135–1160.

Lyberis, N., Manby, G., Poli, J.T., Kalugin, V., Yousouphocaev, H., and Ashirov, T., 1998. Post-Triassic evolution of the southern margin of the Turan plate, *C. R. Acad. Sci., 326*, 137–143.

Maggi, M., Jackson, J., McKenzie, D., and Priestley, K., 2000. Earthquake focal depths, effective elastic thickness, and the strength of the continental lithosphere, *Geology, 28*(6), 495–498.

Masson, F., Anvari, M., Djamour, Y., Walpersdorf, A., Tavakoli, F., Daignières, M., Nankali, H., and Van Gorp, S., 2007. Large-scale velocity field and strain tensor in Iran inferred from GPS measurements: new insight for the present-day deformation pattern within NE Iran, *Geophys. J. Int., 170*, 436–440. doi:10.1111/j.1365-246X.2007.03477.x.

Masson, F., Djamour, Y., Vangorp, S., Chéry, J., Tavakoli, F., Tatar M., and Nankali, H., 2006. Extension in NW Iran inferred from GPS enlightens the behavior of the south Caspian basin, *Earth Planet. Sci. Lett., 252*, 180–188.

McClusky, S., Reilinger, R., Mahmoud, S., Ben Sari, D., and Tealeb, A., 2003. GPS constraints on Africa (Nubia) and Arabia plate motions, *Geophys. J. Int., 155*(1), 126–138. doi:10.1046/j.1365-246X.2003.02023.x.

McDonald, E.V., 1994. The relative influence of climatic change, desert dust, and lithological control on soil-geomorphic processes and hydrology of calcic soils formed on Quaternary alluvial-fan deposits in the Mojave Desert, California, PhD thesis, Univ. of New Mexico, Albuquerque.

McFadden, L.D., McDonald, E.V., Wells, S.G., Anderson, K., Quade, J., and Forman, S.L., 1998. The vesicular layer and carbonate collars of desert soils and pavements: formation, age and relation to climate change, *Geomorphology, 24*, 101–145.

McKenzie, D.P., 1972. Active tectonics of the Mediterranean region, *Geophys. J. Int., 30*(2), 109–185. doi:10.1111/j.1365-246X.1972.tb02351.x.

Phillips, F.M., Zreda, M.G., Flinsch, M.R., Elmore, D., and Sharma, P., 1996. A reevaluation of cosmogenic $^{36}$Cl production rates in terrestrial rocks, *Geophys. Res. Letters, 23*, 949–952.

Phillips, F.M., Zreda, M.G., Gosse, J.C., Klein, J., Evenson, E.B., Hall, R.D., Chadwick, O.A., and Sharma, P., 1997. Cosmogenic $^{36}$Cl and $^{10}$Be ages of Quaternary glacial and fluvial deposits of the Wind River Range, Wyoming, *Geol. Soc. Am. Bull., 109*(11), 1453–1463.

Regard, V., Bellier, O., Braucher, R., Gasse, F., Bourlès, D., Mercier, J., Thomas, J.-C., Abbassi, M.R., Shabanian, E., and Soleymani, S., 2006. $^{10}$Be dating of alluvial deposits

from Southeastern Iran (the Hormoz Strait area), *Palaeogeography, Palaeoclimatology, Palaeoecology, 242*(1-2), 36–53. doi:10.1016/j.palaeo.2006.05.012.

Regard, V., Bellier, O., Thomas, J.-C., Abbassi, M.R., Mercier, J.L., Shabanian, E., Feghhi, K., and Soleymani, S., 2004. Accommodation of Arabia-Eurasia convergence in the Zagros-Makran transfer zone, SE Iran: A transition between collision and subduction through a young deforming system, *Tectonics, 23*, TC4007. doi:10.1029/2003TC001599.

Regard, V., Bellier, O., Thomas, J.-C., Bourlès, D., Bonnet, S., Abbassi, M.R., Braucher, R., Mercier, J., Shabanian, E., Soleymani, S., and Feghhi, K., 2005. Cumulative right-lateral fault slip rate across the Zagros–Makran transfer zone: role of the Minab–Zendan fault system in accommodating Arabia–Eurasia convergence in southeast Iran, *Geophys. J. Int., 162*, 177–203. doi:10.1111/j.1365-246X.2005.02558.x.

Reilinger, R., et al., 2006. GPS constraints on continental deformation in the Africa-Arabia-Eurasia continental collision zone and implications for the dynamics of plate interactions, *J. Geophys. Res., 111*, B05411. doi:10.1029/2005JB004051.

Ritz, J.F., Brown, E.T., Bourlès, D., Philip, H., Schlupp, A., Raisbeck, G.M., Yiou, F., and Enkhtuvshin, B., 1995. Slip rates along active faults estimated with cosmic-ray–exposure dates: Application to the Bogd fault, Gobi-Altaï, Mongolia, *Geology, 23*(11), 1019-1022.

Ritz, J.-F., Nazari, H., Ghassemi, A., Salamati, R., Shafei, A., Solaymani, S., and Vernant, P., 2006. Active transtension inside central Alborz: A new insight into northern Iran–southern Caspian geodynamics, *Geology, 34*(6), 477–480. doi:10.1130/G22319.1.

Ron, H., Freund, R., Garfunkel, Z., and Nur, A., 1984. Block-rotation by strike–slip faulting: structural and paleomagnetic evidence, *J. Geophys. Res., 89*(B7), 6256-6270.

Schimmelpfennig, I., Benedetti, L., Finkel, R., Pik, R., Blard, P.H., Bourlès, D., Burnard, P., and Williams, A., 2009. Sources of in-situ $^{36}$Cl in basaltic rocks. Implications for calibration of production rates, *Quaternary Geochronology*, in press, xxxx doi:10.1016/j.quageo.2009.06.003.

Sella, G.F., Dixon, T.H., and Mao, A., 2002. REVEL: A model for recent plate velocities from space Geodesy, *J. Geophys. Res., 107*(B4), 2081. doi:10.1029/2000JB000033.

Stöcklin, J., 1968. Structural history and tectonics of Iran: A review, *Am. Assoc. Petr. Geol. Bull., 52*(7), 1229–1258.

Stone, J.O.H., 2000. Air pressure and cosmogenic isotope production, *J. Geophys. Res., 105*(B10), 23753-23759.

Stone, J.O.H., Allan, G.L., Fifield, L.K., and Cresswell, R.G., 1996. Cosmogenic chlorine-36 from calcium spallation, *Geochimica et Cosmochimica Acta, 60*(4), 679-692.

Stone, J.O.H., Evans, J.M., Fifield, L.K., Allan, G.L., and Cresswell, R.G., 1998. Cosmogenic chlorine-36 production in calcite by muons, *Geochimica et Cosmochimica Acta, 62*(3), 433-454.

Talebian, M., and Jackson, J., 2002. Offset on the Main Recent Fault of NW Iran and implications for the late Cenozoic tectonics of the Arabia–Eurasia collision zone, *Geophys. J. Int., 150*, 422-439.

Talebian, M., and Jackson, J., 2004. A reappraisal of earthquake focal mechanisms and active shortening in the Zagros mountains of Iran, *Geophys. J. Int., 156*(3), 506–526.

Tapponnier, P., Frederick , J.R., Van der Woerd, J., Mériaux, A.S., and Lasserre, C., 2001. Long-term slip rates and characteristic slip: keys to active fault behaviour and earthquake hazard, *C. R. Acad. Sci. Ser. II, 333*(9), 483–494.

Tavakoli, F., 2007. Present-day kinematics of the Zagros and east of Iran faults, PhD thesis, University of Joseph Fourier, Grenoble.

Taylor, J.R., 1997. An Introduction to Error Analysis, The Study of Uncertainties in Physical Measurements, 2nd ed., University Science Books, Sausalito, CA.

Tchalenko, J.S., 1975. Seismicity and structure of the Kopet Dagh (Iran, USSR), *Phil. Trans. R. Soc. Lond., Series A, 278* (1275), 1–28.

Tchalenko, J.S., Braud, J., and Berberian, M., 1974. Discovery of three earthquake faults in Iran, *Nature, 248*, 661-663.

Trifonov, V., 1978. Late Quaternary tectonic movements of western and central Asia, *Geol. Soc. Am. Bull., 89*, 1059-1072.

Vernant, P., Nilforoushan, F., Hatzfeld, D., Abbassi, M.R., Vigny, C., Masson, F., Nankali, H., Martinod, J., Ashtiani, A., Bayer, R., Tavakoli, F., and Chéry, J., 2004. Present-day crustal deformation and plate kinematics in the Middle East constrained by GPS measurements in Iran and northern Oman, *Geophys. J. Int., 157*(1), 381–398. doi:10.1111/j.1365-246X.2004.02222.x.

Walker, R., and Jackson, J., 2004. Active tectonics and Late Cenozoic strain distribution in central and eastern Iran, *Tectonics, 23*, TC5010. doi:10.1029/2003TC001529.

Walpersdorf, A., Hatzfeld, D., Nankali, H., Tavakoli, F., Nilforoushan, F., Tatar, M., Vernant, P., Chéry, J., and Masson, F., 2006. Difference in the GPS deformation pattern of North and Central Zagros (Iran), *Geophys. J. Int., 167*(3), 1077-1088. doi:10.1111/j.1365-246X.2006.03147.x.

Wells, S.G., McFadden, L.D., and Dohrenwend, J.C., 1987. Influence of Late Quaternary climatic changes on geomorphic and pedogenic processes on a desert piedmont, eastern Mojave Desert, California, *Quaternary Res., 27*, 130–146.

Wells, S.G., McFadden, L.D., Dohrenwend, J.C., Turrin, B.D., and Mahrer, K.D., 1985. Late Cenozoic landscape evolution of lava flow surfaces of the Cima volcanic field, Mojave Desert, California, *Geol. Soc. Am. Bull., 96*, 1518–1529.

Wells, S.G., McFadden, L.D., Poths, J., and Olinger, C.T., 1995. Cosmogenic $^{3}$He exposure dating of stone pavements: implications for landscape evolution in deserts, *Geology, 23*, 613–616.

Westaway, R., 1994. Present-day kinematics of the Middle East and eastern Mediterranean, *J. Geophys. Res., 99*(B6), 12071-12090.

Yamini-Fard, F., Hatzfeld, D., Farahbod, A.M., Paul, A., and Mokhtari, M., 2007. The diffuse transition between the Zagros continental collision and the Makran oceanic subduction (Iran): microearthquake seismicity and crustal structure, *Geophys. J. Int., 170*(1), 182–194.

Zreda, M.G., Phillips, F.M., & Elmore, D., 1994. Cosmogenic $^{36}$Cl accumulation in unstable landforms, 2. Simulations and measurements on eroding moraines, *Water Resources Research, 30*, 3127–3136.

# *Chapter II*

Northeast Iran and specially the Kopeh Dagh were always referred as a key region to demonstrate the geological reliability of the continuous deformation model according which, deformation is uniformly distributed throughout the zone. In the previous chapter, it is revealed that active deformation is focalized along a major fault system discarding such a hypothesis. However, the absence of precise quantitative measures of regional continental deformation has been the chief obstacle in determining which model is able to describe the kinematics of active deformation. In this chapter, we characterize a small but very important region at the northeastern boundary of the Arabia-Eurasia collision, i.e., the Meshkan Transfer Zone, in order to better understand the kinematics of deformation, and respond to a key question: how is transferred the deformation accommodated in the Kopeh Dagh Mountains toward the South? After a review of the geological setting and structural framework of the MTZ, the evidences for Late Cenozoic strike-slip faulting in the MTZ are presented. We merge our results with those discussed in the previous chapter to present a clearer image of the deformation pattern in northeast Iran. Then, we compare our model with kinematic descriptions of the Kopeh Dagh deformation proposed in previous studies.

# New tectonic configuration in NE Iran: active strike-slip faulting between the Kopeh Dagh and Binalud mountains[1]

Esmaeil Shabanian[1,2], Olivier Bellier[1], Lionel Siame[1], Nicolas Arnaud[3], Mohammad R. Abbassi[2], Jean-Jacques Cochemé[4]

[1] CEREGE - UMR CNRS, Université Aix-Marseille, IRD, Collège de France, Europôle de l'Arbois, BP 80, 13545 Aix-en-Provence Cedex 4, France

[2] International Institute of Earthquake Engineering and Seismology (IIEES)

[3] Géosciences Montpellier - UMR CNRS 5243, Groupe GEODE, CC 060, Université de Montpellier 2, Place Eugène Bataillon, 34095 Montpellier Cedex 5, France

[4] Laboratoire de Pétrologie Magmatique, Université Aix-Marseille, Faculté des Sciences de St Jérôme, 13397 Marseille Cedex 20, France

## Abstract

In this paper, a combined approach of geomorphic analyses, detailed geological mapping on SPOT5 satellite images and field surveys, complemented by radiometric dating ($^{40}Ar/^{39}Ar$) allows proposing a new and consistent tectonic configuration for the northeastern Arabia-Eurasia collision zone. It favors a simple strike-slip faulting mechanism in NE Iran accommodating the northward motion of Central Iran with respect to Eurasia between the Binalud and Kopeh Dagh mountains. Our results demonstrate that ~2 mm/yr (~25 per cent) of this northward motion has been transferred from the Binalud to the Kopeh Dagh through the Meshkan Transfer Zone (MTZ) since ~5 Ma. The modern state of stress deduced from fault kinematics analyzes shows N30°E trending maximum stress axis and confirms a dominant strike-slip faulting mechanism. Combining our geological data with other available data, we conclude that kinematics of deformation can be appropriately described by rigid block faulting in NE Iran; instead the continuous deformation as it has been thought during the last three decades.

*Keywords: Alborz, Kopet Dagh, Morphotectonics, Stress states, continental deformation.*

[1] *Shabanian et al. (2009), Tectonics, 28, TC5002, doi:10.1029/2008TC002444.*

## 1. Introduction

At the scale of plate tectonics, the deformation of continental lithosphere seems to be distributed over zones up to a few hundred kilometers wide with the relatively aseismic blocks on both sides. This general character of actively deforming continental domains has led geo-scientists to propose two idealized end-member kinematic models. On one hand, it has been suggested that actively deforming regions are comprised of blocks or microplates. Most of the deformation occurs along major block bounding faults, with minor faulting but little internal deformation of the blocks themselves (*Avouac and Tapponnier*, 1993; *Peltzer and Saucier*, 1996; *Replumaz and Tapponnier*, 2003; *Ryerson et al.*, 2006, *Thatcher*, 2007, and references therein). On the other hand, deformation is uniformly distributed and continents can be treated as a continuously deforming viscous medium, governed by the fluid-like solid-state flow of a viscous material (*England and McKenzie*, 1982; *Vilotte et al.*, 1982; *McKenzie and Jackson*, 1983; *England and Molnar*, 1997; *Flesch et al.*, 2001). In this scheme, faults play a minor role and slip in the brittle upper crust occurs on many faults with comparable slip rates. The strengths and limitations of each model have been widely discussed in review papers (*Molnar*, 1988; *England and Jackson*, 1989; *Gordon and Stein*, 1992; *Thatcher*, 1995; *Thatcher*, 2003, and references therein). However, there are perhaps a general agreement that the major unresolved issue is not which of the two extreme models is unconditionally correct, but how the observed deformation can be most usefully and simply described and which intermediate case is most appropriate (*e.g.*, *Molnar*, 1988; *Thatcher*, 1995).

Interestingly, NE Iran and specially the Kopeh Dagh (Figure 1) were always referred as a key region to demonstrate the geological reliability of the continuous deformation model (*McKenzie and Jackson*, 1983, 1986; *Jackson and McKenzie*, 1984). According to this model, unstable geometry of strike-slip faults combined with the thrusting, oblique to the boundaries of the deforming zone will require faults to rotate about a vertical axis until they become parallel to the zone boundary (*McKenzie and Jackson*, 1983, 1986; *Jackson and McKenzie*, 1984; *Jackson et al.*, 2002; *Hollingsworth et al.*, 2006, 2008). However, in the absence of firm quantitative constraints it is difficult to demonstrate the ability of any kinematics model to describe active deformation in NE Iran. In any case, the absence of precise quantitative measures of regional continental deformation has been the chief obstacle in determining which model is able to describe the kinematics of deformation in actively deforming zones (*Thatcher*, 1995). Quantitative data, particularly offset amounts and slip rates on major faults

hold the key to constrain these models. In this context, the study of the Quaternary faulting yields the most precise average velocities of slip on faults (*e.g.*, *Molnar*, 1988; *Thatcher*, 1995; *Replumaz and Tapponnier*, 2003; *Nyst and Thatcher*, 2004).

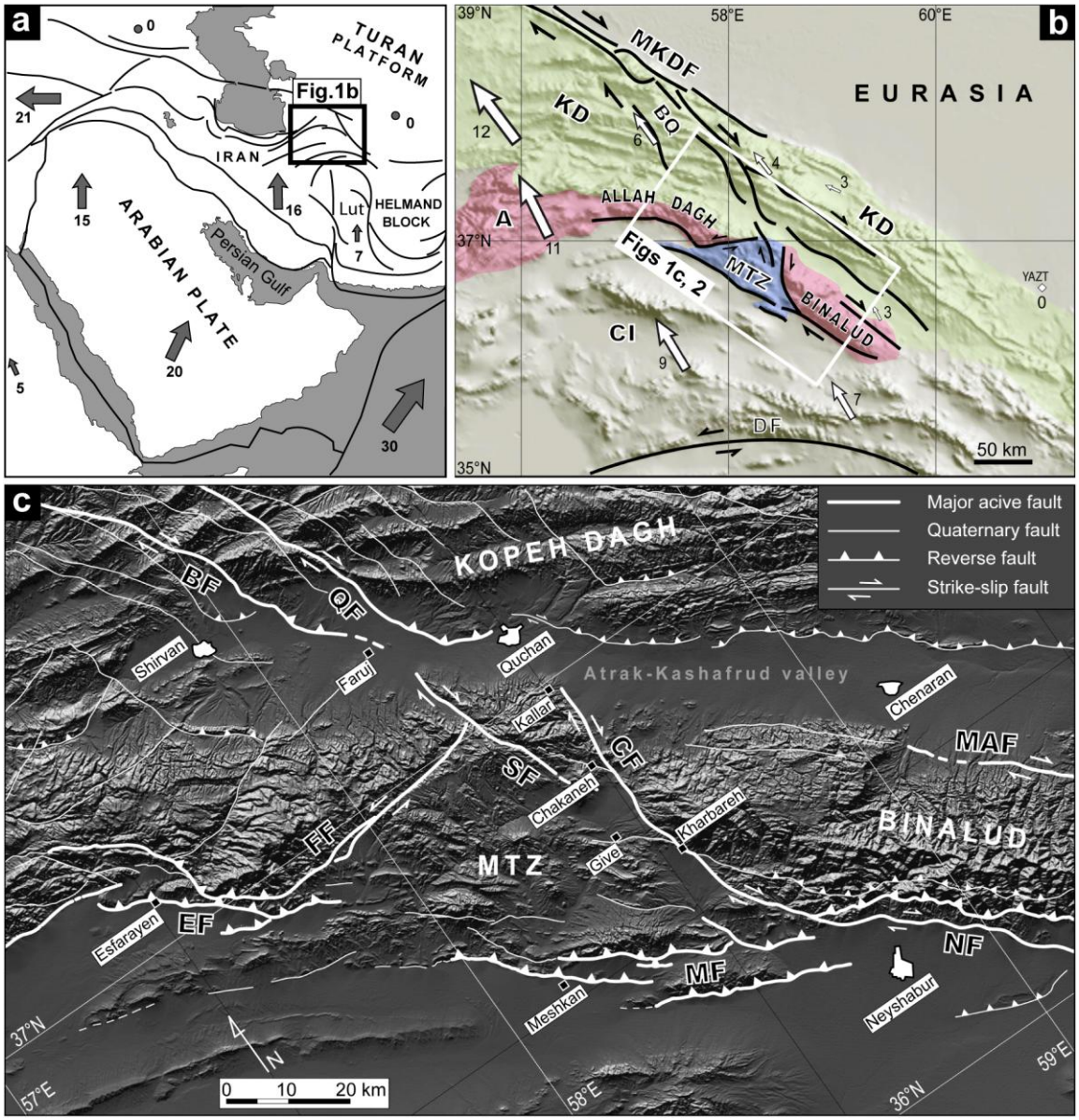


Figure 1. (a) The location of the Meshkan Transfer Zone (MTZ) in the Arabia-Eurasia collision framework. Gray arrows and associated numbers represent Arabia-Eurasia plate velocities (in mm/yr) after *Reilinger et al.* (2006). (b) GTOPO30 topographic image of northeastern Iran showing the MTZ location in the tectonic context of NE Iran. White arrows and associated numbers are GPS horizontal velocities (mm/yr) in a Eurasia-fixed reference frame (YAZT station) (*Tavakoli*, 2007). Abbreviations: MKDF, Main Kopeh Dagh Fault; BQ, Bakharden-Quchan Fault System; DF, Doruneh Fault; KD, Kopeh Dagh; A, Alborz; CI, central Iran. (c) Shaded relief image of the MTZ and surroundings (based on SRTM digital topographic data) showing triangular-liked fault systems of the MTZ, and their structural relationships with the Binalud and Kopeh Dagh fault systems. Fault traces are based on SPOT5 and LANDSAT ETM+ image mapping (after *Shabanian et al.,* 2009, and this study). BF, Baghan Fault; CF, Chakaneh Fault system; EF, Esfarayen Fault; FF, Farhadan Fault system; MAF, Mashhad Fault; MF, Meshkan Fault system; NF, Neyshabur Fault system; QF, Quchan Fault; SF, Sar'akhor Fault.

In this paper, we characterize a small but very important region at the northeastern boundary of the Arabia-Eurasia collision, *i.e.*, the Meshkan Transfer Zone (MTZ), in order to better understand the kinematics of deformation in NE Iran (Figure 1), and respond to a key question: how is transferred the deformation accommodated in the Kopeh Dagh Mountains toward the South? Several approaches of geomorphic analyses, detailed mapping and field surveys, complemented by few radiometric dating ($^{40}Ar/^{39}Ar$) have been used to define and detail the structural and kinematic characteristics of the MTZ.

The data and results presented in this paper have significant impacts on both kinematic and geodynamic interpretations of strike-slip faulting in oblique convergence domains such as NE Iran. First, our data reveal a new tectonic configuration in which strike-slip faulting oblique to the convergence direction and zone boundary plays the major structural role to take up active deformation in the northeastern boundary of the Arabia-Eurasia collision. This configuration is completely different from what was suggested during the last thirty years. Secondly, at a more general scale, our data present another possibility for the evolution of a continued convergence; a way in which crustal thickening and growth in area of the range by thrust faulting parallel to the range is not significant. Finally, our data help to better understand the kinematics of deformation in NE Iran and probably in the similar regions submitted to oblique convergence.

After a review of the geological setting and structural framework of the MTZ, the evidences for Late Cenozoic strike-slip faulting in the MTZ are presented. Then, we describe morphotectonic and geological investigations conducted along two major strike-slip fault systems, allowing us determining individual Plio-Quaternary fault slip rates. We merge our results with those published by *Shabanian et al.* (2009) and analyze the combined data set to present a clearer image of the deformation pattern in NE Iran. Then, we compare our model with kinematic descriptions of the Kopeh Dagh deformation proposed in previous studies examining the validity of both rigid blocks and continuous deformation kinematics model for continental deformation at the northeastern boundary of the Arabia-Eurasia collision.

## 2. Tectonic setting and structural framework

Tectonic deformations in Iran result from the Arabia-Eurasia convergence. This convergence took place by crustal shortening and strike-slip faulting in different intracontinental deformation domains (mountain ranges) such as the Zagros, Alborz and Kopeh Dagh mountains. The northward motion of Arabia with respect to Eurasia is

accommodated at a rate of 22±2 mm/yr at the longitude of Bahrain (*Sella et al*., 2002; *McClusky et al*., 2003; *Vernant et al*., 2004; *Reilinger et al*., 2006). According to the available geodetic (*Vernant et al*., 2004; *Reilinger et al*., 2006; *Masson et al*., 2007; *Tavakoli*, 2007) and geological (*Shabanian et al*., 2009) data, this northward motion is accommodated in north-east Iran at a rate ranging from 4 to 11 mm/yr. A significant part (7±2 mm/yr) of this deformation is localized along the Bakharden-Quchan Fault system (BQFS, Figure 1) within the Kopeh Dagh Mountains (*Tavakoli*, 2007; *Shabanian et al*., 2009). In the Binalud Mountains, the GPS-derived velocity vectors (*Masson et al*., 2007; *Tavakoli*, 2007) indicate 2-4 mm/yr of right-lateral strike-slip movement on both sides of the range. Accepting the plate boundary like character of the Bakharden-Quchan Fault system (*Shabanian et al*., 2009), and the calculated range-parallel GPS rates through the Binalud Mountains (*Masson et al*., 2007; *Tavakoli*, 2007) has two main consequences. First, the northward motion of the Lut Block and Central Iran with respect to Afghanistan (*Regard et al*., 2004; *Vernant et al*., 2004; *Walker and Jackson*, 2004) should be taken up between the Doruneh Fault (Figure 1) and the Kopeh Dagh Mountains with trivial absorption across the northern part of Central Iran. Secondly, part of this motion have to be transferred between the Binalud and Kopeh Dagh mountain ranges, as strike-slip motion along localized major fault systems or in form of distributed deformation (on several faults with comparable slip rates). However, available geological data are insufficient to establish the structural linkage between these deformation domains. Hereafter, we pay a special attention to the structural and geomorphic evidences for active faulting within the transfer region between the Kopeh Dagh and Binalud mountains, *i.e*., the Meshkan Transfer Zone.

The MTZ forms a triangular-shaped zone (70×70×100 km) between three distinct structural domains: (1) the Allah Dagh-Binalud mountains, which can be regarded as the eastern extension of the Alborz mountain ranges (*Alavi*, 1992), (2) the Kopeh Dagh mountains to the north, and (3) Central Iran to the south (Figure 1). The structural pattern in the Meshkan region is dominated by three fault systems in a triangular configuration with clear crosscutting relationships: (1) the left-lateral, Farhadan Fault system consisting of two ENE trending, strike-slip fault segments, and defining the northern margin of the MTZ against the Allah Dagh mountains, (2) the right-lateral, Chakaneh Fault system, constituted by NNW trending, strike-slip fault segments which affected eastern part of the region and separates the MTZ from the Binalud Mountains, and (3) the reverse Meshkan Fault system, constituted by NW trending, reverse fault segments distributed in the southeastern part of the region defining

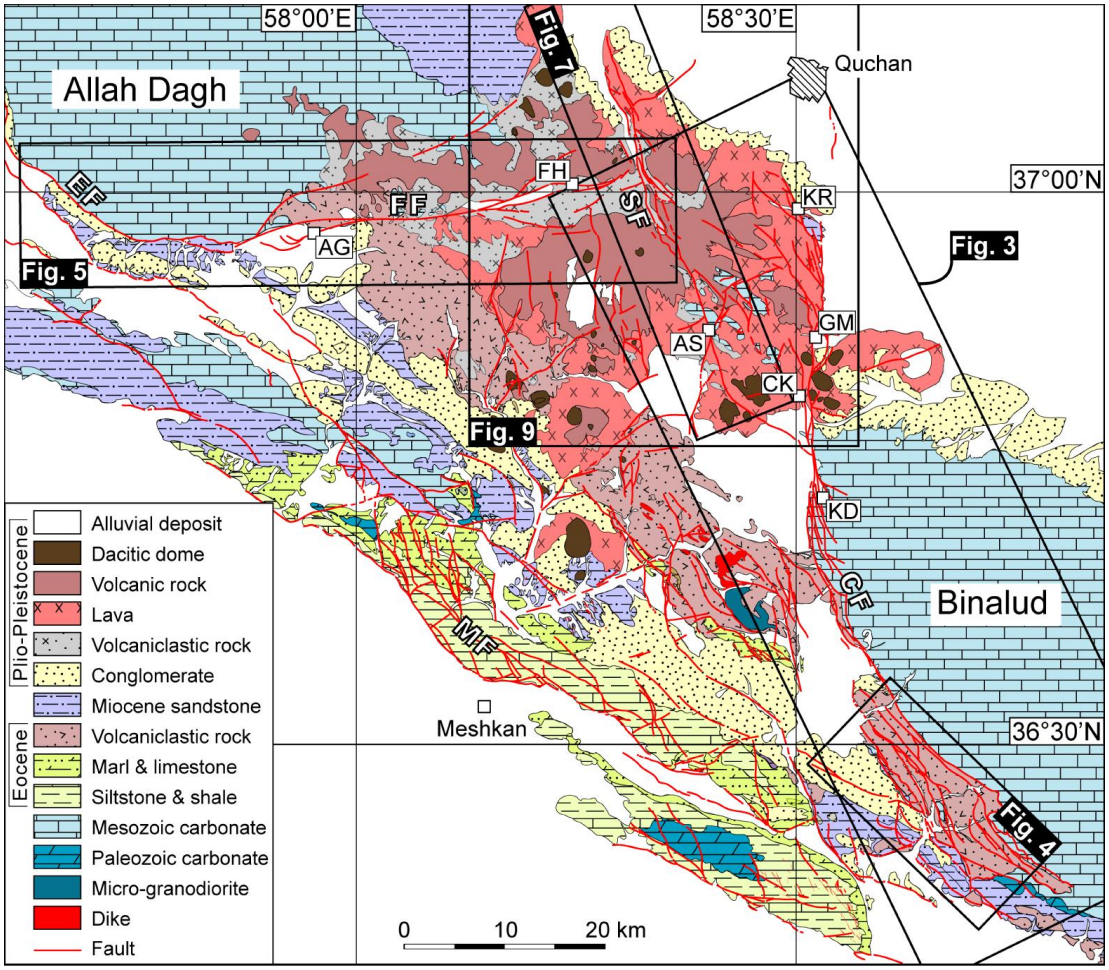
58°00'E
58°30'E
37°00'N
36°30'N
Allah Dagh
Binalud
Quchan
Meshkan
Fig. 3
Fig. 4
Fig. 5
Fig. 7
Fig. 9
EF
FF
SF
MF
CF
FH
AG
AS
KR
GM
CK
KD
0
10
20 km
Plio-Pleistocene
Eocene
Alluvial deposit
Dacitic dome
Volcanic rock
Lava
Volcaniclastic rock
Conglomerate
Miocene sandstone
Volcaniclastic rock
Marl & limestone
Siltstone & shale
Mesozoic carbonate
Paleozoic carbonate
Micro-granodiorite
Dike
Fault

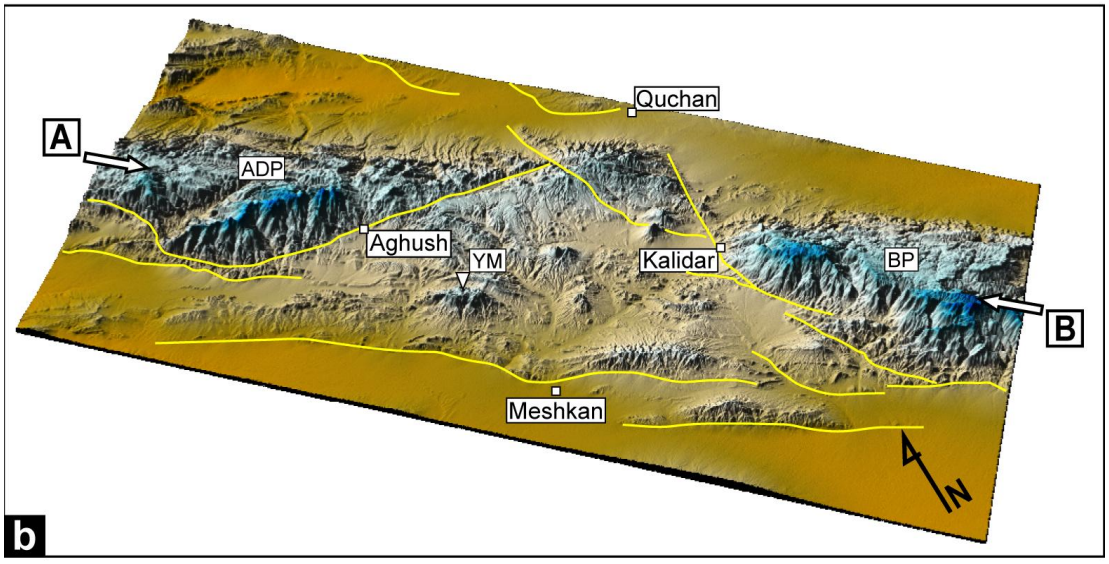
A
B
Quchan
ADP
Aghush
YM
Kalidar
BP
Meshkan
N
b

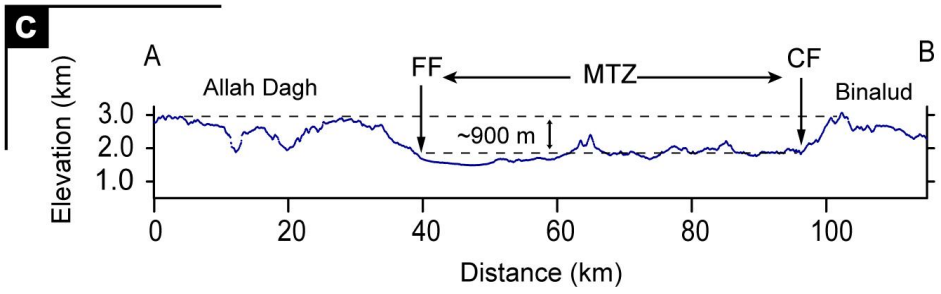
c
A
B
Allah Dagh
FF
MTZ
CF
Binalud
~900 m
Elevation (km)
3.0
2.0
1.0
0
20
40
60
80
100
Distance (km)

the southeastern boundary of the MTZ with Central Iran (Figure 1). Both the geological and topographic boundaries of the MTZ have been controlled by those fault systems (Figure 2).

In comparison with the surrounding structural domains, the MTZ is clearly different both in geomorphic and geological characteristics (Figure 2). This triangular region is conspicuously less elevated than the Allah Dagh and Binalud mountains (Figure 2). The maximum elevation of the Late Cretaceous-early Paleocene paleo-reliefs in the MTZ does not exceed 2300 m for Yarimja summit, which is about 800 m lower than the corresponding land surfaces in the Allah Dagh (3060 m) and Binalud (3100 m) mountains (Figure 2). In the same way, an abrupt elevation change of roughly 900 m is observed comparing the average topographic level of the MTZ with respect to the adjacent mountain ranges on the other sides of the Chakaneh and Farhadan fault systems (Figure 2).

The Cenozoic evolution of the Meshkan region is complex; the MTZ has been involved in geological histories of the adjacent structural domains (Alborz, Kopeh Dagh, Central Iran) intervened by its own Cenozoic tectono-magmatic episodes. Diverse sedimentary and volcanic rocks, mainly of Tertiary age, are cropping out within the study area. The late Eocene or probably early Oligocene tectonic movements uplifted the entire region (*Afshar Harb*, 1979). The Oligocene-Miocene lagoonar to continental sediments fill depressions within syncline fold axis regions constituted by middle-late Eocene layers. These sediments overlie unconformably the folded Eocene rocks and were deformed by the late Miocene compressional movements. The fold axes appear to lie roughly parallel to the northeast dipping fault traces for much of their length. This trend is homogenous throughout the entire region including the Kopeh Dagh, Allah Dagh and Binalud mountain ranges, and probably is representative for uniform episodes of folding since Late Cretaceous. They only have undergone structural deflection in the vicinity of strike-slip faults, given sense of the fault motions. Plio-Quaternary conglomerates have been deposited over the previous folded strata and were gently folded. The folded Eocene and Oligo-Miocene rocks are overlain by thick sequence of Late Cenozoic volcanic rocks. In the final stage of the volcanic activity, Plio-Quaternary dacitic-rhyodacitic dome intruded the previous volcanoes or calderas (*Amini and*

Figure 2. (a) Geological map of the MTZ (modified after *Amini & Khan Nazer*, 2000; *Ghaemi et al.*, 1999; *Sahandi*, 1993). Fault mapping results from this study based on SPOT5 and LANDSAT images. (b) 3d-view of the MTZ showing the general morphology, major fault traces, and Mesozoic paleo-relief (based on SRTM digital topographic data). (c) Topographic profile through the MTZ between A and B on (b). Localities: AG, Aghush; AS, Asheq-Abad; CK, Chakaneh; FH, Farhadan; GM, Golmeym; KD, Kalidar; KR, Kallar; YM, Yarimja Mountain; ADP and BP, Allah Dagh and Binalud paleo-reliefs, respectively; other abbreviations like Figure 1.

*Khan-Nazer*, 2000). Regardless some small volcanic domes and dikes, almost all the volcanic activity was concentrated in the northern part of the Meshkan triangle (Figure 2).

According to geological and geomorphic observations, the Late Cenozoic deformation within the MTZ has been mainly accommodated by three major fault systems, *i.e.*, the Chakaneh, Farhadan, and Meshkan fault systems (section 3) (Figure 1). The interior of the Meshkan triangle was affected by sparse and distributed faults with maximum segment lengths of about 15 km (Figure 2). Occupying narrow and linear valleys, these faults have straight traces cross-cutting the topography, indicating steeply dipping fault segments. Considering the geometry and orientation of these structures, the Chakaneh and Farhadan fault systems are the best possible candidates to transfer the northward motion of Central Iran to the Kopeh Dagh Mountains. Hereafter, we present detailed structural and geomorphic characteristics for these faults, providing evidence for the transferred northward motion of Central Iran beyond the Binalud Mountains.

## 3. Cenozoic faulting in the Meshkan Transfer Zone

In comparison with the adjacent structural domains, the particular geological configuration of the MTZ suggests a complex history of Cenozoic deformation on the boundary fault systems. There is clear evidence for at least two distinct periods of deformation along the fault systems during Cenozoic: (1) An initial fault movement normal to the fault strike, *i.e.*, major component being vertical, creating and then, controlling the margins of the Meshkan Eocene sedimentary basin, (2) the present-day strike-slip movements affecting post-Miocene fold and thrust structures of the MTZ.

There is a striking contrast between Cenozoic rocks on opposite sides of the Chakaneh and Farhadan fault systems. To the north and east are Middle Jurassic-Early Cretaceous marine carbonate rocks while in the central part, are middle Eocene and early Miocene shallow marine to continental sedimentary rocks (Figure 2). This domain has been affected by Late Cenozoic (Miocene to Quaternary) volcanic activities as testified by dike and volcanic domes. The lack of Eocene sedimentation on the surrounding regions indicates direct structural control of the Farhadan and Chakaneh fault systems on the post-Paleocene evolution of the MTZ sedimentary basin. The total vertical slip of the earlier movements along the fault systems is unknown; no rocks of post-Mesozoic have been matched across the fault systems. In the Meshkan triangle, the Mesozoic rocks are overlain by more than 2000 m of Eocene-Oligocene stratified rocks. These strata have no counterpart along the eastern or

northern side of the Chakaneh and Farhadan fault systems, respectively (Figure 2). On the other hand, the present-day average topographic level of reliefs within the MTZ is about 900 m under the Binalud and Allah Dagh Mesozoic highlands level (Figure 2). Therefore, if the earlier movement was normal to the fault traces, a minimum vertical displacement of ~2900 m is necessary.

The inception of fault activity along the Chakaneh and Farhadan fault systems may be suggested in the early Cenozoic, but the general history of movement on those fault systems remains unknown. Nevertheless, there is conspicuous geomorphic and geological evidence for active strike-slip faulting along the two fault systems (next sections). Slip vectors on major and minor fault planes within Plio-Quaternary deposits confirm the Late Cenozoic strike-slip tectonic regime (sections 6).

### 3.1. The Chakaneh Fault system

The 76-km-long Chakaneh Fault system runs southward from Kallar village (14 km south of Quchan), to the Uqay-Gach gypsum quarry (19 km northwest of Neyshabur) (Figure 3). It cuts Plio-Quaternary volcanic rocks and lies along the eastern boundary of the Eocene sedimentary basin against the Late Cretaceous highlands (Figures 2 and 3). The fault system is a complex, Z-shaped structure that consists of at least three distinct fault segments or fault zones (Figure 3) separated by relatively large (up to 15-km-long and 3-km-wide), and intensely sheared relay zones (Figure 3). Late Cenozoic strike-slip movement along the Chakaneh Fault system is recorded by reorientation and/or displacement of preexisting geological structures (*e.g.*, fold axes, stratigraphic contacts as well as volcanic domes) and geomorphic features such as drainage systems, linear crests and alluvial fans within the fault zones. They are significantly rearranged within several hundred-to-thousand meters of the fault zone and particularly within the relay zones (Figures 3).

Detailed geological mapping on SPOT5 satellite images provides convincing evidence for large cumulative strike-slip offsets along the Chakaneh Fault system. Along the Dâmanjan fault segment (Figure 4), folded volcano-sedimentary layered rocks of Cenozoic age show a right-lateral cumulative displacement of 3.8±0.4 km. Total right-lateral cumulative offset along the entire fault zone reaches a sum of 5.8±0.8 km recorded by different stratigraphic markers offset by three fault strands (Figure 4). On both sides of the Dâmanjan fault, equivalent geological units are roughly at the same elevation, suggesting negligible (<3 per cent) coeval vertical component of displacement on the fault, *i.e.*, nearly pure strike-slip

faulting (Figure 4). The inception date of dextral strike-slip faulting along the Chakaneh Fault system can be deduced using stratigraphic ages of the offset geological units. In the southern part of the fault zone, upper Eocene layers are thrusted over Miocene rocks, deforming gently

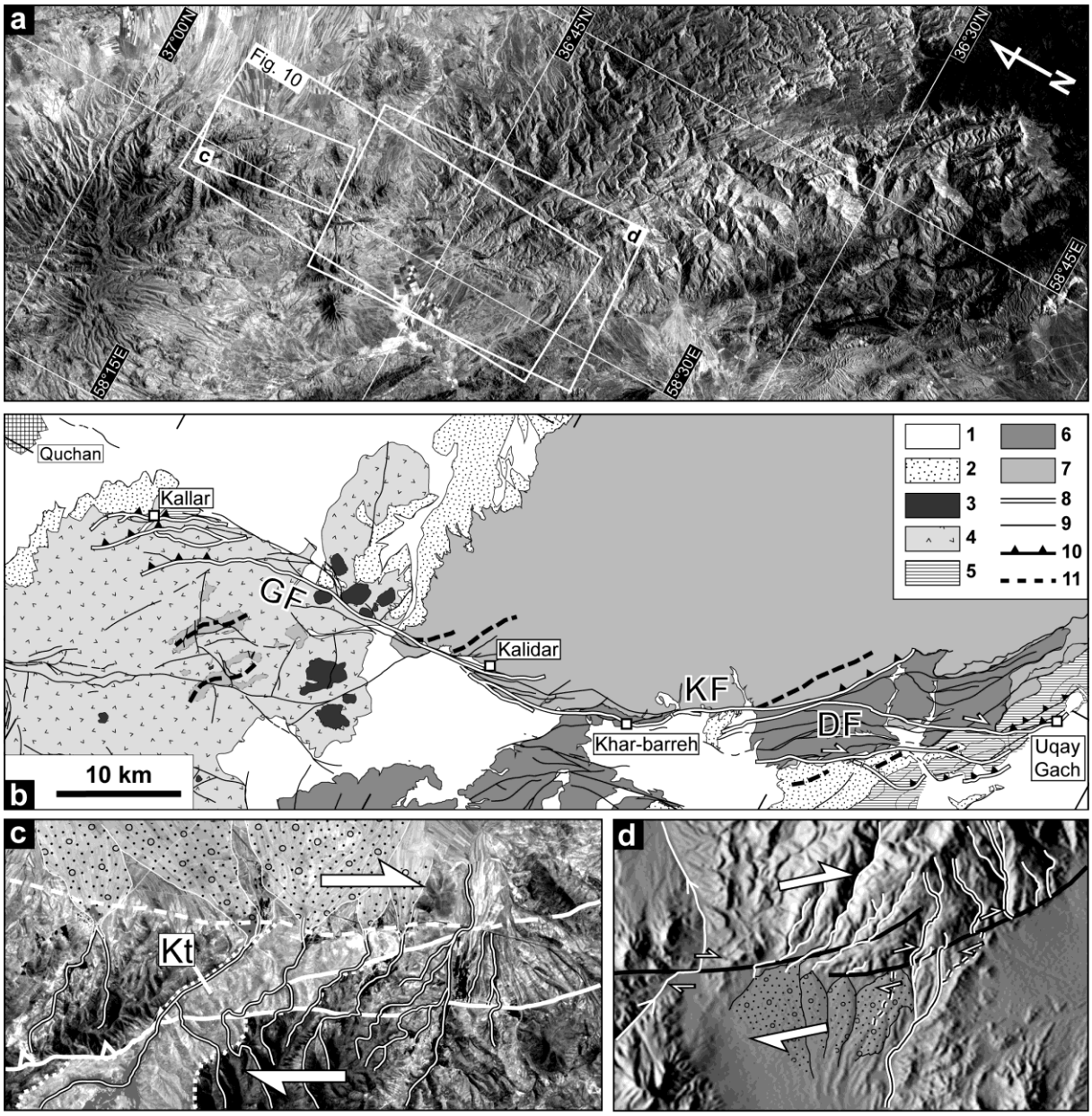


Figure 3. (a) SPOT5 image of the Chakaneh Fault system. (b) Geological map of the area in inset "a" showing the detailed geometry, fault segments and their relay zones. DF, Dâmanjan Fault; GF, Golmeym Fault; KF, Khar-Barreh Fault. 1, Quaternary deposits; 2, Pliocene conglomerates; 3, Plio-Quaternary volcanic domes; 4, Plio-Quaternary pyroclastics; 5, Miocene marl and sandstones; 6, Eocene volcaniclastics; 7. Mesozoic carbonates; 8, Major Quaternary fault segments of the Chakaneh Fault system; 9, Non-classified fault; 10, Reverse fault; 11, Fold axis. (c) SPOT5 image centered on the Golmeym Fault termination indicating right-lateral offsets in a Cretaceous limestone (Kt) and Plio-Quaternary drainage systems. (d) SRTM shaded image centered on the Kalidar region showing sheared or right-laterally offset markers such as drainages, ridge crests, and alluvial fans along and within the relay zone between the Golmeym and Khar-Barreh faults.

folded Plio-Quaternary conglomerates into an overturn synclinal fold structure (Figure 4). The thrust contact is right-laterally displaced by the eastern fault strand (A - A' piercing points in Figure 4). Along the central and western fault strands, the synclinal axis is displaced as approximately the same order as early Miocene rocks (Figure 4). Considering these geological relationships, one can conclude that right-lateral strike-slip faulting along the Chakaneh Fault system started during (not earlier than) Pliocene.

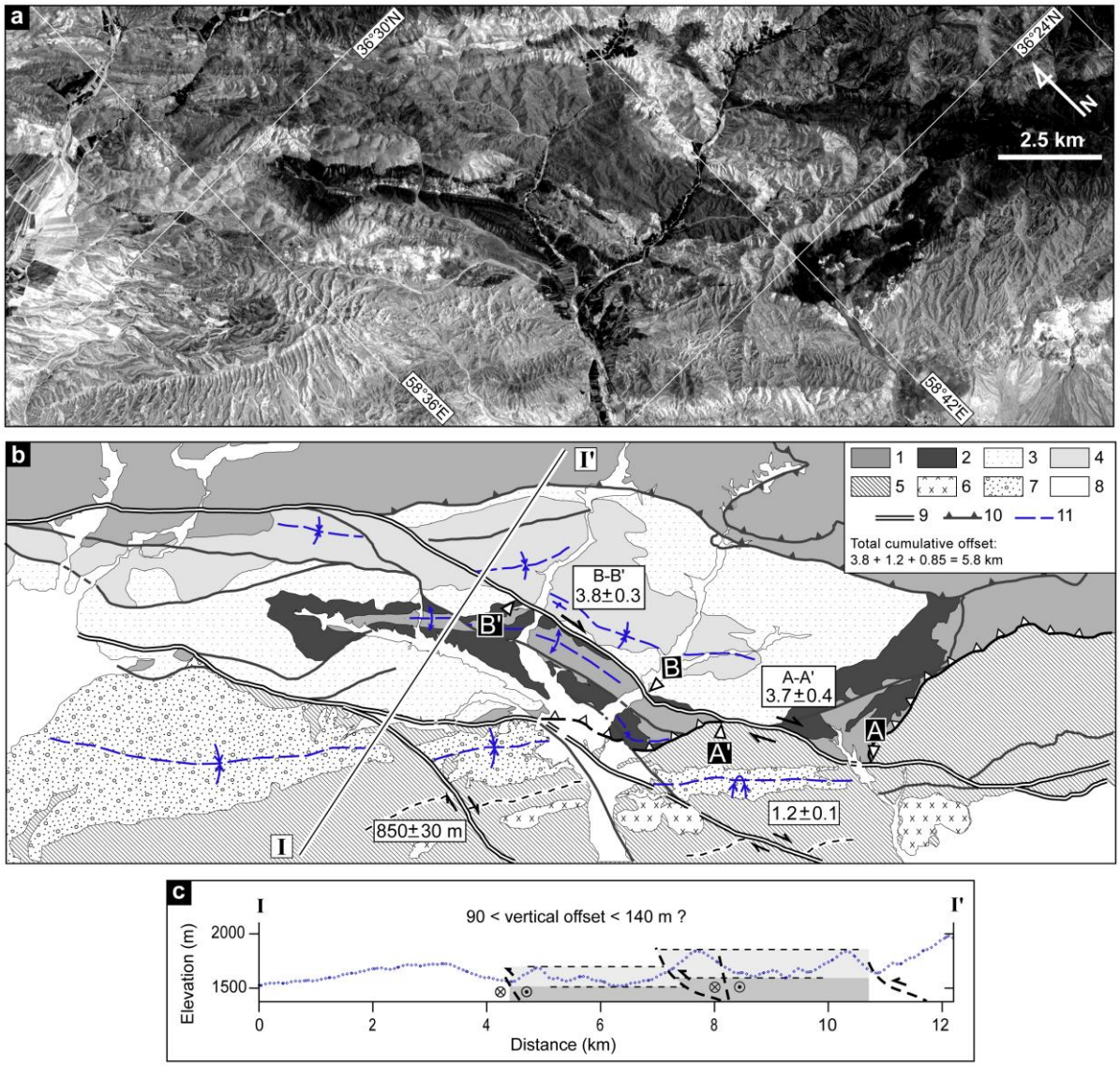


Figure 4. (a) SPOT5 image of the Dâmanjan region. (b) Detailed geological mapping based on (a) along the Dâmanjan Fault. Numbers within white rectangles are right-lateral offset values for each pair of successive piercing points (A-A', B-B') or stratigraphic features (thick-white lines); values are in kilometers. I - I' shows the location of topographic profile across the fault zone. 1, undifferentiated rocks (Mesozoic and early Eocene); 2, Volcanic rocks; 3, Marl and sandstones; 4. Conglomerates (2 to 4 are Eocene rock units); 5, Miocene and Pliocene rocks; 6, Post Miocene extrusive volcanic rocks; 7, Plio-Quaternary conglomerates; 8, Quaternary deposits; 9, Fault; 10, Thrust fault; 11, Fold axis. (c) Topographic profile across the fault zone on the basis of SRTM digital topographic data. Minimum and maximum topographic levels on both sides of the Dâmanjan fault are marked by colored polygons.

### 3.2. The Farhadan Fault system

The Farhadan Fault system runs along the northern boundary of the MTZ. This 65-km-long fault system extends west-southwest from 6 km east of Farhadan village to the village of Jahan in the southwest. In that area, the fault merges with the Esfarayen Fault (Figures 1 and 5). The Farhadan Fault system was partly mapped by *Amini and Khan-Nazer* (2000) and referred as the Bash Mahalleh Fault. In the present study, detailed mapping allow characterizing the whole fault system, which is referred to as the Farhadan Fault system. This fault system consists of two principal faults diverging westward (Figure 5). The eastern one extends on roughly 40 km to the west of Farhadan village, and ends into a thrust-bend termination zone (Figure 5). The western strand runs on ~25 km west from Aghush village, joining the Esfarayen Fault at the western end.

Late Cenozoic movement along the Farhadan Fault system is mainly strike-slip. Along most of its length, the Farhadan Fault system cuts through Quaternary features and provides convincing evidence for its Quaternary activity. The fault system is indicated by linear traces, deflected and beheaded streams, and obvious lithologic contrasts (Figures 5 and 6). Nearly continuous south-facing scarps in Quaternary deposits are observed along the main active fault trace. These scarps probably result from vertical component of displacement along the fault. Left-lateral offset streams, ridges, and rock units are representative for dominant strike-slip motions along the fault system. Around Aghush village, the oldest streams incised in Plio-Quaternary pyroclastic terrains indicate cumulative offset of 5.6±0.2 km along the Farhadan Fault system (Figure 6). In the same area, the restoration of total offset in upper Eocene volcanic units reveals a maximum cumulative displacement of 7.0±0.6 km along the fault. More to the west, the same order of displacement (7.5±0.5) is observed in stratigraphic contact between upper Miocene and Pliocene beds (Figure 5), indicating a Pliocene inception age for the left-lateral movement along the Farhadan Fault system.

### 3.3. The Sar’akhor Fault

South of Faruj, the SE trending Sar'akhor Fault cuts through the Sar’akhor Mountain (Kuh-e Sar’akhor) over a length of 34 km (Figures 1 and 7). The relatively straight fault trace is occupied by two linear valleys on both sides. The Farhadan Fault ends northeast intersecting the Sar'akhor Fault. North of the Sar’akhor Mountain, sharp fault traces underline segments that extend through Plio-Quaternary volcanic rocks parallel to the main trace of the fault (Figure 8). Conspicuous geomorphic features such as offset and/or perturbed drainage

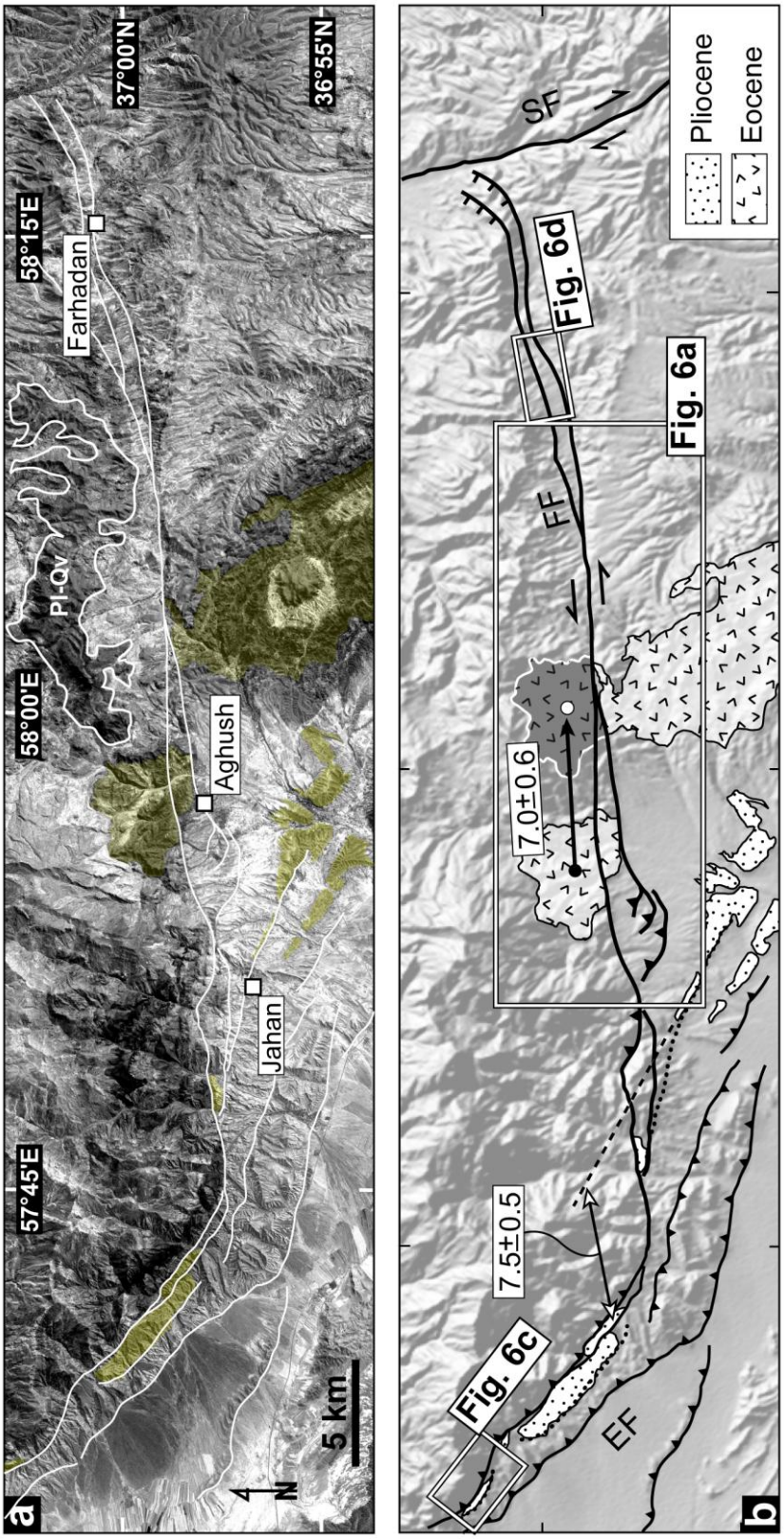


Figure 5. (a) LANDSAT image of the Farhadan Fault system (FF). (b) Simplified geological map of the area based on inset "a". It presents detailed 2D-geometry of the fault, left-lateral offsets of the folded bedrock and the structural relationships of the Farhadan Fault with Esfarayen (EF) and Sar'akhor (SF) faults. Offset values (within white rectangles) are in kilometres. The reconstructed form of Eocene unit is shown by the transparent polygon. The geological contact of Miocene marls and Pliocene conglomerates is shown as dotted line.

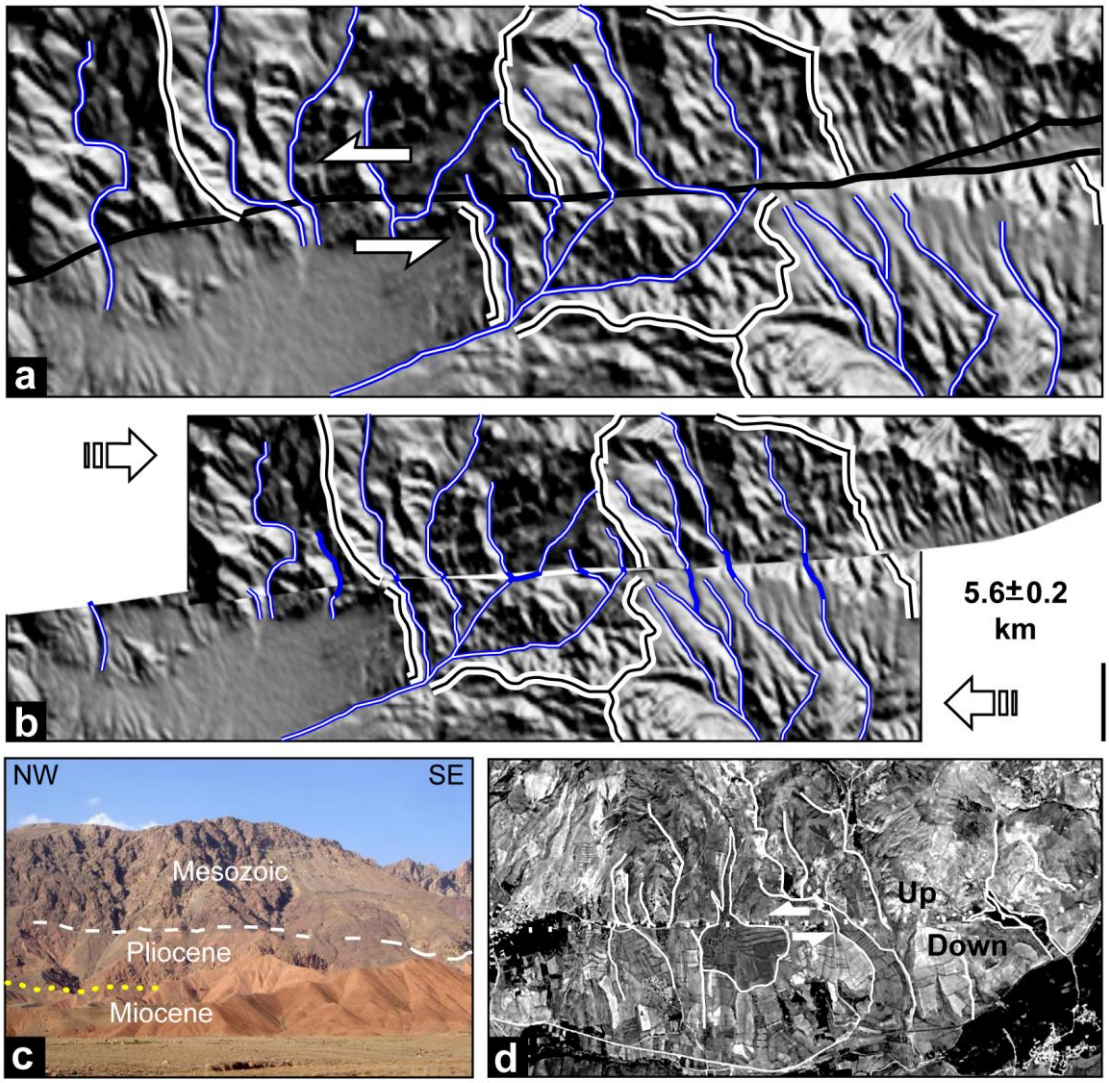


Figure 6. (a) and (b) Morphotectonic reconstruction of two drainage basins and their associated streams left-laterally offset along the fault trace; (a) before, and (b) after the reconstruction. (c) A field photograph showing that the Mesozoic limestone is thrust over the Pliocene conglomerate. Location of the photograph is marked on (Figure 5b). (d) SPOT5 image centered on the eastern segment of the Farhadan Fault system indicating deflected and/or beheaded streams, as well as left-laterally offset alluvium landforms (fan and bed streams).

basins, deflected gullies and streams as well as outcrop-scale knick points represent right-lateral strike-slip fault displacements ranging from 80 to 900 m along the fault traces (Figure 8). Even if the main fault trace is relatively obvious on digital topography and satellite images, the morphologies associated to the fault are relatively degraded and weakly preserved due to erosion and a long human activity. This effect is even more severe along the northwest mid-length of the fault than its southeastern end. However, the preserved fault morphology along the central and southeastern parts provides evidence for the mechanism and amount of cumulative fault displacement. Close to its southeastern termination, the Sar'akhor Fault offsets a ~9-km-long anticline near Asheq-Abad village (Figure 7). The anticline is

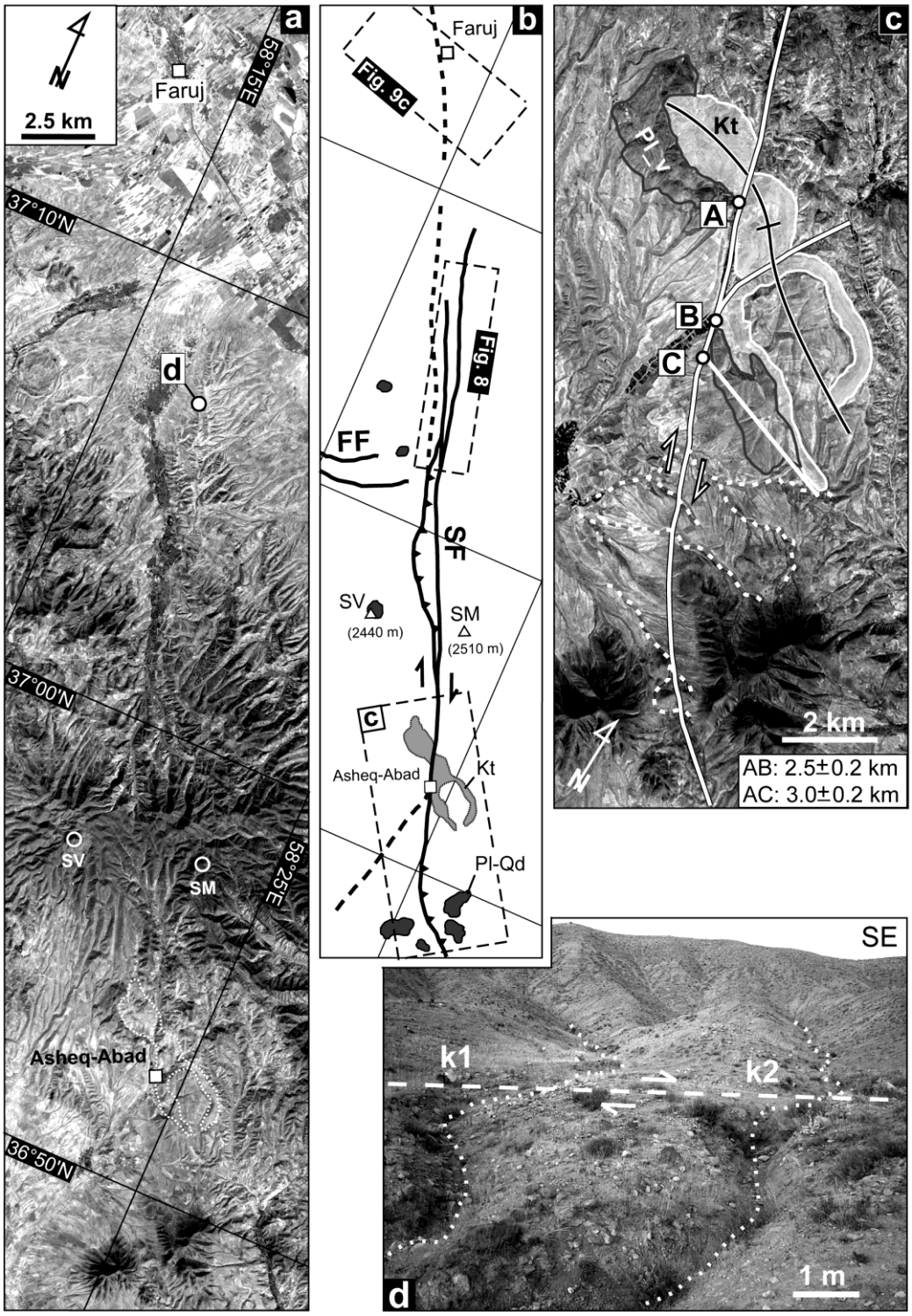


Figure 7. (a) SPOT5 image of the Sar'akhor Mountain (SM). SF, Sar'akhor Fault; SV, Sar'akhor volcano. The inferred continuation of the Baghan and Sar'akhor faults is marked by black dotted line. (b) Morphotectonic map of the Sar'akhor fault based on inset "a". (c) SPOT5 image of the Asheq-Abad anticline deformed along the Sar'akhor Fault (double, white line). Double, black line presents anticline axis and dotted lines are drainages deflected along the fault trace. A, B and C are the piercing points used for offset measurements. Kt, Cretaceous limestone; Pl-v, Plio-Quaternary lava. (d) Field photograph of two right-laterally deflected gullies and associated knick points (K1 and K2) along the northeastern Quaternary trace of the Sar'akhor Fault. Location of the photograph is marked on inset "a". Note that insets "a" and "b" have the same frame.

constituted by Cretaceous limestone (Tirgan formation) and is surrounded by Plio-Quaternary lavas. The assemblage is right-laterally displaced of 2.7±0.3 km by the Sar'akhor Fault (Figure 7). Despite, there is no clear geological evidence for coeval vertical fault displacement; it can be estimated using geometric reconstruction of the conic-shaped Sar'akhor Mountain morphology. Considering the present day shape of the Sar'akhor volcano (Figure 9), one can assume that volcanic materials sourced from the volcano were distributed on a uniform slope around the Sar'akhor Mountain. Accepting this assumption, vertical offset can be estimated through a restoration of the topography affected by the fault. Figure 9 presents topographic contour maps of the Sar'akhor Mountain before and after the restoration. The present-day topographic contours of the Sar'akhor Mountain show obvious apparent offsets along the Sar'akhor Fault. The offsets are opposite at the two fault ends, and the surface of each given topographic level on the northeastern side of the fault is waster than its equivalent on the southwestern side (Figure 9). Theoretically, this feature can be described as differential vertical displacement across a dissected conic- or dome-shaped structure, which is consistent with the rounded geometry of the Sar'akhor Mountain (Figure 9). Therefore, the amount of vertical displacement can be estimated by numeric restoration of each virtually displaced contours area achieving the initial conic-form of the mountain. Such a topographic reconstruction reveals an upward vertical displacement of about 110 m for the northeastern side (block) of the Sar'akhor Fault (Figure 9), that is to say less than 5 per cent of its cumulative lateral offset (~2.5 km).

To the northwest, the Sar'akhor Fault surface expression disappears 10 km southeast of Faruj city, in south flank of the Atrak valley (Figure 1). The morphology of the valley has been reworked by human activities and there is not preserved geomorphic evidence for the continuation of the fault across the valley. The other side of the valley is affected by the Baghan and Quchan faults, which are the major strike-slip faults of the Kopeh Dagh (*e.g.*, *Afshar Harb*, 1979; *Hollingsworth et al*., 2006; *Shabanian et al*., 2009; *Tchalenko*, 1975). The Baghan and Quchan faults start 15 and 7 km north of the northern termination of the Sar'akhor Fault, respectively (Figure 1). Even though subtle geomorphic features have been proposed by *Hollingsworth et al*. (2006), as evidences of their thrust-bend termination in the Atrak Valley, the southern end of the Baghan and Quchan faults remains unclear. A meticulous analysis of SRTM digital topographic data and SPOT5 image reveals a delicate right-lateral geomorphic offset, where a NE trending hill (Neogene marls) appears to be affected by the inferred continuation of the Baghan and/or Sar'akhor fault trace crossing the Atrak valley (Figure 9). All together, the geological and geomorphic observations lead us

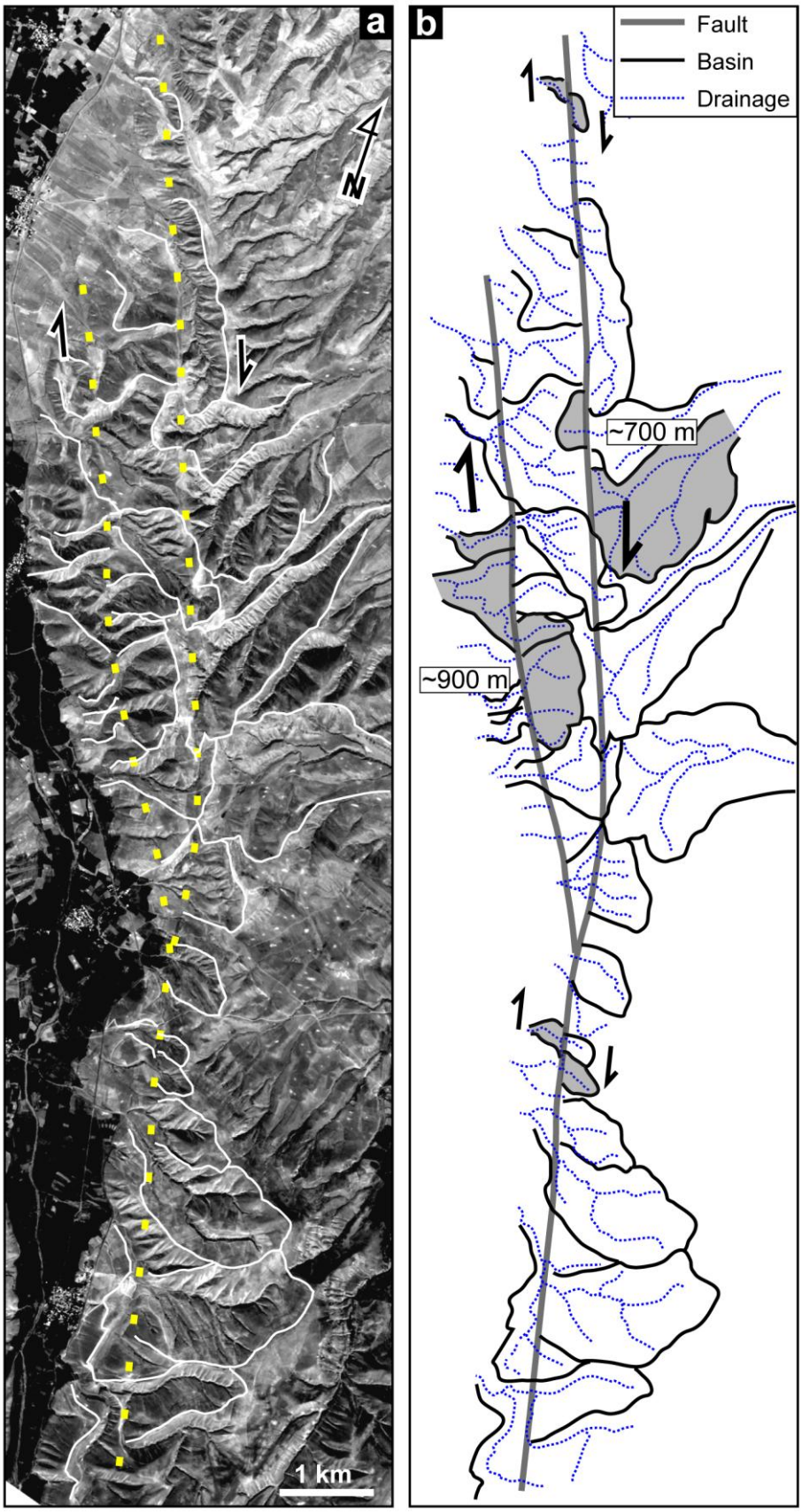


Figure 8. (a) SPOT5 image of the Sar'akhor Quaternary fault traces (yellow, dotted line). (b) Morphotectonic map of drainage systems (drainage basins and streams) affected by the Sar'akhor Fault (based on inset "a"). Rectangles show the values of possible right-lateral offsets deduced from dissected basins (gray polygons).

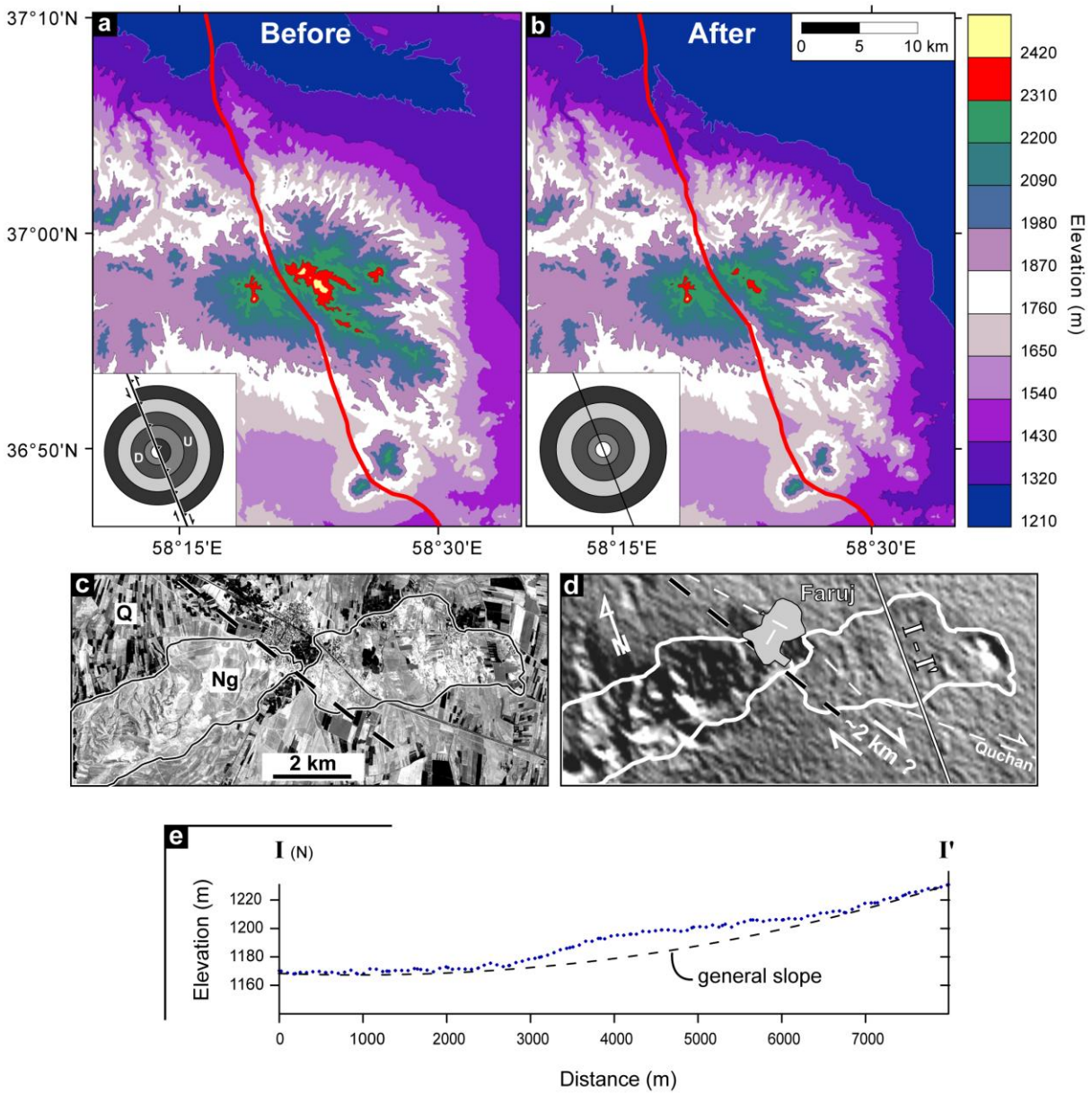


Figure 9. Topographic restoration of vertical displacements recorded by the Sar'akhor volcano. (SRTM data); (a) before, and (b) after the reconstruction. A simple geometric model is presented in the lower left corner of each image. (c) SPOT5 image centered on a right-lateral offset along the inferred continuation of the Baghan Fault (black, dotted line), within the Atrak valley. Ng and Q are the Neogene and Quaternary deposits, respectively. (d) SRTM shaded image of the same area as (c). (e) A topographic profile (I-I' on "d") showing morphology of the affected hill on eastern fault block. See Figures 2 and 7 for location of (a) and (c), respectively.

interpreting the Sar'akhor Fault as a possible candidate for the southern extension of the Baghan Fault beyond the Atrak valley.

## 4. Morphotectonic investigations along the Chakaneh Fault system

The geomorphic expression of strike-slip faulting on the Chakaneh Fault system is characterized by conspicuously offset landforms such as drainage systems, linear crests and alluvial fans. Around the village of Kalidar, valleys show systematic dextral offsets of about

2 km along the relay zone between the northern (Golmeym) and central (Khar-Barreh) fault segments (Figure 10). The streams are deflected parallel to shutter ridges within and along the fault zone forming trapped alluvial basins behind shutter ridges (Figure 10). A key site is selected along the Golmeym Fault, between Golmeym village and Chakaneh city. In that area, the Golmeym Fault splays northwardly to several fault strands forming a 1500-m-wide fault zone. Along the main strand of the fault, several streams indicate systematic right-lateral offsets of 1400 ±50m, while the Chakaneh River shows a maximum geomorphic offset of 1600±200 m (Figure 10). These offset values are lower than the observed offsets more to the south, in the Kalidar region (Figure 10), indicating the northward diminution of displacement along the Chakaneh Fault system. Despite abundant offset markers over whole length of the fault, there are a few landforms providing both geomorphic feature offset and absolute dating possibilities. For instance, along the Golmeym River, surface exposure dating using *in situ*-produced cosmogenic $^{10}$Be was unsuccessful due to intense erosion of the surface. However, a typical landform is found north of Chakaneh city where, the Golmeym Fault runs through volcanic dome structures. In this area, the fault right-laterally displaces a dacitic dome (Figures 10 and 11). This is one of the rare geomorphic features providing favorable conditions for both landform dating ($^{40}$Ar/$^{39}$Ar) and cumulative offset measurements (next section).

### 4.1. Cumulative offset recorded by the volcanic dome

North of Chakaneh city, a series of volcanic structures comprising of distinct dacitic domes is affected by the Golmeym Fault. The domes are elliptical in shape, with NW trending elongated axis. The largest one is clearly truncated and right-laterally offset by the fault (Figure 11). To avoid misinterpreting two distinct volcanic domes as a truncated structure, dependency of the domes (suggested to be parts of the same structure) was examined by combined geomorphic and structural analysis complemented by $^{40}$Ar/$^{39}$Ar dating (section 5).

During extrusion process, older layered rocks (Cretaceous limestones) are pierced by the lava dome tilting them over to create a clear stratified boundary around the volcanic masses. This boundary is also cut and displaced along the fault (Figures 11 and 12) indicating that the two volcanic masses were formerly a single dome structure. Confirming our assertion, we verified consistency of the internal structure of the lava dome in the field. Thermal cracks develop perpendicularly to the isothermal surfaces and to the external surfaces in contact with air and wall rocks. The orientation of the columns relates to the cooling history of the mass.

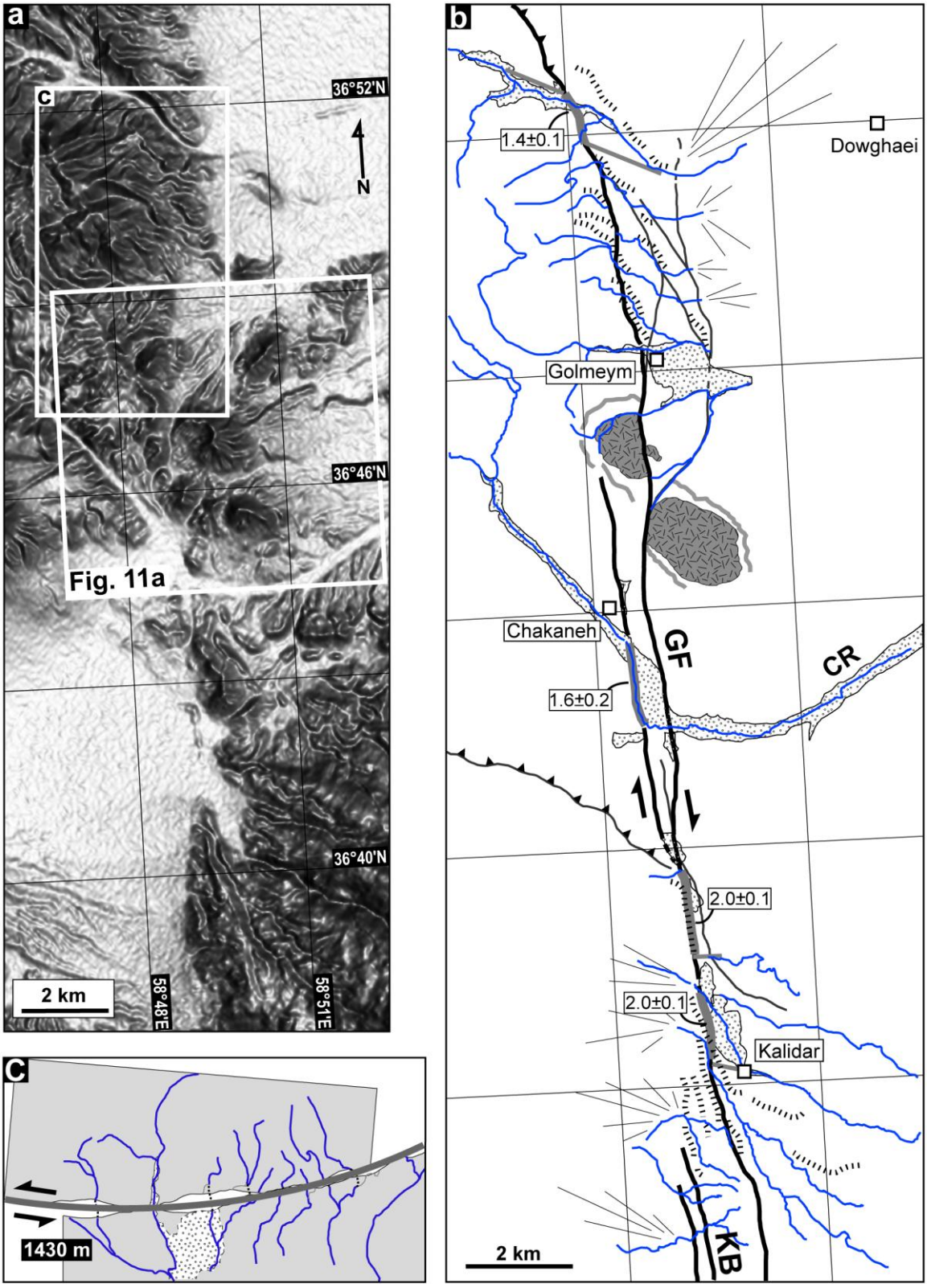


Figure 10. (a) SRTM shaded image of the Golmeym Fault. (b) Morphotectonic map of the Golmeym Fault based on SPOT5 images presenting major fault segment traces (thick, black line), minor faults (thin, black line), deflected drainages (thin, blue line), shutter ridges (thick, dotted line), trapped alluvial basins and bed streams (dotted polygon), and a right-laterally offset volcanic dome (gray polygon). Gray lines show external limit of the tilted strata around the dome. Offset values are expressed in kilometers. CR, Chakaneh River. (c) Final reconstruction of drainage systems deflected along the Golmeym Fault. Note that (a) and (b) have the same frame.

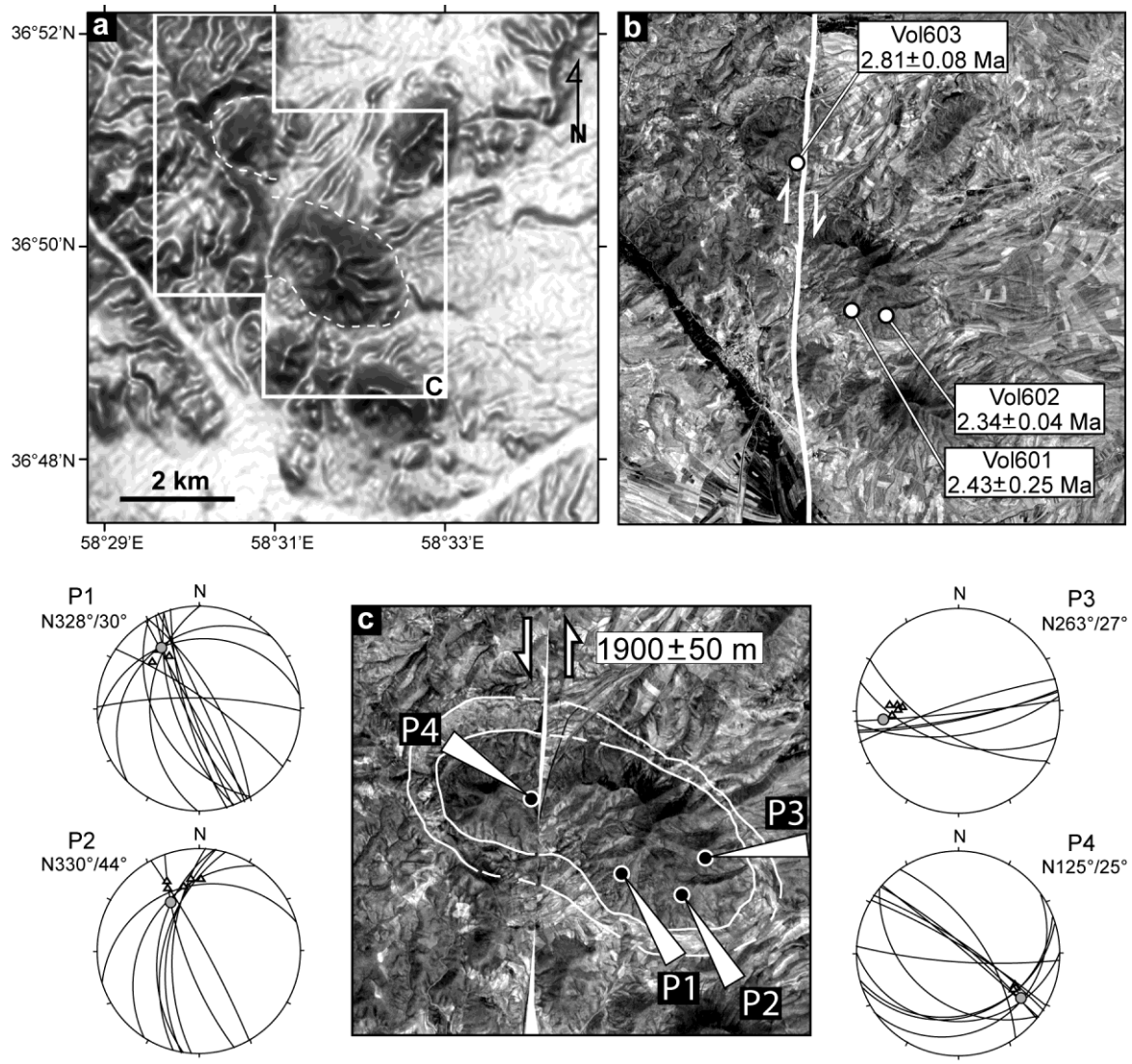


Figure 11. SRTM Shaded (a) and SPOT5 (b) images of the volcanic dome offset along the Golmeym Fault (white line). Names and location of samples as well as their associated radiometric ($^{40}Ar/^{39}Ar$) ages are marked on inset "b". (c) The initial form of the dome after the fault offset restoration. The frame of this figure (before reconstruction) is presented in inset "a". P1 to P4 are average axes of the lava columns measured on the field that pointed in the axis plunge directions. Stereograms represent Smith projection of the measured geometry of cooling features developed in the dome: β-axis (circle) and column axis (triangles).

When viscous dacitic or rhyolitic magmas are extruded, they form a cumulo dome. A section across a lava dome would have a concentric, onion-like structure with radiating columnar joints. In a reconstitution model, two separates blocks of a single dome must fit geometrically. Structural analysis of the orientation of column axes and associated columnar joints was down using measured geometric data at four localities on the offset domes, both sides of the fault (Figure 11). The centre-ward converging column pattern in the main body of the volcanic dome was examined at three localities selected on different sides of the southern dome segment. The fourth one was chosen on the free-face side of the northern segment that

is suggested to be a transversal section along the Golmeym Fault exposing the internal structure of the volcanic dome. The measured data in each site are plotted on separate stereograms (Figure 11) in which, the column orientation is independently indicated by both intersection of the columnar joint planes (β-diagram axis) and column axes directly measured in the field. In stereograms, similar geometry for both the β-diagram and column axes demonstrates that the measured structural data can be confidently considered as igneous columnar features and not tectonic jointing (Figure 11). The centre-ward converging column pattern of the southern dome segment is deduced from the three first stereograms. The fourth one has inappropriate (centre-ward diverging) orientation with respect to the northern dome geometry, when assuming it an individual structure. Restoring the initial dome shape (Figure 11), the four positions show a converging pattern of the cooling columns toward the initial dome centre. This observation reveals that the two segments belong to a single lava dome displaced by the Golmeym Fault and their offset is representative for the cumulative post intrusion fault displacement. The reconstruction of former dome shape shows a cumulative right-lateral offset of 1900±50 m along the Golmeym Fault (Figure 11).

## 5. $^{40}Ar/^{39}Ar$ dating

### 5.1. Sampling and analytical procedure

Three rock samples were collected from the two isolated parts of the offset dacitic dome (section 4). The sample localities and their characteristics are presented in Figure 11 and Table 2. The samples were collected from the less weathered parts of the lava masses. Detail analytical results and sample treatment procedure are presented in Appendix A.

### 5.2. Dating result

Sample VOL601 gives a broadly saddle-shaped age spectra with the lowest ages ranging from 2.17 to 2.55 Ma (Table 1, Figure 12). The fairly strong heterogeneity in the age spectra as well as in the inverse isochron plot suggests excess argon. The low-age steps encompass most of the $^{39}Ar$ released and low chlorine content as shown by the K/Ca and Cl/K proxy plots. The total fusion age of 3.08±0.04 Ma is a maximum while a simple average of those low-age steps at 2.43±0.25 Ma is probably close to the correct age.

Sample VOL602 shows a fairly flat age spectra from which a plateau age of 2.34± 0.04 Ma is extracted on more than 80 per cent of the total $^{39}Ar$ released from the steps with

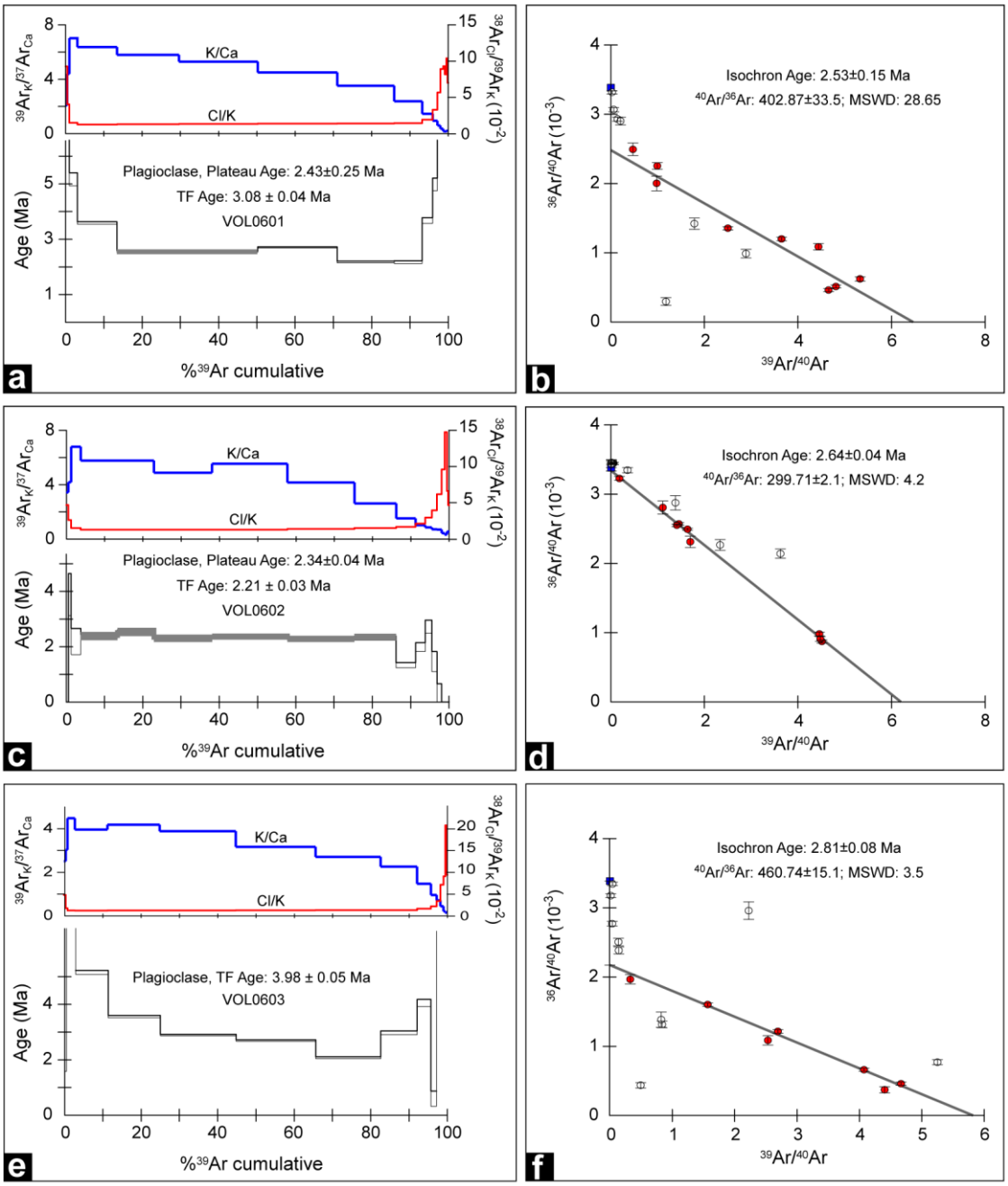


Figure 12. The $^{40}Ar/^{39}Ar$ step-heating results from the offset volcanic dome. Sample names are marked middle of the right hand diagrams. See Figure 11 for sample locations.

highest K and lowest chlorine content. The younger total fusion age is dominated by the low ages at the end of the spectra and is non reliable while the isochron yields a slightly older age of 2.64±0.04 Ma with a MSWD of 4.2 implying scatter above the individual errors. The plateau value is preferred (Figure 12).

Sample VOL603 show a broad saddle-shape age spectra with only one step of minimum age at ca 2.1 Ma (Figure 12). The total fusion age of 3.98±0.05 Ma is clearly a maximum and the isochron age of 2.81±0.08 Ma clearly indicates excess argon ($^{40}Ar/^{36}Ar$ of 461) with a

MSWD of 3.5 which suggest that some scatter remains because excess argon has not been completely resolved through the inverse isochron approach. The inverse isochron age is taken as the best estimate but probably slightly in excess of the real age.

The three samples gives ages at 2.43±0.25 Ma, 2.34±0.04 Ma and 2.81±0.08 Ma (Table 1, Figure 12), the first two being the most robust and indistinguishable within errors, the third being probably overestimated. This yields a robust estimate for the age of dome intrusion at ca 2.3-2.4 Ma, *i.e.*, ca 2.35±0.24 Ma when the age uncertainties are considered. The obtained age is used to calculate long-term slip rates along the MTZ strike-slip fault systems (section 7.2).

Table 1. Dating results from $^{40}Ar/^{39}Ar$ radiochronology for whole rock

| Sample | Longitude (°E) | Latitude (°N) | Total fusion age | Plateau Age (PA) or Simple Mean age (SMA) | Isochron age | $^{40}Ar/^{36}Ar$ | MSWD | Preferred age | Remark |
|---|---|---|---|---|---|---|---|---|---|
| VOL601 | 58,525 | 36,823 | 3.08 ±0.04 | 2.43 ± 0.25 (SMA) | - | - | - | 2.43 ± 0.25 | |
| VOL602 | 58,533 | 36,823 | 2.21 ± 0.03 | 2.34 ± 0.04 (PA) | 2.64 ± 0.04 | 300 | 4,2 | 2.34 ± 0.04 | |
| VOL603 | 58,516 | 36,844 | 3.98 ± 0.05 | - | 2.81 ± 0.08 | 461 | 3,5 | 2.81 ± 0.08 | Max. age |

Ages are given in Ma with their 1σ uncertainty. Max., maximum.

## 6. Modern stress state in the MTZ deduced from fault kinematics analyses

Fault population data consisting of fault planes and associated slip vectors (striations) were measured in eight localities distributed along the boundary faults (Figure 13). Fault kinematic analysis has been performed using a computer program derived from the numerical method of *Carey and Brunier* (1974), and *Carey* (1979). The inversion results include the orientation (azimuth and plunge) of the principal stress axes ($\sigma_1>\sigma_2>\sigma_3$) of computed stress tensors as well as the stress ellipsoid shape parameter R, defined as $R = (\sigma_2-\sigma_1)/(\sigma_3-\sigma_1)$, which describes relative stress magnitudes ranging from 0 to 1 (see *e.g.*, *Carey and Brunier*, 1974; *Mercier et al*., 1991; *Bellier and Zoback*, 1995, and references therein).

We analyzed the modern state of stress, using the youngest striae sets mostly measured in Plio-Pleistocene conglomerates (Figures 13 and 14, Table 2). Separation of distinct families of striations has been done on the basis of geological field data using relative chronology of the striations (crosscutting relationships) and their relationships with regional tectonic events. In all data sets, modern stress state is represented by NNE trending $\sigma_1$ ranging from N10°E to N50°E, and shows two distinct (compressional and strike-slip) stress deviators respecting structural setting of the fault slip data (Figures 13 and 14). In this context, the Chakaneh Fault system is characterized by a strike-slip stress regime. Applying the average N25°E trending horizontal $\sigma_1$ to the geometry of boundary fault systems implies dominant strike-slip faulting

along the Chakaneh and Farhadan fault systems, together with the Sar'akhor fault. Considering the fault orientations, the Chakaneh Fault system and the Sar'akhor fault are characterized by right-lateral and the Farhadan Fault system is characterized by left-lateral motions. The inversion results of the fault slip data are presented in Table 2.

The correlation between the youngest geomorphic expression of the inspected faults and relative chronology of the fault striations, suggests that the computed stress deviators (average N25°E trending $\sigma_1$) can confidently characterized the present-day stress state in the MTZ. This is consistent with the NE trending mean P-axis deduced from focal mechanisms of the rare earthquakes ($5 \geq M \geq 7$) that occurred in the region (Figure 13), as well as the average regional N32°E trending $\sigma_1$ stress axis computed from focal mechanisms inversion of moderate to large earthquakes in northeast Iran (*Zamani et al*., 2007).

Table 2. Results of stress tensor inversion for slip data representing Late Cenozoic stress regimes[a]

| Site | Longitude | Latitude | $\sigma_1$ | | $\sigma_2$ | | $\sigma_3$ | | *R* | *N* | Quality | Age |
|---|---|---|---|---|---|---|---|---|---|---|---|---|
| | (°E) | (°N) | Azim. | Dip | Azim. | Dip | Azim. | Dip | | | | (Formation) |
| 1 | 58,518 | 36,869 | 10 | 17 | 245 | 63 | 107 | 21 | 0,86 | 18 | A | Quaternary |
| 2 | 58,529 | 36,891 | 30 | 1 | 255 | 89 | 120 | 1 | 0,64 | 8 | B | Pl-Q |
| 3 | 58,513 | 36,824 | 44 | 2 | 141 | 71 | 314 | 18 | 0,88 | 14 | A | Cretaceous |
| 4 | 58,515 | 36,724 | 35 | 11 | 187 | 77 | 303 | 6 | 0,46 | 22 | A | Cretaceous |
| 5 | 58,863 | 36,272 | 176 | 11 | 48 | 73 | 268 | 13 | 0,76 | 12 | B | Quaternary |
| 6 | 58,627 | 36,383 | 210 | 1 | 101 | 87 | 300 | 3 | 0,71 | 23 | A | Pl-Q |
| 7 | 57,830 | 36,902 | 25 | 2 | 294 | 22 | 120 | 68 | 0,87 | 19 | A | Quaternary |
| 8 | 57,651 | 36,942 | 208 | 9 | 299 | 8 | 71 | 78 | 0,99 | 17 | A | Quaternary |

Table 2b. Focal mechanisms information[b]

| Ref. no. | Date | Longitude | Latitude | Depth | M | Nodal plane 1 | | | Nodal plane 2 | | | Source |
|---|---|---|---|---|---|---|---|---|---|---|---|---|
| | | (°E) | (°N) | (km) | (mb) | Azim. | Dip | Pit | Azim. | Dip | Pit | |
| 9 | 19690103 | 57,9 | 37,13 | 11 | 5,6 | 132 | 60°S | 85°W | 142 | 30°E | 81°N | M |
| 10 | 19840706 | 58,33 | 36,56 | 10 | 4,8 | 87 | 64°N | 29°E | 163 | 64°W | 29°S | MOS |

[a]Numbers refer to Figures 13 and 14. The used inversion method (*e.g.*, Carey, 1979) assumes that the slip represented by the striation (s) occurs in the direction of the resolved shear. Deviatoric principal stress axes: $\sigma_1$, $\sigma_2$, $\sigma_3$, are the compressional, intermediate and extensional deviatoric axes, respectively. $R = (\sigma_2 - \sigma_1) / (\sigma_3 - \sigma_1)$, is the stress ratio of the deviatoric stress tensor, a linear quantity describing relative stress magnitudes. Ages are reported from the geological map cited in text; Azim., azimuth; *N*, number of fault slip pairs considered for stress calculation; quality: A, excellent, B, good.

[b]Focal mechanisms used for P-axis directions presented in Figure 13. Date (yyyymmdd) follows usual convention and all angles are in degrees. Magnitudes of earthquakes (M) determined using body waves forms. For each focal mechanism, the two nodal planes are characterized by azimuth (Azim.), dip (dip), and pitch (pit) of the inferred motion vector. The last column refers to the source of focal mechanism: M, *McKenzie* (1972); Mos, *Mostriouk and Petrov* (1994).

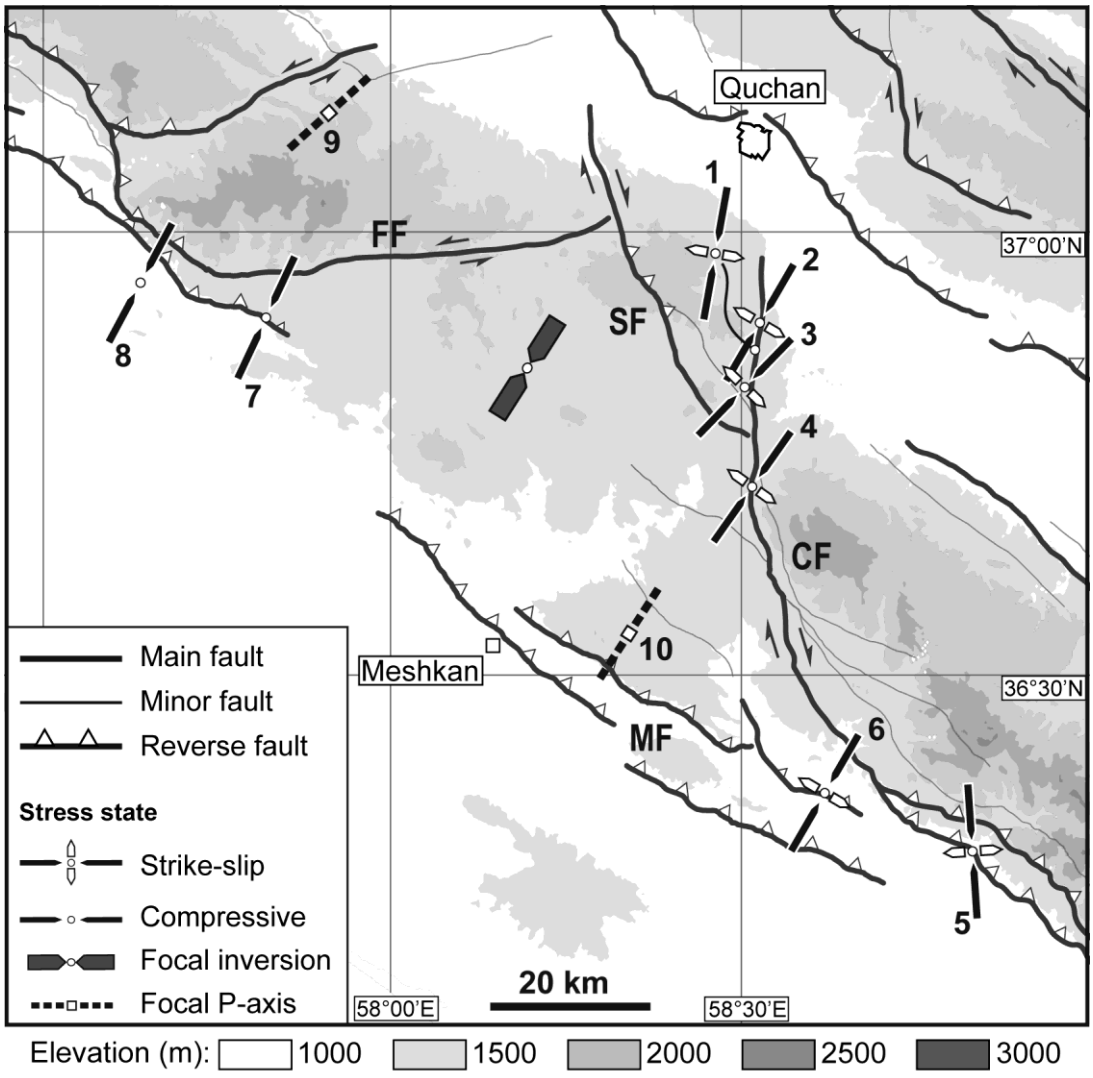


Figure 13. Azimuths of $\sigma_1$ (maximum stress axis) for the strike-slip and compressional stress regimes deduced from the individual fault slip inversions given in Table 2 and Figure 14.

## 7. Summary and discussion

As presented above, major fault segments in the MTZ have been mapped at the regional scale, with the objective to recognize their structural and geomorphic characteristics. At the site scale, analyses of SPOT5 images combined with direct field observations were used to quantify cumulative offsets along the newly recognized active faults. In this context, the Chakaneh and Farhadan fault systems and the Sar'akhor fault were characterized (section 3) as the principal right-lateral (Chakaneh Fault system and Sar'akhor Fault), and left-lateral (Farhadan Fault system) strike-slip structures in the MTZ. Our geological and geomorphic investigations reveal large cumulative lateral offsets (5-8 km) along the Farhadan and Chakaneh fault systems. The same offset amounts recorded by the Eocene and Pliocene

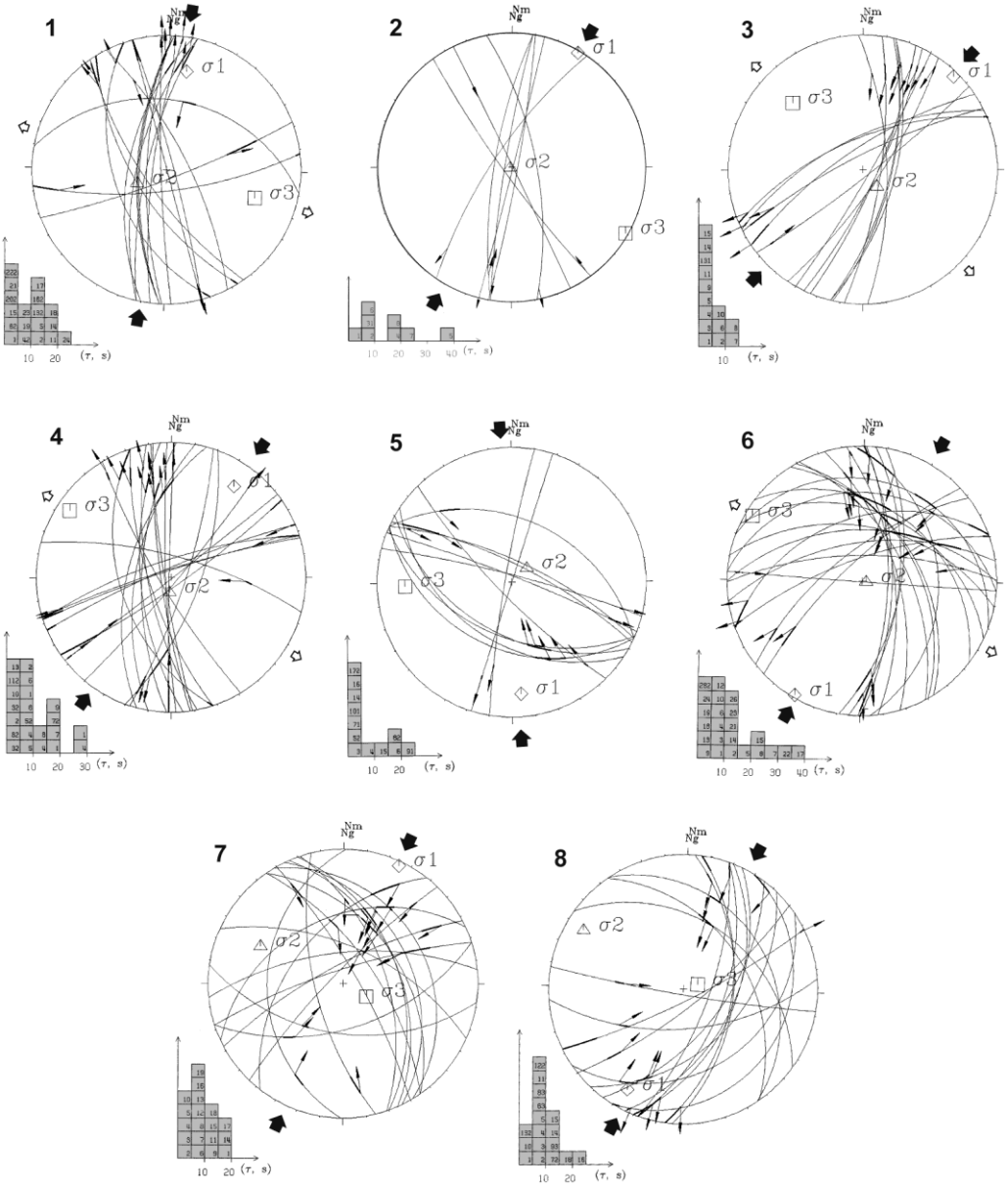


Figure 14. Lower hemisphere stereograms of fault slip data from the MTZ together with inversion results presented in Table 2. Numbers refer to site names marked in Figure 13, and in Table 2. Individual fault planes and measured slip vectors (arrows on fault planes) at each site are plotted. Large arrows outside stereograms represent the azimuth of $\sigma_1$. Histograms show distribution of deviation angles between the measured and calculated slip vectors (*e.g., Bellier and Zoback,* 1995).

geological units indicate that strike-slip faulting should not be starting before Pliocene. All together, the presented results in this paper provide evidence for considerable strike slip faulting through the MTZ since ~5 Ma ago. The triangular arrangement of the MTZ boundary fault systems appears to be a selective combination of predominant fault trends of the Alborz, Kopeh Dagh and Central Iran. Indeed, the Farhadan and Meshkan fault systems were limited or even offset by NNW trending right-lateral faults, *i.e.*, the Chakaneh Fault system and

Sar'akhor fault. This crosscutting relationship is consistent with the major role of right-lateral faults within the structural pattern emplacement that is transferring part of the northward motion of Central Iran to the Kopeh Dagh. The Modern state of stress (section 6) is also in agreement with active strike-slip faulting along the Farhadan (left-lateral) and Chakaneh (right-lateral) Fault systems, and reverse faulting along the Meshkan Fault system at the boundaries of the MTZ.

### 7.1. Reassessment of the historical seismicity pattern in NE Iran

A long and detailed historical record of earthquakes in northeastern Iran spans over the last nine hundred years (*Tchalenko*, 1975; *Ambraseys and Melville*, 1982; *Berberian and Yeats*, 1999; *Berberian and Yeats*, 2001). In the Kopeh Dagh and Binalud mountain ranges, the relationship between seismicity and preexisting faults has already been discussed (*Tchalenko*, 1975; *Ambraseys and Melville*, 1982; *Berberian and Yeats*, 1999; *Berberian and Yeats*, 2001). Since the 12th century, NE Iran (Kopeh Dagh and Binalud) has experienced at least 12 large earthquakes, which, with magnitudes ranging from 6.5 to 7.5, almost all of them occurred in the vicinity of the major fault zones (Figure 15). These large earthquakes (Baghan earthquake: 1929; Quchan earthquakes: 1851(?), 1871-72, 1893(?), 1895; Neyshabur earthquakes: 1209, 1270, 1389, 1405) were directly assigned to the significant structures of the region such as the Baghan, Quchan and Neyshabur faults (*Tchalenko*, 1975; *Ambraseys and Melville*, 1982; *Berberian and Yeats*, 1999; *Berberian and Yeats*, 2001). However, the band of maximum destruction associated to these historical earthquakes appears to follow the trends of Quchan and Baghan faults connecting to the Neyshabur Fault system. Among the earthquakes assigned to the Quchan fault (*Tchalenko*, 1975; *Ambraseys and Melville*, 1982), the macroseismic regions associated to two earthquakes do not certainly correspond with the Quchan Fault trace (1851 and 1893 earthquakes). Noteworthy, such assignments were only based on the facts that the Quchan Fault is the major strike-slip fault in the region, and that there was no data indicating the active faulting through the macroseismic areas, *i.e.*, the MTZ. The documented faults in this paper give therefore new insights to re-interpret this historical seismicity. According to our data and observations, the Chakaneh Fault system and Sar'akhor Fault are the only main active faults in the maximum destruction regions of 1851 and 1893 earthquakes. Indeed, the fault traces correspond well to the well-defined extent of the maximum destruction regions (Figure 15). In such a case, the most reliable possibility is that the Chakaneh Fault system and Sar'akhor Fault have been reactivated during the respective

1851 and 1893 earthquakes. However, there is no evidence for coseismic rupture along the Chakaneh Fault system, associated to the 1851 earthquake (*Tchalenko*, 1975; *Ambraseys and Melville*, 1982). Nevertheless, our discussions with old villagers from Golmeym village revealed a sudden shut in discharge of the Golmeym spring (along the fault trace) as coseismic phenomenon during 1851 earthquake. Our interpretation implies, except two potentially related earthquakes (1833, 1895), that no macroseismic region can be directly assigned to the Quchan Fault (Figure 15). More precisely, there is no documented historical or instrumental seismicity along the most important active strike-slip fault of the Kopeh Dagh (*e.g.*, *Shabanian et al*, 2009). This fact brings into question the seismic behavior of the Quchan Fault and the recurrence interval of the large earthquakes in the Kopeh Dagh.

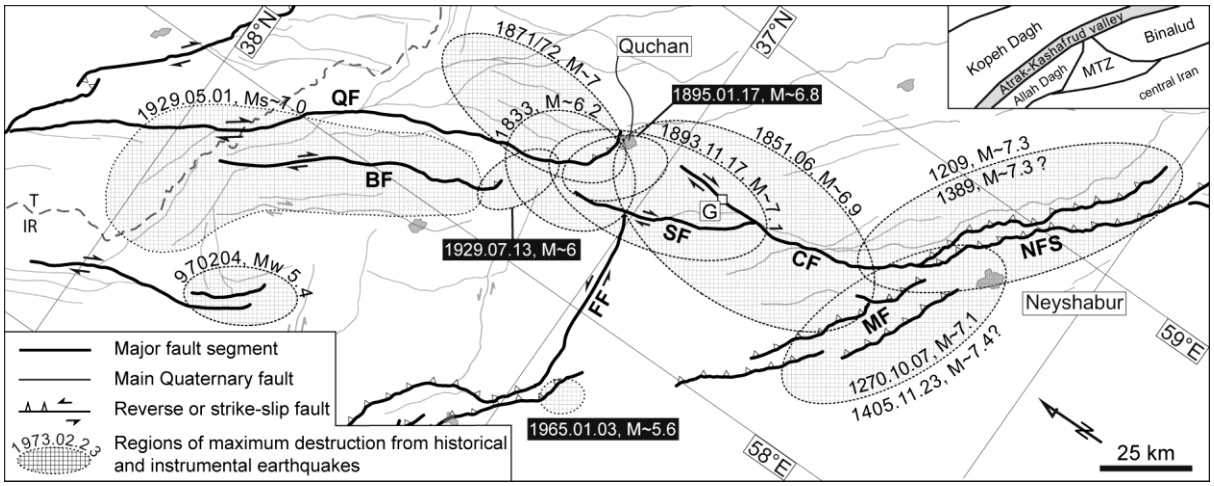


Figure 15. The regions of maximum destruction of earthquakes occurred in NE Iran. The isoseismal regions are based on *Ambraseys and Melville* (1982), *Berberian and Yeats* (1999) and *Tchalenko* (1975). Only one of the 4th February 1997 Garmkhan earthquake is from *Hollingsworth et al.* (2007). Upper right inset is a schematic map of different deformation domains covered by this figure. G, Golmeym village; IR, Iran; T, Turkmenistan; other abbreviations like Figure 1.

### 7.2. Long-term strike-slip rates in the MTZ

In this study, the slip rate estimates are based on the assumption that the fault slip rates remained constant since formation of the offset markers. Because the used time spans to evaluate the rates are large enough (2.5 to 5 Ma), the proposed slip rates are valid if no significant tectonic change has occurred during that period of time.

For the Chakaneh Fault system, the measured cumulative offset of 1900±50 m through the volcanic dome (section 4.1) is dated at maximum ca 2.35±0.24 Ma (*i.e.*, post dating the age of the dome intrusion). The obtained values yield an average slip rate of 0.8±0.1 mm/yr

along the Golmeym Fault (northern segment). For its southern segment (Dâmanjan Fault), a minimum slip rate of about 1.2 mm/yr can be deduced considering the total cumulative fault offset of 5.8±0.8 km (Figure 4) and the suggested maximum inception date of ~5 Ma for the initiation of right-lateral strike-slip faulting in the MTZ (sections 3.1 and 3.2). This is slightly higher than that calculated for the Golmeym Fault (0.8±0.1 mm/yr). Considering the fact that the offset volcanic dome is located near the northern fault termination (Figures 3 and 10), the Golmeym Fault slip rate can be regarded as a lower bound since cumulative fault displacements decrease northward along the Chakaneh Fault system (section 4).

Along the Farhadan Fault, the post-Pliocene (~5 Ma) cumulative offset of 7.3±0.8 km (Figure 5) yields a minimum long-term slip rate of 1.4±0.1 mm/yr. On the other hand, the geomorphic left-lateral offset of 5.6±0.2 km (Figure 6), presented by the oldest drainages incised in pyroclastic terrains, predates the last volcanic extrusion at ca 2.35±0.24 Ma (section 5). This allows limiting the upper bound of the Farhadan Fault slip rate at maximum of 2.3±0.5 mm/yr, and deducing a constrained long-term slip rate of 1.8±0.4 mm/yr.

The Sar'akhor Fault exhibits a cumulative right-lateral offset of 2.7±0.3 km (Figure 7), displacing Plio-Quaternary lavas. Even if the lavas age in unclear, the last volcanic episode at ca 2.35±0.24 Ma ago (domes intrusion), defines a minimum age limit for it. Accepting this assumption, a maximum lateral slip rate of 1.1±0.2 mm/yr is estimated for the Sar'akhor Fault.

### 7.3. Strike-slip faulting between the Binalud and Kopeh Dagh mountains

The possibility of a structural linkage between the Kopeh Dagh and Binalud mountain ranges has already been evaluated in previous studies (*Tchalenko*, 1975; *Afshar Harb*, 1979; *Hollingsworth et al.*, 2006). Despite the lack of clear structural linkage between the Kopeh Dagh and Binalud mountain ranges, the pioneer work by *Tchalenko* (1975) suggested a possible connection between the two deformation domains. Conversely, the lack of knowledge about strike-slip faulting in the MTZ led *Hollingsworth et al*. (2006) to conclude that the strike-slip faulting within the Kopeh Dagh is not transferred southward beyond the Atrak valley. In the other hand, the GPS-derived rate of 2-4 mm/yr for range parallel displacement through the Binalud Mountains (*Masson et al*., 2007; *Tavakoli*, 2007) implies significant right-lateral strike-slip faulting along both sides of the mountains (*i.e.*, the Mashhad and/or Neyshabur fault systems; Figure 16). Such a configuration could not be explained by the known structural pattern in NE Iran. As an important result, the data presented in this study uncovered evidence for clear structural linkage between the Kopeh

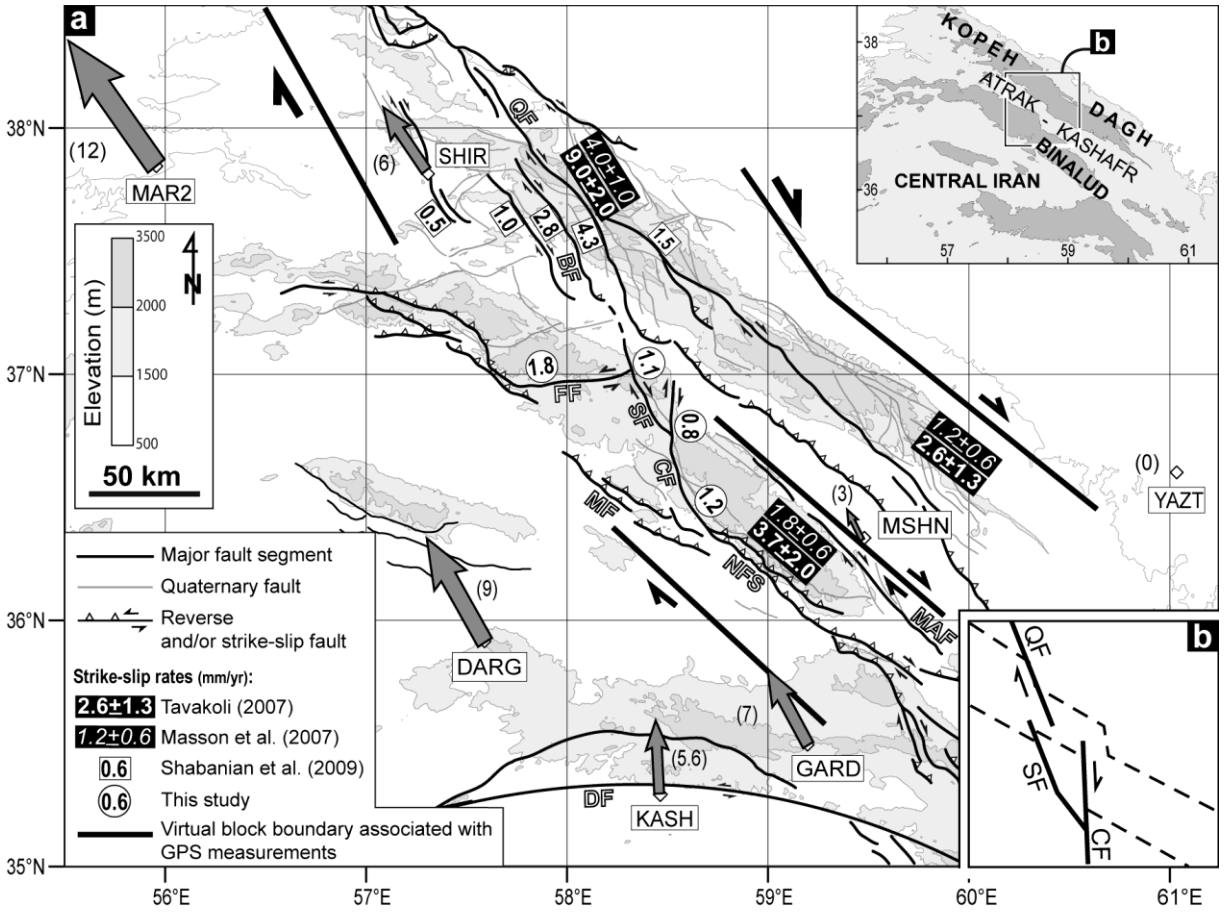


Figure 16. (a) Simplified active fault map (based on *Shabanian et al.* (2009) and this study) of NE Iran showing location of the MTZ in the geodynamic context of the northeastern Arabia-Eurasia collision. Gray arrows and their associated numbers are GPS horizontal velocities in a Eurasia-fixed reference frame (YAZT station) expressed in mm/yr (*Tavakoli,* 2007). The inset shows different mountain ranges and structural domains mentioned in the text as well as the Atrak-Kashafrud valley in the same frame as inset "a". (b) Simplified map centered on the Kopeh Dagh-Meshkan faults relay zone showing the affected morphology of the Atrak-Kashafrud valley by the named faults.

Dagh and Binalud mountains. This leads us to propose a new consistent tectonic pattern for NE Iran in which, part of motion of Central Iran with respect to Eurasia (~2 mm/yr) is transferred northward from the Binalud to the Kopeh Dagh Mountains through the MTZ strike-slip faults (Figure 16). In this context, the Farhadan Fault is considered as the easternmost extension of left-lateral strike-slip faulting within the Kopeh Dagh and the Eastern Alborz (*e.g.*, *Jackson et al*., 2002) favoring the northwestward motion of the Western Kopeh Dagh with respect to its eastern part.

In the Atrak valley, there is no direct geomorphic or geological evidence for the structural linkage between the Kopeh Dagh fault systems and the MTZ fault systems. However, the particular situation of the Atrak valley (*e.g.*, the long-time human settlement and cultivation) would likely removes possible fault surface expressions. Nonetheless,

according to our observations, we cannot rule out that the fault systems dissected or at least, affected the valley because: (1) an apparent right-lateral cumulative offset of ~12 km can be deduced analyzing the topography of the Atrak valley (Figure 16), (2) the band of maximum destruction (macroseismic regions) associated to the historical earthquakes in NE Iran (Figure 15), follows the trends of the Quchan and Baghan faults joining the Neyshabur fault system through the Chakaneh Fault system and the Sar'akhor fault (section 7.1). In this context, at least two macroseismic regions (1895 and 1929 earthquakes) are observed within the Atrak valley having different orientations and locations with respect to the mapped thrust-bend fault terminations proposed by *Hollingsworth et al*. (2006), (3) the observed geomorphic offset along the inferred trace of the Sar'akhor Fault within the valley (Figure 9) implies that the fault runs northward through the Atrak valley joining to the Baghan Fault. All together, these observations indicate that the strike-slip faulting within the Kopeh Dagh does not die out at the northern part of the valley. In other words, the area between the Kopeh Dagh and MTZ fault systems, including the Atrak-Kashafrud valley and thrust-bend terminations (Figures 15 and 16), should be considered as a relay zone between the two fault systems. This in turn, explains the right-lateral offset of the valley and the occurrence of several large earthquakes (M>6) in this area.

### 7.4. Kinematics of continental deformation in NE Iran

NE Iran, including the Kopeh Dagh and Allah Dagh-Binalud mountains, is involved in oblique convergence at the northeastern boundary of the Arabia-Eurasia collision. The Kopeh Dagh Mountains form a NW trending active deformation belt that separates Central Iran from Eurasia (Turan platform) (Figure 1). Mesozoic and Tertiary sediments of the Kopeh Dagh were folded into parallel, asymmetric NW trending folds during the Oligo-Miocene orogenic movements (*Stöcklin*, 1968; *Afshar Harb*, 1979; *Lyberis and Manby*, 1999). These folds are obliquely dissected by strike-slip fault systems that consist of active NNW trending right-lateral, and ENE trending left-lateral strike-slip faults (*e.g.*, *Tchalenko*, 1975; *Afshar Harb*, 1979; *Shabanian et al.*, 2009) extended within the Western and Central Kopeh Dagh. The Allah Dagh-Binalud Mountains (Figure 1) form NW trending Mesozoic paleoreliefs south of the Kopeh Dagh that thrusts over the northern margin of Central Iran. Conversely to the Kopeh Dagh, tectonic evolution of the Binalud is much more complex. A collection of the paleo-Tethys remnants as well as lower Paleozoic, middle and upper Mesozoic, and Cenozoic rocks has been submitted to successive major ductile or brittle tectonic deformation episodes

since the paleo-Tethys closure (pre-late Triassic) (*Alavi*, 1992). However, the Cenozoic tectonics is roughly identical for the entire region.

Late Cenozoic faulting and the accommodation mode of deformations in northeast Iran was already discussed by *Tchalenko* (1975), *Lyberis and Manby* (1999), *Jackson et al.* (2002), *Hollingsworth et al.* (2006, 2008), *Shabanian et al.* (2009) and *Siame et al.* (2009). The first kinematics model for NE Iran was proposed by *McKenzie and Jackson* (1983, 1986). They claimed that continuum mechanisms can appropriately describe the instantaneous deformation in NE Iran. In this context the Kopeh Dagh was considered as an excellent example that exhibits the characteristic features of their 'pinned model' by distributed deformation (Figure 17). According to this model, the overall motion in the Kopeh Dagh is expressed by large blocks bounded by the through-going faults that rotate about two pivot points, one on each plate, that is, Eurasia in the North and Central Iran in the South. Strike-slip fault motions are accompanied by a component of thrust faulting. On the basis of the same model, *Jackson et al.* (2002) expected that the strike-slip faulting within the Kopeh Dagh, which strikes NNW at an oblique angle to the belt, rotates anticlockwise about a vertical axis as the deformation progresses to eventually become parallel to the regional strike (see also *Jackson and McKenzie*, 1984; *Jackson et al.*, 1995). Subsequently, this hypothesis has become a dogma to explain kinematics of deformations in the Kopeh Dagh (*Hollingsworth et al.*, 2006, 2008). *Hollingsworth et al.* (2006) proposed a nearly similar block rotation model to explain the total right-lateral cumulative offset of 35-40 km along the Bakharden-Quchan Fault system as the apparent offsets due to anticlockwise rotation of fault-bounded blocks around vertical axes (Figure 17). According to this model, northward motion of Central Iran was thought to be accommodated between the Turan platform and Central Iran involving: (1) dominant thrust faulting at the southern boundaries of the Kopeh Dagh (north of the Atrak-Kashafrud valley), without significant strike-slip faulting, and (2) anticlockwise block rotation around a vertical axis within the Kopeh Dagh (see also *Jackson et al*., 2002). All the hypotheses mentioned above are based on the idealized continuum model proposed by *McKenzie and Jackson* (1983, 1986) to explain the relationship between finite strain and fault movements within a deforming zone submitted to the oblique convergence or divergence. The fundamental assumptions of such models are that (1) the deformation is uniformly distributed over the deforming zone, *i.e.*, the homogeneous deformation, and (2) the rigid boundaries of the deforming zone remain constant during the deformation process. In this view, the through-going strike-slip faults, oblique to the strike of the zone, are passive structures confined within

the zone boundaries. Consequently, observed deformation on these faults is controlled by kinematic constraints associated with the finite deformation.

Recently, quantitative geological and geomorphic investigations by *Shabanian et al.* (2009) provided the first geological constraints on the Late Cenozoic faulting in the Kopeh Dagh. Examining distribution of post-folding brittle deformation using satellite imagery, SRTM data and field observations, *Shabanian et al.* (2009) shown that (1) the strike-slip brittle deformation is not uniformly distributed within the Kopeh Dagh, but it is focalized on a well-defined intracontinental strike-slip fault system (BQFS) which obliquely dissect the belt, and (2) there is no structural evidence supporting regional anticlockwise block rotation within the Central-Eastern Kopeh Dagh. In this paper, we show that a significant part (≥25 per cent) of the Late Cenozoic brittle deformation within the Kopeh Dagh is taken up by prominent strike-slip faulting through the MTZ being transferred to the Binalud Mountains. Such a mechanism strongly favors a simple strike-slip faulting mechanism that translates the Central Iran northwards relative to the east. Moreover, it implies that the original range-parallel boundaries of both the Kopeh Dagh and Binalud deformation domains was affected by the Late Cenozoic strike-slip faulting focalized on few NNW-striking structures (Fig. 17). All together, the geological-derived results reveal that the distribution pattern of deformation is easily described as the focalized deformation along major block bounding strike-slip faults in NE Iran where previous authors (*McKenzie and Jackson*, 1983, 1986; *Hollingsworth et al.*, 2006, 2008) predict several rotating 'slats' (Fig. 17). With the great benefit of quantitative geological observation we see their model as more complex than is necessary to explain the large-scale kinematics. However, our data and observation propose a simpler model in which Central Iran and the Western Kopeh Dagh are translated northward with respect to Eurasia by focalized intracontinental strike-slip faulting (Fig. 17). It is noteworthy that, in an oblique convergence, an along-strike elongation of the deforming zones can occur due to the obliquity of the strike-slip faults with respect to the zone boundaries. Therefore, in the case of the Kopeh Dagh and Binalud, a NW elongation results from right-lateral fault motions along the NNW trending strike-slip faults (Fig. 17). Such a mechanism simply explains material translation in the Western Kopeh Dagh toward the South Caspian Basin, taken up by lateral motion on the Main Kopeh Dagh Fault and the Shahrud fault system. In summary, our data and deduced results do not support the fundamental assumptions for the popular hypothesis of distributed deformation proposed by *McKenzie and Jackson* (1983), and subsequently followed by *Jackson and McKenzie* (1984), *Jackson et al.* (1995), *Jackson et al.* (2002), and *Hollingsworth et al.* (2006, 2008).

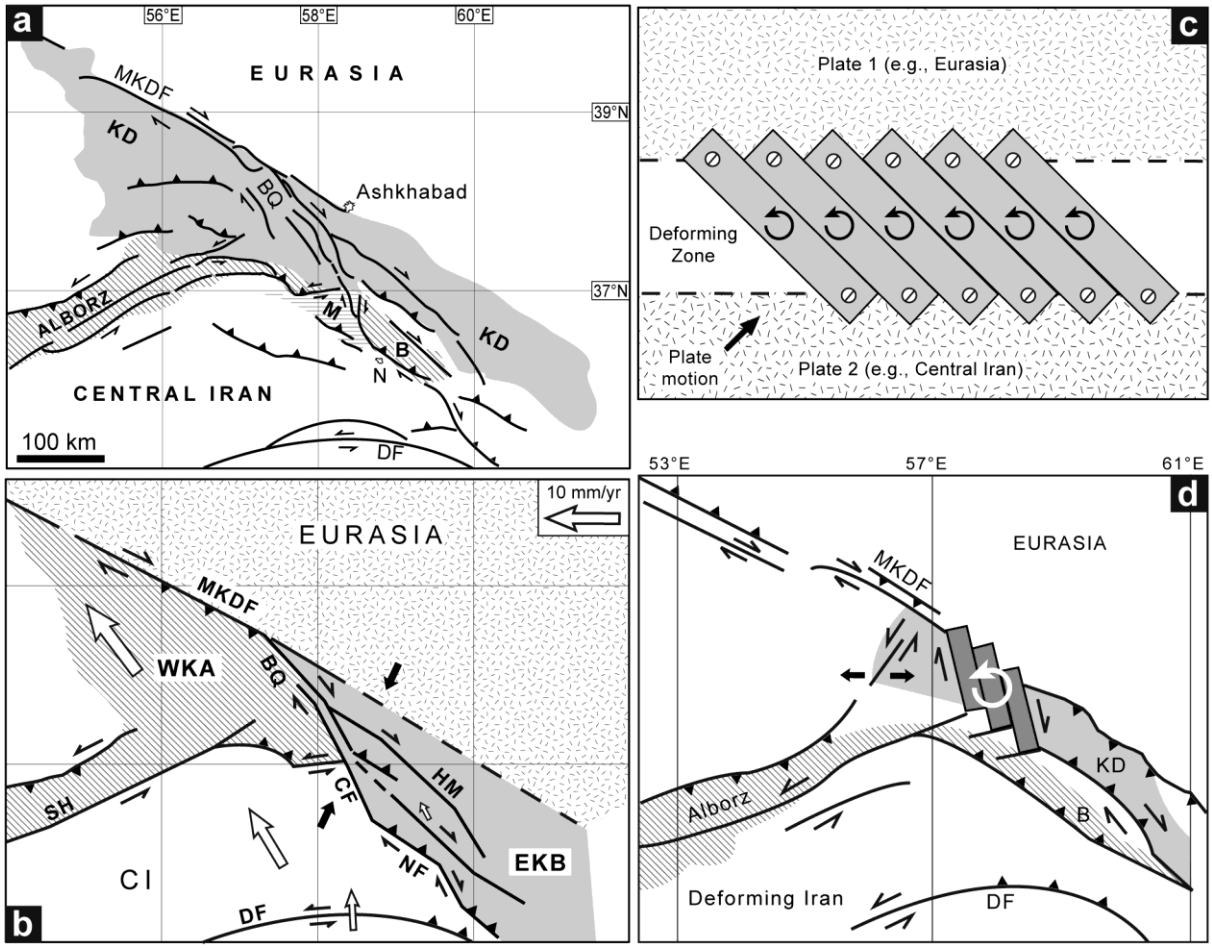


Figure 17. (a) Simplified active fault map together with the main tectonic domains of NE Iran. M, Meshkan Transfer Zone; B, Binalud; N, Neyshabur. (b) Schematic kinematic model showing the new tectonic configuration in NE Iran based on the data and results presented in this paper. WKA, Western Kopeh Dagh-Alborz tectonic domain; EKB, Eastern Kopeh Dagh-Binalud tectonic domain; SH, Shahrud fault system; HM, Hezar Masjed fault system; other abbreviations like Figure 1. White arrows are the same GPS velocity vectors than that Figure 16. Black arrows show the direction of the $\sigma_1$ stress axis (see Figure 13). The inactive NE margin of the Kopeh Dagh is marked by dashed line. (c) The "Pinned block model" modified after *McKenzie and Jackson* (1986); the fault bounded blocks are pinned on the stable plates in either side. (d) Simplified version of the kinematic model proposed by *Hollingsworth et al.,* (2008).

The new tectonic configuration presented here is also consistent with the GPS-derived velocity field (*Tavakoli*, 2007) in NE Iran (Figs 1 and 16). All the stations west of the right-lateral strike-slip fault systems (*i.e.*, BQFS and Chakaneh Fault System) move Northwest with respect to YAZT station in the eastern side (Eurasia). Their relative overall motion is nearly parallel to the regional strike (NNW) of the fault systems. This suggests a clear NW-ward translation of the western side along the right-lateral strike-slip faults, which are considered as the present-day active boundary between Iran and Eurasia. Since major strike-slip faults slip under very low resolved shear stress (*e.g.*, *Mount and Suppe*, 1987; Zoback *et al.*, 1987), these faults can slip in a direction that is not parallel to the relative motion of the microplates or

plates they bound. In such a case, the GPS velocity field indicates a direction different from the both directions of convergence and maximum compressional stress axis ($\sigma_1$).

In the MTZ, the GPS velocity field can also explain the fault kinematics observed on the ENE striking left-lateral faults such as the Farhadan Fault system. Comparing the GPS velocity vectors from GARD and DARG with MAR2 stations, one can estimate a westward motion rate of 3 to 5 mm/yr for the Eastern Alborz and the Western Kopeh Dagh with respect to Central Iran. This relative motion is taken up on ENE-striking left-lateral faults at the southern boundary of the Eastern Alborz and the Western Kopeh Dagh.

### 7.5. Changes in original boundaries of deforming zones

Plate boundary and internal driving forces can change with time, both abruptly and in small increments, leading to deactivation and migration of deforming zones. Active tectonic and magmatic processes also alter both applied forces and rheology, which encourage the temporal migration of patterns of deformation. Each force increment changes the intraplate stress field, altering the shearing and normal stresses across active faults and inactive potential failure planes. The magnitude of the effect depends upon the force increment and the preexisting stress field, either encouraging or discouraging fault slip (*Thatcher,* 2003). As it was suggested by *Zoback and Townend* (2001), if the crust is almost everywhere stressed very near to a state of frictional fault failure, then small stress increments could significantly alter preexisting deformation patterns. In the other hand, as a result of the buoyancy of continental crust, zones of preexisting weakness (mechanical anisotropy in the lithosphere) are effectively 'locked-in' to the continents and can potentially be reactivated many times during successive phases of continental deformation and accretion episodes (*e.g.*, *Thatcher,* 1995; *Storti et al.*, 2003, and references therein). Therefore, it may be expected that major tectonic reorganizations lead to significant structural rearrangements and changes in boundary conditions (forces and geometry) of old deformation belts. Hence, it is important to investigate present-day tectonic configurations in actively deforming zones before describing kinematics of deformation. For instance, all attempts to describe the kinematics of deformation in NE Iran have been based on paleo-tectonic knowledge of this region (*e.g.*, *McKenzie and Jackson*, 1983; *Hollingsworth et al.*, 2006).

In NE Iran, pre-Pliocene shortening perpendicular to the range was expressed in range-parallel folding in the Kopeh Dagh (*Afshar Harb*, 1979; *Lyberis and Manby*, 1999), thrust faulting at the southern side of the Binalud Mountains (*Alavi*, 1992), and folding as well as

thrust faulting in the MTZ (this study). It seems that each deformation domain has its own characteristic deformation. Conversely, post-Miocene deformation is characterized by prominent strike-slip faulting on nearly vertical faults (*Shabanian et al.*, 2009, and this study) oblique to the ranges. These faults dissect and offset the range-parallel fold axes and thrust faults throughout the region. In this context, the major right-lateral strike-slip faults cut through the Kopeh Dagh and Binalud deformation domains creating new boundaries for the deforming zones. This scenario implies major structural rearrangements in NE Iran that is accompanied with major kinematics and geometric evolutions in the northeastern Arabia-Eurasia collision zone (Fig. 17). Within this context, the post-Miocene tectonic reorganization (3-5 Ma – *Shabanian et al.*, 2009, and this study) not only caused regional strike- slip faulting in NE Iran, but also caused a drastic change in the old boundaries of the Kopeh Dagh and Binalud deformation domains, which has an important implication for the evolution of active convergences.

It is suggested that continued convergence will manifest itself by a growth in area of the range or plateau, as thrust faulting leads to crustal thickening on its margins (*Molnar*, 1988). Nonetheless, it seems that this condition cannot be attributed to all active convergences. At least in NE Iran, the deformation pattern and thickening processes within actively deforming mountain belts has been strongly affected by Late Cenozoic tectonic reorganization in the belts. This tectonic reorganization and the consequent structural rearrangement reactivated inherited faults, cutting the boundaries of old deformation zones and to create new tectonic configurations (Figure 17) more consistent with the new tectonic regime. The newly created boundaries take up more easily active deformation between converging plates. Such a deformation pattern does not need to grow in area of the range by thrusting in respond to continued convergence.

From a geodynamic perspective, there is perhaps an agreement that a significant change occurred in the nature of the Arabia-Eurasia collision zone at 5±2 Ma (*e.g.*, *Hempton*, 1987; *Westaway*, 1994; *Axen et al.*, 2001; *Allen et al.*, 2004; *Copley and Jackson*, 2006), though the cause for this change is debated. The widely accepted suggestions for the cause of this change include the arrival of buoyant Arabian continental crust choking the Neo-Tethyan subduction zone (*Axen et al.*, 2001), possible initiation of westward escape of the Anatolian Platelet between the North and East Anatolian faults (*Westaway*, 1994; *Koçyigit et al.*, 2001), slab break-off in the Bitlis-Zagros collision belt (*Authemayou et al.*, 2006, 2009; *Faccenna et al.*, 2006), and uplift of the Turkish-Iranian Plateau and a migration of deformation to its edges due to a dynamically supported increase in crustal thickening (*Allen et al.*, 2002; *Allen et al.*,

2004) or elevation (*Copley and Jackson.*, 2006). However, considering the contemporaneity of this widespread drastic reorganization, we suggest that the occurrence of relatively synchronous tectonic events (5±2 Ma) within different deformation domains throughout the Middle East cannot be entirely explained by only a single cause among those mentioned above. For instance, in regions such as the Kopeh Dagh, there is no evidence for migration of deformation outward of the previously deformed belt (*Allen et al.*, 2004; *Copley and Jackson*, 2006), where pre-Pliocene compressive tectonic regime was replaced by present day strike-slip one. Similar scenarios were also reported for the Makran-Zagros transition zone (*Regard et al.*, 2004, 2005) and the Lesser Caucasus (*Koçyigit et al.*, 2001). On the other hand, because of the 10 Ma sampling interval in the model proposed by *McQuarrie et al.* (2003), we cannot rule out the possibility of changes in plate's behavior and dynamics of the Arabia-Eurasia convergence during the last 10 Ma. In this case, we do not really know if the Pliocene tectonic reorganization is a consequence of possible changes in dynamics of the African-Arabian plates, or due to rearrangement of the involved plates in response to interactions between the causes mentioned above. Anyway, in this scenario relationships between the cause and effects are still unclear.

## 8. Conclusion

The dataset and results presented in this paper reveal that strike-slip brittle deformation within the Kopeh Dagh is transferred southward through the MTZ. This strongly supports the existence of a simple strike-slip faulting mechanism in the northeastern Arabia-Eurasia collision zone, which translate Central Iran to the north with respect to Eurasia. In this context The Chakaneh Fault system and Sar'akhor Fault are responsible for at least 2 mm/yr of the right-lateral strike-slip faulting between the Binalud and Kopeh Dagh mountains. That is to say that ~25 per cent of the northward motion between Central Iran and Eurasia in NE Iran is accommodated by the MTZ strike-slip faults. The present-day strike-slip deformation is taken up by reactivated preexisting structures which controlled Cenozoic tectono-sedimentary and volcanic evolution of the MTZ. This strike-slip faulting has started at ~5 Ma, more probably coeval with the time of the major tectonic reorganization in the Kopeh Dagh (*Shabanian et al.*, 2009). Comparing preexisting GPS data from *Tavakoli* (2007), geological and geomorphic mapping within the Kopeh Dagh by *Shabanian et al.* (2009), and the data and results in this paper, we showed that kinematics of deformation can be described by rigid block faulting in NE Iran. This suggestion is different from the kinematic models proposed

during the last thirty years. As a perspective, detailed geomorphic and geological studies are needed to complement the geodynamic puzzle of NE Iran investigating other strike-slip faults between the Kopeh Dagh and Binalud mountain ranges (*e.g.*, the Mashhad Fault).

**Acknowledgements**

This work was funded by the INSU-CNRS (France) and the International Institute of Earthquake Engineering and Seismology (IIEES, Iran), supervised by D. Hatzfeld and M.G. Ashtiani. We thank M. Mokhtari and M. Zare (IIEES) for support and administrative assistance. Funding was provided by the Dyeti and PNRN programs (INSU-CNRS), and ACI FNS program (French Ministry of Research), within the above mentioned co-operative agreement. SPOT images were provided thanks to the ISIS program (©CNES 2004 to 2007, distribution SPOT images S.A.). The samples were analyzed at the argon geochronology laboratory of the Montpellier University, France. E. Shabanian benefits of a Foreign Affair Ministry (Ministère des Affaires Etrangères) grant through French Embassy in Iran, and a complement support through the "Cotutelle de thèse" program (ACI du Ministère des Affaires Etrangères). We thank V. Grimault, Ch. Duhamel and the staff of the SCAC of the French Embassy in Tehran, for their support. We are grateful to G. Axen, an anonymous reviewer and an associate editor for helpful and constructive reviews. The General governments of Khorassan-e Razavi and Shomali provinces have efficiently helped us during three years.

**References**

Afshar Harb, A. (1979), The stratigraphy, tectonics and petroleum geology of the Kopet Dagh region, northeastern Iran, Ph.D. thesis, Petroleum Geology Section, Royal School of Mines, Imperial College of Science and Technology, London.

Alavi, M. (1992), Thrust tectonics of the Binalood region, NE Iran, *Tectonics, 11*(2), 360-370.

Allen, M. B., S. Jones, A. Ismail-Zadeh, M. Simmons, and L. Anderson (2002), Onset of subduction as the cause of rapid Pliocene-Quaternary subsidence in the South Caspian Basin, *Geology, 30*(9), 775-778, doi:10.1130/0091-7613(2002)030<0775.

Allen, M., J. Jackson, and R. Walker (2004), Late Cenozoic reorganization of the Arabia-Eurasia collision and the comparison of short-term and long-term deformation rates, *Tectonics, 23*, TC2008, doi:10.1029/2003TC00153.

Ambraseys, N., and C. Melville (1982), *A History of Persian Earthquakes*, Cambridge University Press, Cambridge, UK.

Amini, B., and N. H. Khan-Nazer (2000), Geological map of Iran, *Series 7563 (Mashkan sheet), scale 1:100 000*, Geological Survey of Iran, Tehran.

Authemayou, C., D. Chardon, O. Bellier, Z. Malekzade, E. Shabanian, M. and Abbassi (2006), Late Cenozoic partitioning of oblique plate convergence in the Zagros fold-and-thrust belt (Iran), *Tectonics, 25*, TC3002, doi:10.1029/2005TCOO1860.

Authemayou, C., O. Bellier, D. Chardon, L. Benedetti, Z. Malekzade, C. Claude, B. Angeletti, E.Shabanian, and M. R. Abbassi (2009), Quaternary slip-rates of the Kazerun and the Main Recent Faults: active strike-slip partitioning in the Zagros fold-and-thrust belt, Geophys. J. Int., in press, doi: 10.1111/j.1365-246X.2009.04191.x.

Avouac, J.-P., and P. Tapponnier (1993), Kinematic model of active deformation in central Asia, *Geophys. Res. Lett., 20*, 895-898.

Axen, G. J., P. S. Lam, M. Grove, D. F. Stockli, and J. Hassanzadeh (2001), Exhumation of the west-central Alborz Mountains, Iran, Caspian subsidence, and collision-related tectonics, *Geology, 29*(6), 559–562.

Bellier, O., and M. L. Zoback (1995), Recent state of stress change in the Walker Lane zone, western Basin and Range province, United States, *Tectonics, 14*, 564–593.

Berberian, M., and R. Yeats (1999), Patterns of historical earthquake rupture in the Iranian Plateau, *Bull. Seism. Soc. Am., 89*, 120–139.

Berberian, M., and R. Yeats (2001), Contribution of archaeological data to studies of earthquake history in the Iranian Plateau, *J. Structural Geology, 23*, 563-584.

Carey, E. (1979), Recherche des directions principales de contraintes associées au jeu d'une population de failles, *Rev. Geol. Dyn. Geogr. Phys., 21*, 57-66.

Carey, E., and B. Brunier (1974), Analyse théorique et numérique d'un modèle mécanique élémentaire appliqué à l'étude d'une population de failles, *C. R. Acad. Sci., Ser. D, 279*, 891-894.

Copley, A. and J. Jackson (2006), Active tectonics of the Turkish-Iranian Plateau, *Tectonics, 25*, TC6006, doi:10.1029/2005TC001906.

England, P. C., and J. A. Jackson (1989), Active deformation of the continents, *Annu. Rev. Earth Planet. Sci., 17*, 197-226

England, P., and D. McKenzie (1982), A thin viscous sheet for continental deformation, *Geophys. J.R. Astron. Soc., 70*, 295-321.

England, P., and P. Molnar (1997), Active deformation of Asia: From kinematics to dynamics, *Science, 278*, 647-650.

Faccenna, C., O. Bellier, J. Martinod, C. Piromallo, and V. Regard (2006), Slab detachment beneath eastern Anatolia: A possible cause for the formation of the North Anatolian fault, *Earth Planet. Sci. Lett., 242*, 85-97.

Fleck, R. J., J. F. Sutter, and D. H. Elliot (1977), Interpretation of discordant $^{40}Ar/^{39}Ar$ age spectra of Mesozoic tholeiites from Antarctica, *Geochim. Cosmochim. Acta, 41*, 15-32.

Flesch, L. M., A. J. Haines, and W. E. Holt (2001), Dynamics of the India-Eurasia collision zone, *J. Geophys. Res., 106*, 16,435-16,460.

Ghaemi, F., F. Ghaemi, and K. Hosseini (1999), Geological map of Iran, *Series 7766 (Neyshabur sheet), scale 1:100 000*, Geological Survey of Iran, Tehran.

Gordon, R. G., and S. Stein (1992), Global tectonics and space geodesy, *Science, 256*, 333-342.

Hempton, M. R. (1987), Constraints on Arabian plate motion and extensional history of the Red Sea, *Tectonics, 6*(6), 687-705, doi:10.1029/TC006i006p00687.

Hollingsworth, J., J. Jackson, R. Walker, M. R. Gheitanchi, and M. J. Bolourchi (2006), Strike-slip faulting, rotation and along-strike elongation in the Kopeh Dagh Mountains, NE Iran, *Geophys. J. Int., 166*, 1161-1177, doi:10.1111/j.1365-246X.2006.02983.x.

Hollingsworth, J., J. Jackson, J. E. Alarcón, J. J. Bommer, and M. J. Bolourchi (2007), The 4th February 1997 Bojnurd (Garmkhan) earthquake in NE Iran: field, teleseismic, and strong-motion evidence for rupture directivity effects on a strike-slip fault, *Journal of Earthquake Engineering, 11*, 193–214.

Hollingsworth, J., J. Jackson, R. Walker, and H. Nazari (2008), Extrusion tectonics and subduction in the eastern South Caspian region since 10 Ma, *Geology*, *36*(10), 763–766, doi:10.1130/G25008A.1.

Jackson, J. A., A. J. Haines, and W. E. Holt (1995), The accommodation of Arabia–Eurasia plate convergence in Iran, *J. geophys. Res., 100*, 15,205-15,219.

Jackson, J., and D. McKenzie (1984), Active tectonics of the Alpine-Himalayan Belt between western Turkey and Pakistan, *Geophys. J. R. astr. Soc., 77*(1), 185-264.

Jackson, J., K. Priestley, M. Allen, and M. Berberian (2002), Active tectonics of the South Caspian Basin, *Geophys. J. Int., 148*, 214–245.

Koçyigit, A., A. Yilmaz, S. Adamia, and S. Kuloshvili (2001), Neotectonics of East Anatolian Plateau (Turkey) and Lesser Caucasus: implication for transition from thrusting to strike-slip faulting, *Geodinamica Acta*, *14*(1), 177-195, doi:10.1016/S0985-3111(00)01064-0.

Lyberis, N., and G. Manby (1999), Oblique to orthogonal convergence across the Turan block in the post-Miocene, *Am. Assoc. Petrol. Geol. Bull., 83*(7), 1135-1160.

Masson, F., M. Anvari, Y. Djamour, A. Walpersdorf, F. Tavakoli, M. Daignières, H. Nankali, and S. Van Gorp (2007), Large-scale velocity field and strain tensor in Iran inferred from GPS measurements: new insight for the present-day deformation pattern within NE Iran, *Geophys. J. Int., 170*, 436-440, doi:10.1111/j.1365-246X.2007.03477.x.

McClusky, S., R. Reilinger, S. Mahmoud, D. Ben Sari, and A. Tealeb (2003), GPS constraints on Africa (Nubia) and Arabia plate motions, *Geophys. J. Int., 155*(1), 126–138, doi:10.1046/j.1365-246X.2003.02023.x.

McKenzie, D. P. (1972), Active tectonics of the Mediterranean region, *Geophys. J. Int., 30*(2), 109–185, doi:10.1111/j.1365-246X.1972.tb02351.x.

McKenzie, D., and J. Jackson, (1983), The relationship between strain rates, crustal thickening, paleomagnetism, finite strain, and fault movements within a deforming zone, *Earth planet. Sci. Lett., 65*, 182-202.

McKenzie, D., and J. Jackson (1986), A block model of distributed deformation by faulting, *J. Geol. Soc. London, 143*, 349-353.

McQuarrie, N., J. M. Stock, C. Verdel, and B.P. Wernicke (2003), Cenozoic evolution of Neotethys and implications for the causes of plate motions, *Geophys. Res. Lett., 30*(20), 2036, doi:10.1029/2003GL017992.

Mercier, J. L., E. Carey-Gailhardis, and M. Sébrier (1991), Paleostress determinations from fault kinematics: application to the neotectonics of the Himalayan-Tibet and the central Andes, *Philos. Trans. R. Soc. London, Ser. A, 337*, 41-52.

Molnar, P. (1988), Continental tectonics in the aftermath of plate tectonics, *Nature, 335*, 131-137.

Mostriouk, A. O., V. A. Petrov (1994), Catalogue of focal mechanisms of Earthquakes 1964–1990, *Materials of World Data Center B.*, pp. 87, Moscow (available at http://wwwbrk.adm.yar.ru/russian/l_512/stress/fps_cate.htm).

Mount, V. S., and J. Suppe (1987), State of stress near the San Andreas Fault: implications for wrench tectonics, *Geology, 15*, 1143-1146.

Nyst, M., and W. Thatcher (2004), New constraints on the active tectonic deformation of the Aegean, *J. Geophys. Res., 109*, B11406, doi:10.1029/2003JB002830.

Peltzer, G., and F. Saucier (1996), Present-day kinematics of Asia derived from geologic fault rates, *J. Geophys. Res., 101*, 27,943-27,956.

Regard, V., O. Bellier, J.-C. Thomas, M. R. Abbassi, J. Mercier, E. Shabanian, K. Feghhi, and S. Soleymani (2004), The accommodation of Arabia-Eurasia convergence in the Zagros-Makran transfer zone, SE Iran: a transition between collision and subduction through a young deforming system, *Tectonics, 23*, TC4007, doi:10.1029/2003TC001599.

Regard, V., O. Bellier, J.-C. Thomas, D. Bourlès, S. Bonnet, M. R. Abbassi, R. Braucher, J. Mercier, E. Shabanian, S. Soleymani, and K. Feghhi (2005), Cumulative right-lateral fault slip rate across the Zagros–Makran transfer zone: role of the Minab–Zendan fault system in accommodating Arabia–Eurasia convergence in southeast Iran, *Geophys. J. Int., 162*, 177–203, doi:10.1111/j.1365-246X.2005.02558.x.

Reilinger, R., et al. (2006), GPS constraints on continental deformation in the Africa-Arabia-Eurasia continental collision zone and implications for the dynamics of plate interactions, *J. Geophys. Res., 111*, B05411, doi:10.1029/2005JB004051.

Renne, P. R., C. C. Swisher, A.L. Deino, D. B. Karner, T. Owens, and D. J. Depaolo (1998), Intercalibration of Standards, absolute ages and uncertainties in $^{40}Ar/^{39}Ar$ dating, *Chemical Geology, 145*,117–152.

Replumaz, A., and P. Tapponnier (2003), Reconstruction of the deformed collision zone between India and Asia by backward motion of lithospheric blocks, *J. Geophys. Res., 108*(B6), 2285, doi:10.1029/2001JB000661.

Roddick, J. C., R. A. Cliff, and D. C. Rex (1980), The evolution of excess argon in alpine biotites, *Earth and Planetary Sciences Letters, 48*, 185-208.

Ryerson, F. J., P. Tapponnier, R. C. Finkel, A.-S. Meriaux, J. Van der Woerd, C. Lassiere, M.-L. Chevalier, X. Xiwei, and L. Harbing (2006), Applications of morphochronology to the active tectonics of Tibet, *Spec. Pap. Geol. Soc., 415*.

Sahandi, M. R. (1993), Geological quadrangle map of Iran, *No. J-4 (Sabzevar sheet), scale 1:250 000*, Geological Survey of Iran, Tehran.

Sella, G. F., T. H. Dixon, and A. Mao (2002), REVEL: A model for recent plate velocities from space Geodesy, *J. Geophys. Res., 107*(B4), 2081, doi:10.1029/2000JB000033.

Shabanian, E., L. Siame, O. Bellier, L. Benedetti, and M. R. Abbassi (2009), Quaternary slip-rates along the north-eastern boundary of the Arabia-Eurasia collision zone (Kopeh Dagh Mountains, North-East Iran), *Geophys. J. Int., 178*, 1055-1077, doi: 10.1111/j.1365-246X.2009.04183.x.

Siame, L. L., E. Shabanian, and O. Bellier (2009), Comment to Extrusion tectonics and subduction in the eastern South Caspian region since 10 Ma, *Geology*, in press.

Storti, F., R. E. Holdsworth, and F. Salvini (2003), Intra plate strike-slip deformation belts, in *Intra plate strike-slip deformation belts*, edited by F. Storti et al., Geological society, London, Special publications, 210, pp. 1-14.

Tavakoli, F. (2007), Present-day kinematics of the Zagros and east of Iran faults, Ph.D. thesis, University of Joseph Fourier, France, Grenoble.

Tchalenko, J. S. (1975), Seismicity and structure of the Kopet Dagh (Iran, USSR), *Phil. Trans. R. Soc. Lond., Series A, 278* (1275), 1–28.

Thatcher, W. (1995), Microplate versus continuum descriptions of active tectonic deformation, *J. Geophys. Res., 100*, 3885-3894.

Thatcher, W. (2003), GPS constraints on the kinematics of continental deformation, *Int. Geol. Rev., 45*, 191-212.

Thatcher, W. (2007), Microplate model for the present-day deformation of Tibet, *J. Geophys. Res., 112*, B01401, doi:10.1029/2005JB004244.

Vernant, P., F. Nilforoushan, D. Hatzfeld, M. R. Abbassi, C. Vigny, F. Masson, H. Nankali, J. Martinod, A. Ashtiani, R. Bayer, F. Tavakoli, and J. Chéry (2004), Present-day crustal deformation and plate kinematics in the Middle East constrained by GPS measurements in Iran and northern Oman, *Geophys. J. Int., 157*(1), 381–398, doi:10.1111/j.1365-246X.2004.02222.x.

Vilotte, J. P., M. Daignieres, and R. Madariaga (1982), Numerical modeling of intraplate deformation: Simple mechanical models of continental collision, *J. Geophys. Res.*, *87*, 10,709-10,728.

Walker, R., and J. Jackson (2004), Active tectonics and Late Cenozoic strain distribution in central and eastern Iran, *Tectonics, 23*, TC5010, doi:10.1029/2003TC001529.

Westaway, R. (1994), Present-day kinematics of the Middle East and eastern Mediterranean, *J. Geophys. Res.*, *99*(B6), 12071-12090.

York, D. (1969), Least-square fitting of a straight line with correlated errors, *Earth and Planetary Sciences Letters, 5*, 320-324.

Zamani, B., J. Angelier, and A. Zamani (2007), State of stress induced by plate convergence and stress partitioning in northeastern Iran, as indicated by focal mechanisms of earthquakes, *Journal of Geodynamics, 45*, 120–132, doi:10.1016/j.jog.2007.07.003.

Zoback, M. D., and J. Townend (2001), Implications of hydrostatic pore pressures and high crustal strength for the deformation of intraplate lithosphere, *Tectonophysics, 336*, 19-30.

Zoback, M. D., M. L. Zoback, V. S. Mount, J. Suppe, J. P. Eaton, J. H. Healy, D. Oppenheimer, P. Reasenberg, L. Jones, C. B. Raleigh, I. G. Wong, O. Scotti, and C. Wentworth (1987), New evidence on the state of stress on the San Andreas fault system, *Science, 238,* 1105-1111, doi: 10.1126/science.238.4830.1105.

## Appendix A: $^{40}Ar/^{39}Ar$ analytical procedure and data

The minerals (plagioclases) were separated using heavy liquids, a Frantz magnetic separator and finally by hand picking under a binocular microscope to remove all obvious xenocryst from the population with density lighter than 2.56. The samples were then irradiated at the McMaster reactor, Ontario, in the 5C position for 28 h under a $10^{18}$ neutrons $cm^{-2}s^{-1}$ flux. Irradiation interference on K, Ca and Cl were corrected by irradiation of KCl and $CaF_2$ pure salts. J factor was estimated by the use of duplicates of the Fish Canyon sanidine standard with an age of 28.02±0.16 Ma (*Renne et al*., 1998).

Samples were loaded in aluminum foil packets into a double vacuum Staudacher type furnace, which temperature is calibrated by means of a thermocouple, and step heated in a classical protocol of regularly increasing temperature steps. The gas was purified by the means of cold traps with liquid air and Al-Zr getters during five minutes. Once cleaned, the gas was introduced into a VG3600 mass spectrometer, and one minute was allowed for equilibration before analysis. Signals were measured by mean of a Faraday cup with a resistor of $10^{11}$ ohm for $^{40}Ar$ and $^{39}Ar$ while $^{39}Ar$, $^{38}Ar$, $^{37}Ar$ and $^{36}Ar$ were analyzed with a photomultiplier after interaction on a Daly plate. Gain between both collectors was estimated by duplicate analysis of $^{39}Ar$ over both during each analysis, and also by statistical analysis on a period of several years. This gain is, on average, of 54 and is know at better than 1.5%. This error is included in the age calculation. Plateau ages were calculated according to the definition of *Fleck et al*. (1977), and the given error takes the error on the J factor into account. Intercept ages are obtained in an inverse isochron diagram of $^{36}Ar/^{40}Ar$ versus $^{39}Ar/^{40}Ar$ (*Roddick et al*., 1980), which allows homogeneous excess components to be isolated in many occasions. Errors on age and intercept age include individual errors on each point and linear regression by York's method (*York*, 1969). The goodness of fit relative to individual errors is measured by Mean Square Weighted Deviation (MSWD – *York*, 1969). If the inverse isochron age is close to the plateau age and $^{40}Ar/^{36}Ar$ is not significantly different from present day $^{40}Ar/^{36}Ar$ atmospheric ratio (295.5), we consider that the plateau age is reliable. When this is not the case, we prefer to rely on the inverse isochron age if this one is well determined. Isotopic correlation plots of $^{39}Ar$, $^{37}Ar$ and $^{38}Ar$ are used as proxies for K/Ca ($^{39}Ar/^{37}Ar$) and Cl/K ($^{38}Ar/^{39}Ar$) ratios.

Table A1. $^{40}Ar/^{39}Ar$ analytical data.

| Sample | Temperature (°C) | $^{40}Ar/^{39}Ar$ | $^{38}Ar/^{39}Ar$ | $^{37}Ar/^{39}Ar$ | $^{36}Ar/^{39}Ar$ ($10^{-3}$) | $^{39}Ar$ ($10^{-14}$moles) | $F^{39}Ar$ released | $\%^{40}Ar^*$ | $^{40}Ar^*/^{39}Ar$ | Age (Ma) | ± 1σ (Ma) |
|---|---|---|---|---|---|---|---|---|---|---|---|
| VOL601 | 300 | 39,390 | 0,117 | 0,925 | 130,791 | 0,21 | 0,41 | 1,97 | 0,78 | 12,67 | 4,29 |
| | 400 | 6,831 | 0,044 | 0,438 | 20,098 | 0,29 | 0,97 | 13,16 | 0,90 | 14,64 | 0,97 |
| | 500 | 1,006 | 0,016 | 0,274 | 2,324 | 1,08 | 3,09 | 31,41 | 0,32 | 5,16 | 0,24 |
| | 600 | 0,399 | 0,013 | 0,302 | 0,603 | 5,25 | 13,44 | 54,96 | 0,22 | 3,59 | 0,05 |
| | 650 | 0,274 | 0,013 | 0,332 | 0,396 | 8,24 | 29,68 | 57,28 | 0,16 | 2,56 | 0,03 |
| | 700 | 0,208 | 0,013 | 0,363 | 0,181 | 10,43 | 50,22 | 75,20 | 0,16 | 2,55 | 0,02 |
| | 750 | 0,215 | 0,014 | 0,427 | 0,187 | 10,54 | 70,98 | 77,02 | 0,17 | 2,70 | 0,02 |
| | 800 | 0,188 | 0,014 | 0,546 | 0,229 | 7,58 | 85,91 | 70,93 | 0,13 | 2,18 | 0,03 |
| | 850 | 0,225 | 0,015 | 0,807 | 0,410 | 3,70 | 93,18 | 59,01 | 0,13 | 2,17 | 0,05 |
| | 900 | 0,346 | 0,019 | 1,314 | 0,611 | 1,39 | 95,92 | 65,03 | 0,22 | 3,68 | 0,11 |
| | 950 | 0,559 | 0,033 | 2,032 | 1,211 | 0,63 | 97,16 | 54,45 | 0,30 | 4,98 | 0,23 |
| | 1000 | 0,846 | 0,057 | 3,200 | 0,906 | 0,42 | 97,98 | 88,89 | 0,75 | 12,28 | 0,25 |
| | 1050 | 1,017 | 0,090 | 5,281 | 3,118 | 0,36 | 98,68 | 38,86 | 0,40 | 6,47 | 0,52 |
| | 1100 | 2,097 | 0,094 | 10,625 | 7,407 | 0,22 | 99,10 | 25,37 | 0,54 | 8,74 | 0,91 |
| | 1150 | 4,768 | 0,084 | 11,704 | 16,237 | 0,21 | 99,52 | 13,82 | 0,66 | 10,83 | 1,27 |
| | 1200 | 15,717 | 0,113 | 8,948 | 50,048 | 0,14 | 99,80 | 9,22 | 1,46 | 23,69 | 2,33 |
| | 1400 | 34,487 | 0,092 | 12,108 | 116,875 | 0,10 | 100,00 | 1,93 | 0,67 | 10,91 | 3,96 |
| VOL602 | 300 | 20,361 | 0,060 | 0,563 | 70,287 | 0,28 | 0,53 | -1,94 | -0,39 | 0,00 | 0,00 |
| | 400 | 5,614 | 0,029 | 0,462 | 18,220 | 0,39 | 1,25 | 4,23 | 0,24 | 3,88 | 0,76 |
| | 500 | 0,905 | 0,015 | 0,284 | 2,601 | 1,34 | 3,75 | 14,77 | 0,13 | 2,19 | 0,47 |
| | 600 | 0,691 | 0,013 | 0,334 | 1,847 | 5,13 | 13,34 | 21,06 | 0,15 | 2,38 | 0,06 |
| | 600 | 0,712 | 0,013 | 0,334 | 1,887 | 5,11 | 22,90 | 21,75 | 0,15 | 2,53 | 0,07 |
| | 650 | 0,613 | 0,013 | 0,396 | 1,610 | 8,12 | 38,07 | 22,99 | 0,14 | 2,30 | 0,05 |
| | 700 | 0,222 | 0,013 | 0,348 | 0,265 | 10,53 | 57,76 | 65,14 | 0,14 | 2,36 | 0,03 |
| | 750 | 0,225 | 0,014 | 0,464 | 0,316 | 9,36 | 75,26 | 62,04 | 0,14 | 2,28 | 0,03 |
| | 800 | 0,224 | 0,015 | 0,739 | 0,355 | 5,84 | 86,18 | 64,13 | 0,14 | 2,35 | 0,04 |
| | 850 | 0,276 | 0,017 | 1,273 | 0,853 | 2,71 | 91,24 | 29,45 | 0,08 | 1,33 | 0,09 |
| | 900 | 0,429 | 0,021 | 1,899 | 1,361 | 1,34 | 93,75 | 28,31 | 0,12 | 1,99 | 0,16 |
| | 950 | 0,590 | 0,030 | 2,276 | 1,830 | 0,93 | 95,49 | 28,24 | 0,17 | 2,73 | 0,24 |
| | 1000 | 0,727 | 0,040 | 2,769 | 2,658 | 0,71 | 96,82 | 12,26 | 0,09 | 1,46 | 0,36 |
| | 1050 | 2,842 | 0,063 | 2,832 | 10,097 | 0,66 | 98,06 | 0,34 | 0,01 | 0,16 | 0,50 |
| | 1100 | 32,292 | 0,117 | 4,562 | 112,203 | 0,41 | 98,83 | -1,88 | -0,61 | 0,00 | 0,00 |
| | 1150 | 74,016 | 0,195 | 6,245 | 257,272 | 0,31 | 99,40 | -2,23 | -1,66 | 0,00 | 0,00 |
| | 1200 | 157,979 | 0,169 | 3,674 | 547,022 | 0,19 | 99,75 | -2,19 | -3,47 | 0,00 | 0,00 |
| | 1400 | 282,293 | 0,229 | 5,477 | 972,925 | 0,14 | 100,00 | -1,73 | -4,91 | 0,00 | 0,00 |
| VOL603 | 300 | 23,592 | 0,063 | 0,765 | 79,007 | 0,18 | 0,48 | 1,15 | 0,27 | 4,45 | 2,86 |
| | 400 | 6,942 | 0,021 | 0,635 | 16,674 | 0,17 | 0,92 | 29,29 | 2,03 | 32,96 | 1,71 |
| | 500 | 1,194 | 0,013 | 0,428 | 1,657 | 0,73 | 2,84 | 59,49 | 0,71 | 11,58 | 0,27 |
| | 600 | 0,637 | 0,012 | 0,485 | 1,120 | 3,24 | 11,38 | 49,56 | 0,32 | 5,16 | 0,07 |
| | 650 | 0,371 | 0,012 | 0,459 | 0,545 | 5,17 | 25,00 | 58,71 | 0,22 | 3,56 | 0,05 |
| | 700 | 0,245 | 0,012 | 0,495 | 0,264 | 7,52 | 44,84 | 72,32 | 0,18 | 2,90 | 0,03 |
| | 750 | 0,214 | 0,013 | 0,606 | 0,222 | 7,90 | 65,65 | 77,13 | 0,17 | 2,70 | 0,03 |
| | 800 | 0,190 | 0,013 | 0,711 | 0,292 | 6,44 | 82,61 | 66,76 | 0,13 | 2,08 | 0,04 |
| | 850 | 0,227 | 0,013 | 0,852 | 0,259 | 3,62 | 92,14 | 80,24 | 0,18 | 2,98 | 0,07 |
| | 900 | 0,394 | 0,017 | 1,307 | 0,696 | 1,36 | 95,73 | 62,87 | 0,25 | 4,05 | 0,13 |
| | 950 | 0,449 | 0,022 | 2,012 | 1,740 | 0,57 | 97,22 | 8,16 | 0,04 | 0,60 | 0,28 |
| | 1000 | 2,014 | 0,034 | 2,699 | 1,432 | 0,37 | 98,19 | 86,11 | 1,74 | 28,19 | 0,54 |
| | 1050 | 1,212 | 0,072 | 4,378 | 2,574 | 0,31 | 99,01 | 57,47 | 0,70 | 11,39 | 0,72 |
| | 1100 | 3,042 | 0,092 | 9,224 | 7,870 | 0,17 | 99,46 | 41,26 | 1,26 | 20,54 | 1,00 |

| | | | | | | | | | | |
|---|---|---|---|---|---|---|---|---|---|---|
| 1150 | 7,123 | 0,210 | 13,388 | 20,582 | 0,12 | 99,77 | 25,73 | 1,85 | 29,98 | 1,84 |
| 1200 | 27,096 | 0,153 | 11,153 | 77,315 | 0,06 | 99,92 | 18,10 | 4,94 | 79,04 | 4,32 |
| 1400 | 66,632 | 0,133 | 24,083 | 216,415 | 0,03 | 100,00 | 6,18 | 4,19 | 67,18 | 8,54 |

Whole rock is lighter than 2.56 g/cm$^3$

# *Chapter III*

In chapter II, the structural connection between the Kopeh Dagh and Binalud deformation domains was discussed. The active deformation is principally taken up by strike-slip faulting within the Kopeh Dagh and is partly transferred southward through the Meshkan Transfer Zone. In this context, we need to know the contribution of the Binalud that seems to play a major role accommodating the deformation between the Doruneh Fault and Kopeh Dagh Mountains. This chapter focused on the Binalud deformation domain, and aims at characterizing style and rates of quaternary faulting at both sides of the range. After a review of the active tectonic setting of the region, we present the active faulting evidences along the main fault systems (Neyshabur and Mashhad fault systems) at both sides of the range. Then, we describe the morphotectonic investigations conducted along the two fault systems in order to estimate individual Quaternary fault slip rates. As a discussion, geological and geomorphic data are analyzed together to better understand deformation pattern in the Binalud Mountains and its controls on the long-term geomorphic processes.

## Late Quaternary fault slip rates on both sides of the Binalud Mountains (NE Iran)


### Abstract

Investigation of the tectonic geomorphology of active faulting at both sides of the Binalud Mountains, northeast Iran, reveals the geomorphic and tectonic aspects of development of the mountain range produced by quaternary faulting. Detailed Quaternary fault mapping led us to characterize structural pattern and active faulting along two major fault systems at both sides of the Binalud Mountains, *i.e.*, the Neyshabur and Mashhad Fault Systems at its southwestern and northeastern sides, respectively. The distributed nature of deformation within these two fault systems conducted our investigations along seven individual fault segments. We applied combined approaches of morphotectonic analyses based on satellite images (SPOT5 and Landsat ETM+), STRM and site-scale topographic data, and *in situ*-produced $^{10}$Be exposure dating complemented by field surveys to describe rates and kinematics of active deformation processes. Three regional abandonment episodes of alluvial surfaces were dated at 5.3±1.1 kyr ($Q_1$), 94±5 kyr ($Q_3$), and 200±14 kyr ($S_3$). The geomorphic reconstruction of both vertical and horizontal fault offsets postdating these surface abandonment episodes yielded individual slip rates for the late quaternary faulting along the two fault systems. For the Neyshabur Fault System, the respective total horizontal and vertical slip rates of 2.7±0.8 mm/yr and 2.4±0.2 mm/yr are estimated reconstructing cumulative offsets recorded by the $Q_3$ fan surfaces across the fault system. Altogether, these vertical and horizontal slip rates lead us to determine a total slip rate of 3.6±1.2 mm/yr for the Late Quaternary deformation at the southwestern flank of the Binalud Mountains. Reconstructing the cumulative right-lateral offset recorded by the $S_3$ surfaces, a Late Quaternary slip rate of 1.6±0.1 mm/yr is attributed to the Mashhad Fault System. The distribution pattern of slip rates both sides of the Binalud reveals that Late Quaternary strike-slip faulting has been taken up by the Mashhad and Neyshabur Fault Systems at a long-term rate of ~4 mm/yr. This also implies a ~2.4 mm/yr long-term slip rate for vertical deformation which is uplifting the southwestern flank of the Binalud Mountains. Combining our geological observations with geomorphic interpretation of hypsometric analyses of drainage basins nested in the Binalud Mountains we reveal that the locus of active deformation front is migrating southwestward along new reverse faults formed basin-ward. In addition to these typical features of development of fold-and-thrust belts, the basin-ward migration of the Binalud deformation front has apparently been accompanied by backward rotation of older faults making them steepen with time.


*Keywords: Morphotectonics, Mountain front migration; Tectonic geomorphology; Hypsometric integral; Neyshabur Fault; Mashhad Fault*

## 1. Introduction

NE Iran corresponds to the northeastern extension of the Arabia-Eurasia collision zone. In this region, active deformations are principally taken up by strike-slip and reverse faulting within the Kopeh Dagh and Binalud deformation domains (Fig. 1), which are structurally connected through the Meshkan Transfer Zone (*Shabanian et al*., 2009b). The northward motion of Arabia with respect to Eurasia is accommodated at a rate of 22±2 mm/yr at the longitude of Bahrain (*McClusky et al*., 2003; *Reilinger et al*., 2006; *Sella et al.*, 2002; *Vernant et al*., 2004). At the eastern boundary of the Arabia-Eurasia collision, this motion is expressed as right-lateral shear on several major N–S strike-slip fault systems on both sides of the Lut Block (*Meyer and Le Dortz*, 2007; *Regard et al*., 2004; *Tirrul et al.*, 1983; *Walker and Jackson*, 2004). Between the Lut Block and Eurasia, geodetic GPS measurements (*Vernant et al*., 2004; *Tavakoli*, 2007) indicate a rate of 7±2 mm/yr for this right-lateral shear at the eastern boundary of the Arabia-Eurasia collision. Further north, in NE Iran, the available geodetic (*Masson et al*., 2007; *Reilinger et al*., 2006; *Tavakoli*, 2007; *Vernant et al*., 2004) and geological (*Shabanian et al*., 2009a; *Shabanian et al*., 2009b) data, indicate that this northward motion should be accommodated at a rate ranging from 4 to 11 mm/yr (Fig. 1). Comparing the rates representative for the present-day tectonic deformation in eastern Iran with the rates in NE Iran, we suggest that the Arabia-Eurasia northward motion is permanently transferred between eastern Iran faults (*e.g*., Sistan Fault System) and the Kopeh Dagh fault systems. In this context, one key question is to know what the contribution of the main deformation domains (*i.e*., Kopeh Dagh, Meshkan transfer zone, and Binalud) is in the accommodation of this deformation. The distribution and kinematics of deformations in the Kopeh Dagh and Meshkan transfer zone has recently been discussed by *Shabanian et al*. (2009a, 2009b, and 2009c). In the Kopeh Dagh, they shown that the northward motion of central Iran relative to Eurasia is principally (7±2 mm/yr) accommodated by strike-slip faulting localized along the Bakharden-Quchan Fault System. Recent morpho-tectonic investigations by *Shabanian et al*. (2009b) suggested that more than 25 per cent of the strike-slip faulting in the Kopeh Dagh (*e.g*., *Tchalenko*, 1975; *Shabanian et al*., 2009a) should be southwardly transferred through the Meshkan Transfer Zone (Fig. 1). For the Binalud, the GPS-derived rate of range-parallel displacement is comprised between 2 and 4 mm/yr (*Masson et al*., 2007; *Tavakoli*, 2007), implying that considerable right-lateral strike-slip movement should occurs at both sides of this mountain range. However, there is no geological knowledge of the rate and mechanism of active deformation to evaluate the consistency of

such short-term rates with geological long-term rates of quaternary faulting at two different scales of time.

This chapter aims at characterizing rates and kinematics of quaternary faulting that prevail in the Binalud mountains, where a short-term range-parallel slip rate of 2-4 mm/yr is estimated from geodetic GPS measurements without been clearly attributed to individual faults at both sides of the range.

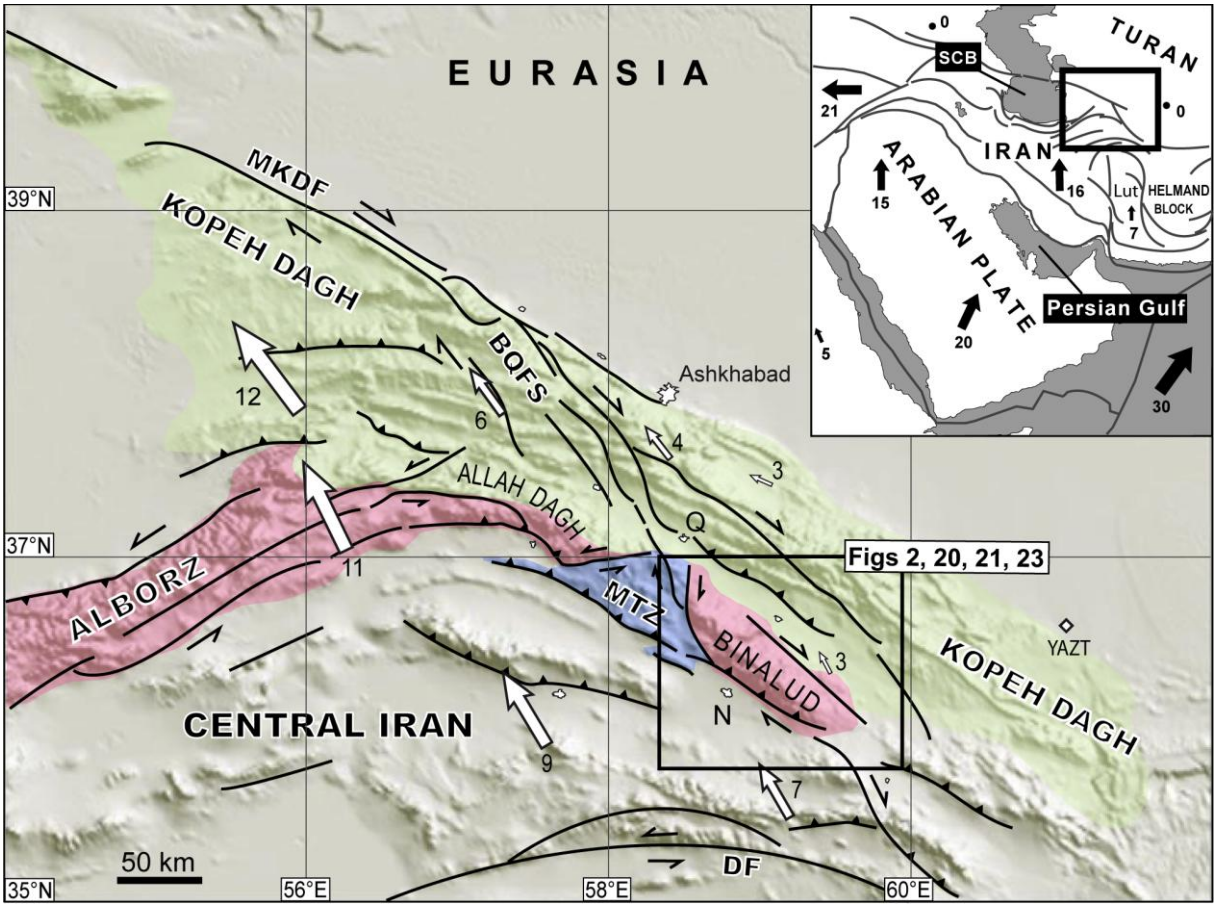


Figure 1. GTOPO30 topographic image showing the regional tectonic setting and major active faults of NE Iran. White arrows and associated numbers are GPS horizontal velocities (mm/yr) in a Eurasia-fixed reference frame (YAZT station; *Tavakoli*, 2007). The inset with the box on the upper right shows the location in the Arabia-Eurasia collision framework. Gray arrows and associated numbers represent Arabia-Eurasia plate velocities (mm/yr) after *Reilinger et al.* (2006). Abbreviations: MKDF, Main Kopeh Dagh Fault; BQFS, Bakharden-Quchan Fault System; DF, Doruneh Fault; MTZ, Meshkan Transfer Zone; SCB, South Caspian Basin.

In this paper, we present the first direct estimation of Late Quaternary slip rates in the Binalud Mountains, combining in situ-produced $^{10}$Be exposure dating, detailed satellite image (Landsat ETM+ and SPOT5) analyses, and morphotectonic field surveys. As a supplementary tool, quantitative geomorphic analysis (*i.e.*, hypsometric integrals for drainage basins) is used to illustrate geomorphic processes linked to active deformation pattern in the Binalud domain.

After a review of active tectonic setting of the region, we present the active faulting evidences along two main fault systems (Neyshabur and Mashhad faults) at both sides of the range. Then, we describe the morphotectonic investigations conducted along the two fault systems in order to estimate individual Quaternary fault slip rates. As a discussion, geological and geomorphic data are analyzed together to better understand deformation pattern in the Binalud Mountains and its controls on long-term geomorphic processes.

## 2. Active tectonic setting

The Binalud deformation domain forms a 130-km-long, NW-trending range, which separates Central Iran from the Eastern Kopeh Dagh (Fig. 2). This asymmetric antiformal range (*Alavi*, 1992) is characterized by a gently sloping NE flank versus a steeply sloping SW flank thrusted over the northeastern margin of Central Iran. The Binalud Mountains correspond to an old deformation domain that suffers from successive major ductile or brittle tectonic deformation episodes since the paleo-Tethys closure (pre-Late Triassic) (*Alavi,* 1992). During the Cenozoic tectonic episodes, folding processes are roughly identical for the entire region including the Kopeh Dagh and Allah Dagh-Binalud mountains. The same orientation of the fold axes within the Kopeh Dagh and Allah Dagh-Binalud mountains was suggested as a result of homogenously directed pre-Pliocene compressional movements, (*Shabanian et al*., 2009b). Such homogeneity is also indicated for the Plio-Quaternary tectonic regimes, deduced from fault kinematics inversion in NE Iran (*Shabanian et al*., 2009c).

From the active deformation point of view, the Binalud domain is bounded by three major inherited fault systems: the Neyshabur and Mashhad Fault Systems at its southwest and northeast flanks, respectively, and the N-trending Chakaneh Fault System along its western side (Fig. 2). This last fault is a right-lateral strike-slip fault system transferring ~25 per cent of the northward motion of Central Iran relative to Eurasia between the Kopeh Dagh and Binalud mountains (*Shabanian et al*., 2009b). Herein after, we focused on the Neyshabur and Mashhad Fault Systems understanding the rate and kinematics of Quaternary deformation at both sides of the Binalud deformation domain.

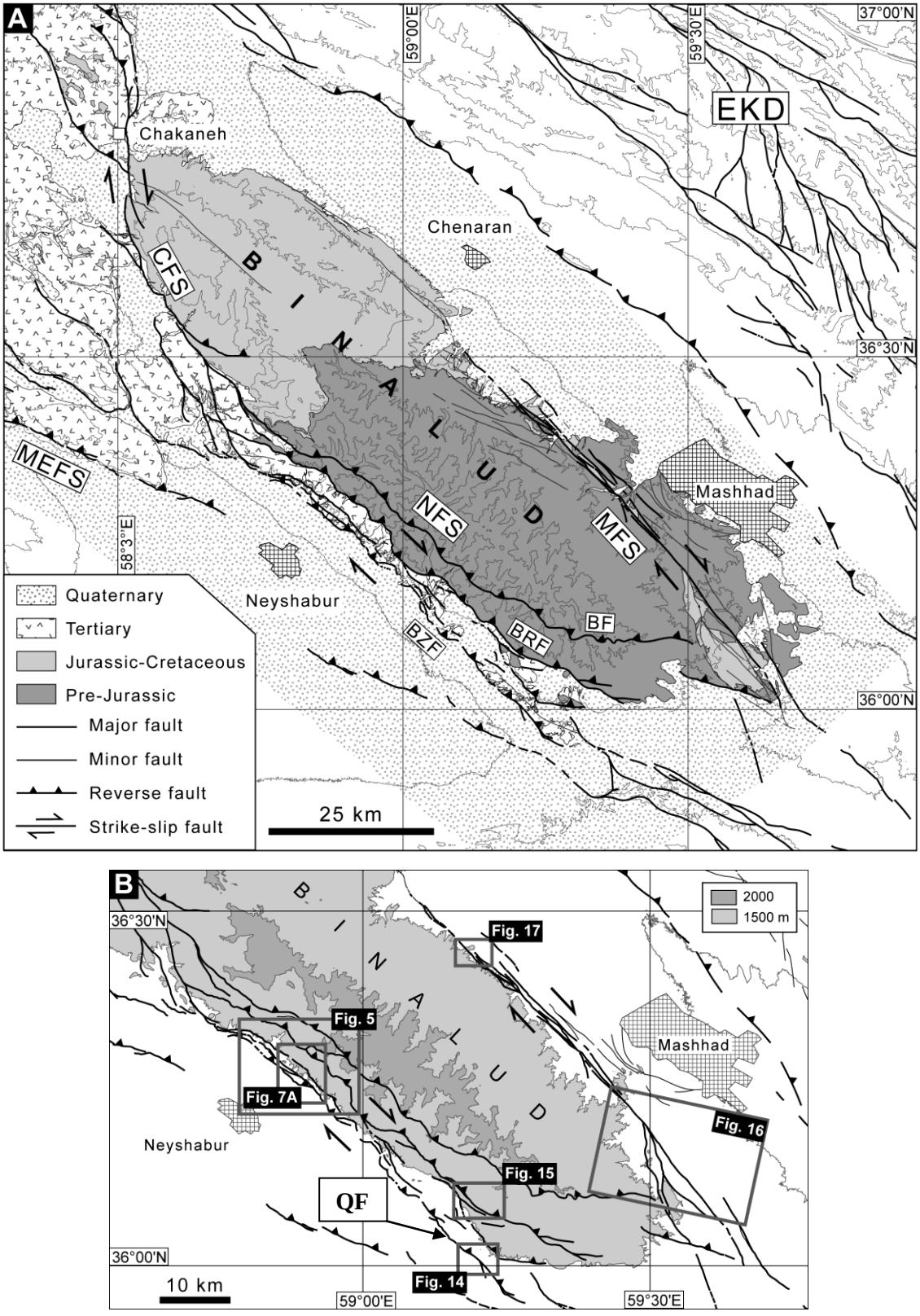


Figure 2. (a) Simplified geological map together with the fault map of the Binalud deformation domain. Fault traces are based on SPOT5 and LANDSAT ETM+ image mapping (after *Shabanian et al*. 2009b and this study). CFS, Chakaneh Fault System; MFS, Mashhad Fault System; NFS, Neyshabur Fault System; MEFS, Meshkan Fault System; BF, Binalud Fault; BRF, Barfriz Fault; BZF, Buzhan fault zone; QF, Qadamgah Fault; EKD, Eastern Kopeh Dagh. (b) Index map of the investigated sites in this paper.

## 3. Methodology

### 3.1. Geomorphic mapping and site selection

At the regional scale, quaternary fault traces were mapped on the basis of Landsat ETM+ images. SRTM digital elevation data was used to quantitative geomorphic analyses of deformed landforms. At the site scale, analyses of SPOT5 images combined with direct field observations were used to quantify geomorphic offsets along the recognized active fault segments, and to select key sites offering two advantages for understanding the displacement history of the Neyshabur and Mashhad Fault Systems: (1) Maximum total offset on a single fault strand, and (2) well-preserved alluvial fan surfaces to ensure constrained fault offset values and readily datable markers. Differential kinematic GPS surveys were performed when more 3-D details of offset markers is needed.

### 3.2. Sampling and estimating surface exposure ages

To select the sampled boulders on the offset fan surfaces, both the geomorphic setting and the surface characteristics were carefully considered. Boulders ranging from 0.3 to 1 m in diameter, embedded on the fan surfaces were sampled avoiding angular, visibly broken and non-rooted boulders. Considering exponential drop off in situ-produced $^{10}$Be concentrations, boulders showing spalled surfaces were avoided and samples were collected from the upper 1-8 cm on top of boulders. Additionally, the sampled surfaces were also selected on the fact that they did not suffer from overland flows and extensive surface erosion by sheet flow (*Wells et al*., 1985, *Wells et al*., 1987; *McDonald*, 1994), ensuring that such post-depositional processes have had a negligible impact on the initial morphology of the sampled surfaces. Consequently, there is no evidence that the sampled boulders might have been moved and/or buried before their exposition at the present surfaces. For all the sampled sites, the shielding by the surrounding topography, snow cover, and sample geometry are found to be of negligible impact on the surface production rates. The sampled surfaces are located away from recent incision rills, and show a relatively fresh morphology (Fig. 3). Even if special efforts have been paid during sampling to minimize the effects of erosional processes on fan surfaces, our cosmogenic ages provide minimum ages of fan abandonment ages, and thus age initiation of offset. As a consequence, all the slip rates discussed hereafter should be considered as maximum rates.

We used in situ-produced $^{10}Be$ resulting from spallation and muonic reactions on Silicon and Oxygen in quartz minerals. After sieving (fraction comprised between 1 and 0.250 mm), sediment samples passed through magnetic separation, and non-magnetic fraction undergone selective etchings in fluorosilicic ($H_2SiF_6$) and hydrochloric acids (HCl) to eliminate all mineral phases but quartz. Quartz minerals then undergone a series of selective etching in hydrofluoric acid to eliminate potential surface contamination by $^{10}Be$ produced in the atmosphere. The cleaned quartz minerals were then completely dissolved in hydrofluoric acid after addition of a $^{9}Be$ carrier solution (*Merchel et al*., 2008). Beryllium was separated from these solutions by successive solvent extractions and precipitations. Beryllium oxides were mixed with Niobium for target packing and samples were analyzed by Accelerator Mass Spectrometry (AMS). Measurements were performed both at ASTER (Aix-en-Provence) AMS National facilities (Table1). The measured isotopic ratios are directly calibrated against the National Institute of Standards Technology (NIST) standard reference material 4325 using the values recently reevaluated by *Nishiizumi et al*. (2007) which are: $^{10}Be/^{9}Be = (2.79\pm0.03).10^{-11}$ and $^{10}Be_{1/2}=(1.36\pm0.07).10^{6}$ years ($\lambda^{10}Be=(5.10\pm0.26).10^{-7}$ $yr^{-1}$). To determine production rates, scaling factors for latitude and altitude corrections were calculated according to *Stone* (2000) and using a modern $^{10}Be$ production rate at sea level and high latitude of 4.5±0.3 atoms/g-$SiO_2$/yr to account for the reevaluation of absolute calibration of $^{10}Be$ AMS standards proposed by *Nishiizumi et al*. (2007).

To illustrate cosmogenic-derived minimum exposure age data and their associated uncertainties, we used the sum of the Gaussian probability distributions (*e.g*., *Deino and Potts*, 1992), already used by different authors for dating purposes (*e.g*., *Daëron et al*., 2004; *Lowell*, 1995), according to (*e.g*., *Taylor*, 1997):

$$p_{sum}(t) = \sum_i e^{-(t-a_i)^2/2\sigma_i^2} / \sigma_i\sqrt{2\pi}$$

where t is time, $a_i$ is the exposure age of sample i and $\sigma_i$ is the associated uncertainty. A probability value less than 0.05 indicates that there is a significant amount of non analytical error in the data set, and that one or more samples are outliers. In such a case, cumulative frequency plots are generally bimodal in shape, with the secondary peak identifying outliers.

## 4. Morphotectonic investigations along the Neyshabur Fault System

In the Binalud region, the Neyshabur Fault System corresponds to a NNW-trending fault assemblage at the southwestern side of the Binalud Mountains (Fig. 2). This fault system is constituted of three nearly parallel fault zones running southeastwardly over a length of ~90 km from the southeastern termination of the Chakaneh fault system (Fig. 2). From NE to SW, the faults are the Buzhan Fault zone, the Binalud and Barfriz Fault systems of which the first one is the youngest ones. It is noteworthy that the WNW-striking faults northwest of Neyshabur City (Fig. 2), referred to as the Neyshabur and North Neyshabur faults by *Berberian and Yeats* (1999) are clearly crosscut by the Chakaneh and Neyshabur Fault Systems. In fact, those faults belong to the Meshkan reverse fault system (*Shabanian et al*., 2009b) showing different orientation and kinematics (reverse faulting) than that (oblique-slip right-lateral faulting) of the Neyshabur Fault System (*Shabanian et al*., 2009c, and this study).

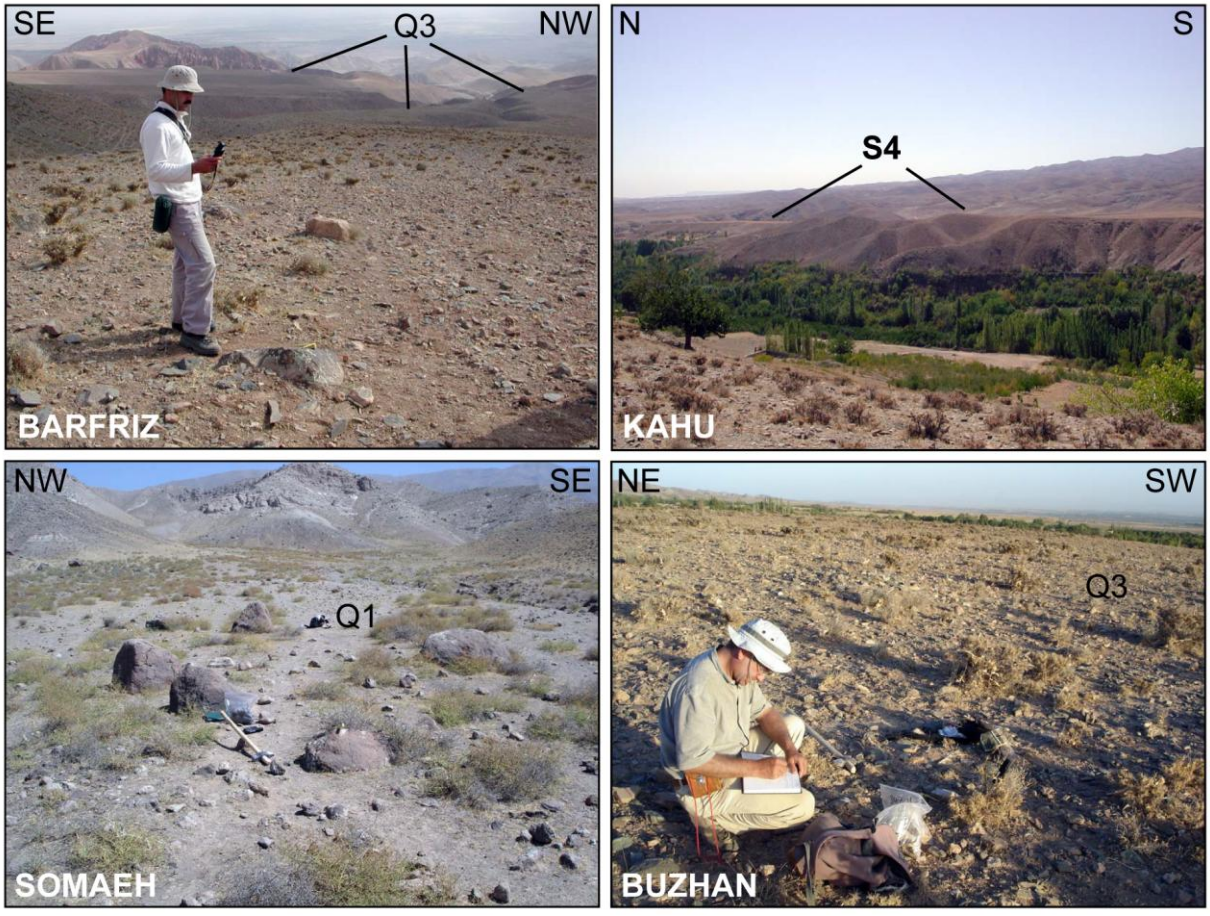


Figure 3. Field photographs of the sampled alluvial fan surfaces illustrating general situation of the dated surfaces. Name of each sampling area is marked lower left of the photographs.

### 4.1. The Binalud Fault zone

Along the NE-dipping Binalud Fault zone, Devonian dolomitic limestones (Bahram Formation) are thrusted over the Triassic metamorphic Mashhad phylites (*Aghanabati*, 1986). The ~90-km-long Binalud Fault zone was originally a low-angle (~30°) thrust fault associated with mylonite zones indicating ductile behavior of the involved rocks at the time of thrusting (*Alavi*, 1992). The topographic expression of the fault indicates that it is nowadays back-tilted and steeply-dipping (50-70°). The northwestern termination of the Binalud Fault zone joins to the Chakaneh Fault system (*Shabanian et al*., 2009b) at an oblique angle (Fig. 2). In that area, systematic deflections of drainage networks that cross through the fault zone suggest a right-lateral component of motion along the northwestern part of the Binalud Fault zone. The onset of right-lateral faulting along the Chakaneh fault system is estimated at <5 Ma (*Shabanian et al.*, 2009b), suggesting that the northwestern part of the Binalud Fault zone may was reactivated during the late Cenozoic. However for the main portion of the Binalud Fault, there is no convincing evidence indicating its activity during the Plio-Quaternary. Therefore, we consider that the Binalud Fault zone is a back-tilted inactive thrust fault with a minimum length of about 65 km, extending in the central and southeastern part of the Binalud Mountains, without significant contribution for accommodating the present-day tectonic deformation in NE Iran. The northwestern fault segment can be considered as a fault splay of the Chakaneh Fault system.

### 4.2. The Barfriz Fault

The Barfriz Fault extends at the southwestern front of the Binalud Mountains (Fig. 2). This NE-dipping, 80-km-long fault was initially a low-angle (20-40°) thrust fault (*Alavi*, 1992) that displaced the Triassic metamorphic Mashhad phylites over Tertiary deposits (*Aghanabati*, 1986). At its northwestern termination, the Barfriz Fault joins to the Chakaneh fault system (Fig. 2). To the southeast, the fault ends into a horsetail splay termination. During the Plio-Quaternary, the Barfriz fault has been reactivated into an oblique-slip reverse fault (next sections). Along which affected Quaternary landforms such as alluvial geomorphic terraces and drainages incised in, provide evidence for both reverse and right-lateral fault offsets (Figs 4, 7 and 8). Spectacular triangular facets at the scale of the mountain front (Fig. 4) and Quaternary fault escarpments along the fault trace (Figs 4, and 8) express the significant vertical component of faulting on the Barfriz fault.

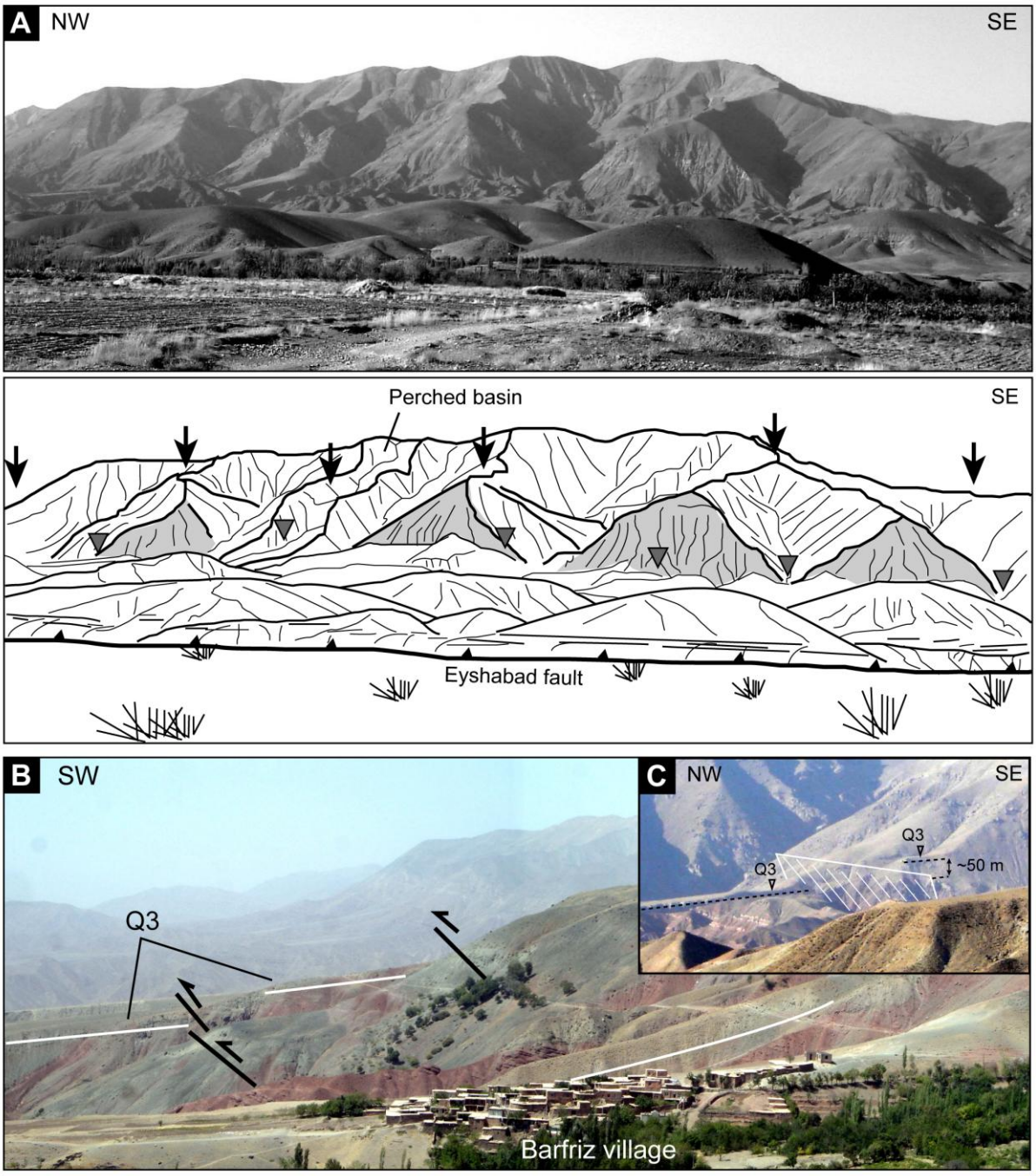


Figure 4. (a) General view of the Binalud Mountains taken from ~2 km SW of Eyshabad village showing spectacular triangular facets, perched watersheds and different levels of fault escarpments across the Neyshabur Fault System. Traces of the Binalud and Barfriz faults are indicated by black arrows and gray triangles, respectively. The foothills domain is represented by rounded hills between the Barfriz Fault and the Eyshabad fault segment belong to the Buzhan Fault zone. The hills are capped by Q3 fan surfaces. (b) and (c) show two Q3 surfaces vertically offset across the Barfriz Fault. Location of the photographs is marked in Figure 5.

Along the northwest half length of the fault, deformation is focalized along a narrow 100-m-wide fault zone, but, faulting is more distributed on its southeastern half length (Fig 2). The Barfriz Fault corresponds to the relic Binalud Mountain front separating the mean 2500 m-high Binalud Mountains on the hanging wall from a band of 1.5–5 km-wide eroded

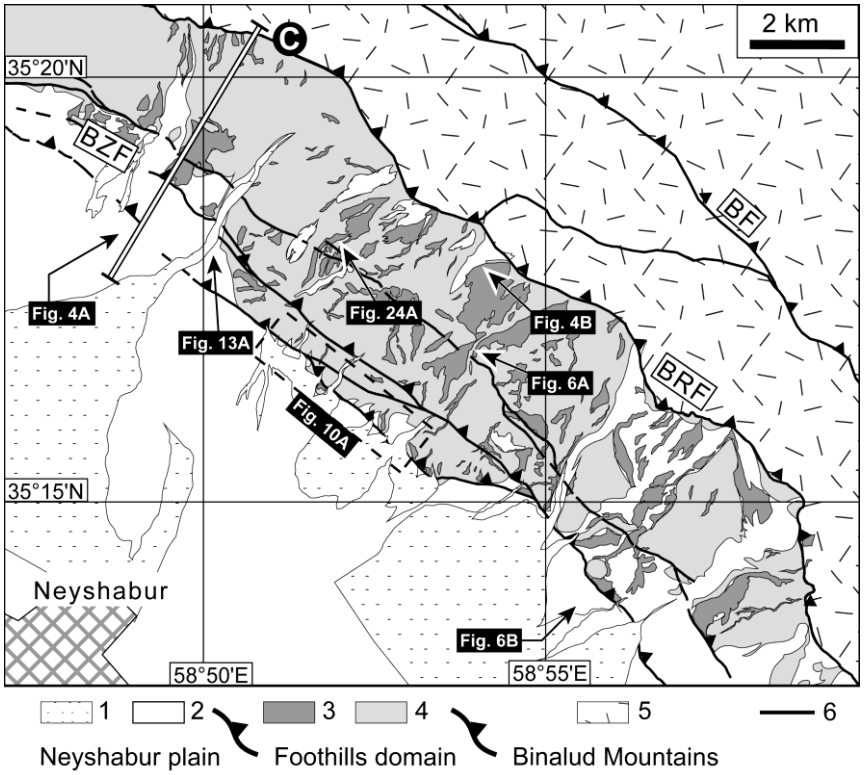


Figure 5. Simplified morphotectonic map of the foothills domain representing major fault segments together with quaternary alluvial units. Abbreviations like in Figure 2. 1, Recent alluvium; 2, Undifferentiated Q1 and Q2 alluvial surfaces; 3, Q3 fan surface; 4, Tertiary rock; 5, Pre-Cenozoic rock; 6, Fault. Location of the topographic profile "C" in Figure 9 is marked. Figure numbers refer to the location of photographs presented in this chapter. The Buzhan Fault zone (BZF), from SW to NE; the Somaeh, Eyshabad, and Buzhan faults.

foothills in the footwall. This domain is a distinct structural and geomorphic unit between the Barfriz and the Buzhan Fault zones (Fig 2 and 5). In the foothills domain, analysis of SPOT5 satellite images allowed us identifying three main abandoned alluvial surfaces from their distinct morphology and geomorphic setting. The higher alluvial fan surface ($Q_3$) comprises of old eroded surfaces that spread within the foothills domain on the hanging wall of the Buzhan Fault, uphill from the Buzhan Fault zone front (Fig. 5). It represents elevated remnants of gently sloping Quaternary surfaces overlying the Tertiary folded rocks. Flat tops of $Q_3$ surfaces can be observed from place to place, but in most cases they are rounded or totally eroded, and thus only transposed in the morphology (Fig. 6). The distribution pattern of the $Q_3$ remnants indicates that the folded Tertiary rocks of the foothills domain have been completely covered by these Quaternary surfaces forming an old alluvial plain at the front of the Barfriz Fault, *i.e.*, relic deformation locus of the southeast Binalud flank. This strongly suggests that the Quaternary front of the Binalud Mountains corresponded to the Barfriz Fault and that the present foothills domain has been under deposition (Fig. 6). The $Q_3$ alluvial fans are now offset both laterally and vertically along the Barfriz Fault (Figs 6, 7, and 8).

An intermediate alluvial surface ($Q_2$) is inset within $Q_3$ alluvial surfaces. This generation is found in narrow patches spread along large stream beds extending on the footwall of the fault. The lowest geomorphic surface ($Q_1$) consists in the youngest abandoned alluvial fan surfaces, extending from the southwestern expression of the Buzhan Fault to the Southwest of the Neyshabur plain (Fig. 5). Active streams incise in $Q_1$ surfaces and discharge their deposits in form of thin, gently sloping alluvial fans dissipating toward southwest, beyond the fault zone (Fig. 5).

### 4.3. Cumulative fault offsets along the Barfriz Fault

Along the Barfriz Fault, most of drainages exhibit systematic deflections or offsets, providing evidence for a right-lateral faulting component on the fault. Vertical component of faulting is clearly expressed in the morphology of the mountain front and Late Quaternary fault escarpments (Figs 4, 7 and 8). However, geomorphic markers suitable for both offset measurement and dating are rare. To A key site was selected near Barfriz village, where a series of offset $Q_3$ fan surfaces and their associated drainages (Figs 7 and 8) provide conspicuous geomorphic evidences indicating both vertical and right-lateral component of faulting along the Barfriz Fault. The lateral-lateral offsets are expressed in deflected or beheaded streams and consequent stream captures (Figs 7 and 8). Generally, the initial form of the $Q_3$ alluvial surfaces has been either degraded by erosion or modified by the younger fan aggradation episodes. This makes relationships between $Q_3$ surfaces and watersheds on the other side of the fault unclear. In such a situation individual $Q_3$ surfaces cannot appropriately be correlated with corresponding drainage basin outlets. Here, drainages incised in $Q_3$ surfaces are considered as favorable candidates to quantify the cumulative fault offsets. However, application of such geomorphic features needs to particular attentions to relevance of the offset they present to the age of the surface abandonment. For drainage with the same morphology (length, depth and width) incised in a Quaternary surface one can attribute the same age postdating the abandonment of the surface. In such a case, older drainages have ages closer to the abandonment age of the surface.

Along the Barfriz Fault trace, a combination of geomorphic and geometric approaches allowed us to reconstruct both horizontal and vertical cumulative offsets recorded by $Q_3$ surfaces. The geomorphic reconstruction of drainages incised in the $Q_3$ fan surfaces indicates a cumulative right-lateral offset of 240±10 m along the Barfriz Fault, allowing us to appropriately reconstruct the initial pattern of the offset drainages (Fig. 7). A part of vertical

fault displacements is expressed by a continuous SW-facing escarpment (Fig. 8) running along a 20-km-long fault segment. Both sides of the fault escarpment, $Q_3$ surfaces have been tilted upward over a distance of 70 m (Fig. 8). Away from the tilted domain, the surfaces slope on both the footwall and hanging wall (eroded bedrock) is identical. In that area, there is evidence for both vertical offsets and tilting in $Q_3$ surfaces due to a reverse faulting component on the NE-dipping Barfriz Fault. This feature indicates that the observed fault escarpment, which corresponds to near-fault cumulative vertical offset, postdates the abandonment of $Q_1$ fan surface. This relationship allows us determining minimum cumulative vertical offset coeval with the lateral offset we measured along the Barfriz Fault (Fig. 8). The geomorphic analysis of topographic profiles (based on SRTM data) across the fault reveals a minimum vertical offset of ~55 m (Fig. 8). But this near-fault displacement is not representative for the total cumulative vertical deformation of the fault. At the scale of the foothills domain, it appears that $Q_3$ surfaces are entirely tilted upward relative to their initial geomorphic position. To measure total vertical deformations recorded by $Q_3$ surfaces, across the Neyshabur fault system, the initial geomorphology of the surface (*i.e.*, depositional surface) should be reconstructed. Doing so, we assume that the downhill segments of the $Q_3$ surfaces are undeformed geomorphic surfaces far away from any identified deformation and significant fan depositions. Using topographic measurements from the downhill segments, we were able to reconstruct the depositional morphology of the $Q_3$ surfaces using a series of equation developed by *Troeh* (1965). These equations utilize three points of known radial distance from the fan apex to predict the elevation of any point on the fan. *Troeh's* equations can thus be used to reconstruct an entire radial profile of an alluvial fan (see *Keller et al*., 2000 for tectonic implications). We applied the reconstructed morphology of the alluvial fan produced by *Troeh's* equations as a landscape model to estimate vertical displacement postdating the $Q_3$ fans. Comparing the reconstructed average elevation of the fan apex at the time of $Q_3$ deposition and the present-day elevation of the fan apex, we infer an averaged total vertical displacement of 230 m of which, for the mountains front, a cumulative vertical offset value of 140-160 m is attributed to the Barfriz Fault since the deposition of the $Q_3$ surfaces (Fig. 9). For the Barfriz Fault, combining both vertical and horizontal offsets allows deducing a total oblique slip of 280 m and a calculated rake angle of 33°, which is the direction of the fault slip vector projected on a vertical plane parallel to the strike of the fault.

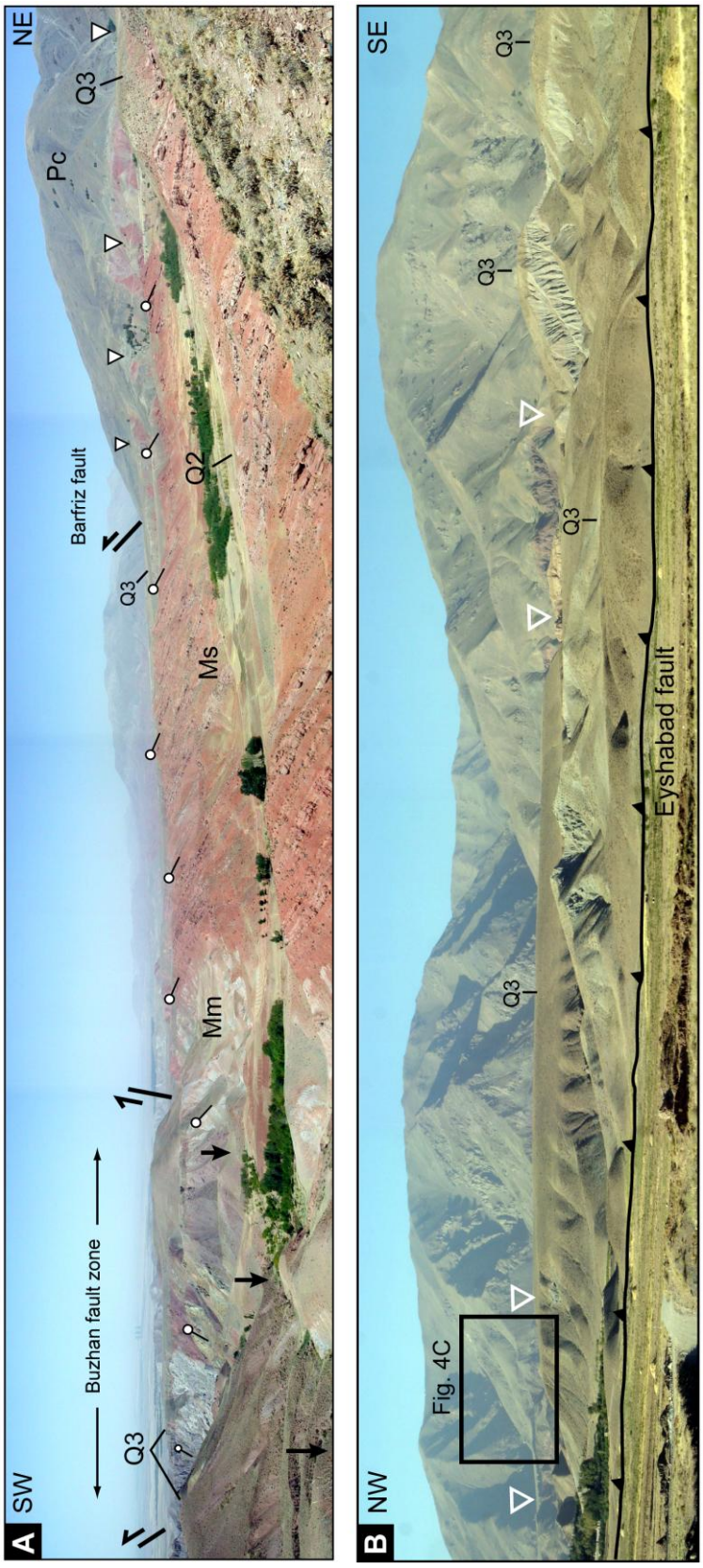


Figure 6. (a) Panoramic view of the foothills domain taken from the Barfriz area. Dip of bedding of the folded Miocene rocks between the Barfriz fault and the Buzhan fault zone is indicated. Mm, Miocene marls; Ms, Miocene sandstones. (b) Geomorphic expression of the $Q_3$ surfaces in the hanging wall of the Eyshabad fault. Trace of the Barfriz fault is pointed by white triangles. See Figure 5 for location of the photographs.

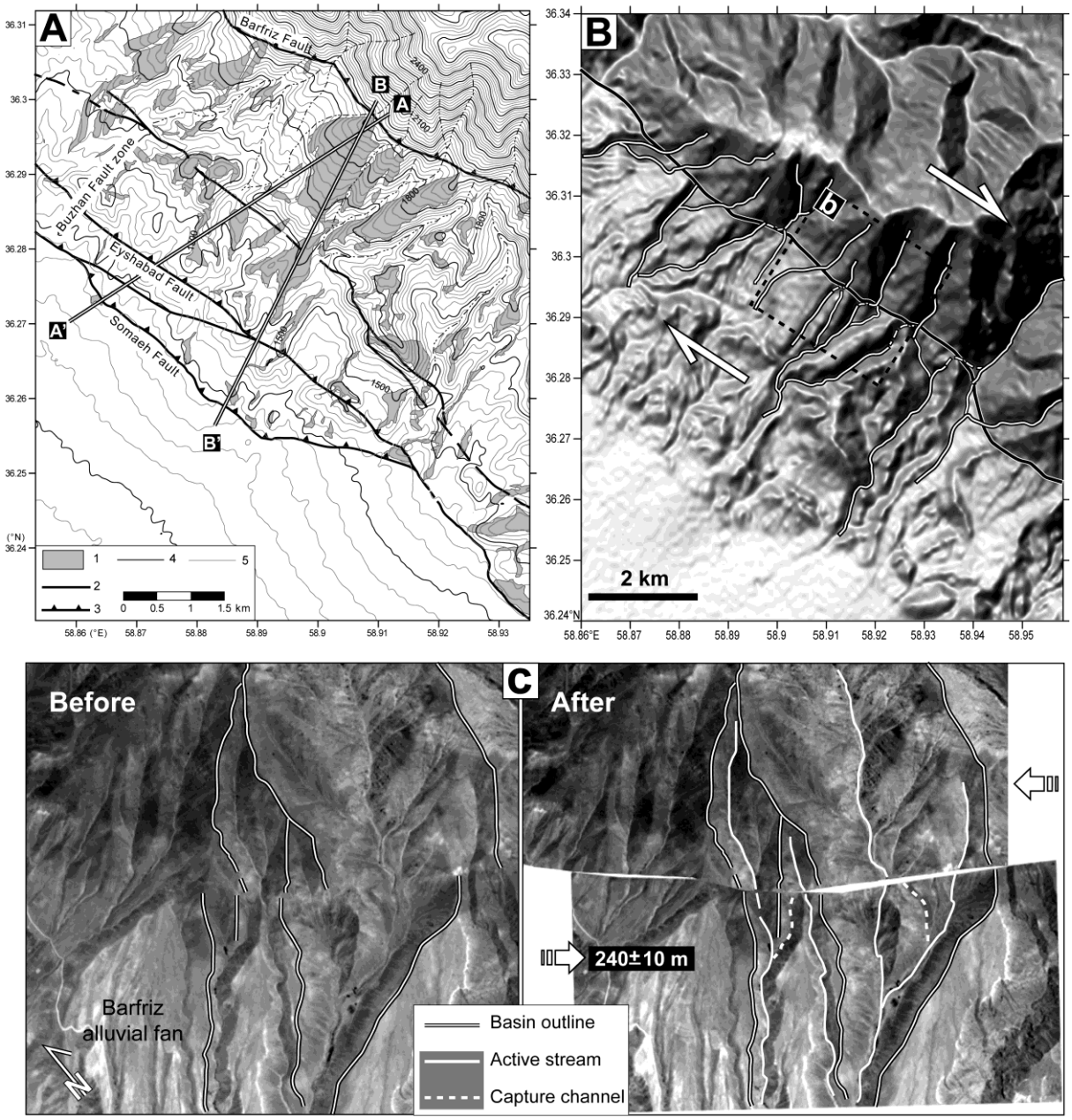


Figure 7. (a) Regional distribution of $Q_3$ surfaces. 1, $Q_3$ alluvial surfaces; 2, Fault; 3, Reverse fault segments (sawteeth mark the hanging wall side of reverse faults); 4, Topographic contour lines with 100 m interval; 5, Topographic contour lines with 20 m interval. A-A' and B-B' show location of the topographic profiles presented in Figure 9. (b) Shaded relief map of the Barfriz area based on SRTM data. White double lines are streams; Captured segments of the streams are marked by dashed lines. Barfriz Fault is shown as black double line. (c) SPOT5 image centered on the Barfriz $Q_3$ surfaces and their associated drainage systems. The situation of offset markers is presented before and after the offset restoration.

### 4.4. The Buzhan Fault zone

At the SW flank of the Binalud Mountains, the 60-km-long, NE-dipping Buzhan Fault zone corresponds to the frontal fault zone of the foothills domain, and consists in parallel fault segments, with lengths ranging from 10 to 30 km (Fig. 2). Conversely to the Barfriz Fault,

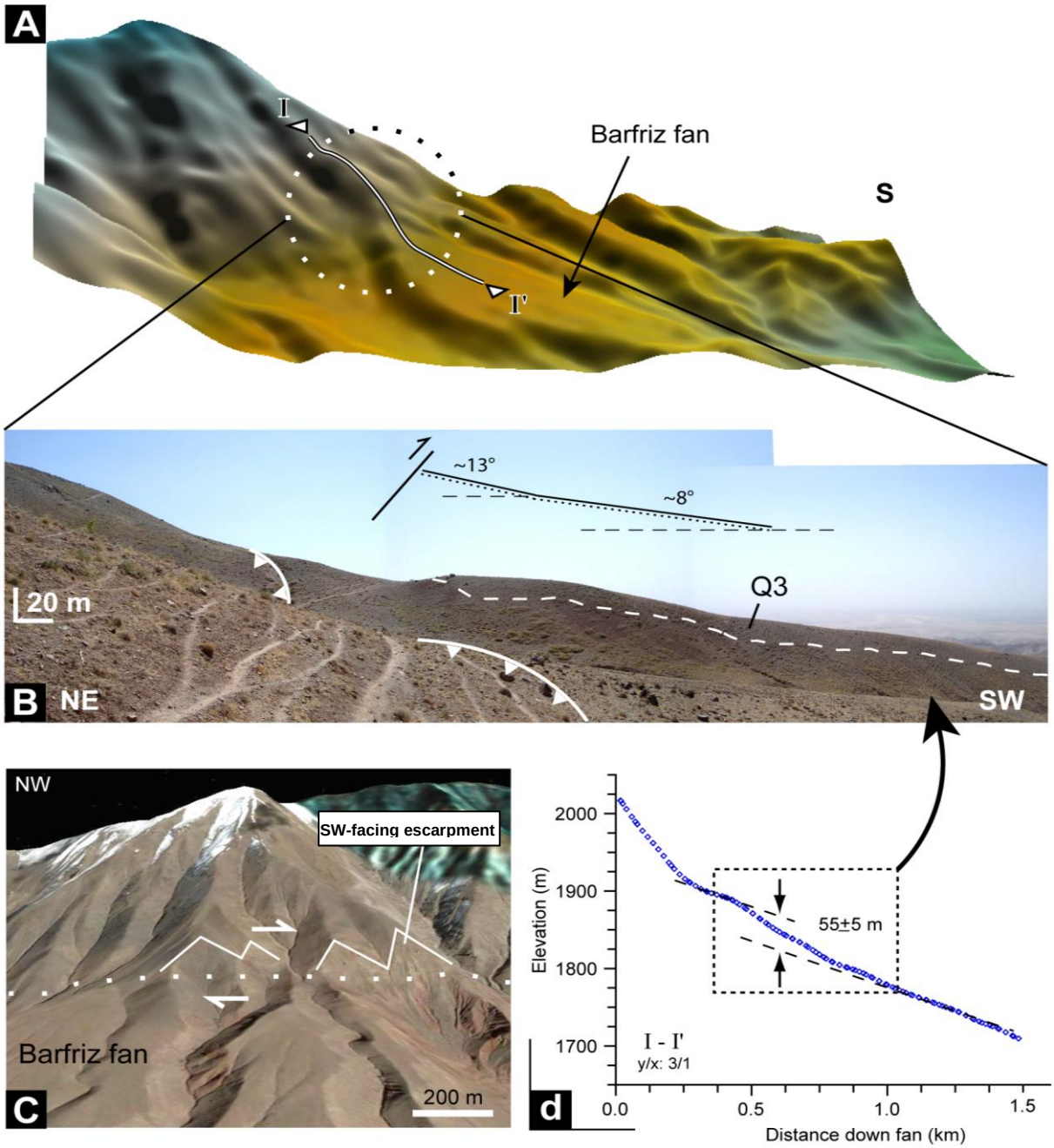


Figure 8. Geomorphic analyses of the Barfriz fan. (a) 3-D view of the Barfriz fan based on SRTM data. (b) Filed photograph from the apex of the Barfriz fan. The Barfriz Fault is marked by white thick lines (sawteeth point the hanging wall side). (c) 3-D view of the Barfriz fan (Quickbird image-GoogleEarth) showing the fresh triangular facets in form of a SW-facing escarpment along the Barfriz Fault. (d) Topographic profile through the Barfriz fan apex affected by the Barfriz Fault (SRTM data).

faulting along the Buzhan Fault is distributed over a 3-km-wide zone in which fault-related morphologies such as fault scarps and geomorphic markers affected by the fault become relatively younger toward the Southwest**.** In the foothills domain, the stratified Miocene marls and sandstones were folded into overturned anticlines or synclines striking parallel to the Buzhan Fault zone with gently-dipping northeastern and steeply-dipping to overturned

southwestern limbs (Fig. 6). Such geometry most probably results from the contraction of the Tertiary strata between the faults at both sides of the foothills domain (Fig. 6). In the northwestern part of the area (north of Ouqay Gach quarry), the Miocene rocks were covered by the Pliocene conglomerates and were folded together into an overturned syncline (*Shabanian et al*., 2009b). This indicates that folding is at maximum Pliocene in age, and consequently, faulting along the Buzhan Fault zone should have occurred during the Pliocene. Afterwards, the folded rocks were covered by $Q_3$ alluvial surfaces, which have in turn been incised and inset by younger erosional and depositional units. Within the Buzhan Fault zone, remnants of $Q_3$ surfaces are observed at the top of the most preserved reliefs (Fig. 6). It suggests that during $Q_3$ aggradation episode, the fault zone was inactive and that the foothills domain was totally covered by $Q_3$ alluvial fans. The Buzhan Fault zone reactivated during the Late Quaternary, uplifting the foothill domain and affecting the $Q_3$ fan surfaces. The youngest abandoned alluvial fans ($Q_1$) are affected by the southwestern segments of the Buzhan Fault zone, and recent streams transport eroded materials away from the fault zone creating the present-day alluvial cones on the footwall (Fig. 5). These features represent the present-day activity along the southwestern segments of the Buzhan Fault zone. Altogether, geological and geomorphic evidences suggest that the present-day faulting along the Buzhan Fault zone is the expression of late Quaternary reactivation of preexisting faults along which the first fault motions could not be older than the Pliocene. Considering the fault arrangement and structural pattern the Buzhan Fault zone, it is divided to two distinct parts; the northwest part constituted by two major parallel fault segments (the Eyshabad and Somaeh faults), and the southeastern part characterized by localized deformation along a single fault. There are conspicuous geological and geomorphic evidences indicating prominent reverse faulting along the northeastern part, while evidence for lateral faulting component is not so clear and abundant. Conversely, the southeastern segment is characterized by right-lateral oblique-slip faulting with a predominated lateral component of faulting.

### 4.5. Quantification of the Late quaternary fault offsets along the Buzhan Fault zone

Along the Buzhan Fault zone, our morphotectonic investigations were conducted at three key sites along the northwestern (*i.e*., the Somaeh and Eyshabad fault segments) and southeastern (Qadamgah fault segment) half lengths of the fault zone (Fig. 2B). The first site is located ~2 km to the north of Somaeh village, where geomorphic and structural expressions of the Somaeh fault segment imply that it has reactivated for at least four times during the late

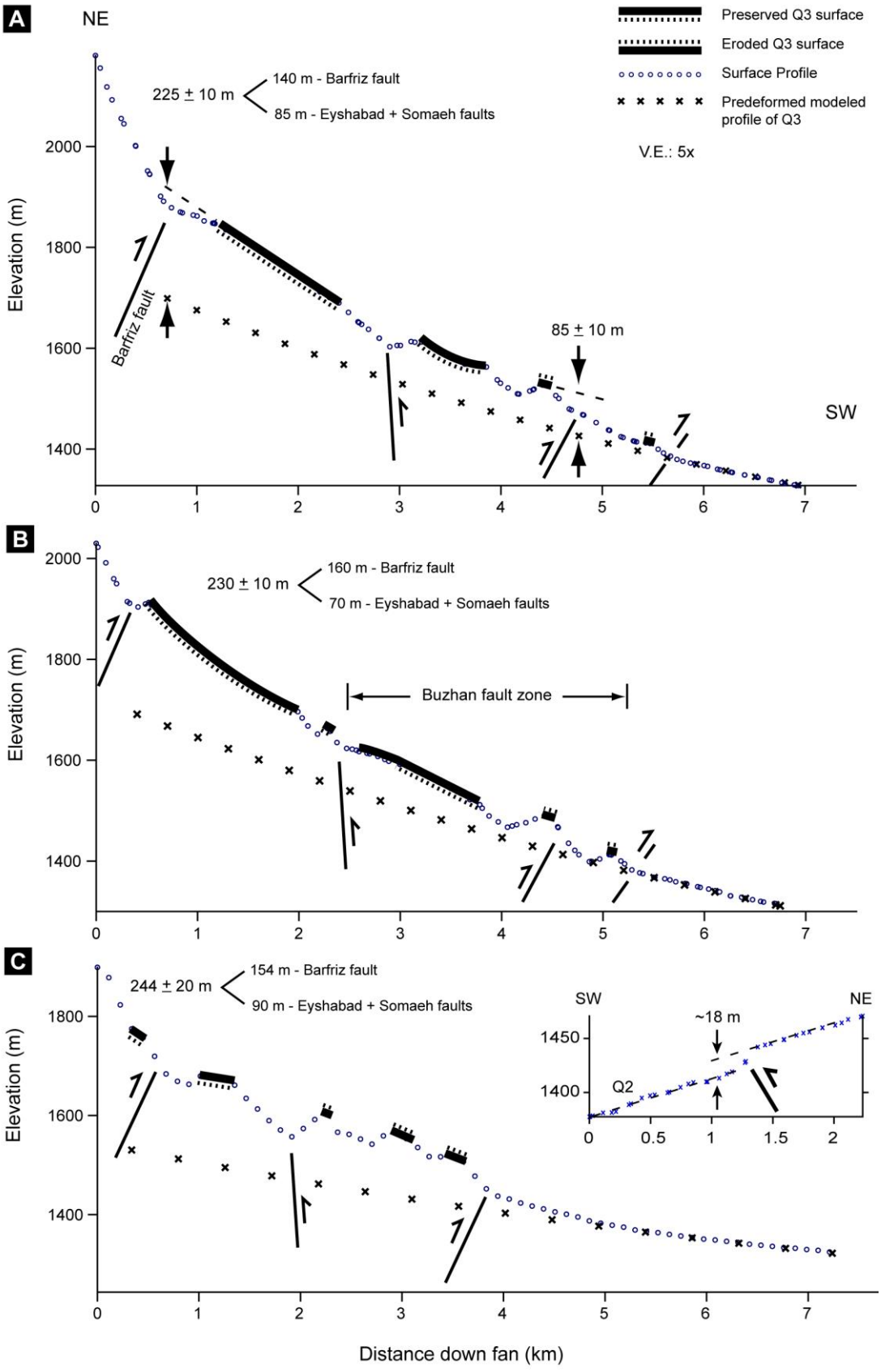


Figure 9. Reconstruction of $Q_3$ alluvial surfaces using *Troeh* (1965) equations. For the profile locations: "A" and "B" in Figure 7; "C" in Figure 5. Upper right in "C" is a detailed profile across the Eyshabad fault scarp to illustrate the vertical offset value recorded by the $Q_2$ surface. Profiles are based on SRTM data.

Quaternary. On the hanging wall (NE side) of the fault, the highest reliefs are the geomorphic expression of the cumulative vertical fault displacements. The reliefs are armed by Tertiary rocks that have been covered by $Q_3$ alluvial surfaces before the reactivation of the Buzhan Fault zone in the Late Quaternary. Except for few places, the $Q_3$ alluvial material has been entirely eroded away from the top of these reliefs. This reveals that the current topography of the foothills domain is due to cumulative vertical deformations since the abandonment of the $Q_3$ alluvial surfaces. The initial topographic level of the $Q_3$ surface was reconstructed following the same method employed for the Barfriz Fault (section 4.3). The preserved remnants of $Q_3$ surfaces were used to reconstruct the undeformed depositional position of the $Q_3$, and consequently, to estimate a minimum vertical offset of about 80 m across the Buzhan Fault zone (Fig. 9). On the hanging wall of the Somaeh fault, $Q_3$ surfaces were intensely eroded away from the top of the reliefs. In such a situation, a constrained value cannot be estimated for cumulative vertical offsets on the Somaeh fault segment. Therefore, the vertical offset of ~20 m estimated from the profile reconstruction (Fig. 9) should be considered a minimum displacement.

At the site scale, the Somaeh Fault is evidenced by multiple fault scarps that represent occurrences of several faulting episodes during the Late Pleistocene and Holocene times (Figs 10-12). The geomorphic expression of the fault escarpment is characterized by vertically offset markers in different ages, such as Quaternary surfaces and drainage catchment areas displaced along the fault. These offset features show various elevations in agreement with the relative age of the geomorphic landforms. Among catchment areas affected by the fault, the relatively youngest ones are systematically offset of about 2.5 m along the fault in a way that they are currently perched on the hanging wall of the fault (Figs 10-12). In the same area, the Somaeh fault cuts $Q_1$ alluvial fans (300×400 m in diameter) through which the fault is underlined by a ~1.5-m-high fault scarp (Fig. 12). Further southwest, the youngest surface expression of the fault runs nearly parallel to the main trace of the main fault trace. This surface rupture, or nearly more co-seismic surface rupture, can either be observed on the high resolution satellite imagery or in the field (Figs 10 and 11). Using kinematic DGPS, we constructed individual high resolution digital elevation models (DEM) and topographic profiles for two offset features, *i.e.*, one catchment area and a $Q_1$ alluvial fan. The geomorphic analysis of these DEMs allowed us to estimate vertical offset values of 240 and 125 cm for the selected catchment area and alluvial fan, respectively. in the same way, a vertical offset value of 80 cm was estimated across the fault rupture (Fig. 12). About 2 km to the southeast of the studied site, the fault rupture was directly observed thanks to a sand

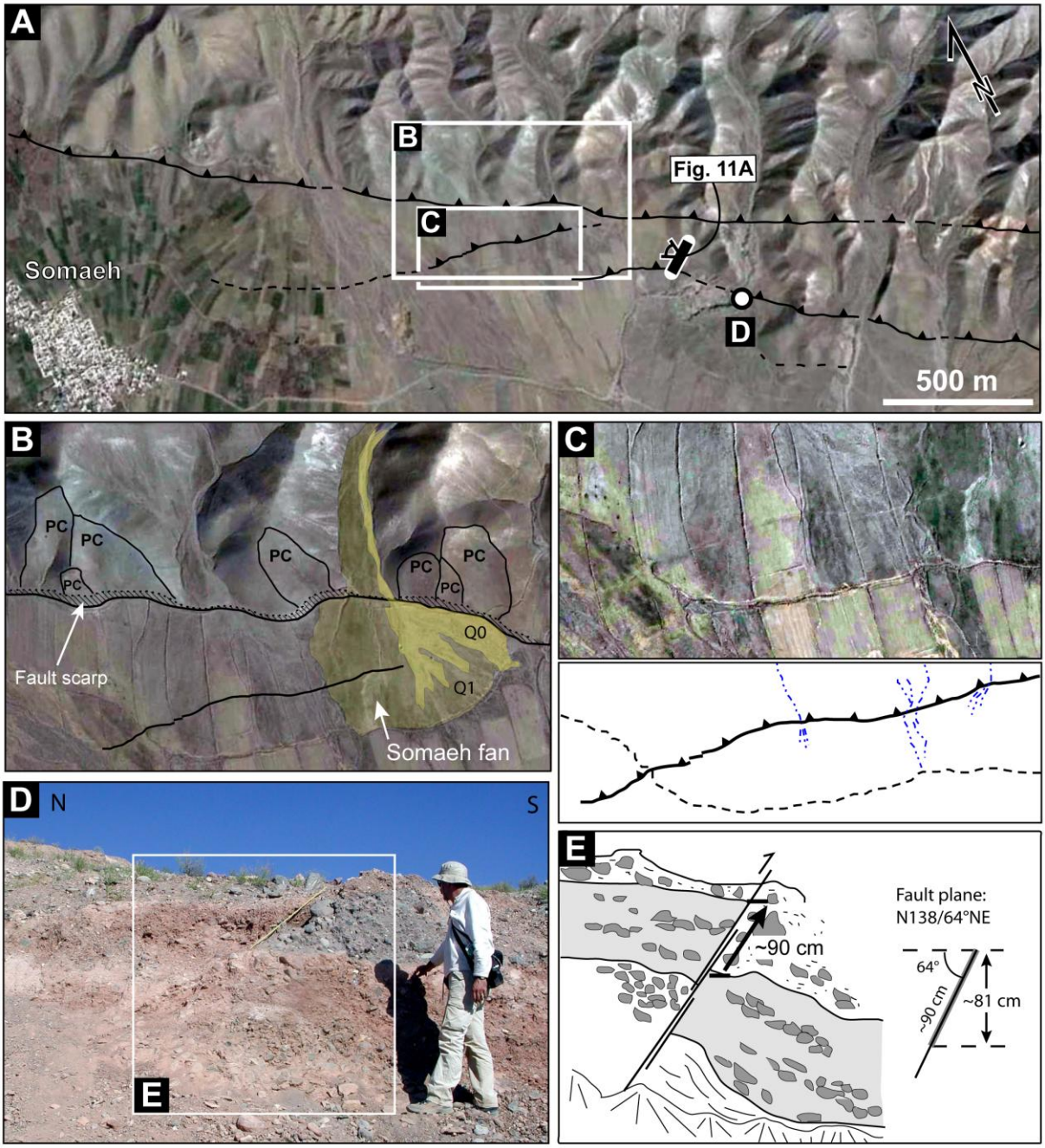


Figure 10. (a) Quickbird image (GoogleEarth) centered on the Somaeh area. Black lines are faults; south-westernmost segments are the new recognized fault ruptures. (b) Quickbird image (GoogleEarth) centered on the Somaeh fan and perched drainage basins. Hatched lines show the fault scarp along the Somaeh Fault clearly visible in the field (see Figure 11). (c) A segment of the Somaeh Fault rupture analyzed here; dotted line is an artificial waterway. (d) Fault rupture in a cross-section thanks to quarry excavations ("D" in inset "a"). (e) Field sketch of "D".

quarry excavation. In a trench wall, a 64°NE-dipping fault plane clearly cut the youngest abandoned fan deposits ($Q_1$), and offsets the layered fanglomerates of ~90 cm on the fault plane (Fig. 10). Resolving the fault parallel vertical displacement on a vertical plane yields an offset value of ~81 cm. Interestingly, this vertical fault displacement is comparable to the

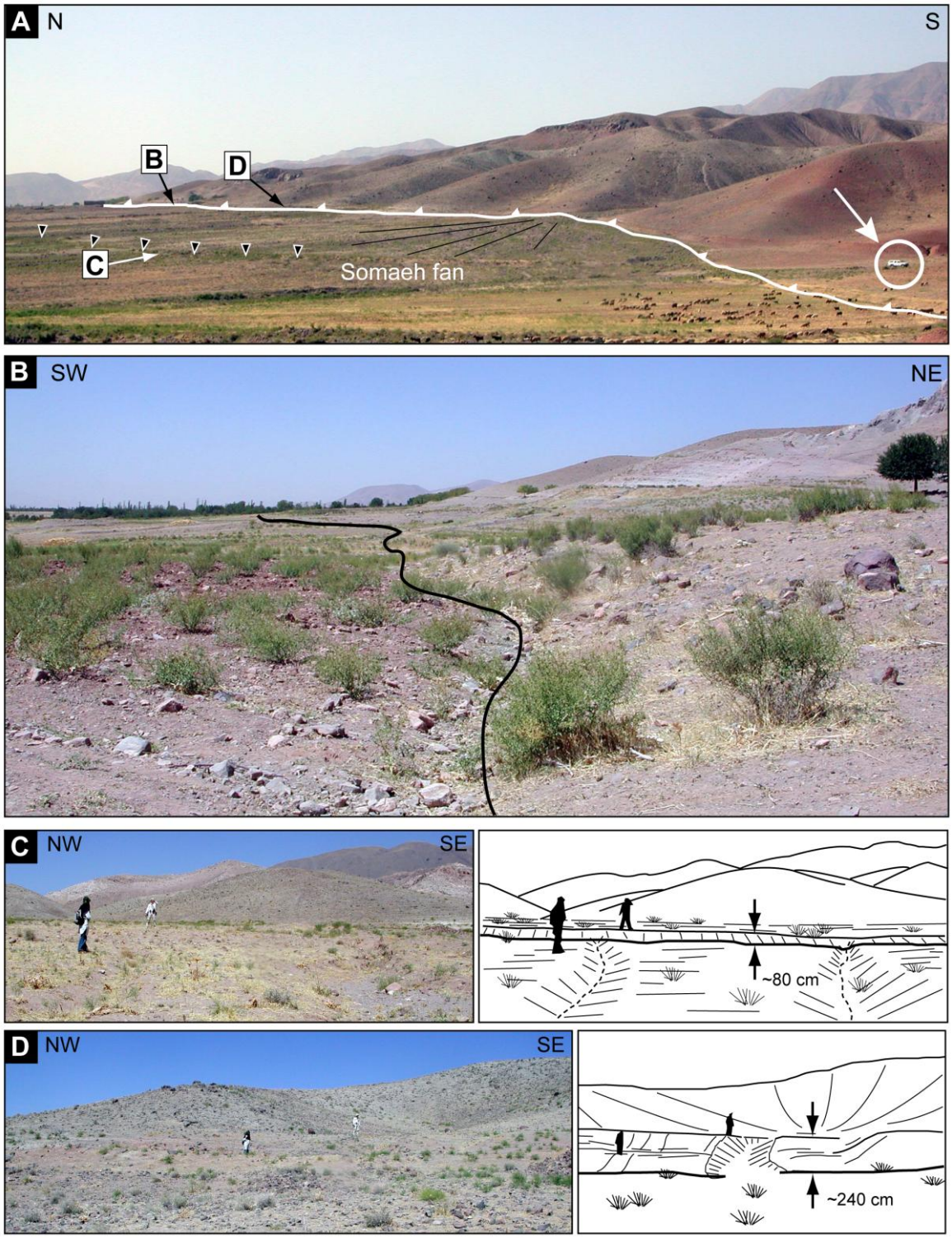


Figure 11. (a) General view of the Somaeh Fault escarpment; see Figure 5 for location of the field photograph. (b) Field photograph of the ~2-m-high multiple fault scarp of the Somaeh Fault. (c) Expression of the fault rupture at the Somaeh fan surface. (d) Perched catchment area and associated fault scarp.

offset value obtained from geomorphic analysis of the topographic profiles. Comparing the cumulative offsets recorded by the basin (~240 cm), alluvial fan (~125 cm), and the youngest fault rupture (~80 cm), it seems that the ~240 cm-high scarp resulted from repetitive

occurrences of 60-80 cm characteristic vertical offsets (cf., *Schwartz and Coppersmith*, 1984) on the Somaeh Fault. Accepting this assumption, at least four characteristic faulting events are required to constitute the fault scarps described above. In this case, the offsets recorded by the alluvial fan, including both offsets along the fault scarp and the fault rupture can be representative for three faulting events since the $Q_1$ fan surface abandonment.

Along the Eyshabad fault segment, a key site was selected to the southeast of Eyshabad village (Figs 5 and 13). At this site, a spectacular cross-section of the fault is exposed thanks to cut-bank erosion of the right-hand side of the Eyshabad River, allowing us to measure the geometry and kinematics of the fault (Fig. 13). On the trench wall, $Q_2$ alluvial deposits are vertically offset of ~17 m by the Eyshabad Fault (N140°E, 55°NE). Fault slip vectors measured on the fault plane indicate a predominated reverse faulting kinematics, which is associated to a minor component of right-lateral strike-slip faulting (rake angle of 85°NW). This kinematics is consistent with the geomorphic expression of the fault. *i.e.*, the vertically offset feature observed in the Eyshabad outcrop. Taking into account the geometry and kinematics of the fault, a right-lateral offset value of ~1.5 m is estimated for the Eyshabad Fault. At the surface, at least two Quaternary surfaces ($Q_2$ and $Q_3$) have vertically been displaced along the fault illustrating a multiple fault escarpment (Fig. 13). The higher geomorphic surface represents cumulative vertical displacements of the fault during the Late Quaternary. At the foot of the escarpment, an inactive fault branch is observed in the river bank few meters northeast of the active fault trace. Remnants of $Q_3$ alluvial surfaces are observed capping the tops of the rounded topography on the uplifted side (Fig. 13), suggesting that the older reactivation of the fault postdates the abandonment of $Q_3$ surface. Topographic analysis of the $Q_3$ surfaces along a profile running across the foothills domain enabled us to reconstruct the depositional $Q_3$ surface morphology on the hanging wall of the Eyshabad Fault (Fig. 9). This allowed us to estimate a cumulative vertical offset of ~90 m, representative for minimum vertical deformation on the Eyshabad Fault since the abandonment of $Q_3$ surfaces. The lower terrace is comparable to $Q_2$ surfaces and corresponds to a ~18-m-high fault scarp formed along the youngest Eyshabad fault trace (Fig. 9). This minimum offset value is consistent with the vertical offset measured on the fault plane in the river trench.

At the third site, our morphotectonic investigations are conducted along the southeastern segment of the Buzhan Fault zone, *i.e.*, the Qadamgah Fault (Fig. 14). In that area, dispersed remnants of $Q_3$ surfaces are observed at the top of rounded hills on the fault hanging wall (NE side). Apparently, the entire area was initially covered by $Q_3$ fan surfaces, which subsequently were incised by streams (~3 km-long) flowing southwestward across the fault. These streams

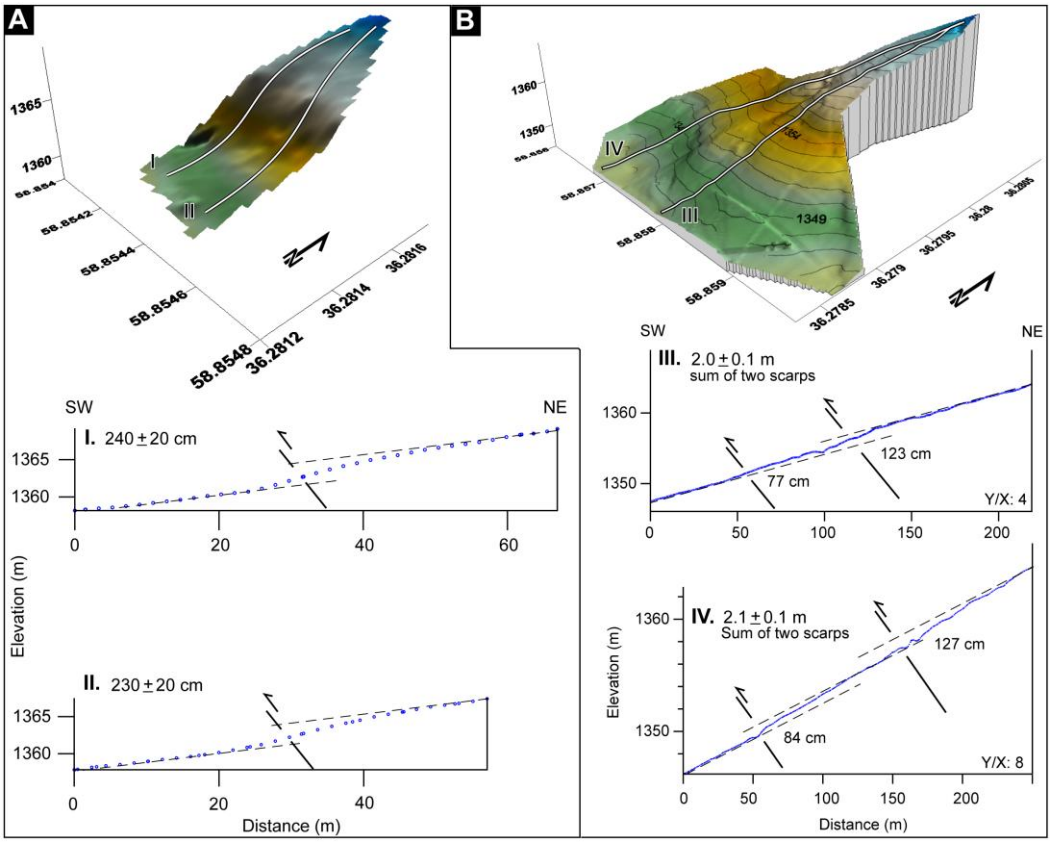


Figure 12. (a) DGPS-derived DEM from the perched basin presented in Figure 11, together with two topographic profiles. (b) DGPS-derived DEM of the Somaeh fan together with two topographic profiles.

have been tight-laterally offset providing evidence for strike-slip faulting along the Qadamgah Fault. The geomorphic reconstruction of the offset steams indicates a right-lateral offset value of ~260 m postdating the abandonment of $Q_3$ fan surfaces (Fig. 14). This cumulative lateral offset is not consistent with the predominant reverse faulting observed along two other major fault segments of the Buzhan fault zone, *i.e.*, the Eyshabad and Somaeh faults, but, is compatible with the lateral offset estimated for the Barfriz Fault. On the other hand, along the southeast portion of the Barfriz Fault, a preliminary geomorphic analysis of offset drainage systems reveals a cumulative right-lateral offset of ~2 km recorded by catchment areas incised in the Mesozoic bedrock (Fig. 15). However, there is no evidence for active strike-slip faulting. These observations lead us to consider the Qadamgah Fault a possible continuation of the Barfriz Fault taking up the Late Quaternary right-lateral strike-slip faulting along the southeastern part of the Neyshabur Fault System. This seems reasonable when considering the structural complexity in the fault pattern at the center part of the Neyshabur Fault System (longitude 59°E); where several faults run between the Barfriz Fault and the Buzhan Fault zone to form a short-cut zone. If accepted, the lateral offset recorded by drainage systems

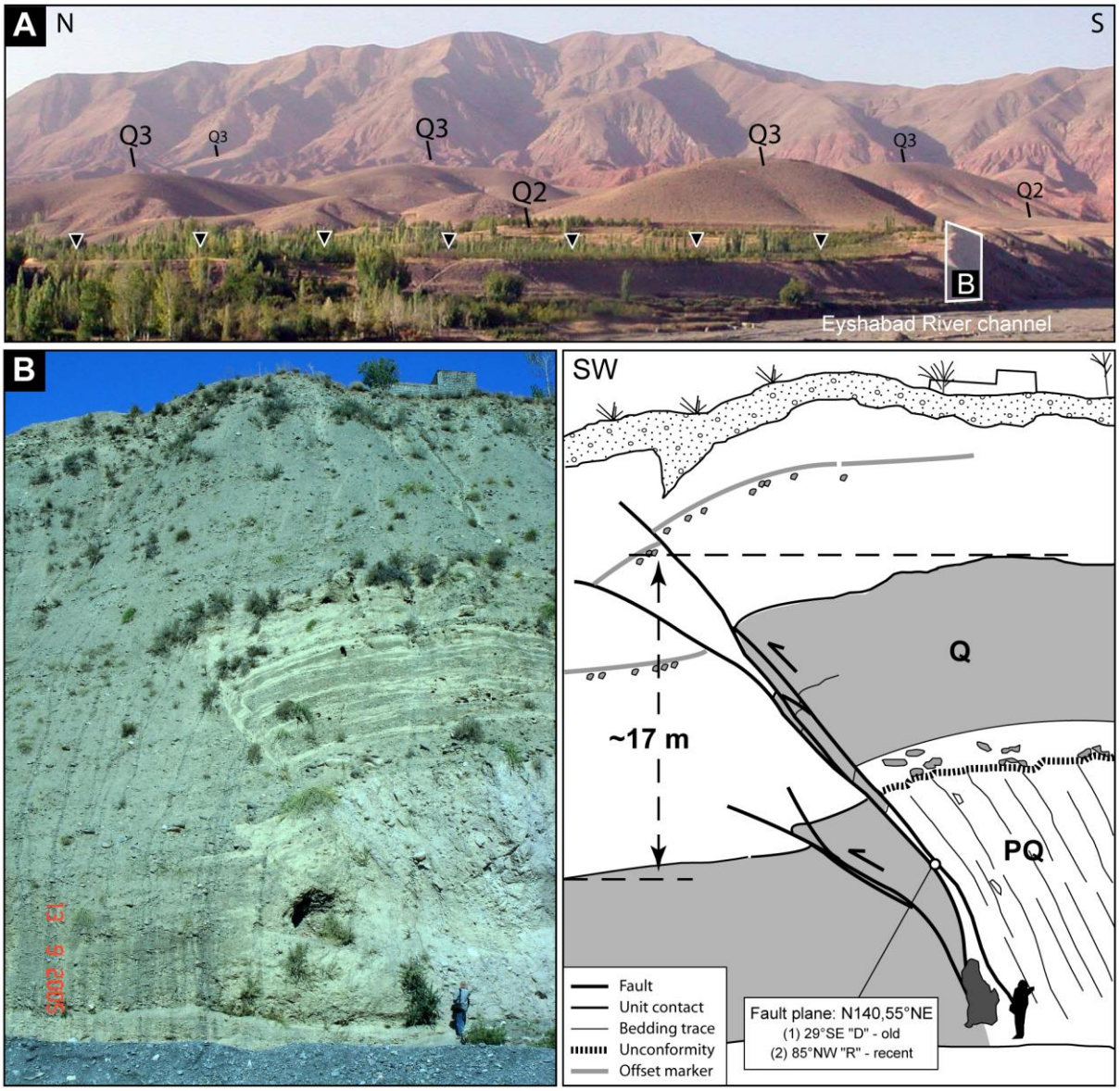


Figure 13. (a) General view of the Eyshabad fault escarpments; see Figure 5 for location of the photograph. The Eyshabad Fault is marked by black triangles. Natural section across the Eyshabad Fault thank to the Eyshabad river bank; Q, Quaternary; PQ, Pre-Quaternary up-righted strata.

along the southeastern portion of the Barfriz Fault (Fig. 15) may represent the expression of lateral motions along the Neyshabur Fault System, before transferring the motions to the Qadamgah Fault.

## 5. Morphotectonic investigations along the Mashhad Fault System

The northeast side of the Binalud Mountains is bounded by the Mashhad Fault System. This ~125-km-long fault system strikes northwest, nearly parallel to the Neyshabur Fault System (Fig. 2). The Mashhad Fault System is constituted by several NW-striking fault

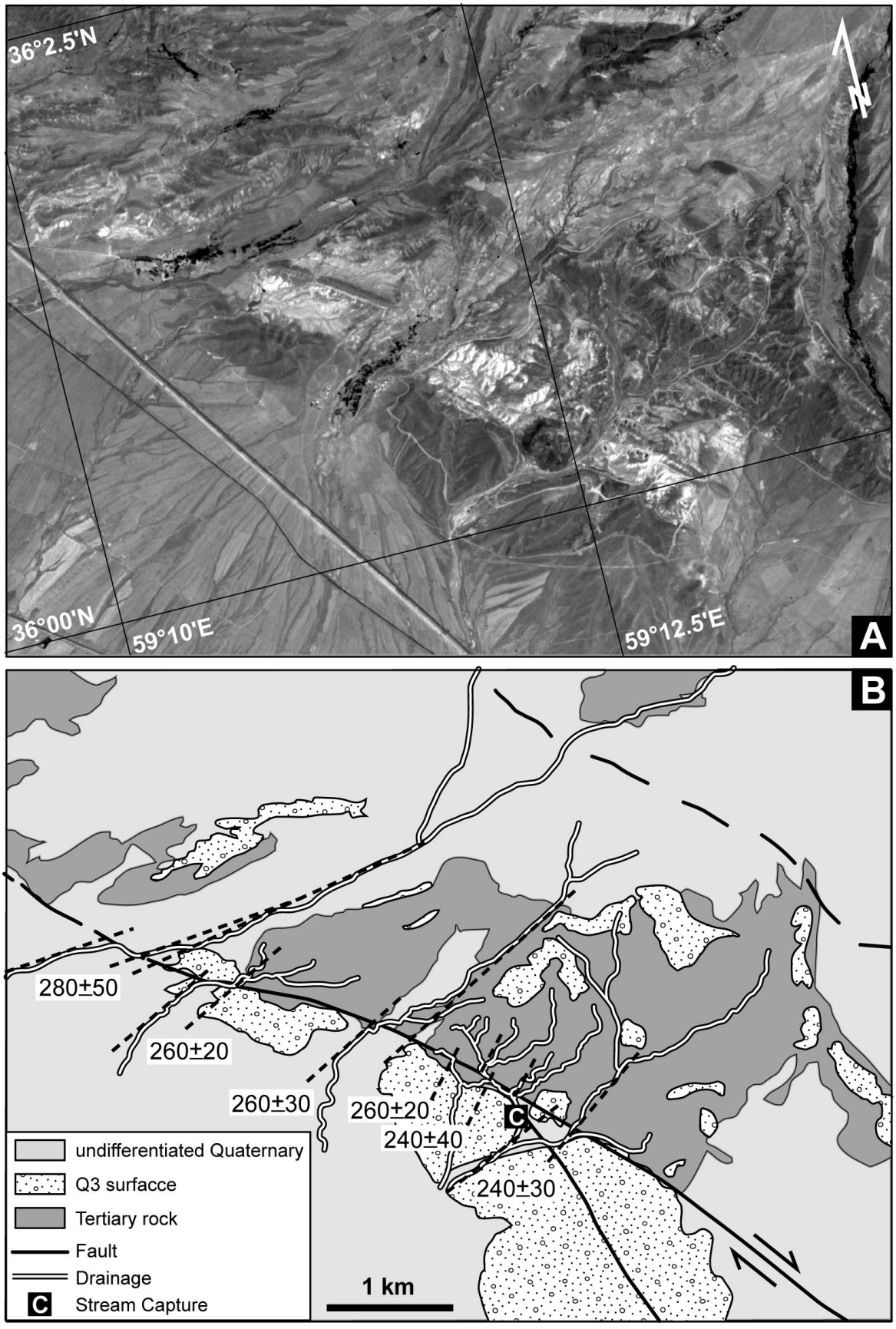


Figure 14. (a) SPOT5 image centered on the Qadamgah Fault. (b) Simplified morphotectonic map of the area covered in (a).

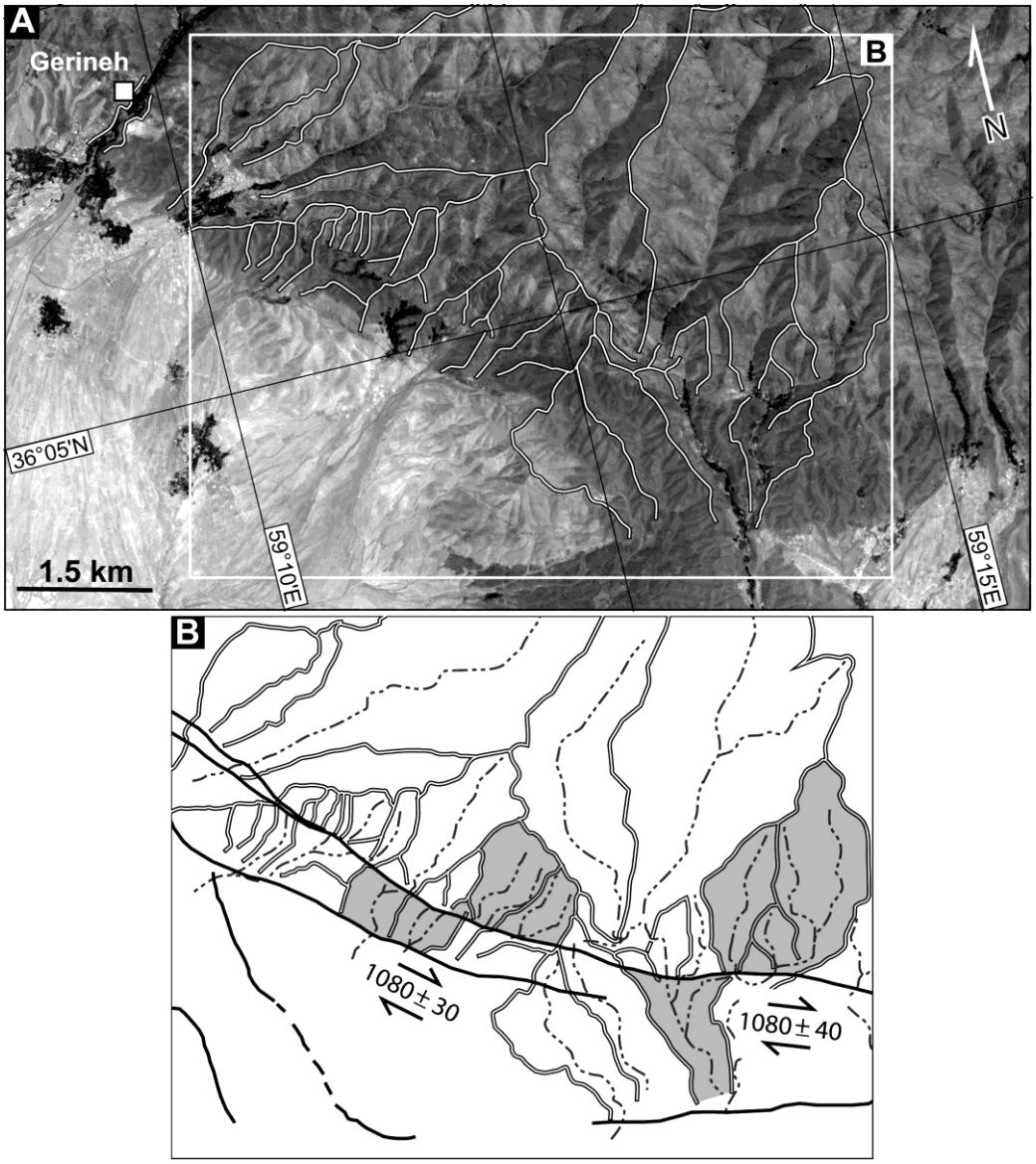


Figure 15. Simplified Morphotectonic map of the Gerineh area along the southeastern portion of the Barfriz Fault. Perturbed basin outlines (double white lines) and streams (dotted lines) are described by right-lateral offsets (expressed in meters) along the fault.

segments some of which are considered as the remnant of the paleo-Tethys suture zone (*e.g.*, *Majidi*, 1978). In the present-day tectonic context, active deformations are taken up along a localized fault zone, herein after the Mashhad fault zone, consisting in at least three Quaternary fault segments (Fig. 2). On satellite imageries and topographic maps of the region, the Mashhad Fault System appears as sharp, linear fault traces extending through the uniformly slopping northeast flank of the Binalud Mountains. The lack of significant changes in elevation on either sides of the fault together with its straight trends indicate that the fault zone is nearly vertical and purely strike-slip. To the southeast, strike-slip faulting along the Mashhad fault zone is localized along a single fault segment, but, to the northwest, faulting is

distributed along a 1 to 8 km-wide fault zone (Fig. 2) despite that active strike-slip faulting is nearly more focalized along the central fault segment. North of latitude N36°, several parallel fault segments runs northwest over a distance of ~40 km from Chenaran town (Fig. 2). Their linear traces in the Mesozoic bedrock are underlined by systematic, but ambiguous deflections in drainage system. Those faults may have considered as the continuation of the Mashhad Fault System, however, in a lack of filed data and direct evidence for their Quaternary activity it is difficult to assert whether those are the old expression of inherited structures in the bedrock or those exhibit the northwest propagation of the Mashhad Fault System. Even thought, our quantitative geomorphic analysis (section 8.2) provides indirect evidence for possible Quaternary activities along these structures.

At the northeast flank of the Binalud Mountains, at least four distinct Quaternary surfaces can be distinguished. The higher surface ($S_4$) spreads in the southeastern part of the region in form of tilted and intensely eroded terraces (Fig. 16). This surface had initially covered the entire SE region. The remnants of $S_4$ surface are currently observed at different elevation levels ranging from 1200 to 1800 m (above the sea level). The distribution pattern of the $S_4$ remnants as well as the geometry of the uniformly slopping NE flank of the Binalud, where the surface was formed, implies that the $S_4$ surface was an old alluvial plain. Subsequently, this surface has been uplifted due to vertical deformations of the Binalud Mountains. The South Mashhad Fault runs through this abandoned surface affecting the surface and its associated geomorphic features such as stream beds, ridges (Fig. 16).

In the northwestern part of the region, the $S_4$ surface is absent suggesting that either it was totally removed from the uplifted region or it never formed there. In that region, the higher Quaternary surfaces ($S_3$) correspond to uplifted and partly eroded Quaternary alluvial fans at the piedmont of the Binalud Mountains (Fig. 17). Younger alluvial fans ($S_2$ and $S_1$) are inset in the $S_3$ fan surfaces and distributed along the northwestern, half length of the Mashhad fault zone, downhill the trace. The higher fan surfaces ($S_3$) and streams incised in these surfaces were affected by the fault providing evidence for cumulative right-lateral displacements (Fig. 17).

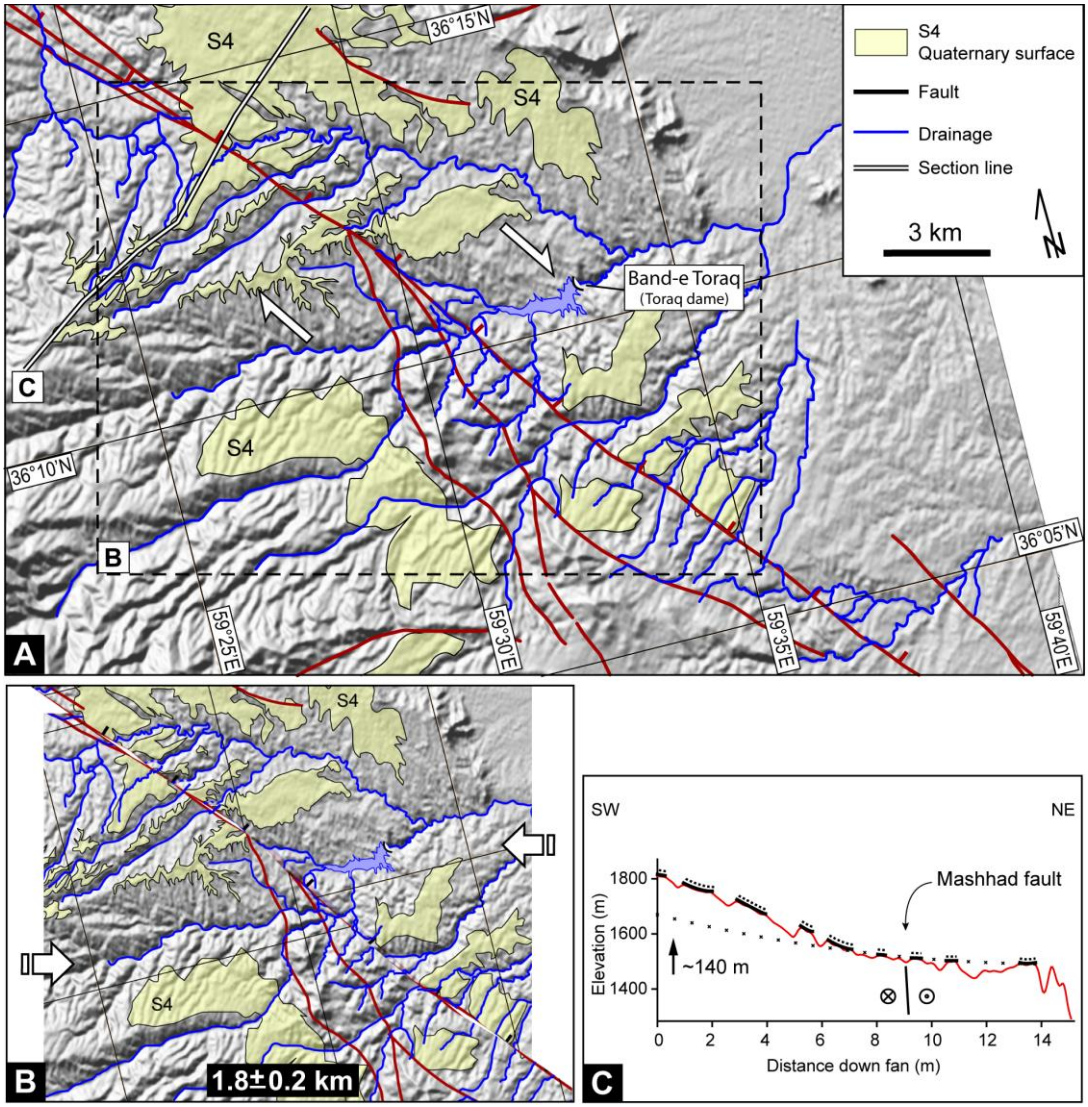


Figure 16. Morphotectonic map of the SE Mashhad area along the southeastern segments of the Mashhad Fault System before (a) and after (b) offset reconstruction. (c) Landscape model (see Figure 9 for symbol and indications) indicating a minimum 140 m vertical deformation recorder by the S4 surfaces, south of Mashhad.

### 5.1. Quantification of the cumulative fault offsets along the Mashhad Fault zone

On the northeast flank of the Binalud Mountains, numerous streams have incised in $S_4$ surfaces flowing eastward, perpendicular to the South Mashhad Fault (Fig. 16). Those streams exhibit systematic right-lateral offsets along the South Mashhad Fault. Our geomorphic analyses (based on Spot images and SRTM topographic data) of the $S_4$ surfaces and incising drainages allow us to estimate cumulative vertical and horizontal displacements along the fault trace (Fig. 16). The geomorphic reconstruction of the main streams gives a maximum cumulative right-lateral offset of ~1.8 km, since the abandonment of the $S_4$ Quaternary surface. To estimate vertical deformation recorded by the $S_4$ surface, a topographic profile

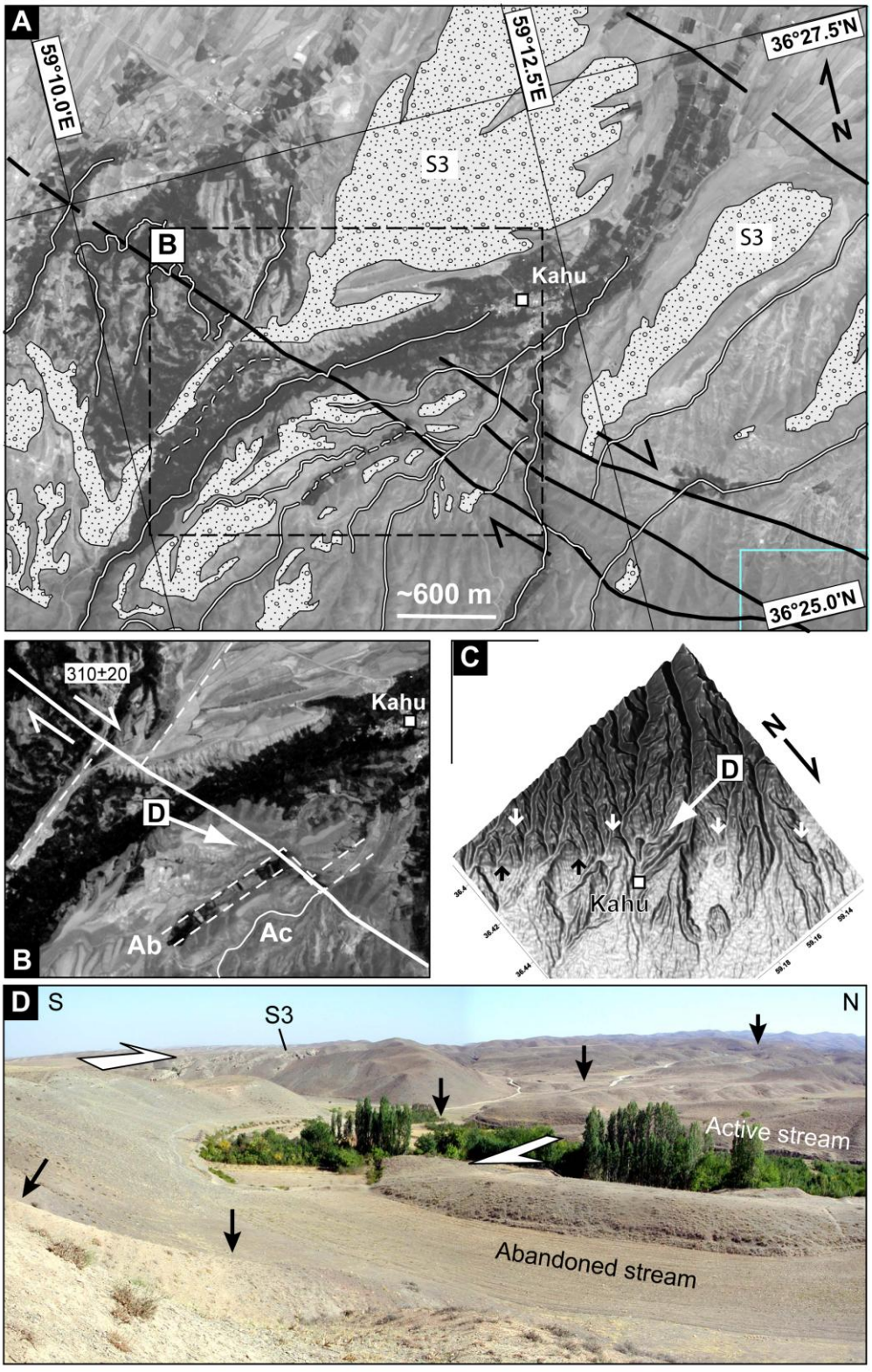


Figure 17. (a) Morphotectonic map of the Kahu area along the northwestern segments of the Mashhad Fault System based on SPOT5. Polygons show the remnants of the $S_3$ alluvial fan surface. Black line is fault. Drainages are marked by double white lines. (b) SPOT5 image centered on the Kahu fan representing the piercing point or lines (dashed line) used to estimate the cumulative lateral fault offset. Ab, Abandoned stream; Ac, Active stream. (c) Oblique view (vertical angle 80°) of the Kahu fan surfaces; arrows point fault traces. (d) Panoramic view of the offset and abandoned stream used as a piercing line. Black arrows mark the trace of the Mashhad Fault.

was analyzed across the South Mashhad fault (Fig. 16). Along this profile, the depositional morphology of the $S_4$ surface was reconstructed using at least three points on the undeformed part of the surface, far away from uplifted areas (see section 4.3). It is noteworthy that the $S_4$ surface is composed of fine grain, loosely cemented deposits, which have facilitated erosional processes removing a significant part of the surface. Hence, our geomorphic analysis leads to a rough estimate of ~140 m for vertical deformations recorded by the $S_4$ surfaces (Fig. 16). Interestingly, nearly all the deformation is due to regional uplifts of the northeast flank of the Binalud Mountains. In other words, no significant vertical deformation is detected across the South Mashhad Fault.

Along the northeastern part, strike-slip faulting is characterized by right-lateral offsets in geomorphic markers such as $S_3$ alluvial fans and their associated drainage systems. Near the village of Kahu, a key offset marker is found suitable for both offset quantification and cosmogenic dating, *i.e.*, the Kahu alluvial fan surface (Fig. 17). The Kahu alluvial fan belongs to $S_3$ alluvial unit, and has been right-laterally offset by the main segment of the Mashhad Fault System. In the southwestern side of the fault, the remnant part of the fan apex can be correlated to the fan body in the northeastern side (Fig. 17). Geomorphic reconstruction (fan body against apex and axial stream) of the Kahu fan yields a cumulative offset of ~310 m postdating abandonment of the fan surface. In the same area, identical offset value is exhibited by drainages incised in the $S_3$ surface (Fig. 17), strengthening the reliability of the offset value estimated for the Kahu alluvial fan (Fig. 17). There, a stream was cut and offset along the fault. In upstream, the stream appears beheaded and inactive (Fig. 17), but, its downstream segment has captured another stream uphill the fault. The geomorphic reconstruction of the offset stream parts indicates the same offset value (~310 m) than the offset recorded by the Kahu fan (Fig. 17).

## 6. Dating of the studied offset features

### 6.1. Neyshabur Fault System

The Barfriz alluvial fan belongs to $Q_3$ surfaces and has been offset by the Barfriz Fault (section 4.2). On the Barfriz fan surface, five embedded sandstone boulders were collected from the most preserved parts and analyzed (Fig. 18 and Table 1). Measured *in situ*-produced cosmogenic $^{10}$Be concentrations allow calculating minimum exposure ages ranging between 84±14 and 110±18 kyr. For the Barfriz surface samples, the sum of the Gaussian age probability distributions ($P_{sum}$) shows a sharp-peaked distribution that corresponds to a small

value of σ (*e.g.*, *Taylor*, 1997), and a weighted-mean $^{10}$Be minimum exposure age of 94±5 kyr (Fig. 19 and Table 1). This weighted-mean $^{10}$Be minimum exposure age is calculated assuming that there has been no significant erosion acting on the fan surface since its abandonment.

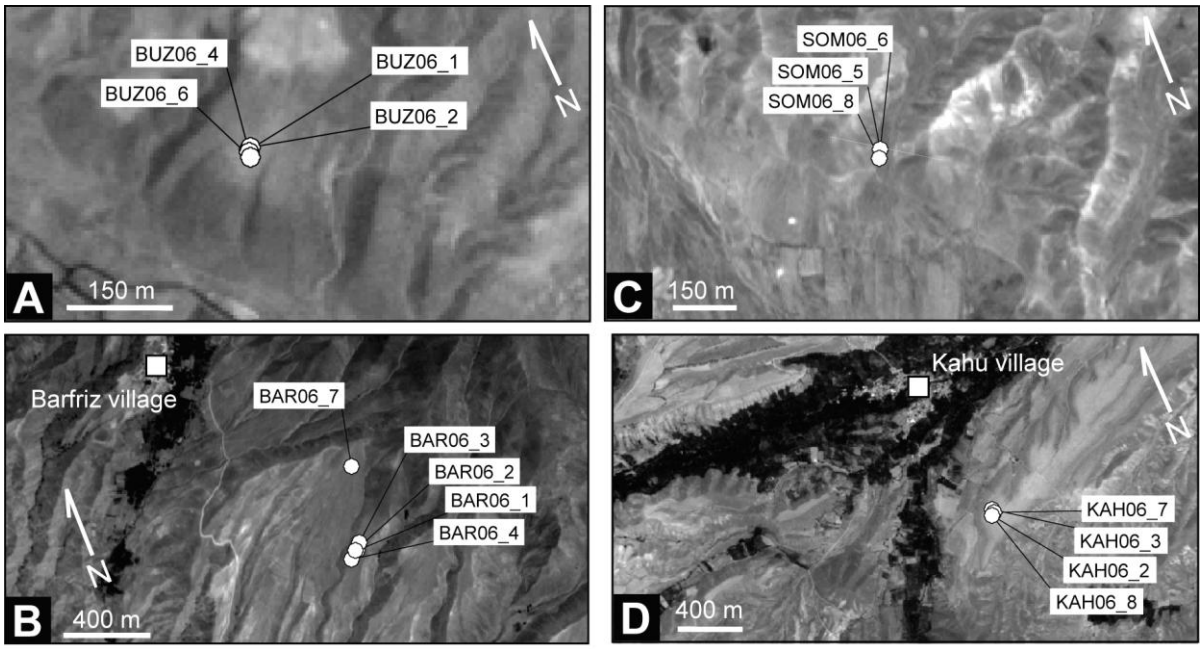


Figure 18. General situation of the fan surfaces together with the location of the sampled boulders. Insets (a) and (b) show the $Q_3$ surface in the Buzhan and Barfriz areas, respectively. (c) $Q_1$ fan surface in the Somaeh area. (d) $S_3$ fan surface in the Kahu area.

We already discussed about the regional distribution of $Q_3$ surfaces and their implications for quantification of fault offsets over the foothills domain (section 4). To verify the synchronicity of these surfaces, four other samples were collected from another $Q_3$ fan surface (Buzhan region) approximately 7 km to the south of the Barfriz fan (Fig. 17). The selected surface is one of the rare preserved $Q_3$ surfaces on the hanging wall of the Eyshabad Fault. Those samples yield minimum $^{10}$Be exposure ages ranging from 74±12 and 100±17 kyr with a weighted-mean of 87±6 kyr, strengthening our confidence for an isochronous abandonment age of the regional $Q_3$ surfaces (Fig. 19).

In the Somaeh region, only three of ten collected samples of granite boulders embedded in a displaced $Q_1$ alluvial fan surface provided minimum pure quartz mass necessary for the analytical procedure of $^{10}$Be dating. The analyzed samples from this fan yield minimum exposure ages of 2.3±0.7, 4.3±1.2 and 5.3±1.1 kyr (Fig. 19). Since erosional processes acting on the fan surface may be responsible for boulder exhumation from deeper positions within the alluvial material, the oldest age may be the closest to the actual age of abandonment, which is the more reliable estimation that can be done considering the dataset.

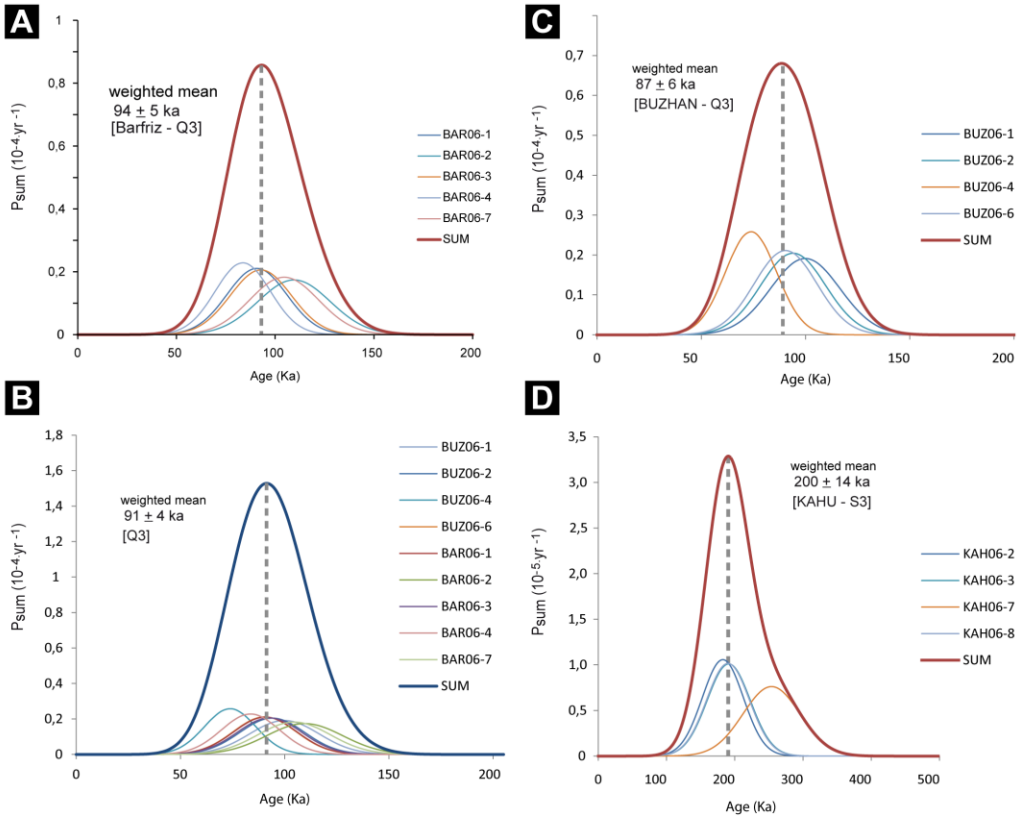


Figure 19. *In situ*-produced $^{10}$Be exposure ages of samples collected on $Q_3$ (insets "a", "b" and "c") and $S_3$ (inset "d") surfaces. Inset (b) represent the regional exposure age of $Q_3$ surfaces obtained from all the samples collected from the Barfriz and Buzhan areas. Thick curves are age probability sum, and thin curves represent the age probability for each individual sample.

Table 1. Sample characteristics and exposure ages.

| Sample | Longitude (°E) | Latitude (°N) | Elevation (m) | $^{10}$Be production rate (atoms/g-SiO2/yr) | $^{10}$Be (atoms/g-SiO2) | Age kyr |
|---|---|---|---|---|---|---|
| BAR06-1 | 58,9081 | 36,2926 | 1843 | 16,6701124 | 1477917 ± 60787 | 91 ± 15 |
| BAR06-2 | 58,9079 | 36,2923 | 1839 | 16,62038235 | 1771386 ± 73503 | 110 ± 18 |
| BAR06-3 | 58,9078 | 36,2923 | 1840 | 16,6345474 | 1506829 ± 62308 | 93 ± 15 |
| BAR06-4 | 58,9075 | 36,2920 | 1841 | 16,64501092 | 1362434 ± 56382 | 84 ± 14 |
| BAR06-7 | 58,9086 | 36,2957 | 1915 | 17,52567713 | 1784065 ± 72804 | 105 ± 17 |
| BUZ06-1 | 58,9325 | 36,2345 | 1457 | 12,64092437 | 1230674 ± 50785 | 100 ± 17 |
| BUZ06-2 | 58,9325 | 36,2345 | 1463 | 12,69732659 | 1165681 ± 41690 | 94 ± 16 |
| BUZ06-4 | 58,9325 | 36,2345 | 1465 | 12,71428879 | 921267 ± 38630 | 74 ± 12 |
| BUZ06-6 | 58,9325 | 36,2344 | 1462 | 12,68887315 | 1121215 ± 45581 | 90 ± 15 |
| KAH06-2 | 59,2088 | 36,4352 | 1466 | 12,7909586 | 2229050 ± 73958 | 182 ± 30 |
| KAH06-3 | 59,2089 | 36,4355 | 1463 | 12,76257517 | 2323869 ± 76485 | 191 ± 31 |
| KAH06-7 | 59,2090 | 36,4353 | 1463 | 12,76252342 | 3038968 ± 99334 | 254 ± 42 |
| KAH06-8 | 59,2088 | 36,4352 | 1465 | 12,77956774 | 2314219 ± 77596 | 190 ± 31 |
| SOM06-5 | 58,8583 | 36,2809 | 1390 | 12,0070892 | 64009 ± 8477 | 5.3 ± 1.1 |
| SOM06-6 | 58,8583 | 36,2809 | 1390 | 12,0070892 | 27345 ± 7242 | 2.3 ± 0.7 |
| SOM06-8 | 58,8582 | 36,2807 | 1389 | 11,99891658 | 51622 ± 11131 | 4.3 ± 1.2 |

### 6.2. Mashhad Fault System

In the northeastern part, the Mashhad Fault right-laterally displaced a series of S3 fan surfaces and drainages incised in the surfaces (Fig. 17). We dated a total of 4 samples of quartz boulders embedded in the most preserved parts fan surface in the northeastern block of the fault (Fig. 18 and Table 1). The analyzed samples from this surface yield minimum exposure ages ranging from 182±30 to 254±42 kyr. Among the sampled boulders, one sample is significantly older (254±42 kyr). To interpret this age distribution, one can consider that the oldest sample is bearing inherited cosmogenic $^{10}$Be, indicating a previous exposure episode in the source area. But, for all samples, the sum of the Gaussian age probability distributions ($P_{sum}$) shows a uni-modal distribution that is not consistent with this suggestion (Fig. 19). In such a case, the weighted-mean minimum $^{10}$Be exposure age of 200±14 kyr is the closest evaluation of the actual abandonment age. On the other hand, as the more conservative estimation, the oldest age (254±42 kyr) may be the closest to the actual age of abandonment. This seems reasonable because erosional processes acting on the fan surface may be responsible for exhumation of the boulders from deeper positions within the alluvial material.

In the lack of direct erosional features (*i.e.*, even young gullies and/or differential erosion) on the sampled parts of the fan surfaces, sensitivity of the surface exposure ages to erosion can be distinguished from the boulder age distribution patterns. In other words, soil erosion (whatever the involved mechanism) produces a distribution of apparent ages between the actual surface age and some younger age limit. The width of the distribution being proportional to the surface age and the actual age, being close to the maximum of the distribution (*Phillips et al*., 1997; *Wells et al*., 1995; *Zreda et al*., 1994). Considering this suggestion as a guide in interpreting the age distributions observed on the offset fan surfaces, the relatively well-clustered exposure age distributions of both the $Q_3$ and $S_3$ boulders imply small erosion depths on the fan surfaces. In such a case, the weighted-mean boulder exposure ages of 94±5 kyr and 200±14 kyr can be interpreted as the best estimate of the true abandonment age for the Barfriz and Kahu alluvial fan surfaces, respectively.

## 7. Late Quaternary fault slip rates on both sides of the Binalud Mountains

In this study, slip rate evaluations are based on three main assumptions: (1) there has been no erosion of the sampled surfaces since their abandonment, (2) the fault slip rates remained constant since formation of the offset Quaternary markers and (3) the main traces of the faults are assumed to have accumulated all of the strain at studied sites. Accepting these

assumptions, the accuracy of our slip rates depends on the geomorphic relevance, and analytical accuracy of the obtained minimum $^{10}$Be exposure ages respect to the cumulative fault offsets. For instance, drainages incised in the same Quaternary surface postdate the abandonment of that surface. If one assumes that drainage with the same morphology (length, depth and width) and physical conditions (geologic and climatic parameters) have been formed at the same time, the more developed drainages are the oldest ones. But, all drainages incised in a surface are younger than that surface implying (1) that fault offsets recorded by the drainages should be less than that cumulated by the surface, and (2) that the initiation of the offsets should be post-dating surface abandonment. Therefore, to estimate reliable fault slip rates from geomorphic analyses of offset drainages, the markers with ages closer to the abandonment age of the incised surface are preferred.

### 7.1. Neyshabur Fault System

In the Barfriz area, $Q_3$ fan surfaces and their associated drainages were offset along the Barfriz Fault. The sampled surfaces are well-preserved and there is no evidence of post-offset deposition on the surfaces. Our geomorphic analyses and dating results indicate that the Barfriz fan surface was abandoned at minimum 94±5 kyr and subsequently offset by 280±40 m. this allows us to estimate a maximum long-term slip rate of 3.0±0.5 mm/yr for the oblique motion on the Barfriz Fault. Considering the 33°NW rake angle calculated for this fault (section 4.3), this total slip rate can be resolved to maximum rates of 2.6±0.2 and 1.6±0.2 mm/yr for horizontal and vertical displacements, respectively.

In the Somaeh area, an alluvial fan ($Q_1$) has recorded a cumulative vertical offset value of ~1.2±0.1 m along the Somaeh Fault, and subsequently a coseismic vertical offset of ~80 cm along a younger fault splay SE of the main fault trace (Fig. 12). Abandonment of the fan surface occurred between 2.3±0.7 and 5.3±1.1 kyr ago. Dividing the total offset value of 2.0±0.1 m by this bracketed age yields Holocene slip rates between 0.4±0.1 and 0.9±0.3 mm/yr$^{-1}$ for vertical motion on the Somaeh Fault (Fig. 12).

A minimum 80±20 m cumulative vertical offset estimated from the geomorphic reconstruction of $Q_3$ surfaces (Fig. 9) deformed on the hanging wall of the Eyshabad fault yields a minimum slip rate of 0.9±0.2 mm/yr averaged over a time of 94±5 kyr since the abandonment of the $Q_3$ surfaces.

For the Qadamgah Fault, drainages incised in $Q_3$ surfaces recorded a 260±80 m cumulative offset due to right-lateral displacements along the fault (Fig. 14). Assuming that

abandonment of $Q_3$ surfaces was regionally synchronous at 94±5 kyr (section 6.1); a maximum slip rate of 2.8±0.9 mm/yr is estimated for strike-slip motion along the southeastern segment of the Buzhan Fault zone.

To determine the late Quaternary rate of deformation at the southwest flank of the Binalud Mountains we sum the slip rates estimated for each individual fault segments within the Neyshabur Fault System. A horizontal slip rate of 2.7±0.8 mm/yr is the average of slip rates obtained for the Barfriz Fault and the south-easternmost fault segment of the Buzhan Fault zone. The total 230±20 m vertical deformation deduced from geomorphic reconstruction of $Q_3$ fan surfaces across the Neyshabur Fault System (Fig. 9) yield a vertical slip rate of 2.4±0.2 mm/yr averaged over 94±5 kyr. All together, these vertical and horizontal slip rates lead us to estimate a total slip rate of 3.6±1.2 mm/yr for the late Quaternary deformation at the southwestern flank of the Binalud Mountains.

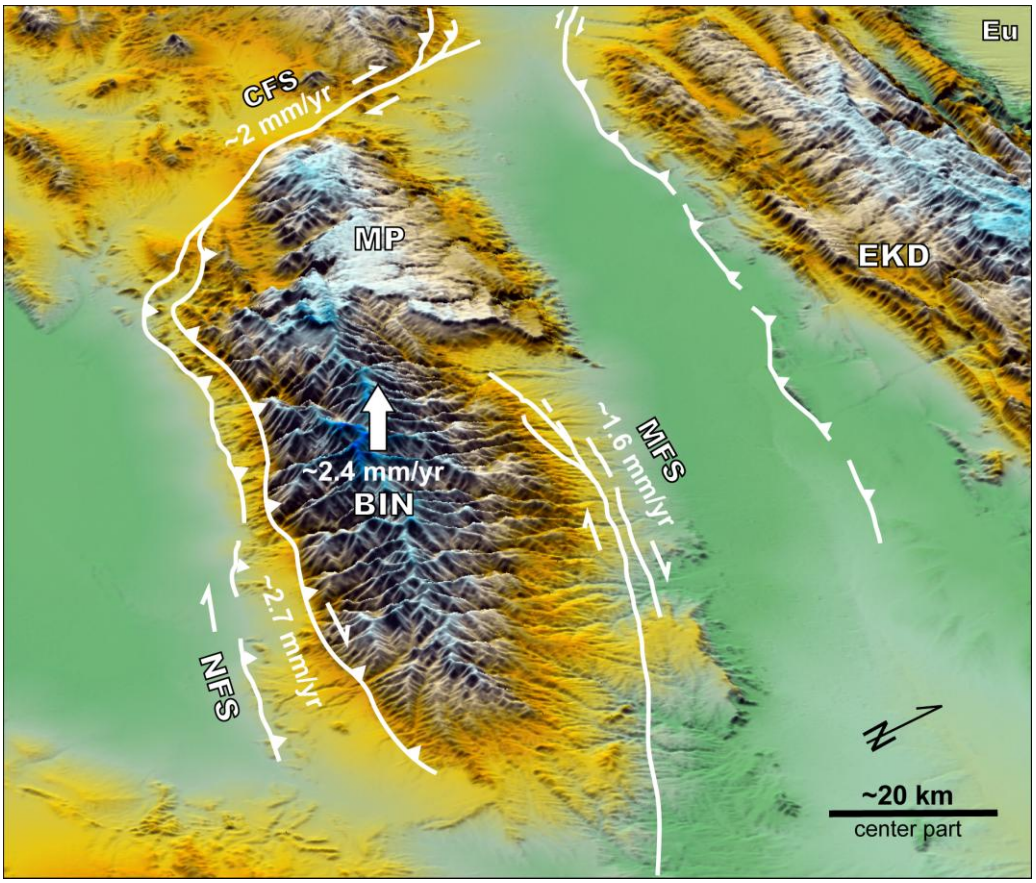


Figure 20. 3-D view of the Binalud Mountains based on SRTM topographic data representing general morphology of the mountains, major fault systems (thick white lines), as well as the calculated vertical and horizontal slip rates at the sides of the range. Slip rate for the Chakaneh Fault System (CFS) was taken from *Shabanian et al.* (2009b). BIN, Binalud; MFS, Mashhad Fault System; NFS, Neyshabur Fault System; EKD, Eastern Kopeh Dagh; EU, Eurasian plate.

### 7.2. Mashhad Fault System

The Kahu alluvial fan has recorded a right-lateral cumulative displacement of 310±20 m along the northwestern part of the Mashhad Fault System (Fig. 17). Since the age of abandonment of the Kahu surfaces is comprised between the weighted-mean minimum $^{10}$Be exposure age of 200±14 kyr and minimum exposure age of 254±42 kyr (the oldest sample in the dataset), the Late Quaternary slip rate should be on the order of 1.6±0.1 mm/yr for the Mashhad Fault System.

## 8. Summary and discussion

In this chapter, new geomorphic and geological data are provided through a combination of detailed structural mapping, quantitative geomorphic analyses and *in situ*-produced $^{10}$Be cosmogenic exposure dating, complemented by field surveys. These led us to characterized quaternary faulting at both sides of the Binalud Mountains. Quaternary offset markers are used to quantify cumulative offsets along the Neyshabur and Mashhad Fault Systems. Sixteen boulder samples were analyzed in order to determine abandonment ages of these markers through measurement of in situ-produced cosmogenic $^{10}$Be concentrations. Altogether, the approaches applied here allowed us to determine maximum vertical and horizontal slip rates of the five most significant fault segments responsible for the Late Quaternary deformation within the Binalud mountain range. The distribution pattern of slip rates both sides of the Binalud reveals that Late Quaternary strike-slip faulting has been taken up by the Mashhad and Neyshabur Fault Systems at a long-term rate of ~4 mm/yr. This also implies a ~2.4 mm/yr long-term slip rate for vertical deformation which is uplifting the southwestern flank of the Binalud Mountains.

### 8.1. Deformation pattern of the Binalud Mountains

The Binalud Mountains is bounded by three major fault systems (Fig. 2). These are the Neyshabur and Mashhad Fault Systems along its northeastern and southwestern sides, respectively, as well as the Chakaneh fault system at the northwestern side of the mountains (Fig. 20). The dataset presented in this study implies that right-lateral strike-slip motion resulting from the northward motion of central Iran relative to Eurasia is accommodated at a mean rate of ~4 mm/yr along the Neyshabur and Mashhad Fault Systems (Fig. 20). This is consistent with the 3.7±2.0 mm/yr of the Present-day range parallel slip rate deduced from

geodetic GPS measurements (*Tavakoli*, 2007). In addition to the strike-slip faulting component, a vertical slip rate of ~2.4±0.2 mm/yr is estimated to be taken up along the Neyshabur Fault System (Fig. 20). Unlikely, for the Mashhad Fault System, there is no evidence for significant vertical displacement during Quaternary. Considering the new fault configuration proposed by *Shabanian et al*. (2009b), the Chakaneh fault system is transferring part of active strike-slip faulting from the Kopeh Dagh Mountains towards the Neyshabur Fault System. To the southeast, this fault system terminates into a complicated horsetail structural zone that consists of strike-slip and reverse fault segments (Fig. 2). Along the northeast flank of the Binalud, the Mashhad Fault System slips right-laterally with a rate of ~1.6 mm/yr. To the northwest, it terminates without clear structural connection to the Kopeh Dagh fault systems (Fig. 2). Such a structural pattern implies that the Binalud Mountains are deformed as a transpressional relay zone between the two fault systems at its sides (Fig. 20).

From the geomorphic point of view, the Binalud is an asymmetric mountain range. The southwest side is a short, steeply-slopping flank incised by catchment areas that are characterized by a mean width/length ratio of 0.45. Conversely, the northeast flank is long and gently-slopping occupied by elongate and nearly more linear basins with a mean width/length ratio of 0.1. This morphology could be described by significant uplift of the southwestern side versus uniform back-tilting of the northeast flank due to a differential vertical deformation caused by active reverse faulting along the Neyshabur Fault System versus strike-slip faulting along the Mashhad Fault System. This pattern is only observed within the southeast half of the range, where the Binalud Mountains are restrained between two overlapping fault systems (Figs 20 and 21). Significant (~4 mm/yr) right-lateral strike-slip faulting components along the fault systems together with their right-handed arrangement make the southeast half of the Binalud Mountains a restraining step-over in which shortening is intensified by considerable (~2.4 mm/yr) reverse faulting components at its southwestern side. Conversely to the intensely deformed southeast part, Mesozoic paleo-reliefs have been preserved in the northwestern half of the Binalud Mountains (Figs 20 and 21). During Paleozoic, the Lower Triassic metamorphic core of the Binalud Mountains was unconformably covered by Upper Mesozoic marine carbonates. During Cenozoic, these rocks were totally removed from the southeastern part, while they are present in the northwest half covering the metamorphic core. This differential denudation indicates that long-term erosional effect should be directly controlled by structural pattern and long-term fault kinematics. Interestingly, more preserved parts of the Mesozoic paleoreliefs are found far from the relay zone, where the paleoreliefs are bounded by the Chakaneh fault system. During the Late Cenozoic, this fault system was

reactivated as a strike slip fault transferring strike-slip faulting from the Kopeh Dagh southwards. Such a mechanism does not favor significant vertical deformations in the northeast half of the mountains. The intensity of deformation, and consequently erosion effects on the paleoreliefs increase southeastward closer to the Chakaneh Fault termination, where it connects to the Neyshabur Fault System (Figs 20 and 21). Altogether, these observations suggest that the deformation pattern of the Binalud Mountains can be described as a restraining right-lateral step-over between the bounding fault systems. Such a structural pattern not only has caused different deformation patterns but also it controlled the long-term effects of erosion and denudation processes forming different large-scale geomorphic features in the northwest and southeast parts of the Binalud deformation domain.

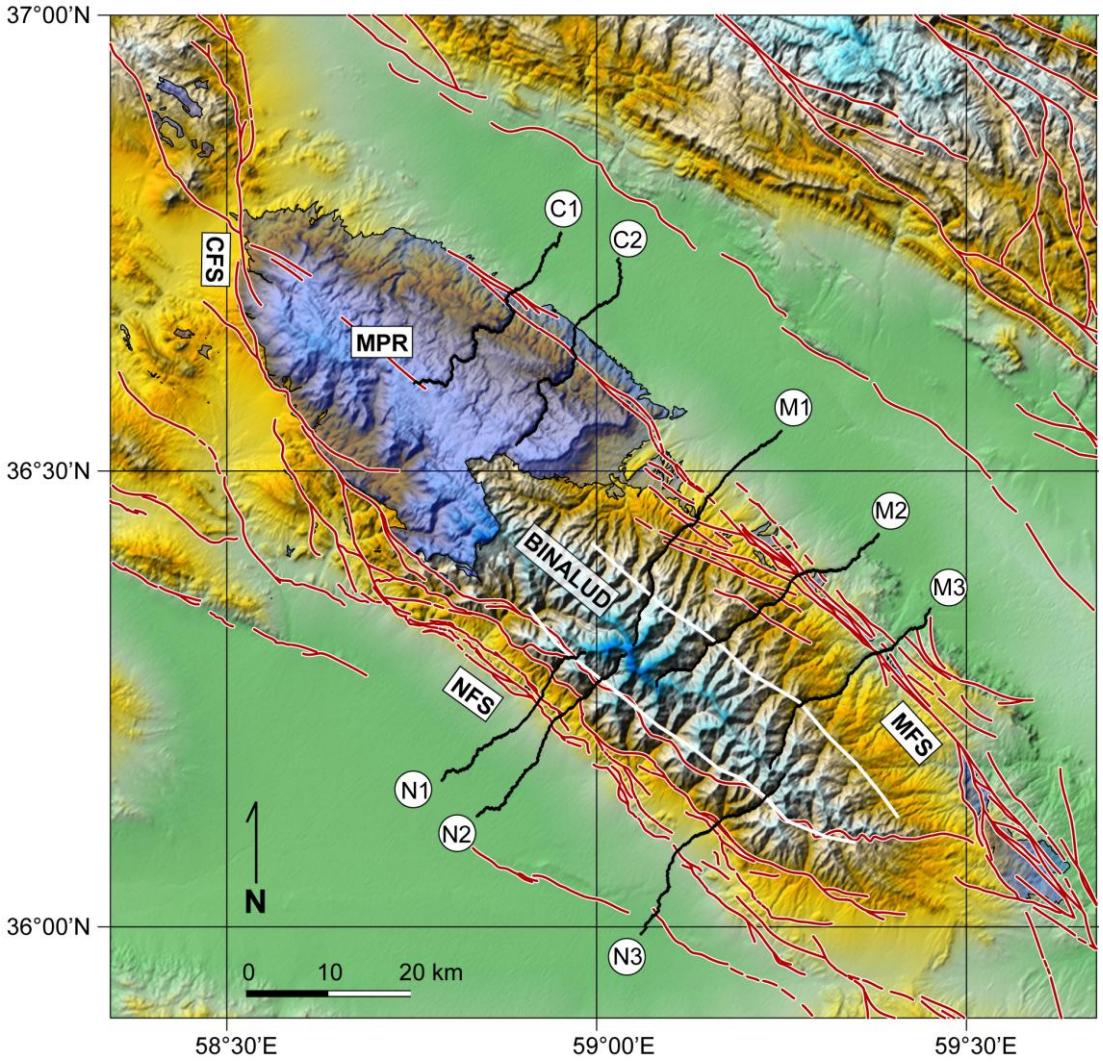


Figure 21. Shaded relief map of the Binalud Mountains superposed by the fault map of the region (red lines) and remnants of the Mesozoic plateau (MPR - blue polygons). Black lines show location of the stream-channel profiles presented in Figure 22. White lines are the geomorphic break-lines.

### 8.2. Examining active deformation pattern through geomorphic analysis

As mentioned in section 8.1, drainage basins incised in the southwest flank of the Binalud Mountains are characterized by large circular watersheds with a mean width/length ratio of 0.45, whereas basins in the NE flank are elongate with a mean width/length ratio of 0.1. In addition to this geomorphic aspect, other differences in the basin morphologies are observed. In the NE flank a drastic change is observed in the shape of basins illustrating a sharp break-line in their morphology (Fig. 21). The longitudinal profiles of the main streams exhibit upstream increasing slope gradient (Fig. 22). In the SW flank, there is no remarkable variation in shape of the basins, but, a drastic step-like change is observed in the longitudinal profiles of axial streams (Fig. 22). The limit of this change for main basins is a continuous break-line from which the upstream segments of the basins show a lower slope gradient relative to the downstream parts. Two parts are usually separated by a scarp-like steep slope (Fig. 22). The field expressions of this geomorphic pattern are back-tilted upstream parts separated from the downstream basin parts through a steep slope (Fig. 22).

In order to better understand relationships between the large-scale geomorphic features and Quaternary deformation processes in the Binalud Mountains, we calculated percentage hypsometric curves and derived integrals (cf. *Strahler*, 1952; *Keller and Pinter*, 1996) for 159 third- to fifth-order (*Horton*, 1945) drainage basins. This geomorphic analysis was performed on the basis of SRTM digital elevation data using "RiverTools-2.4" computer software. The basin outlines were defined in relation to major fault segments to make the obtained hypsometric integral values more meaningful in terms of active tectonics. For the basins showing drastic changes in their morphology, three classes of hypsometric curves are provided. For instance in a given basin, those are two individual hypsometric curves for sub-basins (third- or fourth-order) defined in the upstream and downstream of the geomorphic break-line, as well as a curve for the entire basin (fourth- or fifth-order). Basins are developed on similar types of rock suggesting that a lithologic influence on evolution of the basins is negligible.

For the region without structural and tectonic controls, two percentages have been considered as boundaries of the youthful, mature, and old stages in a geomorphic cycle. In such a situation, transition from the imbalance (youthful) stage to the equilibrium (mature) stage corresponds roughly to a hypsometric integral of 0.60. Whereas, where inselbergs become conspicuous features, the hypsometric integrals drop below 0.35 (*Strahler*, 1952). In the region submitted to active tectonics and without important lithological variations,

significant variations in hypsometric integrals with respect to the expected values corresponding to the present-day geomorphic stage of the basins can be interpreted as tectonic effects.

Hypsometric integrals for the basins developed in the Binalud domain are presented in Figure 23. The integral values range from 0.18 to 0.68. At a first glance, the lower bound (0.18) of this range appears abnormal with respect to the real geomorphic stage of the basins. Except the Paleozoic plateau at the NW corner, the main body of the mountain range is occupied by well-developed basins; so that evidence for neither the initial landmass flat surface, nor remnants of eroded old surfaces are observed within or between the basin outlines. Considering these topographic and geomorphic patterns, apart from geomorphic anomalies due to tectonic deformations, the large-scale geomorphic features of the region can be generally classified between the imbalance (youthful) and equilibrium (mature) stages, while the calculated hypsometric integrals for some basins show a percentage blow the hypsometric integral representative for transition from the mature to old stages.

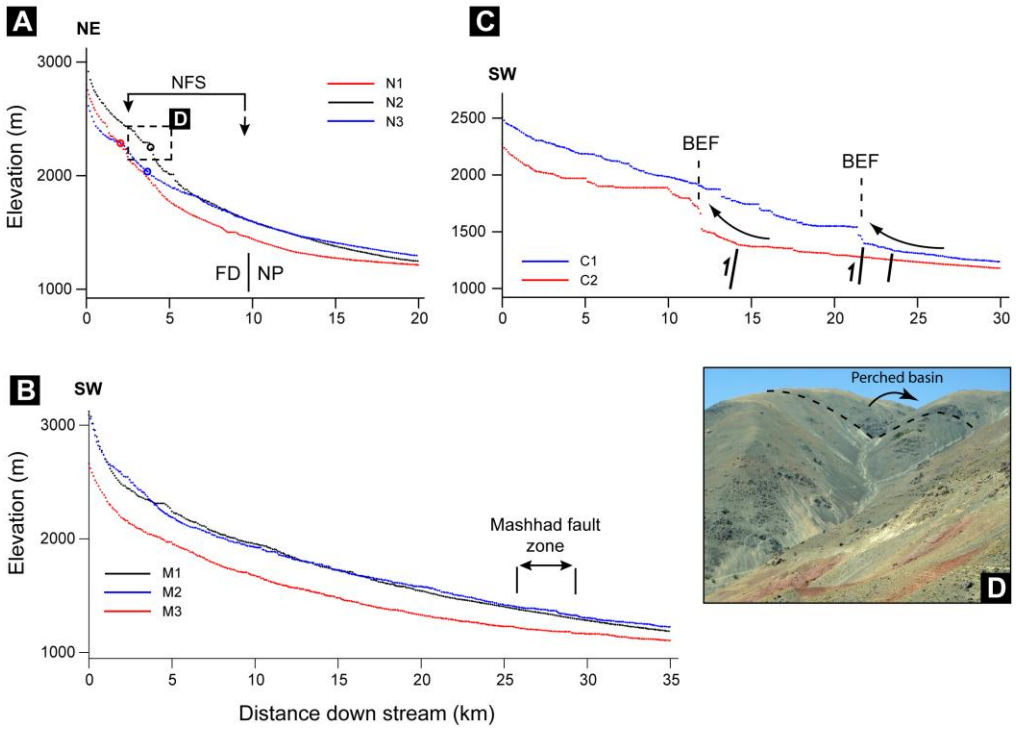


Figure 22. Stream-channel profiles of the major streams incising in the Binalud mountains (see Figure 21 for profile's locations). (a) Streams incising in the southwestern flank of the range across the Neyshabur Fault System; FD, Foothills domain; NP, Neyshabur plain; NFS, Neyshabur Fault System. Small circles show the approximate location of the Binalud Fault in each profile (b) Streams incising in the northeastern flank of the range across the Mashhad Fault System. (c) Streams incising in the northwestern part of the northeastern flank of the range, across the new defined faults; BEF, Backward erosional front (retrogressive erosion). (d) Field photograph of a perched basin at the southwestern flank of the range, along profile N1; dashed line is a fault trace.

In the Binalud Mountains, three distinct classes of hypsometric values are distinguished (1) the moderate integral values between 0.40 and 0.60, (2) the high hypsometric integrals higher than 0.60, and (3) the integral values lower than 0.40. The first class is attributed to the basins with moderate integral values. These basins are distributed throughout the region with a preferred clustering in the northeast flank of the Binalud Mountains. Such a distribution is consistent with our geomorphic description suggesting that large-scale geomorphic features of the region show transition from the imbalance to equilibrium stages. As an exception, the NW part of the Binalud Mountains has been occupied by youthful drainage basins (imbalance stage).

For the second class, distribution of the basins with high hypsometric integrals (>0.60) illustrates meaningful relationships with mechanisms of active deformation along the major fault systems. The basins located at both contractional terminations of the Chakaneh fault systems present high hypsometric integral values. A group of basins belonging to the same class is observed in the northeast flank of the Binalud where an active back-tilting is expected in the hanging wall of the Neyshabur Fault System. A similar mechanism can describe the high integral values for the basins on NE flank of the Kalidar Mountain. The close agreement between high hypsometric integral values and the zone of active contractional deformation may indicate that before the achievement of an equilibrium system, the basins underwent an acceleration of stream erosion rates with increasing relief as a result of active northward tilting of the region associated with fault-related uplifts on the hanging wall of the Neyshabur Fault System. In the northwestern part of the region, where the Mesozoic plateau is cropping out, a large proportion of upland surface has not yet been transformed into valley-wall slopes (Fig. 21), but the hypsometric integrals (ranging from 0.3 to 0.5) are lower than the expected range for such a geomorphic stage (>0.60). This may indicate the effect of slight back-tilting of the basins due to young uplifts along the NE boundary of the mountains. The existence of several small basins at this boundary may testify our suggestion (Fig. 23). If accepted, the faults recognized at the continuation of the Mashhad Fault System (Figs 2 and 23) should be considered as Quaternary faults, whatever their structural importance.

The basins in the southwest flank of the Binalud Mountains produce unusually low hypsometric integrals, between 0.2 and 0.3 (Fig. 23). The majority of these basins are observed in the hanging wall of the Binalud Fault, though; some of them are extended between the Barfriz and Binalud Faults. At the first order, this pattern is surprising; the lowest hypsometric integrals are from a zone, which has been submitted to significant (~2.4 mm/yr) vertical deformations. More precise analysis of the basin hypsometric integrals uncovers

further details. Generally, the basins with low integral values are focalized along, and nearly more, in the hanging wall of the Binalud Fault, where no evidence for quaternary faulting is observed (section 4.1). Moreover, in the area between the Binalud Fault zone and the Barfriz Fault, basins represent increasing integral values relative to the basins incised in the hanging wall of the inactive segment of the Binalud Fault zone. The mismatch of hypsometric integrals to the predicted values, in accordance with the actual place of the basins in a geomorphic cycle, as well as the meaningful relationships between long-term geomorphic evolution and structural pattern of the Binalud Mountains suggest that geomorphic processes are closely controlled by kinematics of deformation.

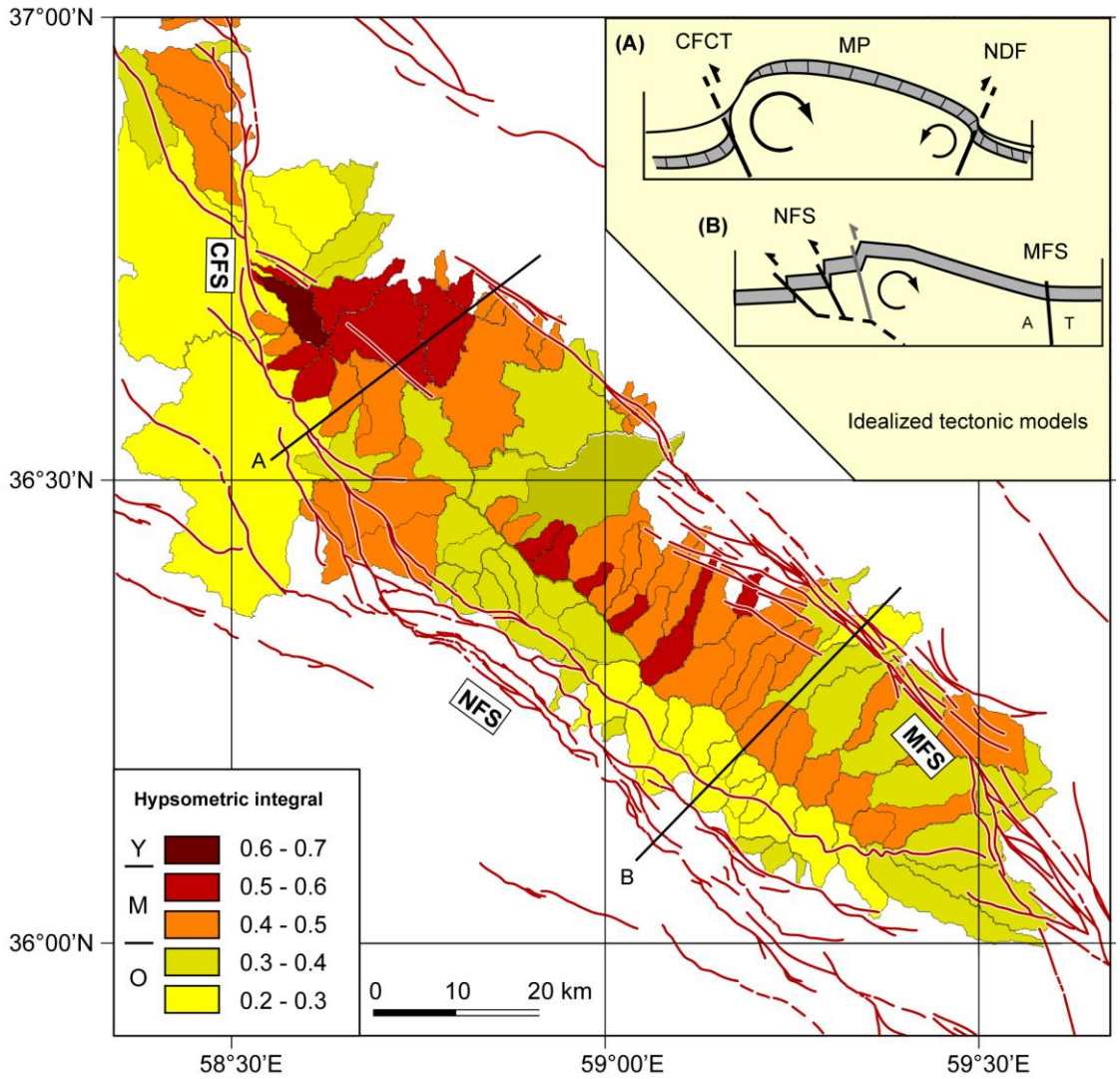


Figure 23. Hypsometric integral values calculated for drainage basins nested in the Binalud mountain range. The geomorphic stages presented in the map legend are: Y, Youthful; M, Mature; O, Old. The upper right inset illustrates idealized tectonic models describing the inferred deformation processes responsible for the long-term geomorphic evolution of the range; pivoting arrows show sense of fault-related tilting. CFCT, Chakaneh Fault contractional termination; NDF, New defined faults; MP, Mesozoic Plateau; A and T indicate the right-lateral sense of fault motions. Gray line marks inactive faults.

For the areas at contractional fault terminations and corresponding back-limb areas, uplifts caused by reverse faulting components persists against the river corrasion to retain basins in the youth stage, producing high hypsometric integral values. At the northeast side, the predominant strike-slip mechanism of the Mashhad Fault System implies that tectonic uplift and the consequent back-tilting are insignificant. Conversely, vertical motions along reverse to oblique-slip faults of the Neyshabur Fault System have caused significant uplift at the southwest front of the Binalud Mountains. The Binalud Mountains exhibit an asymmetric antiformal geometry (*e.g.*, *Alavi*, 1992), which in northeast side (gently sloping limb), is confined to the Mashhad Fault System that is a deep-seated back-stop structure (Paleo-Tethys suture - *Majidi, 1978*; *Alavi*, 1992). Considering this geometric constraint, uplift at the SW front is followed by tilting of the NE flank, producing relatively high hypsometric integral values (Fig. 23). But, such a mechanism could not adequately explain the unusually low hypsometric integrals from basins confined between the Barfriz Fault and the inactive segment of the Binalud Fault zone.

The Binalud Fault zone is nowadays a back-tilted steeply-dipping structure that was originated from a low-angle thrust fault (section 4.1). On the other hand, the locus of Quaternary deformations, and consequently, the depositional setting of $Q_1$, $Q_2$, and $Q_3$ alluvial fans has been migrated basin-ward across the Neyshabur Fault System. Before ~94 kyr ago (abandonment of the $Q_3$ surfaces), the Binalud active mountain front corresponded to the Barfriz Fault, where the $Q_3$ alluvial surfaces formed. The abandonment of the $Q_3$ fan is suggested to be concurrent with the onset of Late Pleistocene thrust faulting along the Buzhan Fault zone. The consequent contraction of the zone between the Barfriz and Buzhan Faults uplifted, and even folded $Q_3$ fan surfaces forming the foothills domain. Subsequently, a significant part of the uplifted $Q_3$ surfaces was removed from the Foothills domain due to erosion. The eroded materials were discharged at the new deformation front along the Buzhan Fault zone downhill into gently sloping alluvial fans, which in turn are affected by Holocene activities ($\leq$5 kyr) along the southwestern most fault segments(*e.g.*, the Somaeh Fault). The youngest fault activities are represented by co-seismic fault ruptures or up-warped alluvial fans (section 4.5) at the present active deformation front into the basin. The Late Pleistocene-Holocene reverse faulting along the Buzhan Fault zone has rejuvenated old drainages incised in Q3 surfaces. This rejuvenation is expressed by active stream captures, intense incisions inset in older stream beds and spectacular knick point that mark the last progression of the new erosional regime. These observations indicate that the Binalud deformation front is migrating southwestward along new reverse faults formed basin-ward. Such a pattern of

deformation has been observed in fold-and-thrust belts in various localities in the world, including Taiwan (*Davis et al*., 1983), India and Pakistan (*Yeats*, 1986), the Transverse Ranges (*Bullard and Lettis*, 1993; *Namson and Davis*, 1988) and the San Joaquin Valley of California (*Keller et al*., 2000). The topographic expression of active fold-and-thrust belts is mostly produced by the ongoing thrust faulting and folding. The deformation commonly migrates away from the highlands of the range toward the adjacent flanks such that youngest structures are at the edge of the fold-and-thrust belt. Interior faults of the system may become relatively inactive as the active tectonic processes are transferred to frontal fault systems (*Davis*, 1983; *Yeats*, 1986 and references therein). According to this model, as a mountain front develops, new buried reverse faults form basin-ward and new folds and a new mountain front develop. Older alluvial fans are folded, faulted, and incorporated within the mountain range. An older, now-intermountain front is abandoned in the interior of the range, and new fans are developed basin-ward. In the case of the Binalud mountains, in addition to these typical features of the development of fold-and-thrust belts, the basin-ward migration of the deformation front has apparently been accompanied by backward rotation of older faults (*i.e*., Binalud Fault) making it steepen with time. If accepted, the areas above steepen faults are tilted back decreasing the slop gradient of catchment areas incised in hanging walls of the faults. This will produce perched drainage catchments (Figs 4, 22 and 24) with unusually low hypsometric integrals (Fig. 23). Such a mechanism may appropriately be described by the back-stop role of the Mashhad Fault System, which persists against the hinterland development of deformation, and makes the backward rotation of thrust faults an adapted mechanism to take up shortening across the belt. The sudden changes in morphology of the basins may also explained by episodic character of the tectonic processes controlling the long-term geomorphic evolutions of the Binalud Mountains. Both the migration of the Binalud deformation front and the episodic character of deformations are consistent with successive faulting along the Neyshabur Fault System suggested by (*Alavi*, 1992).

## 9. Conclusion

According to the data and deduced results presented here, late Cenozoic faulting at both sides of the Binalud Mountains is taken up by two major fault systems, *i.e*., the Neyshabur and Mashhad Fault Systems (Figs 2 and 20). The present-day northward motion of Central Iran relative to Eurasia is accommodates by strike-slip faulting along the Mashhad Fault System at a rate of ~1.6 mm/yr averaged over ~200 kyr. The Neyshabur Fault System slips at

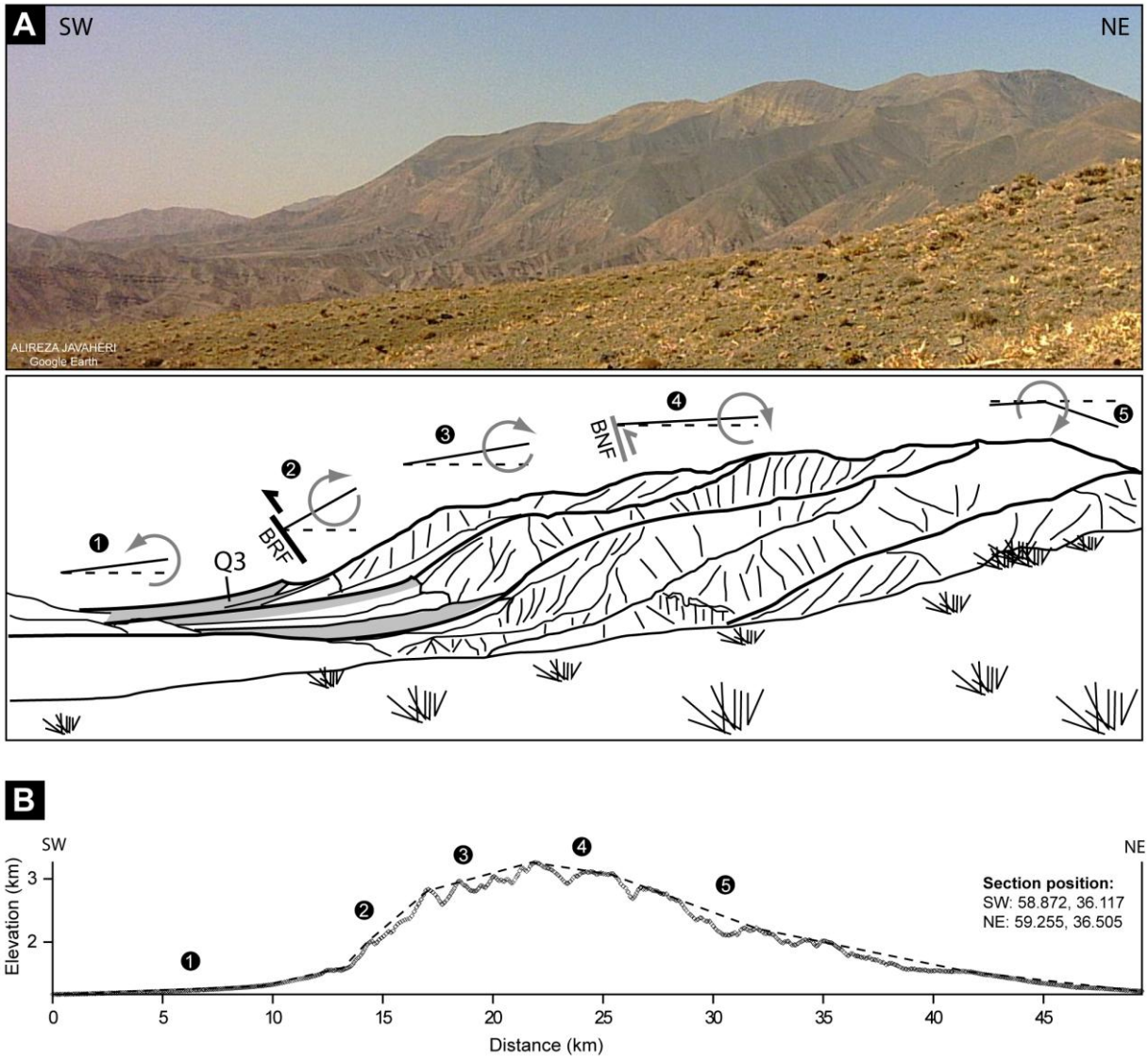


Figure 24. (a) General view of the Binalud Mountains together with the inferred deformation processes due to migration of the locus of active reverse faulting and vertical deformation along the southwestern flank of the range. Pivoting arrows show sense of fault-related tilting. BFR, Barfriz Fault; BNF, Binalud Fault. Gray line marks inactive faults. (b) Topographic profile across the Binalud mountains based on SRTM data; circled numbers help to correlate corresponding geomorphic slopes interpreted in (a).

a total oblique-slip rate of ~3.6 mm/yr, which is resolved into a rate of ~2.4 mm/yr for vertical faulting component being accommodated along at least three parallel faults (*i.e.*, the Barfriz, Somaeh and Eyshabad faults), and into the respective rates of 2.6 and 2.8 mm/yr for right-lateral faulting component taken up by the Barfriz Fault and the southeastern fault segment of the Buzhan Fault zone.

Considering the geometry and kinematics of the two fault systems, deformation pattern of the southeast Binalud Mountains can be described by a restraining step-over arrangement in which contractional deformation is intensified by oblique-slip reverse faulting along the

Neyshabur Fault System. Such a structural arrangement has controlled the long-term erosion and denudation history of the mountains, making the geomorphic evolution of the southeast part different from the northwest evolution history. The southeast part, confined between the restraining step-over, is characterized by an elongate dome shape topography in which drainage catchments are well developed (Figs 22 and 23). The Mesozoic paleoreliefs are absent and suggested to be totally removed from this area. A ~140 m variation in height of the highest Quaternary surfaces ($S_4$) in the northeast flank confirm this assumption. Conversely, in the northwest part, beyond the restraining step-over, the Mesozoic formations form well preserved, plateau-like paleoreliefs characterized by drainage basins in the youth stage. This pattern strongly indicates the non-uniform pattern of deformation in the Binalud Mountains.

The Mashhad Fault System has experienced successive deformation episodes since the closure of Paleo-Tethys (*e.g*., *Majidi*, 1978). Conversely for the Neyshabur Fault System, geomorphic and geological observations suggest that the deformation front has migrated southwestward across the fault system. The geomorphic analysis of drainage systems reveals close relationships between Quaternary deformation processes and long-term geomorphic evolutions. This analysis provides evidence for (1) backward rotation of older faults in the hanging walls of new produced or reactivated faults due to the southwestward migration of the mountain front and structural imbrications, and (2) tilting of the northeast flank of the Binalud Mountains due to reverse faulting along the Neyshabur Fault System and the back-stop role of the Mashhad Fault System.

From the geodynamic point of view, the Mashhad and Neyshabur fault systems have the significant contribution, *i.e*., ~5 mm/yr of total slip rates, to accommodate active deformations due to the Arabia-Eurasia convergence, taken up in northeast Iran. The range parallel strike-slip faulting at both sides of the Binalud Mountains confidently suggests that the northward motion of central Iran relative to Eurasia has not wholly been absorbed by crustal shortening and thrust faulting in the range, but, it is transferred toward the Northwest. Further north in the Kopeh Dagh, the Arabia-Eurasia related deformation is principally (~80 per cent) taken up by localized strike-slip faulting along the Bakharden-Quchan fault system (*Shabanian et al*., 2009a). The strike-slip deformation is transferred southward through the Meshkan transfer zone (*Shabanian et al*., 2009b and 2009c), between the Binalud and Kopeh Dagh mountains. Our knowledge of the range parallel strike-slip faulting at both sides of the Binalud Mountains add another segment to the geodynamic puzzle of northeast Iran in which central Iran and western Kopeh Dagh are translated towards northwest with respect to Eurasia (*Shabanian et al*., 2009a, 2009b, and 2009c). In the Binalud deformation domain, age relation

of successive faulting episodes indicates that the initiation of strike-slip faulting cannot be older than the Quaternary. This strengthens the suggestion that a new tectonic configuration (*Shabanian et al.*, 2009b) was established during the Plio-Quaternary. Such a configuration implies that the late Cenozoic shortening and crustal thickening, at the regional scale, were replaced by strike-slip faulting localized along well-defined fault systems. However, more detailed morphotectonic works are needed to characterize other active faults (*e.g.*, the Dorbadam and Hezar Masjed fault systems in the Eastern Kopeh Dagh) to reconstruct a complete image of active deformation at the northeastern boundary of the Arabia-Eurasia collision.

**References**

Aghanabati, A. (1986), Geological quadrangle map of Iran, Mashhad sheet, scale 1:250,000, Geol. Survey of Iran, Tehran.

Alavi, M. (1992), Thrust tectonics of the Binalood region, NE Iran, *Tectonics, 11*(2), 360-370.

Berberian, M., and Yeats, R. (1999), Patterns of historical earthquake rupture in the Iranian Plateau, *Bull. Seism. Soc. Am., 89*, 120–139.

Bullard, T. F., and Lettis, W. R. (1993), Quaternary fold deformation associated with blind thrust faulting, Los Angeles basin: California: *Journal of Geophysical Research, 98*, 8349–8369.

Daëron, M., Benedetti, L., Tapponnier, P., Sursock, A. and Finkel, R. C. (2004), Constraints on the post ~25-ka slip rate of the Yammoûneh fault (Lebanon) using in situ cosmogenic $^{36}$Cl dating of offset limestone-clast fans, *Earth Planet. Sci. Lett., 227*, 105-119.

Deino, A. and Potts, R. (1992), Age-probability spectra from examination of single-crystal $^{40}$Ar/$^{39}$Ar dating results: Examples from Olorgesailie, Southern Kenya Rift, *Quaternary International, 13/14*, 47-53.

Davis, D., Suppe, J., and Dahlen, F. (1983), Mechanics of Fold-and-Thrust Belts and Accretionary Wedges, *J. Geophys. Res., 88*(B2), 1153-1172.

Dixon, T. H, Norabuena, E. and Hotaling, L. (2003), Paleoseismology and Global Positioning System: Earthquake cycle effects and geodetic versus geologic fault slip rates in the Eastern California shear zone, *Geology, 31*, 55-58.

Friedrich, A. M., Wernicke, B. P., Niemi, N. A., Bennett, R. A. and Davis J. L. (2003), Comparison of geodetic and geologic data from the Wasatch region, Utah, and implications for the spectral character of Earth deformation at periods of 10 to 10 million years, *J. Geophys. Res., 108*(B4), 2199. doi:10.1029/2001JB000682.

Horton, R. E. (1945), Erosional development of streams and their drainage basins: hydrophysical approach to quantitative morphology, *Geol. Soc. Am., Bull., 56*(3), 275-370.

Keller, E. A. and Pinter, N. (1996), Active Tectonics, Earthquakes, Uplift and Landscape, Prentice Hall, Upper Saddle River, 338 p.

Keller, E. A., Seaver, D. B., Laduzinsky, D. L., Johnson, D. L. and Ku, T. L. (2000), Tectonic geomorphology of active folding over buried reverse faults: San Emigdio Mountain front, southern San Joaquin Valley, California, *Geol. Soc. Am. Bull., 112*(1), 86–97.

Lowell, T. V. (1995), The application of radiocarbon age estimates to the dating of glacial sequences: an example from the Miami sublobe, Ohio, USA, *Quaternary Science Reviews, 14*, 85– 99.

Majidi, B. (1978), Etude petrostructurale de la région de Mashhad, Iran: Les problèmes des métamorphites, serpentinites, et granitoïdes hercyniens, Thèse de doctorat, l'Université Scientifique et Médicale de Grenoble, France, 274 p.

Masson, F., Anvari, M., Djamour, Y., Walpersdorf, A., Tavakoli, F., Daignières, M., Nankali, H. and Van Gorp, S. (2007), Large-scale velocity field and strain tensor in Iran inferred from GPS measurements: new insight for the present-day deformation pattern within NE Iran, *Geophys. J. Int., 170*, 436–440. doi:10.1111/j.1365-246X.2007.03477.x.

McClusky, S., Reilinger, R., Mahmoud, S., Ben Sari, D. and Tealeb, A. (2003), GPS constraints on Africa (Nubia) and Arabia plate motions, *Geophys. J. Int., 155*(1), 126–138. doi:10.1046/j.1365-246X.2003.02023.x.

McDonald, E. V. (1994), The relative influence of climatic change, desert dust, and lithological control on soil-geomorphic processes and hydrology of calcic soils formed on Quaternary alluvial-fan deposits in the Mojave Desert, California, PhD thesis, Univ. of New Mexico, Albuquerque.

Merchel, S., Arnold, M., Aumaître, G., Benedetti, L., Bourlès, D. L., Braucher, R., Alfimov, Freeman, V., S.P.H.T., Steier, P., and Wallner, A. (2008), Towards more precise 10Be and 36Cl data from measurements at the 10−14 level: Influence of sample preparation, Nuclear Instruments and Methods in Physics Research Section B: Beam Interactions with Materials and Atoms, 266(22), 4921-4926.

Meyer, B., and K., Le Dortz (2007), Strike-slip kinematics in Central and Eastern Iran: Estimating fault slip-rates averaged over the Holocene, *Tectonics, 26*, TC5009, doi:10.1029/2006TC002073.

Namson, J., and Davis, T. L. (1988), Seismically active fold and thrust belt in the San Joaquin Valley, central California: *Geol. Soc. Am. Bull., 100*, 257–273.

Nishiizumi K., Imamura M., Caffee M. W., Southon J. R., Finkel R. C., and McAninch J. (2007), Absolute calibration of 10Be AMS standards, *Nuclear Instruments and Methods in Physics Research, B258*, 403-413.

Phillips, F. M., Zreda, M. G., Gosse, J. C., Klein, J., Evenson, E. B., Hall, R. D., Chadwick, O. A., and Sharma, P. (1997), Cosmogenic $^{36}$Cl and $^{10}$Be ages of Quaternary glacial and fluvial deposits of the Wind River Range, Wyoming, *Geol. Soc. Am. Bull., 109*(11), 1453–1463.

Regard, V., Bellier, O., Thomas, J.-C., Abbassi, M. R., Mercier, J. L., Shabanian, E., Feghhi, K., and Soleymani, S. (2004), Accommodation of Arabia-Eurasia convergence in the Zagros-Makran transfer zone, SE Iran: A transition between collision and subduction through a young deforming system, *Tectonics, 23*, TC4007. doi:10.1029/2003TC001599.

Reilinger, R., et al. (2006), GPS constraints on continental deformation in the Africa-Arabia-Eurasia continental collision zone and implications for the dynamics of plate interactions, *J. Geophys. Res., 111*, B05411. doi:10.1029/2005JB004051.

Schwartz D. P., and K. J., Coppersmith (1984), Fault behavior and characteristic earthquakes: Examples from the Wasatch and San Andreas Fault zones. *J. Geophys. Res., 89*, 5681-5698.

Sella, G. F., Dixon, T. H., and Mao, A. (2002), REVEL: A model for recent plate velocities from space Geodesy, *J. Geophys. Res., 107*(B4), 2081. doi:10.1029/2000JB000033.

Shabanian, E., L. Siame, O. Bellier, L. Benedetti, and M. R. Abbassi (2009a), Quaternary slip-rates along the north-eastern boundary of the Arabia-Eurasia collision zone (Kopeh Dagh Mountains, North-East Iran), *Geophys. J. Int., 178*, 1055–1077, doi: 10.1111/j.1365-246X.2009.04183.x.

Shabanian, E., O. Bellier, L. Siame, N., Arnaud, M. R. Abbassi, and J.-J. Cochemé (2009b), New tectonic configuration in NE Iran: active strike-slip faulting between the Kopeh Dagh and Binalud mountains, *Tectonics, 28*, TC5002, doi:10.1029/2008TC002444.

Shabanian, E., O. Bellier, M. R. Abbassi, L.L. Siame, and Y. Farbod, (2009c), Plio-Quaternary stress states in NE Iran: Kopeh Dagh and Allah Dagh-Binalud mountains, *Tectonophysics*, accepted.

Stone, J. O. H. (2000), Air pressure and cosmogenic isotope production, *J. Geophys. Res., 105*(B10), 23753-23759.

Strahler, A. N. (1952), Hypsometric (area-altitude) analysis of erosional topology, *Geol. Soc. Am. Bull., 63* (11), 1117–1142.

Tavakoli, F. (2007), Present-day kinematics of the Zagros and east of Iran faults, PhD thesis, University of Joseph Fourier, Grenoble.

Taylor, J. R. (1997), An Introduction to Error Analysis, The Study of Uncertainties in Physical Measurements, 2nd ed., University Science Books, Sausalito, CA.

Tchalenko, J. S. (1975), Seismicity and structure of the Kopet Dagh (Iran, USSR), *Phil. Trans. R. Soc. Lond., Series A, 278*(1275), 1-28.

Tirrul, R., Bell, I. R., Griffis, R. J., and Camp, V. E. (1983), The Sistan suture zone of eastern Iran, *Geol. Soc. Am. Bull., 94*, 134 – 150.

Troeh, F. R. (1965), landform equations fitted to contour maps: *American Journal of Science, 263*, 616-627.

Vernant, P., Nilforoushan, F., Hatzfeld, D., Abbassi, M.R., Vigny, C., Masson, F., Nankali, H., Martinod, J., Ashtiani, A., Bayer, R., Tavakoli, F., and Chéry, J. (2004), Present-day crustal deformation and plate kinematics in the Middle East constrained by GPS measurements in Iran and northern Oman, *Geophys. J. Int., 157*(1), 381–398. doi:10.1111/j.1365-246X.2004.02222.x.

Walker, R., and Jackson, J. (2004), Active tectonics and Late Cenozoic strain distribution in central and eastern Iran, *Tectonics, 23*, TC5010. doi:10.1029/2003TC001529.

Wells, S. G., McFadden, L. D., and Dohrenwend, J. C. (1987), Influence of Late Quaternary climatic changes on geomorphic and pedogenic processes on a desert piedmont, eastern Mojave Desert, California, *Quaternary Res., 27*, 130–146.

Wells, S. G., McFadden, L. D., Dohrenwend, J. C., Turrin, B. D., and Mahrer, K. D. (1985), Late Cenozoic landscape evolution of lava flow surfaces of the Cima volcanic field, Mojave Desert, California, *Geol. Soc. Am. Bull., 96*, 1518–1529.

Wells, S. G., McFadden, L. D., Poths, J., and Olinger, C. T. (1995), Cosmogenic $^{3}$He exposure dating of stone pavements: implications for landscape evolution in deserts, *Geology, 23*, 613–616.

Yeats, R. S. (1986), Active faults related to folding, in Active Tectonics, Washington, D.C., National Academy Press, 63-79.

Zreda, M. G., Phillips, F. M., and Elmore, D. (1994), Cosmogenic $^{36}$Cl accumulation in unstable landforms, 2. Simulations and measurements on eroding moraines, *Water Resources Research, 30*, 3127–3136.

# *Chapter IV*

In the three previous chapters, different lines of evidences were presented for the rate and distribution of active strike-slip faulting in northeast Iran. Moreover, it was revealed that a major tectonic reorganization occurred at ~5 Ma. This major tectonic change corresponds to the onset of late Cenozoic strike-slip faulting in northeast Iran indicating that the Kopeh Dagh and Binalud deformation domains have not been uniformly deformed during the Cenozoic. Such an important change in tectonic configuration defines the temporal boundary between paleo- and modern- tectonic regimes. However, even if one accepts that the present-day tectonic configuration remained identical during the last 5 Ma; the key question is whether the kinematics of post-reorganization tectonic movements has been constant or not. The focus of this chapter is to identify changes in the Plio-Quaternary state of stress (since ~5 Ma) by inversion of both geologically and seismically determined faults slip vectors. After a brief review of the tectonic setting and applied methodology, we document significant changes in the Plio-Quaternary state of stress. Then, we describe geomorphic and geological observations related to the reliability of the identified Plio-Quaternary stress states. Finally, the validity of preexisting models, proposed for the northeast Iran geodynamics, was examined by integrating our geological data and deduced results in the models.

# Plio-Quaternary stress states in NE Iran: Kopeh Dagh and Allah Dagh – Binalud mountain ranges*

Esmaeil Shabanian[1,2], Olivier Bellier[1], Mohammad R. Abbassi[2], Lionel Siame[1], Yassaman Farbod[1,2]

[1] CEREGE - UMR CNRS, Université Aix-Marseille, IRD, Collège de France, Europôle de l'Arbois, BP 80, 13545 Aix-en-Provence Cedex 4, France

[2] International Institute of Earthquake Engineering and Seismology (IIEES), BP 19395-3913 Tehran, Iran

## Abstract

NE Iran, including the Kopeh Dagh and Allah Dagh-Binalud deformation domains, comprises the northeastern boundary of the Arabia-Eurasia collision zone. This study focuses on the evolution of the Plio-Quaternary tectonic regimes of northeast Iran. We present evidence for drastic temporal changes in the stress state by inversion of both geologically and seismically determined fault slip vectors. The inversions of fault kinematics data reveal distinct temporal changes in states of stress during the Plio-Quaternary (since ~5 Ma). The paleostress state is characterized by a regional transpressional tectonic regime with a mean N140±10°E trending horizontal maximum stress axis ($\sigma_1$). The youngest (modern) state of stress shows two distinct strike-slip and compressional tectonic regimes with a regional mean of N030±15°E trending horizontal $\sigma_1$. The change from the paleostress to modern stress states has occurred through an intermediate stress field characterized by a mean regional N trending $\sigma_1$. The inversion analysis of earthquake focal mechanisms reveals a homogeneous, transpressional tectonic regime with a regional N023±5°E trending $\sigma_1$. The modern stress state, deduced from the youngest fault kinematics data, is in close agreement with the present-day stress state given by the inversions of earthquake focal mechanisms. According to our data and the deduced results, in northeast Iran, the Arabia-Eurasia convergence is taken up by strike-slip faulting along NE trending left-lateral and NNW trending right-lateral faults, as well as reverse to oblique-slip reverse faulting along NW trending faults. Such a structural assemblage is involved in a mechanically compatible and homogeneous modern stress field. This implies that no strain and/or stress partitioning or systematic block rotations have occurred in the Kopeh Dagh and Allah Dagh-Binalud deformation domains. The Plio-Quaternary stress changes documented in this paper call into question the extrapolation of the present-day seismic and GPS-derived deformation rates over geological time intervals encompassing tens of millions of years.

*Keywords: Kopet Dagh; stress state; slip-vector chronology; Cenozoic tectonics; strain/stress partitioning; Neyshabur Fault.*

* *Shabanian et al. (2009), Tectonophysics, in press, doi:10.1016/j.tecto.2009.10.022.*

## 1. Introduction

Over the last three decades, attempts to characterize the tectonics of northeast Iran have revealed different structural and geodynamic aspects of the Cenozoic deformation (*Tchalenko*, 1975; *Afshar Harb*, 1979; *Hollingsworth et al*, 2006; *Masson et al.*, 2007; *Shabanian et al.*, 2009a, 2009b). The recognition of a major tectonic reorganization responsible for the late Cenozoic strike-slip faulting in northeast Iran by *Shabanian et al.* (2009a, 2009b) indicated that the Kopeh Dagh and Allah Dagh-Binalud deformation domains (Figure 1) have not been uniformly deformed during the Cenozoic. This important change in tectonic configuration occurred ~3.5 Ma (*Shabanian et al.*, 2009a) defining the temporal boundary between paleo- and modern- tectonic regimes throughout the region. On the other hand, recent GPS (Global Positioning System) measurements (*Vernant et al.*, 2004; *Masson et al.*, 2007; *Tavakoli*, 2007) significantly clarified the present-day tectonics of NE Iran (Figure 1), presenting instantaneous motion rates for distinct tectonic domains with respect to Eurasia. Subsequently, the present-day slip rates derived from the GPS observations were used to interpret cumulative geological fault offsets providing geodynamic models for the late Cenozoic tectonics of NE Iran, and furthermore, to explain the late Cenozoic geodynamics of the Arabia-Eurasia collision (*e.g.*, *Hollingsworth et al.*, 2006, 2008; *Masson et al.*, 2007). Such interpretations are based on the hypothesis that geological displacement vectors (including rate and direction of relative geological motions) remained constant throughout the late Cenozoic. Considering the post-Miocene (<5 Ma) tectonic change recognized in NE Iran (*Shabanian et al.*, 2009a, 2009b), it is clearly invalid to extrapolate the present-day instantaneous deformation rates over a time before Pliocene. However, even if one accepts that the present-day tectonic configuration remained identical during the last 5 Ma; the key question is whether the rates and kinematics of post-reorganization tectonic movements has been constant or not.

This paper looks to identify changes in the Plio-Quaternary state of stress (since ~5 Ma) in NE Iran (Figure 1) by inversion of both geologically and seismically determined fault slip vectors. After a brief review of the tectonic setting and applied methodology, we present the original results deduced from inversions of fault kinematics data documenting significant changes in the Plio-Quaternary state of stress. Then, we describe geomorphic and geological observations related to the reliability of the identified Plio-Quaternary stress states. Slip vectors obtained from earthquake focal mechanisms were inverted to determine the present-day kinematics of the region and its consistency with the modern state of stress determined from the inversion of fault kinematics data. Finally, the validity of preexisting models,

proposed for NE Iran's geodynamics, was examined by integrating our geological data and deduced results in the models.

## 2. Tectonic setting

In Iran, tectonic deformations result from the Arabia-Eurasia convergence. The northward motion of Arabia with respect to Eurasia is accommodated at a rate of 22±2 mm/yr at the longitude of Bahrain (*Sella et al.*, 2002; *McClusky et al.*, 2003; *Vernant et al.*, 2004; *Reilinger et al.*, 2006). In the Iranian plateau, the Arabia-Eurasia convergence took place by (1) crustal shortening and strike-slip faulting in intracontinental deformation domains such as the Zagros, Alborz and Kopeh Dagh mountain ranges, and (2) the active subduction along the Makran destructive continental margin. According to the available geodetic data, this northward motion should be accommodated in the Kopeh Dagh and Allah Dagh-Binalud mountains (NE Iran) at a rate of between 4 and 10 mm/yr (*Vernant et al.*, 2004; *Reilinger et al.*, 2006; *Masson et al.*, 2007; *Tavakoli*, 2007) (Figure 1).

The Kopeh Dagh Mountains form a NW trending active belt that separates central Iran from Eurasia (Turan platform) (Figure 1). Mesozoic and Tertiary sediments of the Kopeh Dagh were folded into parallel, asymmetric folds during the Oligo-Miocene orogenic movements (*Stöcklin*, 1968; *Afshar Harb*, 1979; *Lyberis and Manby*, 1999). The first folding episode and subsequently, emplacement of the Kopeh Dagh Mountains are characterized by these NW trending folds that result from a NE trending compressional tectonic regime during the late Cenozoic (*Afshar Harb*, 1979; *Lyberis et al.*, 1998; *Lyberis and Manby*, 1999). These folds are obliquely cut by strike-slip fault systems that consist of active NNW trending, right-lateral, and ENE trending left-lateral strike-slip faults (*e.g.*, *Tchalenko*, 1975; *Afshar Harb*, 1979; *Shabanian et al.*, 2009a) extending within the Western and Central Kopeh Dagh. The entire belt accommodates a significant part of the Arabia-Eurasia convergence involving thrust faulting, left-lateral strike-slip (on minor faults) in the west, and right-lateral strike-slip in the Central-Eastern Kopeh Dagh (*Afshar Harb*, 1979; *Jackson and McKenzie*, 1984) mainly along a large intracontinental fault system (*Shabanian et al.*, 2009a, 2009b). In this context, the Bakharden-Quchan Fault System (Figure 1) has accommodated about 80% of the Kopeh Dagh share (*i.e.*, 35-40 km) of Arabia-Eurasia northward motion during the last ~3.5 Ma (*Shabanian et al.*, 2009a).

The Allah Dagh-Binalud mountain ranges (Figure 1) form NW trending Mesozoic paleoreliefs south of the Kopeh Dagh that thrusts over the northern margin of Central Iran.

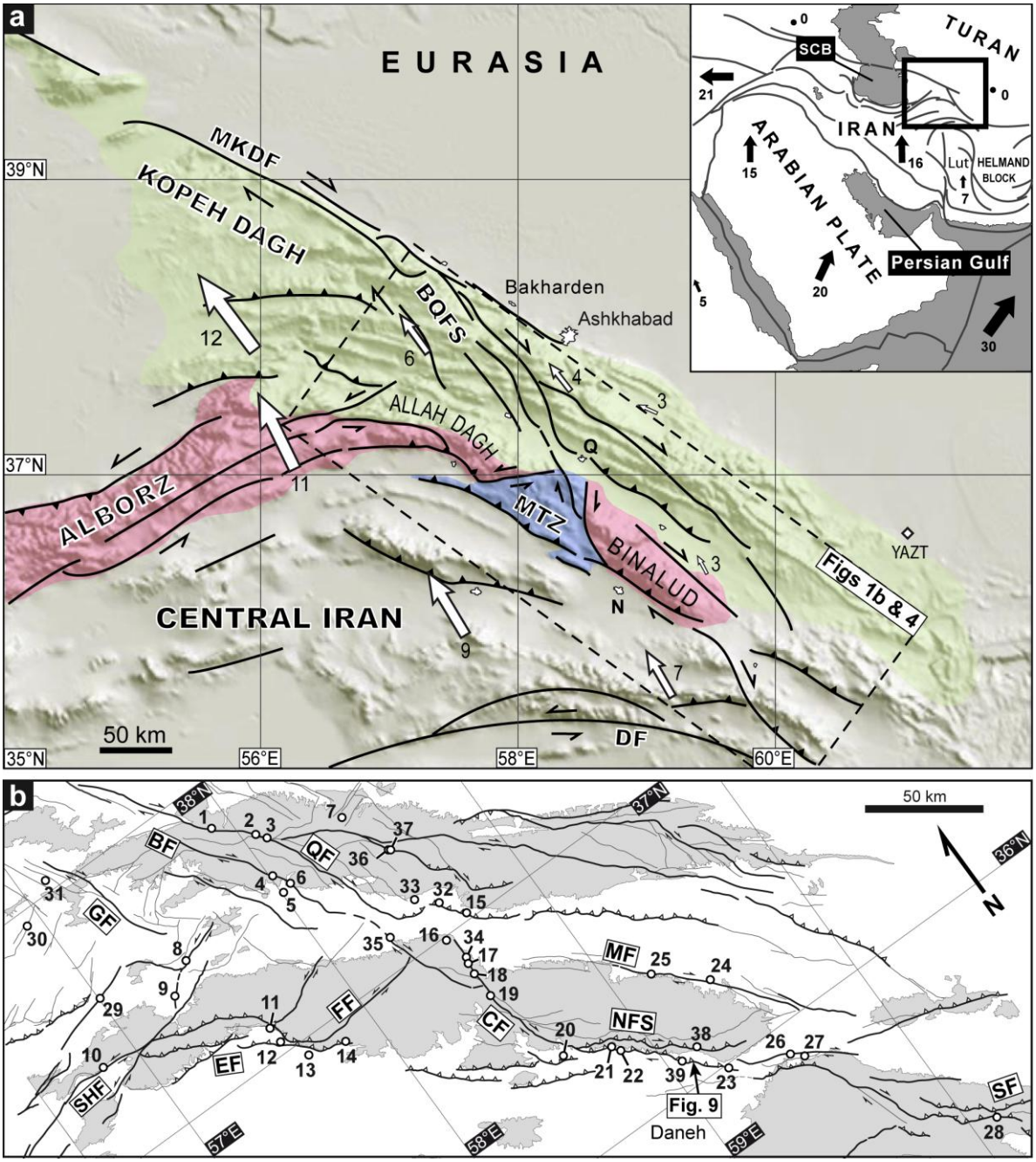


Figure 1. (a) GTOPO30 topographic image showing the regional tectonic setting and the major active faults of NE Iran. White arrows and associated numbers are GPS horizontal velocities (mm/yr) in a Eurasia-fixed reference frame (YAZT station (*Tavakoli*, 2007)). The inset with the box on the upper right shows the location in the Arabia-Eurasia collision framework. Gray arrows and associated numbers represent Arabia-Eurasia plate velocities (in mm/yr) after *Reilinger et al.* (2006). Abbreviations: MKDF, Main Kopeh Dagh Fault; BQFS, Bakharden-Quchan Fault System; DF, Doruneh Fault; MTZ, Meshkan Transfer Zone; N, Neyshabur; Q, Quchan; SCB, South Caspian Basin. (b) Fault map of the Kopeh Dagh and Allah Dagh-Binalud deformation domains representing major active faults (thick, black lines), other quaternary faults (thin, grey lines) together with the locations and corresponding site numbers of the fault kinematic measurements. Fault traces are based on SPOT5 and LANDSAT ETM+ image mapping (after *Shabanian et al.,* 2009a, 2009b, and this study). Colored areas are the region higher than 1500 m. BF, Baghan Fault; CF, Chakaneh Fault; EF, Esfarayen Fault; FF, Farhadan Fault; GF, Gholaman Fault; MF, Mashhad Fault; NFS, Neyshabur Fault System; QF, Quchan Fault; SF, Surestan Fault; SHF, Showqan Fault.

Conversely to the Kopeh Dagh, tectonic evolution of the Binalud is much more complex. A collection of the paleo-Tethys remnants as well as Lower Paleozoic, Middle and Upper Mesozoic, and Cenozoic rocks has been submitted to successive major ductile or brittle tectonic deformation episodes since the Paleo-Tethys closure (pre-Late Triassic) (*Alavi*, 1992). However, the same orientation of the fold axes within the Kopeh Dagh and Allah Dagh-Binalud mountains was suggested to be a result of homogenously directed compressional tectonic regimes, during Cenozoic folding episodes (*Shabanian et al.*, 2009b). The active tectonic framework of the Allah Dagh-Binalud domain consists of NE dipping active reverse faults at the southwestern boundary, ENE trending left-lateral strike-slip faults in the western part (Allah Dagh), and NW trending right-lateral strike-slip to oblique-slip reverse faults in the southeastern part (Figure 1). The central part of the range is considered as a transfer zone between the Kopeh Dagh and Binalud mountains, *i.e.*, the Meshkan transfer zone, which transfers ~25% of the northward motion between central Iran and Eurasia involving ENE trending left-lateral and N trending right-lateral strike-slip faults across the range (*Shabanian et al.*, 2009b). However, our knowledge of the late Cenozoic kinematics is largely insufficient despite attempts to characterize northeast Iran's tectonics (*e.g.*, *Tchalenko*, 1975; *Afshar Harb*, 1979; *Hollingsworth et al*, 2006; *Masson et al.*, 2007; *Shabanian et al.*, 2009a, 2009b).

## 3. Methodology: Inversion method, data separation and results interpretation

### 3.1. Inversion of fault-slip data

To determine the Plio-Quaternary states of stress in northeast Iran, we performed a quantitative inversion of distinct families of fault slip data measured at individual sites (Figure 1), using the method originally proposed by *Carey* (1979). This fault kinematics inversion method computes a mean best fitting deviatoric stress tensor from a set of striated faults by minimizing the angular deviation (misfit angle) between a predicted slip-vector and the observed striations (*Carey and Brunier*, 1974; *Carey*, 1979). The inversion results include the orientation (azimuth and plunge) of the principal stress axes ($\sigma_1>\sigma_2>\sigma_3$, corresponding to maximum, intermediate and minimum stress axis, respectively) of a mean deviatoric stress tensor as well as a "stress ratio" $R = (\sigma_2-\sigma_1)/ (\sigma_3-\sigma_1)$. This linear parameter (R) is equal to $1-\varphi$, $\varphi$ being another commonly used stress ratio (*e.g.*, *Angelier*, 1979; *Zoback*, 1989), and describes relative stress magnitudes ranging from 0 to 1 (*e.g.*, *Carey and Brunier*, 1974; *Mercier et al.*, 1991; *Bellier and Zoback*, 1995, and references therein).

### 3.2. Inversion of earthquake focal mechanism data

The present-day state of stress responsible for active faulting in northeast Iran was determined by inversion of focal mechanisms from moderate to large earthquakes (4.5 <M<7.5) using the method proposed by *Carey-Gailhardis and Mercier* (1987). In this method, computation of states of stress from populations of focal mechanisms of earthquakes requires the knowledge of the seismic slip-vectors and consequently the selection of the preferred seismic fault plane from each pair of nodal planes. The selection can be made directly from the observation of coseismic ruptures as well as the spatial epicenter distribution of the aftershock sequence, or by inverse computation. In the last alternative, the selection is possible because only one of the two slip-vectors of a focal solution is the seismic fault slip-vector in agreement with the principal stress axes (see *Carey-Gailhardis and Mercier*, 1987, 1992) defined using the dihedra method (*Angelier and Mechler*, 1977; *Carey-Gailhardis and Vergely*, 1992) before the inversion of focal mechanisms. In this study, we used the computation method mentioned above to select the seismic fault planes of each focal mechanism. Generally, the state of stress computed from focal mechanism of major earthquakes is in agreement with the state of stress deduced from inversions of active faulting kinematics measured in the field (*e.g.*, *Mercier et al.*, 1991; *Bellier et al.*, 1991, 1997; *Regard et al.*, 2004; *Authemayou et al.*, 2006).

Inversion of fault kinematics is based on several basic assumptions (*Mercier et al.*, 1991; *Carey-Gailhardis and Mercier*, 1992): (1) the slip responsible for the striation occurs on each fault plane in the direction and sense of the maximum shear stress resolved on the fault plane, (2) the slips on the fault planes are independent, (3) the faulted material is homogeneous, and (4) fault displacements are small with respect to the faults length, and no ductile deformation and rotation of the fault planes has occurred during the faulting. As a consequence, all the motions shown by striated faults or by focal mechanisms are not necessarily significant of the regional tectonic regime. Thus, only the coherence of results shown, for instance, by a statistical analysis of the principal stress directions obtained at numerous sites (see *Mercier et al.*, 1991) is a convincing argument for reliable information on the regional principal stress directions (*Carey-Gailhardis and Mercier*, 1992).

### 3.3. Data separation

In all fault kinematic inversion schemes, the main assumption is that slip responsible for the striation occurs on each fault plane in the direction and sense of the shear stress resolved

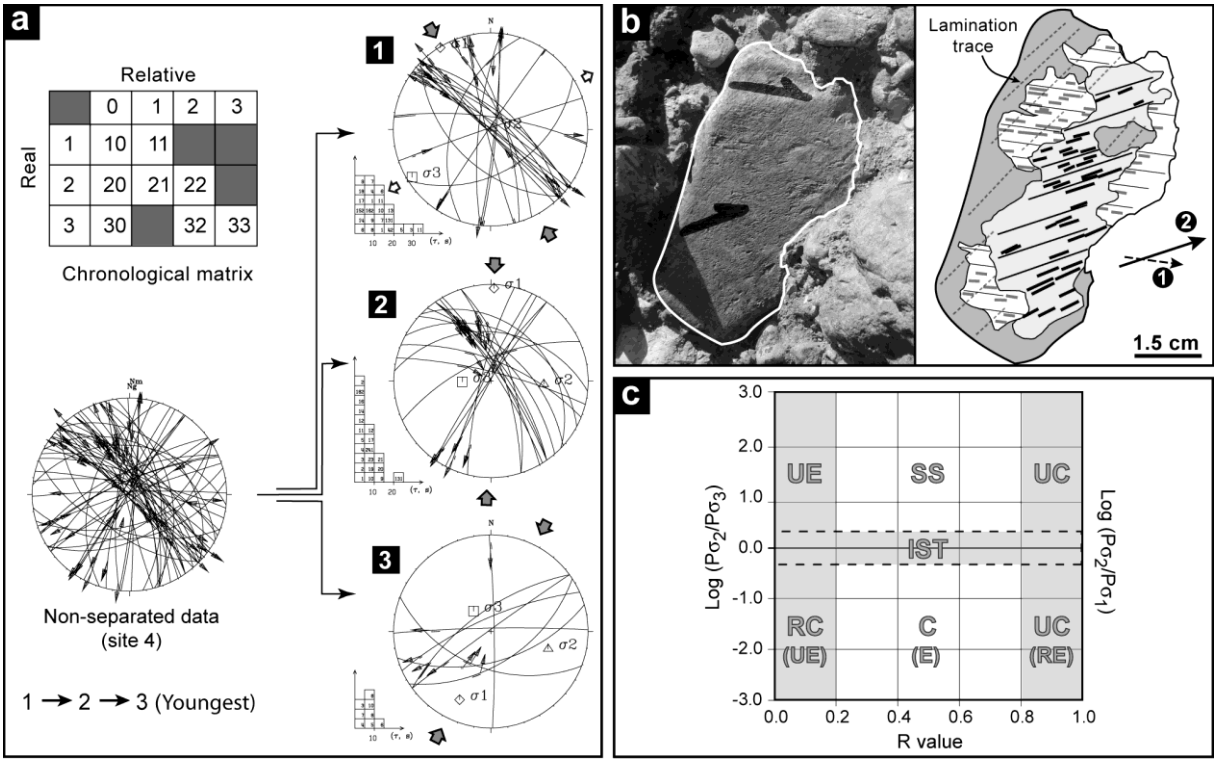


Figure 2. (a) A summary of the slip data separation strategy performed in this study. Upper left, the chronological matrix showing the relationships between relative slip chronologies observed in the field and the corresponding real chronologies used in the fault kinematic inversions (see text for more explanation). Lower-hemisphere stereograms represent an example of fault slip data separation; the left stereoplot is a non-separated data set, the right ones are the consequent separated data sets and corresponding deviatoric stress solutions: 1, paleostress; 2, intermediate stress; 3, modern stress states determined for site 4. Numbers refer to different slip generations. Fault planes and measured slip vectors (arrows on fault planes) are plotted. Large arrows outside stereograms represent the direction of minimum ($\sigma_3$, divergent, white arrows) and maximum ($\sigma_1$) horizontal stress axes. Histograms show distribution of deviation angles between the measured and calculated slip vectors (*e.g.*, *Bellier and Zoback*, 1995). (b) An example of crosscutting relationships between two distinct slip generations recorded on a pebble face within Quaternary conglomerates (site 25). (c) LP diagram illustrating strike-slip and compressional tectonic regimes in terms of individually determined deviatoric stress tensors. The horizontal axis presents the R values (ranging from 0 to 1), and the vertical axis is decadic logarithm of the $\sigma_2/\sigma_3$ plunge ratio (LP) for each individual solution. The corresponding end-members for a transtensional tectonic regime ($\sigma_2/\sigma_1$ plunge ratio) are presented in parentheses.

on the fault plane. Therefore, a distinct stress deviator ($\sigma_1$, $\sigma_2$, $\sigma_3$, and R) can only produce one slip direction on a given fault plane. In the field, often more than one generation of striae are detected on a fault plane and/or at the same measurement site. This may be due to (1) multiple slip within single event, (2) changes in slip directions due to changes in the fault strength or local boundary conditions, or (3) temporal changes in regional state of stress due to changes in boundary conditions at the scale of plate tectonics expressed by distinct tectonic regimes. In a homogeneous stress field determined at the regional scale, stress deviators affected by (1)

and (2) are represented as local heterogeneities that are easily distinguishable from the regional changes in the state of stress linked to (3). However, the separation of fault slip data from different tectonic regimes remains problematic in the utilization of fault kinematic inversion schemes (to characterize stress states) despite the efforts made for automatic data separation during the two last decades (*e.g.*, *Angelier*, 1984, 1990). Generally, the chronology of different stress states can be determined from the age of the rock formations affected by corresponding tectonic regimes. In our study, the fault kinematic data have been measured in Cretaceous to late Quaternary age deposits. Among the total thirty nine inspected outcrops (Figure 1) only eight sites were measured in Cretaceous formations. Those formations are cut by major faults that were produced or reactivated during post-Miocene tectonic events. The majority of the striated fault planes (thirty one sites) were measured from faults cross-cutting the Pliocene and Pleistocene deposits (Table 1). Such a measurement strategy eliminated the slip evidence of pre-Pliocene tectonic regimes in our data sets. In spite of this systematic geological selection of data, in almost all measured outcrops, we always observed two or sometimes three slip generations exhibited by clear crosscutting striations on fault planes (Figure 2). However, in NE Iran, the age of the Quaternary deposits is not well-constrained. In such a case, distinct datasets were separated using (1) direct evidence of relative chronology showing successive fault movements expressed by crosscutting relationships between different fault slip-vectors and/or fault planes, and (2) indirect evidence, which is the compatibility of fault movements with regional tectonic regimes deduced from well-constrained stress solutions, after a careful qualitative field study of geological structures.

Fault slip data population constituted by fault slips belonging to two different tectonic regimes can be manually separated into appropriate data sets. In our measurements, the observed relative chronologies were often expressed in two crosscutting striations while data sets were measured in the outcrops affected by two or three different tectonic regimes. This situation makes the real slip chronologies (the chronology of distinct tectonic regimes) different from the relative chronologies (*i.e.*, the chronology of slip vectors directly observed in the field). Such a situation needs a careful data separation process. In other words, data separations only based on the observed slip chronologies can lead to erroneous data sets with inconsistent chronologies, and consequently, deviatoric stress solutions without geological reliability. The conceptual graphical matrix presented in Figure 2 illustrates such complicated relationships between the real and corresponding relative chronologies that can be observed on a fault plane. For instance, in an outcrop affected by three tectonic regimes, a certain fault slip direction compatible with the last tectonic regime (real chronology 3) can appear as: (1) a

single slip direction on a fault plane with only one slip direction (*i.e.*, unclear chronology or 30 in Figure 2), (2) the second slip generation on a fault plane showing two different slip directions (32 in Figure 2) or (3) the third slip generation on a fault plane showing three different slip directions (33 in Figure 2). Considering this complexity, an intermediate stress tensor would result from the analysis of three categories of fault data: (1) a few fault planes on which three distinct slip directions were recorded showed clear crosscutting relationships, (2) fault planes striated by two slip directions and clear relative chronology that one of them is incompatible with either paleostress or modern stress solutions, and (3) fault planes with only one striation direction incompatible with the paleo-and modern-stress solutions (Figure 2). Altogether, it is a delicate job to calculate reliable stress tensors from the inversion of mixed populations of striated fault planes that may not belong to the same tectonic regime (see *Carey, 1979*; *Ritz and Taboada*, 1993). For this reason, the third group of fault planes was added to the solutions only if a stable stress tensor was achieved from the computation of the two first categories. A summary of the strategy we used for the separation of fault data is presented in Figure 2.

### 3.4. Evaluation of stress tensor qualities

An uncritical use of inversion methods, whatever the computation program used, can lead to stress tensors that are not representative for a geological reality (*e.g.*, *Carey-Gailhardis and Mercier*, 1992; *Ritz and Taboada*, 1993). These are usually poorly-constrained and/or revolution solutions (*Ritz and Taboada*, 1993), always, obtained when incompatible fault planes are taken into account for stress determination. The probability of obtaining anomalous revolution stress tensor solutions increases with the number of tectonic regimes observed in the field, and/or by incorporating data from different tectonic settings. More precisely, mixed populations of striated fault planes or focal mechanisms corresponding to different states of stress may apparently yield excellent solutions that are not geologically reliable (*Carey-Gailhardis and Vergely*, 1992).

However, the reliability of stress tensor solutions can be tested following a series of criteria (*e.g.*, *Etchecopar*, 1984; *Carey-Gailhardis and Mercier*, 1992; *Bellier and Zoback*, 1995): (1) the number and spatial dispersion of fault planes, (2) the value of the mean deviation angle between calculated shear stresses and measured striation directions as well as its standard deviation, and (3) the mechanical consistency of fault planes with the stress tensor solution (*e.g.*, *Ritz and Taboada*, 1993). Using these criteria, we evaluated quality of the stress

tensor computed at each individual site (Table 1). The standard solutions were classified into three distinct quality levels (A, B and C) representative for well-constrained, constrained, and poorly-constrained solutions, respectively. For the fault data populations comprised of less than four well-distributed fault directions, a fixed solution (*Bellier and Zoback*, 1995) was applied, in which the principal stress axes are fixed to lie in horizontal and vertical planes. In this fixed inversion one requires only two independent fault sets examining compatibility of fault planes with a homogeneous regional stress field or stress tensors deduced from nearby sites in the same tectonic context. The results were marked as CF quality to distinguish them from poorly-constrained standard solutions (Table 1). Both C and CF quality deviatoric stress tensors are only used for deducing the direction of principal stress axes, not used for R value interpretation.

### 3.5. R values analysis

The stress ratio, $R = (\sigma_2-\sigma_1)/(\sigma_3-\sigma_1)$, describes the relative stress magnitudes of the calculated mean deviatoric stress tensors. The significance of stress-ratio in interpreting inversion results is well understood (*e.g.*, *Ritz and Taboada*, 1993; *Bellier and Zoback*, 1995). Here, we present a simple graphical way that allows us to analyze regional tectonic regimes in terms of R values and corresponding stress regimes deduced from inversions of fault kinematics. To illustrate both strike-slip and compressional stress regimes versus corresponding R ratios, stress solutions were plotted on a diagram in which the horizontal axis presents the R values (ranging from 0 to 1), and the vertical axis is a decadic logarithm of the $\sigma_2/\sigma_3$ ($\sigma_2/\sigma_1$ for transtensional tectonic regimes) plunge ratio (LP) for each individual solution (Figure 2). Using the LP, one can plot $\sigma_2/\sigma_3$ plunge ratios between 0.01/89.9 and 89.9/0.01 along a short logarithmic-scale axis. Therefore, for a given stress solution, while the corresponding stress regime is plotted along the vertical axis from compressional (-3>LP>-0.3; vertical $\sigma_3$ axis) to strike-slip (0.3>LP>3; vertical $\sigma_2$ axis), the horizontal axis presents the R value of the solution. In this way, the proposed diagram allows to illustrate regional tectonic regimes in terms of individually determined deviatoric stress tensors (Figure 2). The line of LP = 0, parallel to the horizontal axis, represents unstable stress regimes characterized by oblique $\sigma_2$ and $\sigma_3$ axes with a plunge of 45°. For well-constrained deviatoric stress tensors computed from inversions of natural striated fault planes measured in the field, the minimum and intermediate stress axes ($\sigma_3$ and $\sigma_2$, respectively) show a plunge fluctuation between 0° and 30° with respect to the quasi-vertical or quasi-horizontal positions (*e.g.*, *Angelier et al.*,

1981; *Carey-Gailhardis and Mercier*, 1992; *Bellier et al.*, 1997). Out of this fluctuation range (plunge values of 45°±15° for $\sigma_3$ and $\sigma_2$ axes) are considered as the instability domain for computed stress regimes (Figure 2) that may be induced by tilted fault planes as well as local rotations around vertical axes, and/or mixed data sets from different stress states. For a transpressional tectonic regime, the corners of the diagram illustrate four distinct domains of revolution stress tensors that are radial (RC) and uniaxial compression (UC) end-members for compressional stress regimes, as well as uniaxial compression and uniaxial extension (UE) end-members for strike-slip regimes. The corresponding end-members for a transtensional tectonic regime are also presented in Figure 2.

## 4. Fault kinematics and stress regimes

Following the methodology explained in section 3, the separation of fault kinematics data reveals the existence of three distinct slip generations which are representative for three successive but discontinuous tectonic regimes (section 5). Inversions of the separated data sets allow us to distinguish three episodic changes in the Plio-Quaternary stress state in NE Iran. According to the clear chronology of tectonic regimes corresponding to these changes, the determined stress states are classified into paleostress state, intermediate and modern stress states having well-known relative chronologies. The paleostress state is the oldest stress state distinguished since 5 Ma. The pre-Pliocene kinematics history and especially transition from the tectonic regime responsible for Miocene folding to the Plio-Quaternary paleostress state remains unclear.

### 4.1. Modern state of stress

The modern sate of stress was deduced from analyses of the youngest fault slips observed at individual inspected sites where the majority of fault slip data was measured in Plio-Quaternary conglomerates. The computed deviatoric stress tensors, which belong to the modern stress state of the Kopeh Dagh and Allah Dagh-Binalud deformation domains, reveal a homogenous stress field (Figures 3 and 4, Table 1). The direction of both horizontal stress axes ($\sigma_{hmin}$ and $\sigma_{hmax}$) of modern stress solutions are presented in Figure 3a. The modern stress field is characterized by N030±15°E trending horizontal maximum stress axes ($\sigma_1$) for almost all the studied sites. However, five out of thirty two sites (21, 22, 23, 17, and 26) show perturbed direction of $\sigma_1$ axes with respect to the regional pattern (Figures 3 and 4). The last three are poorly-constrained stress tensors or show slight variation in the $\sigma_1$ direction. Only

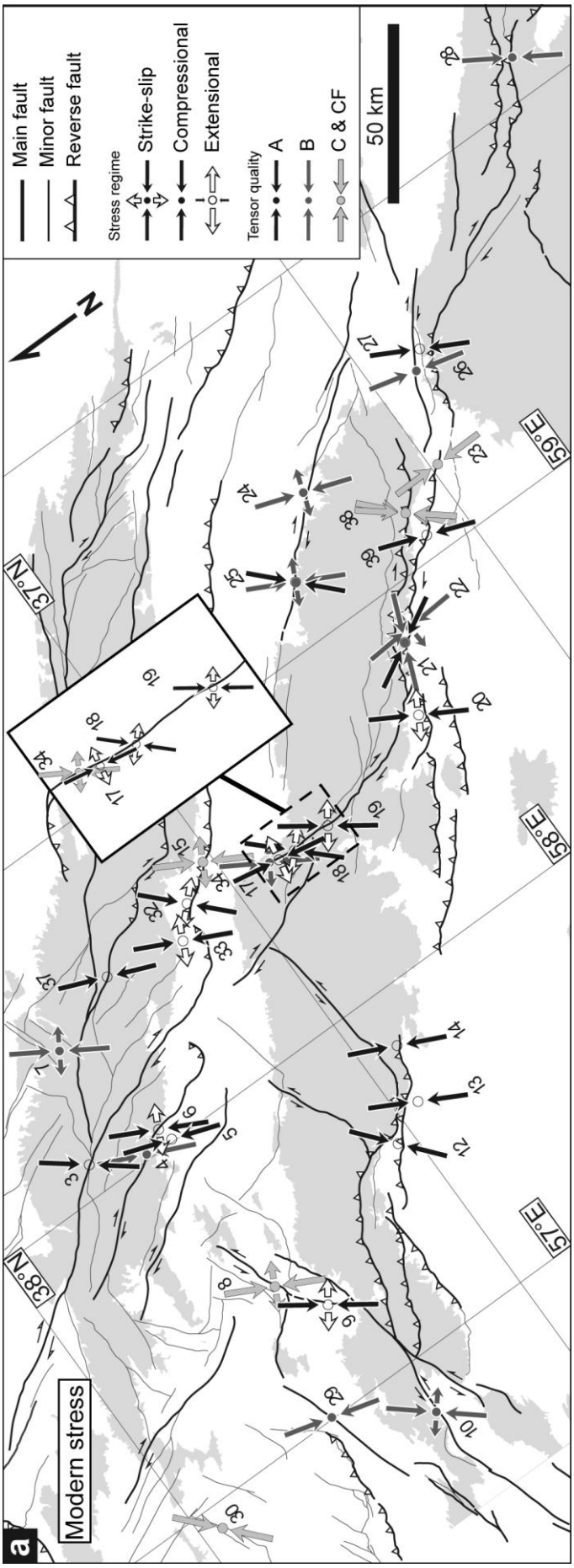


Figure 3. Direction of $\sigma_1$ (maximum horizontal stress) axis for the strike-slip, compressional, and extensional stress regimes deduced from the fault kinematics inversions given in Table 1 and Figures 4, 5, 6. (a) Modern state of stress. (b) Intermediate state of stress. (c) Paleostress state. Shaded regions are topographic reliefs based on SRTM digital topographic data.

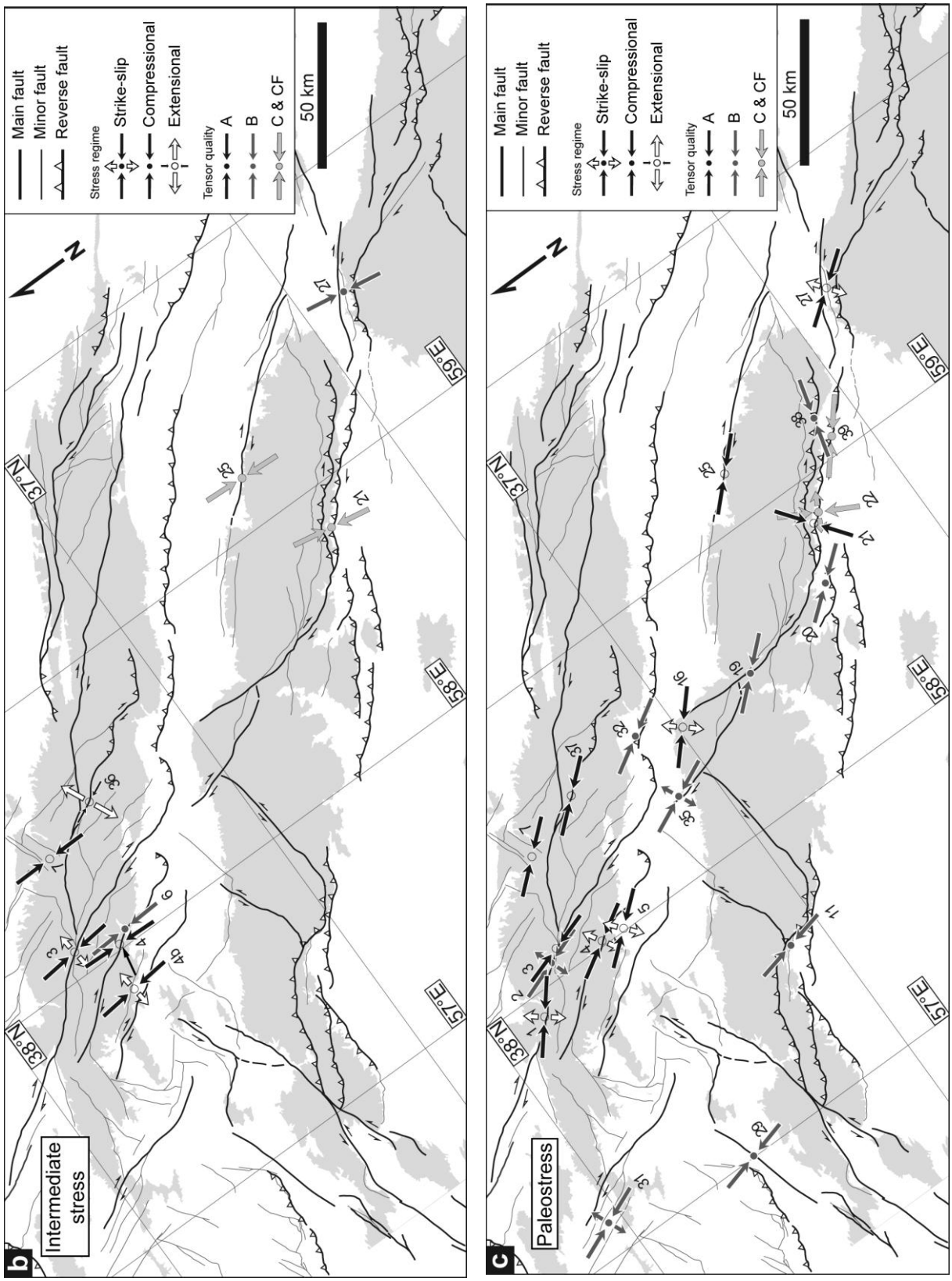


Figure 3. Continued

the stress tensors from sites 21 and 22 are obviously different from the regional modern stress state pattern. Those two sites are situated at the junction of the N trending Chakaneh Fault system with the NW trending Neyshabur Fault system where pure strike-slip motions along the Chakaneh Fault system is transferred to the Neyshabur Fault system (*Shabanian et al.*, 2009b) leading to different kinematics (oblique-reverse faulting) (Figure 3). Such a structural setting may cause significant perturbations in both the direction of stress axes and stress ratio by producing local stress state at strike-slip fault terminations to adjust incompatibility of the fault movements (*e.g.*, *Homberg et al.*, 1997).

Two distinct stress regimes have been distinguished throughout the region (1) strike-slip faulting regimes presented by the sites along major strike-slip faults of the Kopeh Dagh and Meshkan transfer zone, as well as the Mashhad and Showqan faults, and (2) compressional stress regime (reverse faulting) along NW trending reverse faults such as the Esfarayen and Neyshabur faults (Figure 3). The two compressional tensors (3, 4) along the Baghan and Quchan strike-slip faults are clearly controlled by local changes in the fault geometries where the fault traces bent to NW-striking restraining bends. The clear N trending alignment of the sites showing strike-slip regimes between the Kopeh Dagh and Binalud mountains confirms that a significant part of strike-slip deformation within the Kopeh Dagh is distributed southward through the Meshkan transfer zone (*Shabanian et al.*, 2009b). Moreover, the Showqan and the Mashhad faults have to be considered as left-lateral and right-lateral strike-slip faults, respectively.

### 4.2. Intermediate state of stress

The fault kinematics inversions also reveal the remnants of an intermediate state of stress, which is presented by eight regionally-distributed deviatoric stress tensors (Figures 3 and 5, Table 1). All solutions show a regional N180±10°E trending mean $\sigma_1$ axis. Except sites 3 and 4b along the Quchan and Baghan faults, the other stress tensors indicate compressional stress regimes. One stress solution is an extensional (normal faulting) stress regime characterized by a NE trending minimum stress axis ($\sigma_3$). The deduced extensional direction results from a local effect of which significance and relationship with the regionally consistent stress regime are not understood. Considering their structural setting, they cannot be described as normal faults that commonly form above growing anticlines due to flexure or in releasing bends of strike slip faults.

We attribute them to other local effects and refrain from further interpretations. The good quality of the computed stress tensors (Table 1) and the homogenous pattern of the

Table 1. The Results of fault kinematics inversions characterizing the Plio-Quaternary stress regimes in NE Iran.

| Site | Longitude | Latitude | Paleostress | | | | | | | Modern stress | | | | | | | Intermediate stress | | | | | | | Lithology | Formation age |
|---|---|---|---|---|---|---|---|---|---|---|---|---|---|---|---|---|---|---|---|---|---|---|---|---|---|
| | | | Stress axis (trend/plunge) | | | R | N | Q | Rm | Stress axis (trend/plunge) | | | R | N | Q | Rm | Stress axis (trend/plunge) | | | R | N | Q | Rm | | |
| | (°E) | (°N) | $\sigma_1$ | $\sigma_2$ | $\sigma_3$ | | | | | $\sigma_1$ | $\sigma_2$ | $\sigma_3$ | | | | | $\sigma_1$ | $\sigma_2$ | $\sigma_3$ | | | | | | |
| 1 | 57,910 | 37,837 | 129/06 | 012/76 | 221/12 | 0,748 | 19 | A | S | _ | _ | _ | _ | _ | _ | _ | _ | _ | _ | _ | _ | _ | _ | Limestone | Cretaceous |
| 2 | 58,062 | 37,722 | 160/07 | 281/77 | 068/11 | 0,834 | 7 | B | S | _ | _ | _ | _ | _ | _ | _ | _ | _ | _ | _ | _ | _ | _ | Conglomerate | Quaternary |
| 3 | 58,095 | 37,686 | 162/04 | 255/36 | 066/54 | 0,887 | 17 | A | C | 218/04 | 309/05 | 092/84 | 0,852 | 15 | A | C | 174/16 | 010/73 | 265/05 | 0,389 | 10 | A | S | Conglomerate | Quaternary |
| 4 | 58,020 | 37,562 | 329/01 | 084/87 | 239/03 | 0,846 | 22 | A | S | 204/14 | 107/27 | 320/59 | 0,707 | 7 | B | C | 002/02 | 093/33 | 268/57 | 0,785 | 21 | A | C | Limestone | Cretaceous |
| 4B | 58,020 | 37,562 | _ | _ | _ | _ | _ | _ | _ | _ | _ | _ | _ | _ | _ | _ | 175/21 | 349/69 | 084/02 | 0,520 | 15 | B | S | Limestone | Cretaceous |
| 5 | 58,007 | 37,487 | 140/09 | 245/60 | 045/29 | 0,816 | 29 | A | S | 019/04 | 109/04 | 240/84 | 0,657 | 26 | A | C | _ | _ | _ | _ | _ | _ | _ | Conglomerate | Neogene |
| 6 | 58,059 | 37,499 | _ | _ | _ | _ | _ | _ | _ | 207/03 | 304/68 | 116/22 | 0,833 | 23 | A | S | 177/10 | 267/01 | 003/80 | 0,494 | 8 | B | C | Conglomerate | Quaternary |
| 7 | 58,440 | 37,584 | 319/06 | 228/06 | 094/82 | 0,877 | 9 | A | C | 032/13 | 169/72 | 300/12 | 0,830 | 9 | B | S | 179/04 | 089/05 | 307/83 | 0,822 | 12 | A | C | Conglomerate | Quaternary |
| 8 | 57,442 | 37,495 | _ | _ | _ | _ | _ | _ | _ | 207/00 | 117/00 | 302/90 | 0,740 | 4 | CF | C | _ | _ | _ | _ | _ | _ | _ | Limestone | Cretaceous |
| 9 | 57,301 | 37,414 | _ | _ | _ | _ | _ | _ | _ | 035/12 | 158/69 | 301/17 | 0,458 | 26 | A | S | _ | _ | _ | _ | _ | _ | _ | Conglomerate | Quaternary |
| 10 | 56,826 | 37,355 | _ | _ | _ | _ | _ | _ | _ | 040/06 | 146/68 | 307/21 | 0,570 | 12 | B | S | _ | _ | _ | _ | _ | _ | _ | Conglomerate | Quaternary |
| 11 | 57,576 | 37,108 | 167/02 | 258/14 | 069/76 | 0,213 | 10 | B | C | _ | _ | _ | _ | _ | _ | _ | _ | _ | _ | _ | _ | _ | _ | Claystone | Neogene |
| 12 | 57,578 | 37,042 | _ | _ | _ | _ | _ | _ | _ | 050/04 | 143/36 | 314/54 | 0,735 | 16 | A | C | _ | _ | _ | _ | _ | _ | _ | Conglomerate | Pl-Q |
| 13 | 57,651 | 36,942 | _ | _ | _ | _ | _ | _ | _ | 208/09 | 299/08 | 071/78 | 0,990 | 17 | A | C | _ | _ | _ | _ | _ | _ | _ | Conglomerate | Quaternary |
| 14 | 57,830 | 36,902 | _ | _ | _ | _ | _ | _ | _ | 025/02 | 294/22 | 120/68 | 0,872 | 19 | A | C | _ | _ | _ | _ | _ | _ | _ | Conglomerate | Quaternary |
| 15 | 58,654 | 37,024 | _ | _ | _ | _ | _ | _ | _ | 209/00 | 118/90 | 299/00 | 0,939 | 6 | CF | S | _ | _ | _ | _ | _ | _ | _ | Micro-conglo. | Quaternary |
| 16 | 58,500 | 36,986 | 132//13 | 275/73 | 040/10 | 0,785 | 12 | A | S | _ | _ | _ | _ | _ | _ | _ | _ | _ | _ | _ | _ | _ | _ | Conglomerate | Neogene |
| 17 | 58,518 | 36,869 | _ | _ | _ | _ | _ | _ | _ | 010/17 | 245/63 | 107/21 | 0,859 | 18 | A | S | _ | _ | _ | _ | _ | _ | _ | Conglomerate | Quaternary |
| 18 | 58,513 | 36,824 | _ | _ | _ | _ | _ | _ | _ | 044/02 | 141/71 | 314/18 | 0,879 | 14 | A | S | _ | _ | _ | _ | _ | _ | _ | Limestone | Cretaceous |
| 19 | 58,515 | 36,724 | 318/15 | 060/39 | 212/47 | 0,881 | 6 | B | T | 035/11 | 187/77 | 303/06 | 0,457 | 22 | A | S | _ | _ | _ | _ | _ | _ | _ | Limestone | Cretaceous |
| 20 | 58,627 | 36,383 | 141/10 | 048/17 | 261/70 | 0,158 | 5 | B | C | 210/01 | 101/87 | 300/03 | 0,708 | 23 | A | S | _ | _ | _ | _ | _ | _ | _ | Conglomerate | Pl-Q |
| 21 | 58,837 | 36,305 | 053/11 | 144/06 | 260/78 | 0,607 | 19 | A | C | 151/12 | 052/36 | 257/51 | 0,858 | 23 | A | C | 190/05 | 282/16 | 083/73 | 0,468 | 6 | C | C | Conglomerate | Quaternary |
| 21A | 58,837 | 36,305 | _ | _ | _ | _ | _ | _ | _ | 292/18 | 200/06 | 091/71 | 0,679 | 6 | B | C | _ | _ | _ | _ | _ | _ | _ | Conglomerate | Quaternary |
| 22 | 58,863 | 36,272 | 208/00 | 113/90 | 298/00 | 0,807 | 4 | CF | S | 176/11 | 048/73 | 268/13 | 0,761 | 12 | B | S | _ | _ | _ | _ | _ | _ | _ | Crush zone | Quaternary |
| 23 | 59,230 | 35,983 | _ | _ | _ | _ | _ | _ | _ | 179/00 | 089/00 | 278/90 | 0,849 | 4 | CF | C | _ | _ | _ | _ | _ | _ | _ | Conglomerate | Quaternary |
| 24 | 59,404 | 36,289 | _ | _ | _ | _ | _ | _ | _ | 019/09 | 152/78 | 288/09 | 0,447 | 10 | B | S | _ | _ | _ | _ | _ | _ | _ | Metamorphic | Triassic |
| 25 | 59,194 | 36,437 | 135/02 | 227/37 | 043/53 | 0,733 | 7 | A | C | 207/13 | 330/66 | 113/19 | 0,940 | 9 | B | S | 183/03 | 092/03 | 325/86 | 0,797 | 6 | C | C | Conglomerate | Quaternary |
| 25A | 59,194 | 36,437 | _ | _ | _ | _ | _ | _ | _ | 046/02 | 137/19 | 309/71 | 0,314 | 7 | A | C | _ | _ | _ | _ | _ | _ | _ | Conglomerate | Quaternary |
| 26 | 59,505 | 35,890 | _ | _ | _ | _ | _ | _ | _ | 184/06 | 093/13 | 296/75 | 0,668 | 10 | B | C | _ | _ | _ | _ | _ | _ | _ | Conglomerate | Quaternary |
| 27 | 59,542 | 35,857 | 143/04 | 033/79 | 233/10 | 0,952 | 19 | A | S | 028/12 | 121/12 | 255/72 | 0,858 | 12 | A | C | 189/23 | 092/18 | 327/61 | 0,722 | 5 | B | C | Claystone | Neogene |
| 28 | 60,124 | 35,248 | _ | _ | _ | _ | _ | _ | _ | 033/08 | 297/37 | 132/52 | 0,703 | 5 | B | C | _ | _ | _ | _ | _ | _ | _ | Conglomerate | Quaternary |
| 29 | 57,006 | 37,571 | 165/05 | 257/25 | 064/64 | 0,429 | 13 | B | C | 015/02 | 106/21 | 279/69 | 0,533 | 18 | B | C | _ | _ | _ | _ | _ | _ | _ | Conglomerate | Quaternary |
| 30 | 56,926 | 37,947 | _ | _ | _ | _ | _ | _ | _ | 048/00 | 138/00 | 317/90 | 0,519 | 6 | CF | C | _ | _ | _ | _ | _ | _ | _ | Limestone | Cretaceous |
| 31 | 57,124 | 38,044 | 337/02 | 237/78 | 068/11 | 0,868 | 7 | B | S | _ | _ | _ | _ | _ | _ | _ | _ | _ | _ | _ | _ | _ | _ | Sandstone | Cretaceous |
| 32 | 58,576 | 37,115 | 329/11 | 066/34 | 223/54 | 0,557 | 6 | B | C | 046/06 | 299/70 | 138/19 | 0,633 | 18 | A | S | _ | _ | _ | _ | _ | _ | _ | Conglomerate | Quaternary |
| 33 | 58,490 | 37,178 | _ | _ | _ | _ | _ | _ | _ | 017/13 | 150/72 | 284/13 | 0,310 | 18 | A | S | _ | _ | _ | _ | _ | _ | _ | Conglomerate | Quaternary |
| 34 | 58,530 | 36,892 | _ | _ | _ | _ | _ | _ | _ | 031/02 | 292/76 | 121/13 | 0,821 | 9 | B | S | _ | _ | _ | _ | _ | _ | _ | Tuff | Pl-Q |
| 35 | 58,293 | 37,118 | 339/05 | 224/78 | 070/11 | 0,830 | 6 | B | S | _ | _ | _ | _ | _ | _ | _ | _ | _ | _ | _ | _ | _ | _ | Conglomerate | Pl-Q |
| 36 | 58,528 | 37,385 | _ | _ | _ | _ | _ | _ | _ | _ | _ | _ | _ | _ | _ | _ | N203/68 | N335/15 | N069/15 | 0,891 | 12 | A | E | Limestone | Cretaceous |
| 37 | 58,538 | 37,380 | 319/13 | 054/22 | 200/64 | 0,727 | 15 | A | C | 022/14 | 116/14 | 251/70 | 0,882 | 27 | A | C | _ | _ | _ | _ | _ | _ | _ | Limestone | Cretaceous |
| 38 | 59,165 | 36,117 | 105/06 | 014/06 | 240/80 | 0,263 | 9 | B | C | 047/07 | 139/14 | 291/75 | 0,129 | 9 | C | C | _ | _ | _ | _ | _ | _ | _ | Conglomerate | Pliocene |
| 38* | 59,165 | 36,117 | _ | _ | _ | _ | _ | _ | _ | 223/00 | 133/00 | 314/90 | 0.640 | 9 | CF | C | _ | _ | _ | _ | _ | _ | _ | Conglomerate | Pliocene |
| 39 | 59,070 | 36,106 | 130/03 | 040/10 | 239/78 | 0,929 | 5 | C | C | 020/00 | 110/24 | 290/66 | 0,845 | 10 | A | C | _ | _ | _ | _ | _ | _ | _ | Conglomerate | Quaternary |

intermediate state of stress throughout the Kopeh Dagh and Allah Dagh-Binalud deformation domains, suggests that this state of stress is representative for an intermediate tectonic regime between the paleostress and modern stress ones.

### 4.3. Paleostress state

To determine the paleostress state in NE Iran, the inversion analyses are individually performed for the fault populations including the oldest fault kinematics and other compatible fault planes measured at the same sites (Figures 3 and 6, Table 1). The computed paleostress field shows a regional pattern of N140±10°E trending horizontal compression ($\sigma_1$). This is significantly homogenous in the entire region including the Kopeh Dagh, Meshkan transfer zone, and the Allah Dagh-Binalud deformation domains (Figure 3). Two stress tensors calculated from data of sites 21 and 22 show perturbed direction of $\sigma_1$ axis with respect to the regional trend (Figures 3 and 6). These anomalous solutions correspond to the sites that are characterized by the different direction of modern $\sigma_1$ axis with respect to the regional trend (section 4.1), confirming that the local state of stress at sites 21 and 22 is controlled by a particular structural setting at the junction of the Chakaneh and Neyshabur Fault systems (Figure 3). There is evidence for both compressional and strike-slip stress regimes. Most of the strike-slip regimes are observed along the major strike-slip faults of the Kopeh Dagh, while the compressional stress regimes are distributed throughout the entire region.

## 5. Evidence for slip generation chronologies from the fault zone observations

Late Cenozoic tectonics in northeast Iran are characterized by reverse, oblique-slip, and strike-slip faulting that reactivated inherited Mesozoic structures and produced new faults. Inversions of fault slip data collected along both major and minor fault zones indicate three Plio-Quaternary states of stress keeping in mind that the paleostress state is different from the pre-Pliocene tectonic regimes responsible for the emplacement of NW trending parallel fold

Table 1. The used inversion method (*e.g.*, *Carey*, 1979) assumes that the slip represented by the striation occurs in the direction of the resolved shear. Deviatoric principal stress axes: $\sigma_1$, $\sigma_2$, $\sigma_3$, are the compressional, intermediate and extensional deviatoric axes, respectively. $R = (\sigma_2 - \sigma_1) / (\sigma_3 - \sigma_1)$, is the stress ratio of the deviatoric stress tensor, a linear quantity describing relative stress magnitudes. Site numbers refer to Figures 1 and 3-6. *N*, number of fault slip pairs considered for stress calculation; Rm, stress regime: C, compressional; E, extensional; S, strike-slip; Q, quality: A, well-constrained; B, constrained; C, poorly-constrained solutions. For the fault data populations comprised of less than four well-distributed fault directions, a "fixed" solution (*Bellier and Zoback*, 1995) was applied, in which the principal stress axes are fixed to lie in horizontal and vertical planes; the results were marked as "CF" quality. The site numbers marked by "A" or "B" indicate additional deviatoric stress tensors obtained at those sites. For site 38, two modern stress solutions (Fixed and standard) are presented due to the restricting effects of fault planes nearly parallel to the $\sigma_1$ axis, on the deviatoric stress tensor determined by the standard solution. All angles are in degree.

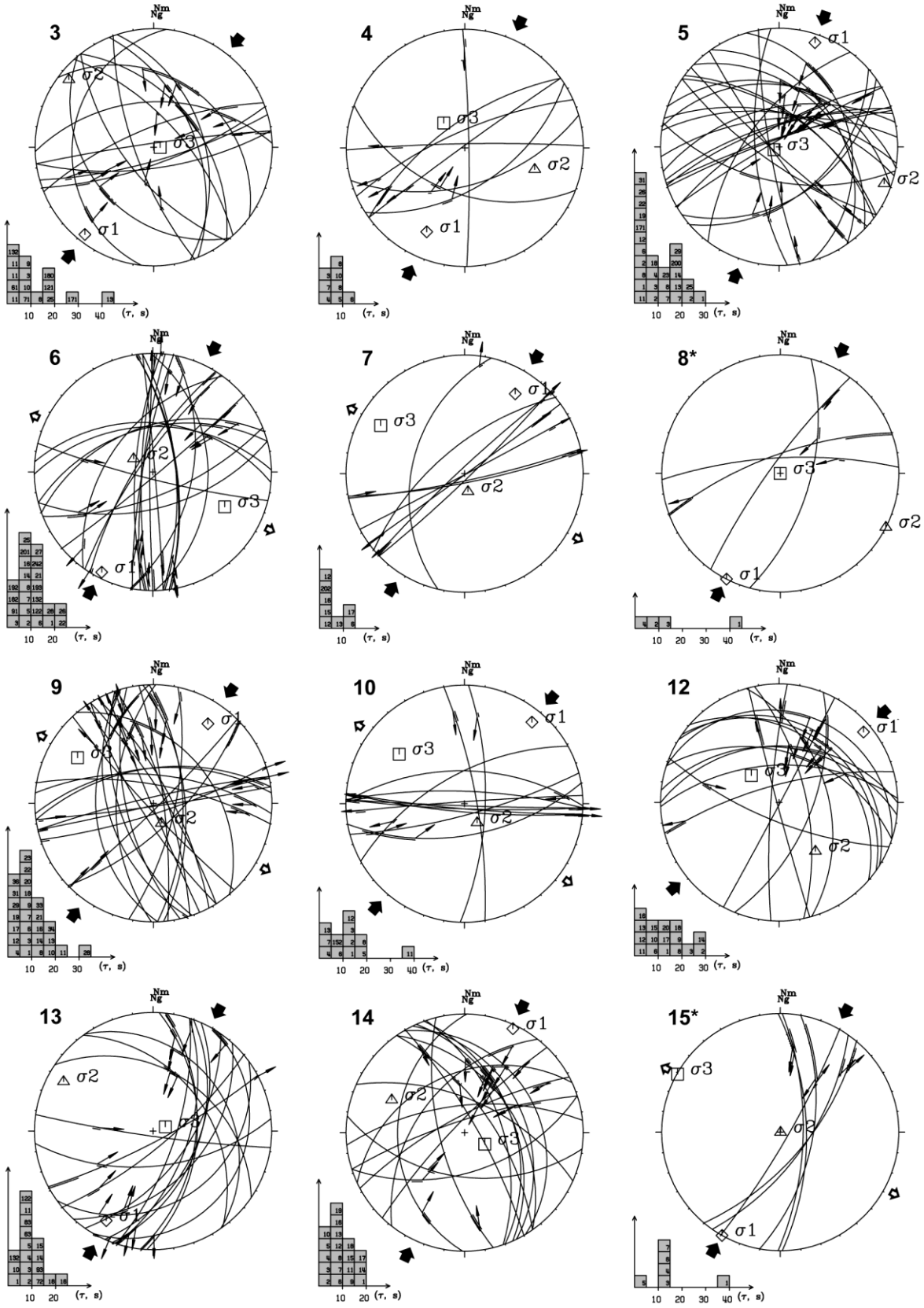


Figure 4. Lower hemisphere stereograms of fault slip data together with the inversion results of the modern state of stress presented in Table 1. Numbers refer to sites marked in Figures 1 and 3, as well as in Table 1. The stereograms indicated by asterisk are the "fixed" solutions (*Bellier and Zoback*, 1995) for fault data populations comprised of less than four well-distributed fault directions. See the caption of Figure 2 for stereoplot descriptions.

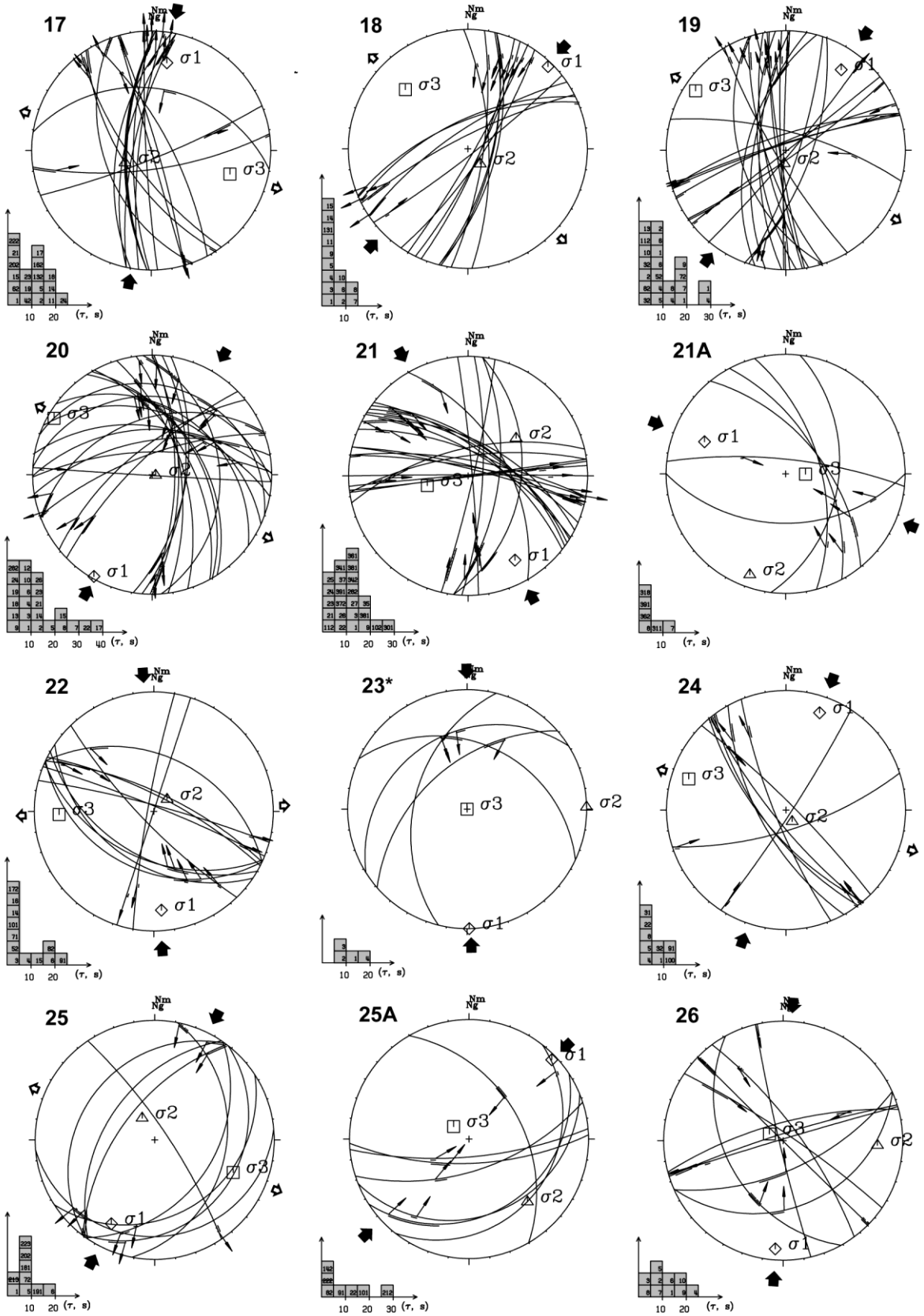


Figure 4. Continued

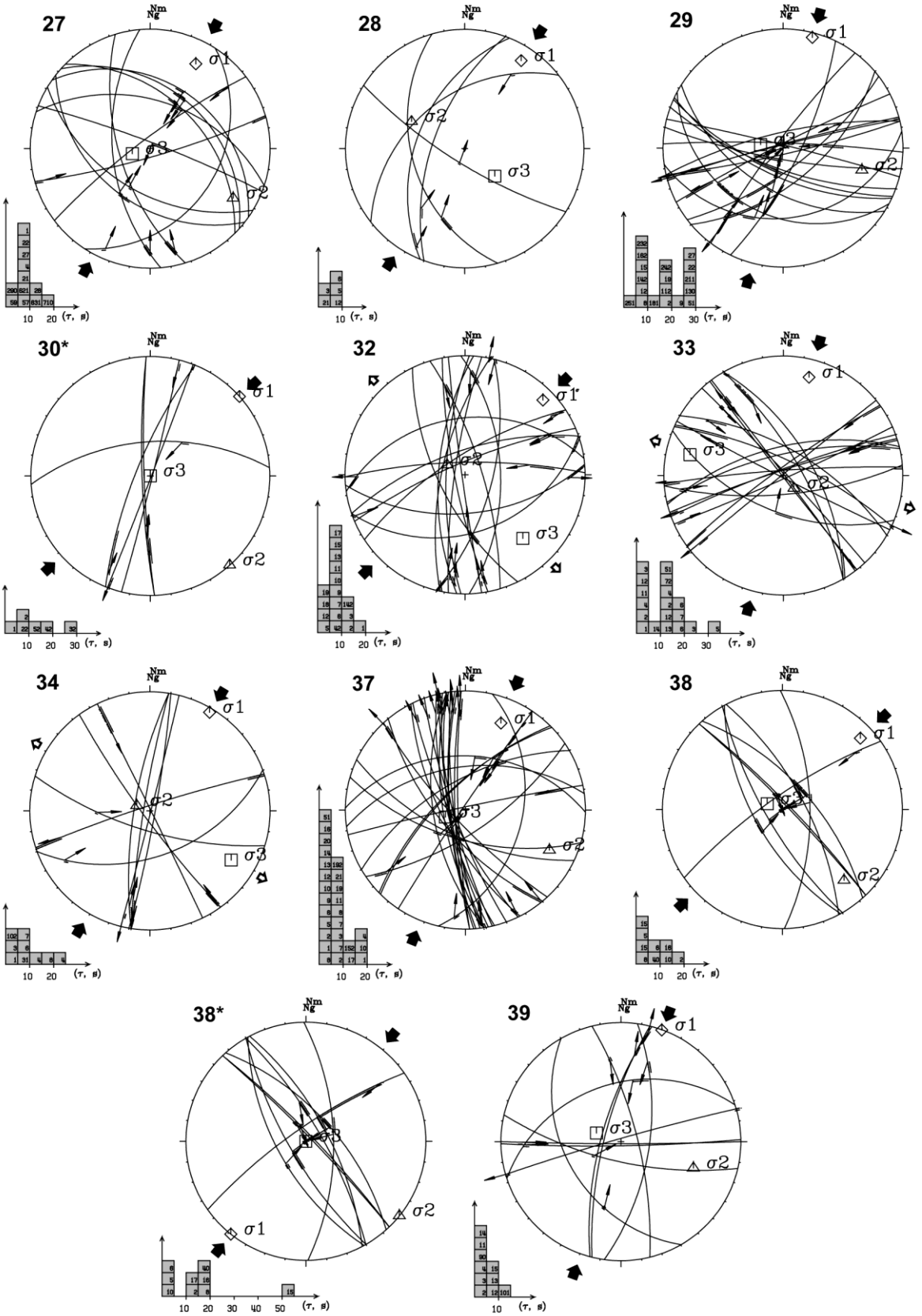


Figure 4. Continued

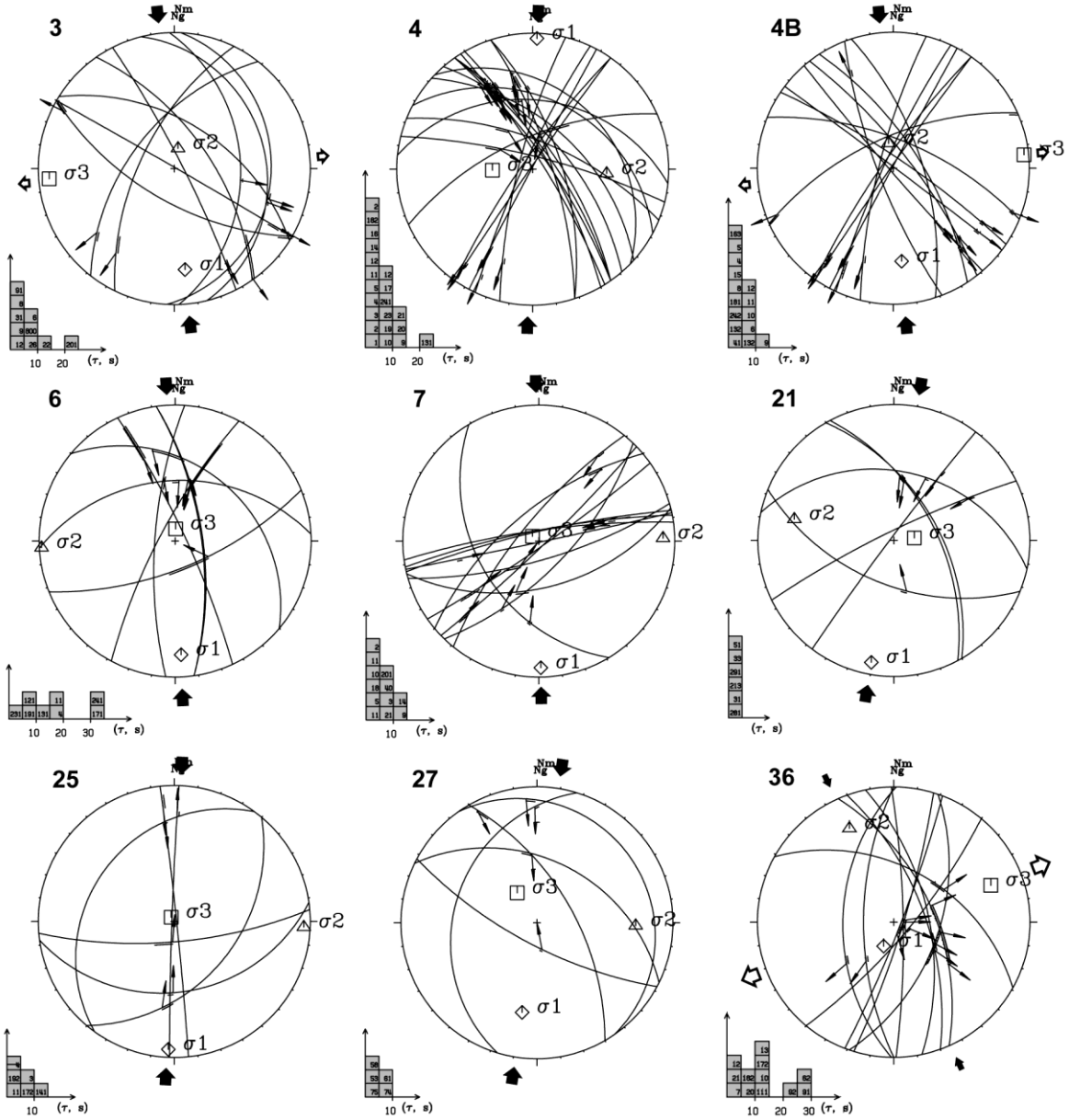


Figure 5. Lower hemisphere stereograms of fault slip data together with the inversion results of the intermediate stress state presented in Table 1. Other descriptions like Figure 4.

and thrust structures. The homogeneity of the inversion results obtained from almost all the inspected sites indicates that the stress states we determined are regionally significant in northeast Iran (Figures 3, 4, 5, 6, Table 1). There are only few sites where fault kinematics related to the intermediate state of stress (N-S compression) has been observed. However, those sites are distributed throughout the region indicating a certain degree of regional significance. In this section we document structural and geomorphic evidences from different investigated deformation domains (*i.e.*, Kopeh Dagh, Binalud, and Meshkan transfer zone) demonstrating the geological reliability of the distinct computed states of stress and changes in the Plio-Quaternary tectonic regimes.

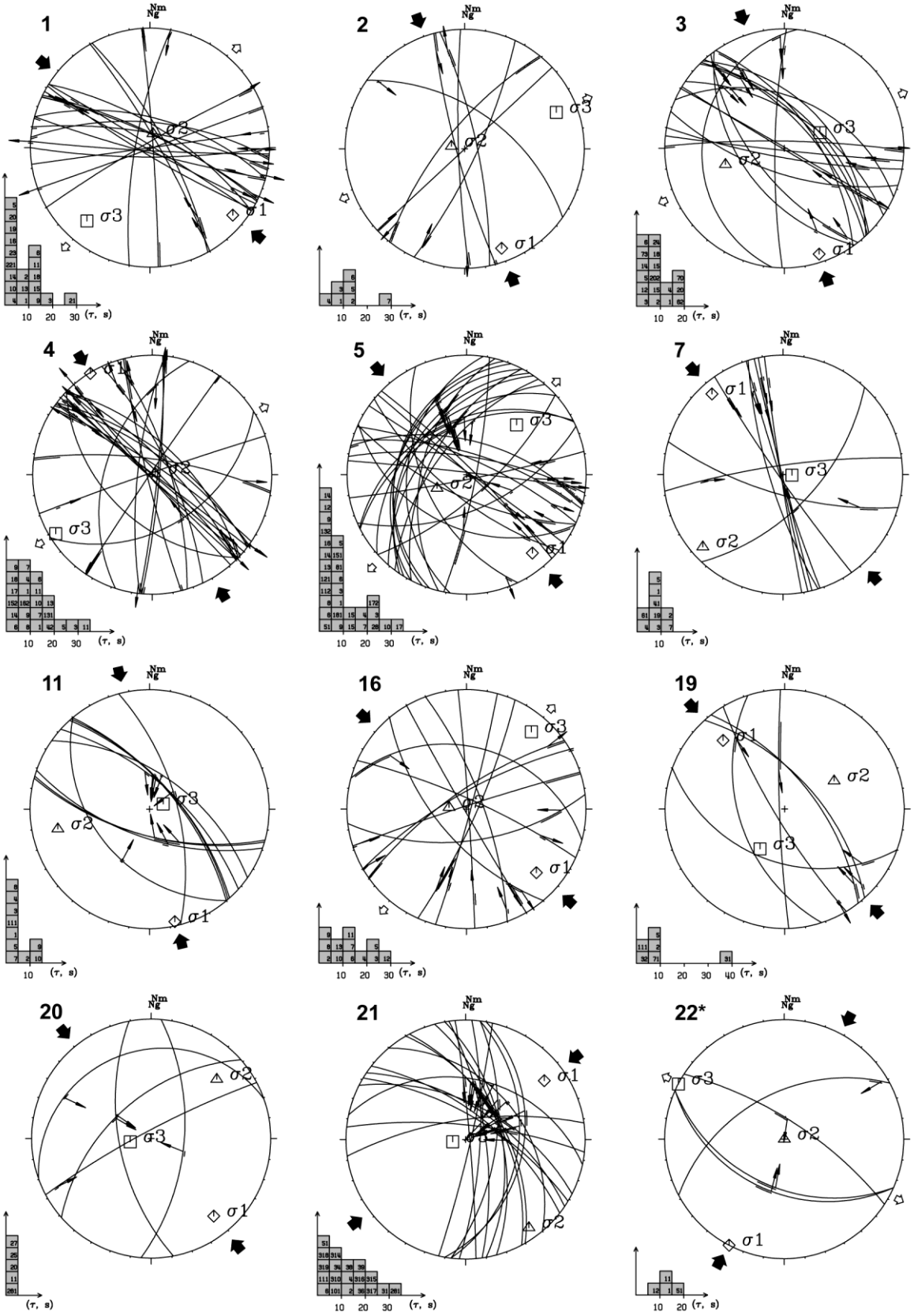


Figure 6. Lower hemisphere stereograms of fault slip data together with the inversion results of the paleostress state presented in Table 1. Other descriptions like Figure 4.

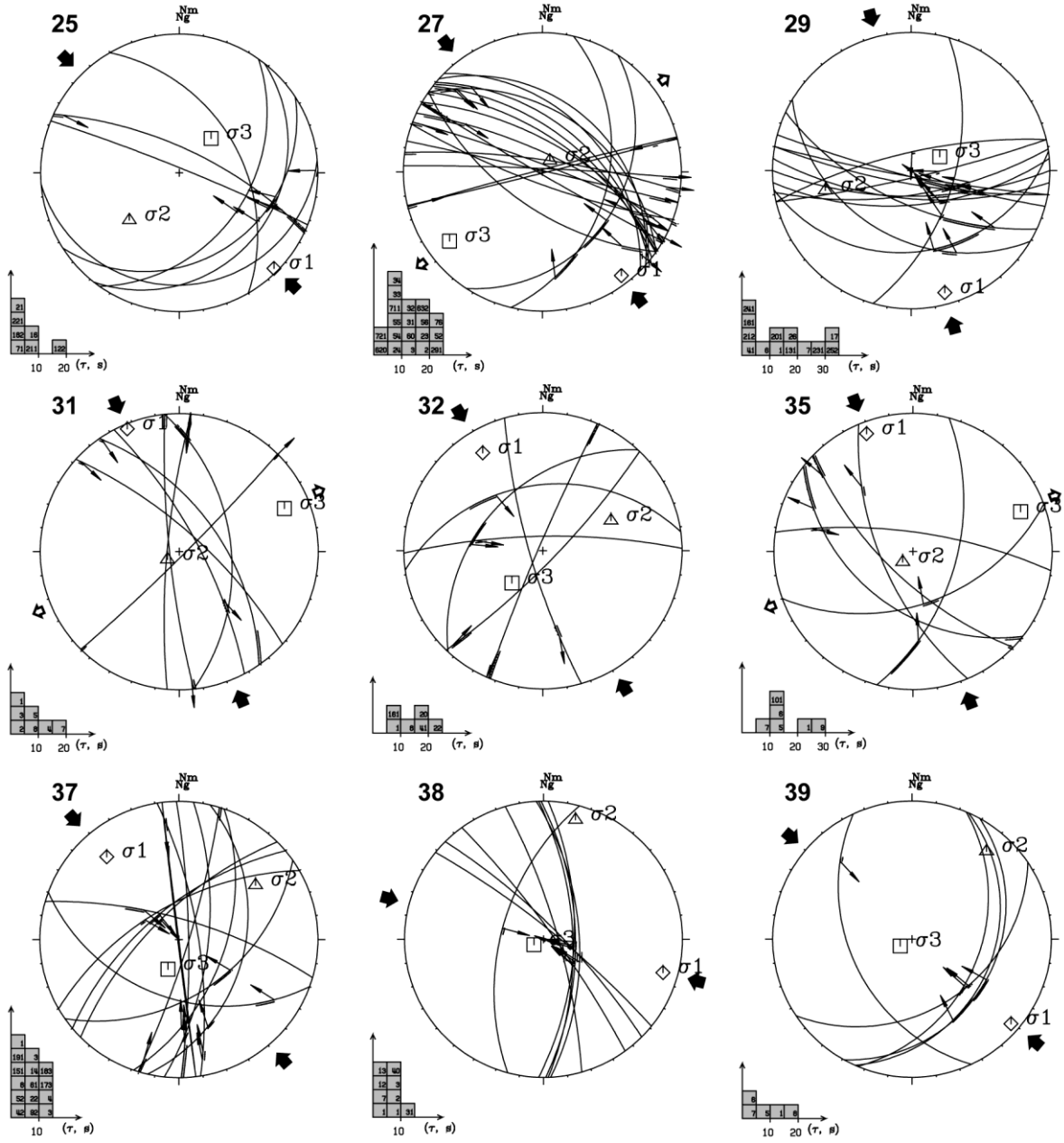


Figure 6. Continued

## 5.1. Structural evidence for the changes in the Plio-Quaternary states of stress

### 5.1.1. Central Kopeh Dagh

Clear geological expressions of both the modern and paleostress states are observed at site 37 (Figure 1) in the central Kopeh Dagh (Figure 7). In this area, an old NW dipping pure reverse fault has been reactivated as an oblique-slip left-lateral fault. This change of mechanism is clearly indicated by crosscutting striations which show a difference in rake angle of 60°. The reverse faulting slip episode was overprinted by a younger left-lateral strike-slip faulting. The oldest (reverse) slip was recorded geologically in parallel rough

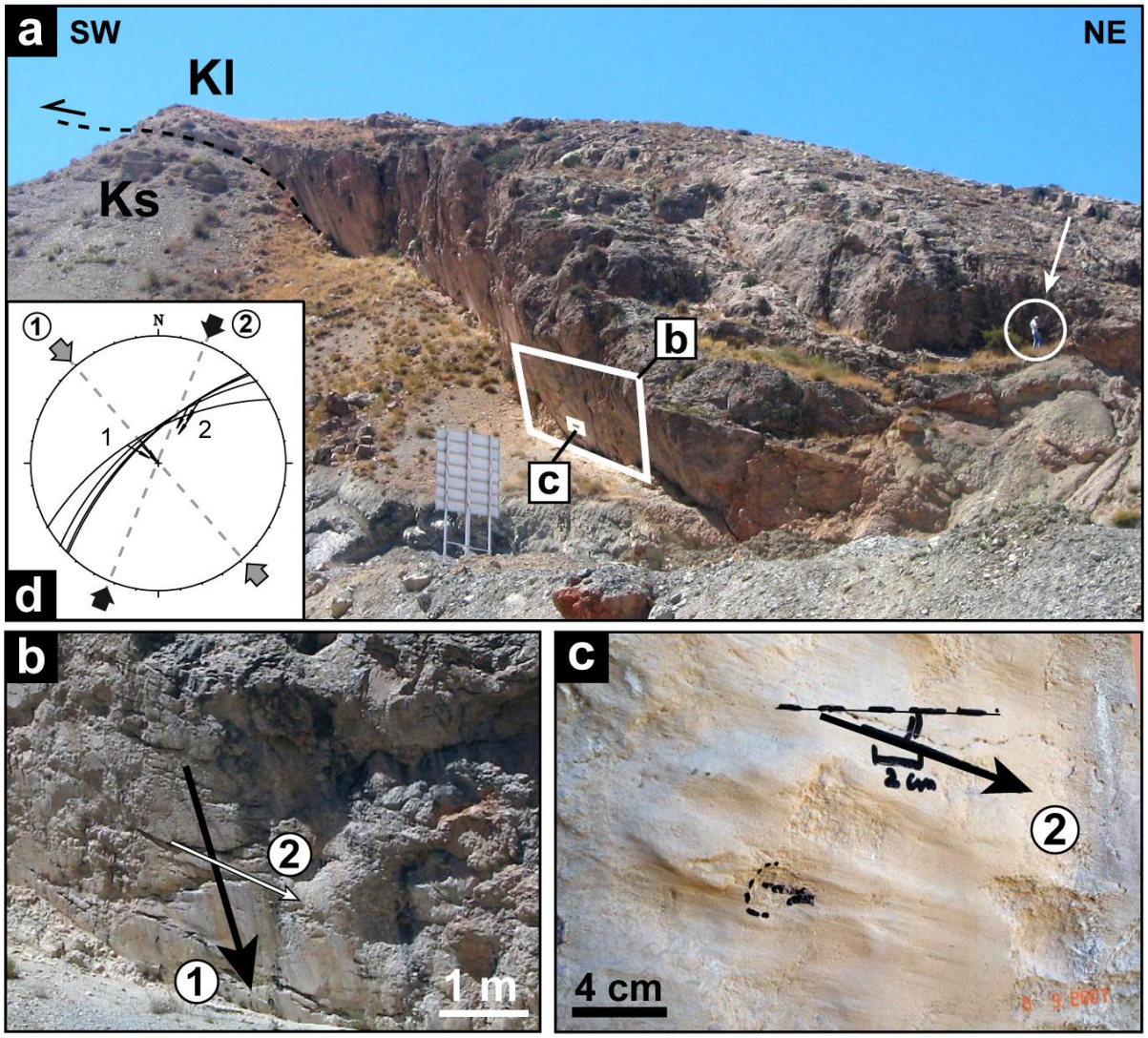


Figure 7. Fault-scale geological expression of the paleostress and modern stress states in the Central Kopeh Dagh. (a) A NW dipping pure reverse fault (1 in inset b) has been reactivated as an oblique-slip left-lateral fault (2 in inset b). (b) The old reverse slip episode (1) expressed in parallel rough grooves that were overprinted by the younger left-lateral strike-slip striations (2 in inset c). (d) The successive reverse slip episode (1) and the left-lateral one (2) are consistent with the paleostress (1) and modern stress (2) states, respectively, deduced from the inversion of fault slip data from site 37 (Figures 3, 4, 5, Table 1).

grooves, while the youngest slip is recorded in thin frictional strike-slip striations smoothing the fault plane (Figure 7). The corresponding modern and paleostress tensors computed from separation of data collected at site 37 (Figures 3, 4, 5, Table 1) are consistent with the successive slip episodes recorded on the fault plane.

### 5.1.2. Western Kopeh Dagh

In the Western Kopeh Dagh, a key outcrop was investigated in the village of Tangeh Turkeman (Site 30; Figures 1 and 8) representing the geological relationships between tectonic regimes concurrent with the modern and paleo stress regimes. In that location, a

limestone member of the Aitamir Formation (Cretaceous) shows a systematic fracturing perpendicular to bedding azimuth (Figure 8), which is parallel to the regional N092°E trending folding axis. These fractures (several tens of meters in length) are originally extensional joints filled by calcites (a thickness of 2 to 10 cm) in which elongated minerals are perpendicular to the joint planes (Figure 8), and were considered as fold-related extensional joints perpendicular to the fold axis. The angular relationship between the joints and the fold axis, as well as the extensional character of the joints, imply that the joints were created parallel to the direction of the Miocene NNE trending compression in the Western

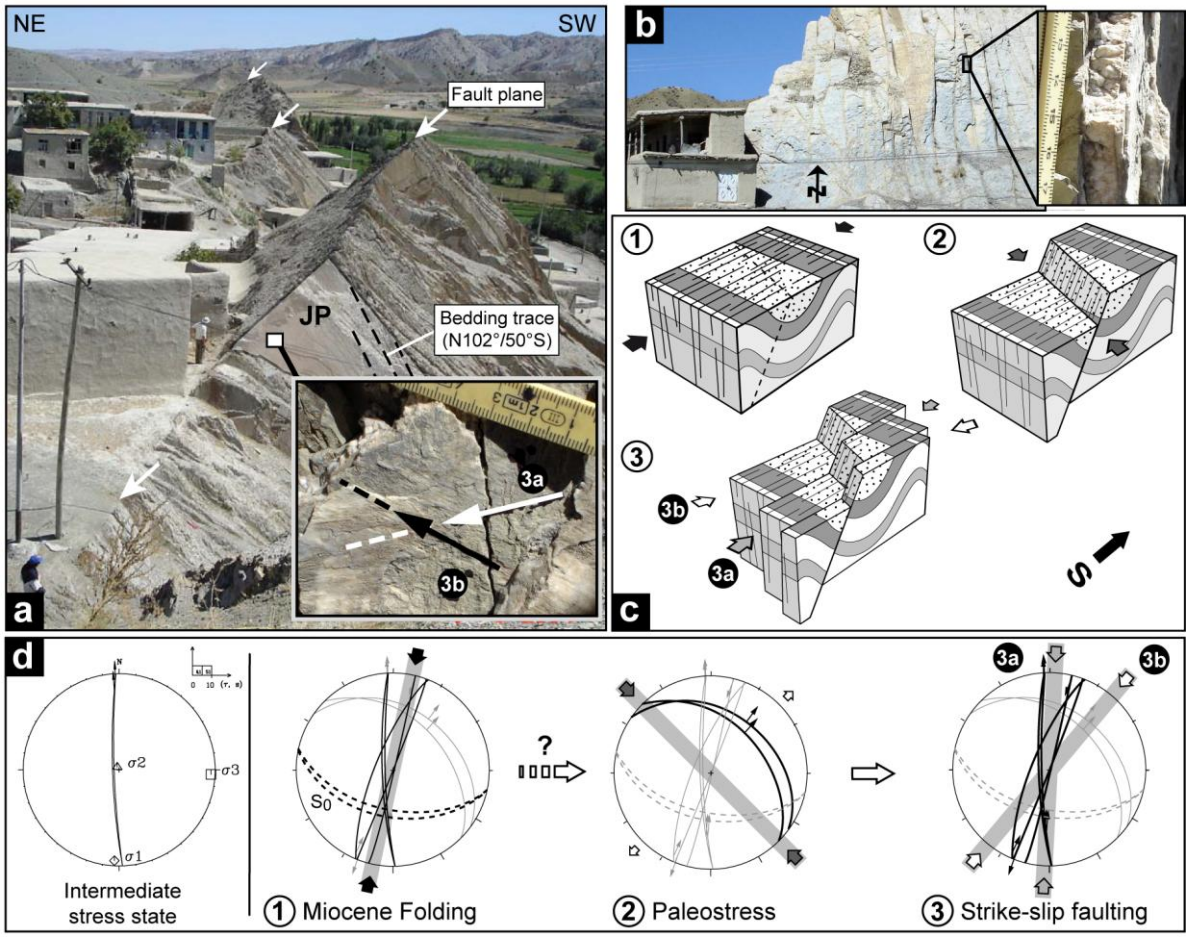


Figure 8. (a) A NW dipping normal fault cut folded strata and fold-related extensional joints perpendicular to the fold axis in the western Kopeh Dagh (site 30). JP shows a free-surface of the extensional joints, on which two distinct right-lateral slips were recorded (3a and 3b in the lower right box). (b) General view of the nearly vertical extensional joints affecting the southern block of the normal fault in inset (a). The calcite filling of the extensional joints is shown in the right box. (c) Schematic block diagrams illustrating the deformation chronologies observed at site 30; numbers correspond to the successive tectonic regimes presented in inset (d). (d) At right, a stereoplot showing mechanical compatibility of the first strike-slip generation (3a) with the regionally consistent intermediate stress state. Other stereograms represent the chronological relationships between the geological structures observed at site 30 and the regional tectonic regimes responsible for: 1, Miocene folding; 2, post-Miocene paleostress state; 3a, intermediate; 3b, modern stress states.

Kopeh Dagh. Subsequently, both the joint and bedding structures were affected by a NE dipping normal fault that permanently cuts the structures. The normal fault is nearly perpendicular to the Miocene compression, but parallel to the regional direction of the paleostress compression ($\sigma_1$) determined in this study. In the last stage, the extensional joints have been reactivated into right-lateral strike-slip faults displacing the initially predominated normal fault as a passive structure (Figure 8). Moreover, as indicated in Figure 8, the calcite filling of the extensional joints was overprinted by two distinct right-lateral slip striations with a clear chronology. The inversion of the youngest fault slip-vector of the reactivated right-lateral strike-slip faults indicates a stress solution consistent with the modern state of stress (site 30 in Figure 4). The successive tectonic regimes, deduced thanks to convincing relative chronologies, are representative for three distinct deformation episodes corresponding to the Miocene folding, the post-folding paleostress state, and the modern stress state determined in this paper. Examining compatibility of the older strike-slip striae recorded on the reactivated joint planes in term of the regional mean of intermediate and modern states of stress, we found that the first slip direction is consistent with the intermediate state of stress (Figure 8). This compatibility indicates the geological reliability of the intermediate stress state, even if there are few stress solutions of this regime throughout the region.

### 5.1.3. Binalud Mountains

There is also convincing geological evidence for changes in the Plio-Quaternary stress state from paleostress to modern stress in the Binalud deformation domain. North of Daneh village, southeast of Neyshabur (Figure 1), a 1-m-thick layer of pedogenic carbonate was affected by the youngest trace of the Neyshabur Fault (Figure 9). On the northern fault block, the carbonate layer crops out (at the surface) due to reverse component of the Neyshabur Fault motion, whereas, this layer is buried below ~2 m of younger alluvial fanglomerates in the southern side of the fault (Figure 9). The inversion of fault slip data measured in two nearby sites (38 and 39; Figures 3 and 4), and in strata older than the carbonate layer reveals a NE trending maximum stress axis for the modern stress state in agreement with the regional direction of $\sigma 1$ computed for the modern stress regime in NE Iran (Figure 3). Several meters north of the main fault trace (Neyshabur Fault), another N trending fault zone (~50-cm-wide) is observed in Quaternary deposits, expressed in colored lithologic contrasts between two mud-supported and pebble-supported conglomerates (Figure 9). The striae measured on fault planes indicate reverse left-lateral kinematics of the fault zone that is not consistent with the modern state of stress. The measured striated fault planes are compatible with the paleostress

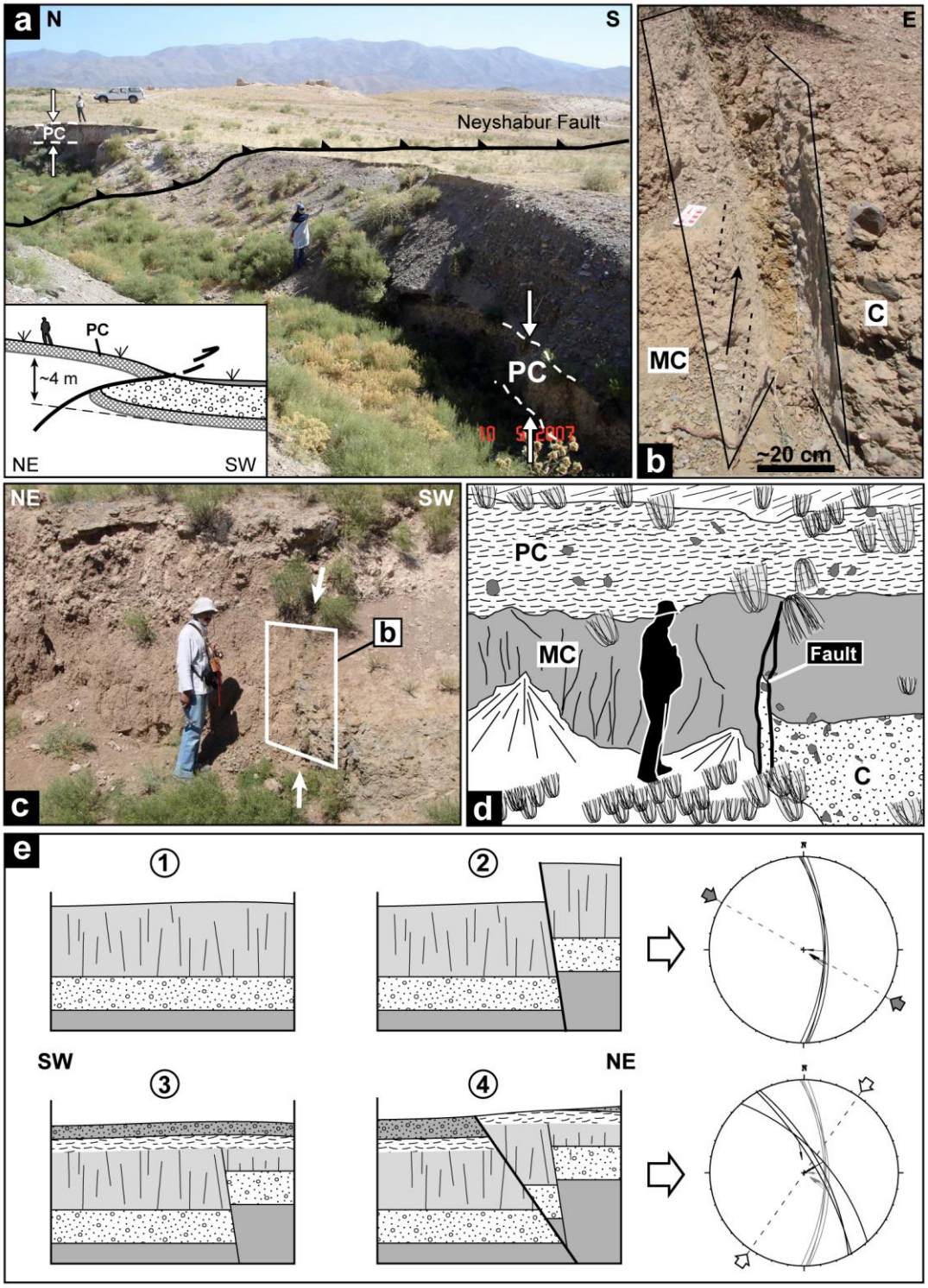


Figure 9. Fault-scale geological evidences for the changes in the stress state along the Neyshabur Fault system, north of Daneh village. (a) The pedogenic carbonate horizon (PC) vertically displaced by the youngest fault strand of the Neyshabur Fault system. (b) The N trending fault zone and its associated fault planes between Quaternary mud-supported (MC) and pebble-supported (C) conglomerates. Black arrow shows oblique-slip reverse fault striation. (c) The N trending fault zone did not affected the pedogenic carbonate horizon (see inset "d" for more information), (e) the chronological relationships between the geological features presented in insets "a, b, c and d" and the corresponding regional tectonic regimes responsible for paleostress and modern stress states; 2, reactivation of the N trending fault zone; 4, the present-day Neyshabur Fault reactivation.

state determined at site 38 (Figure 6). Interestingly, this small Quaternary fault zone was buried by the pedogenic carbonate layer (Figure 9), which in turn has been displaced by the youngest trace of the Neyshabur Fault reactivated within the modern stress field.

### 5.2. Geomorphic evidence for stress changes from paleostress to modern stress states

Among several geomorphic instances representing the Plio-Quaternary stress changes in northeast Iran, we present the paradox of geomorphic observations along the Plio-Quaternary trace of the Golmeym Fault, *i.e.*, the northern segment of the Chakaneh Fault system (*Shabanian et al.*, 2009b). The present-day kinematics of the Chakaneh Fault system is characterized by right-lateral strike-slip faulting along N-striking faults. The West dipping Golmeym Fault makes a sharp boundary between elevated Plio-Quaternary pyroclastic terrains in the western side and a gently sloping piedmont covered by Quaternary alluvial fans in the eastern side (Figures 10 and 11). This topographic contrast is expressed as an east-facing 300-m-high escarpment along the main fault trace. Considering the maximum lateral displacement of ~6 km along the Chakaneh Fault system (*Shabanian et al.*, 2009b), there is no corresponding counterpart to be correlated with the elevated western side of the fault. Therefore, the observed topographic contrast cannot be considered as a differential strike-slip fault escarpment. On the other hand, the westward dip of the fault implies a reverse component of faulting forming such a topographic contrast. But, such a mechanism is not consistent with the present-day transtensional kinematics of the fault. Our kinematic analyses along the Chakaneh Fault system (sites 16, 17, 19 and 34; Figures 3-6) indicate strike-slip faulting mechanisms that have been accompanied by two different minor components of motion corresponding to the paleostress and modern stress states: (1) an old component of reverse faulting, *i.e.*, transpressional stress regime (sites 16, 19), and (2) a present-day minor component of normal faulting, *i.e.*, transtensional stress regime (sites 17, 19, 34). North of Golmeym village, conspicuous geomorphic and structural evidences (at the site-scale) for the present-day normal faulting component along the Golmeym Fault were observed thanks to a road trench (Figure 10). There, rarely stratified Quaternary deposits affected by the fault zone, which is consisted of three fault strands, show normal offsets due to the extensional component of the fault motions. At the surface, the normal component is geomorphologically expressed by a west-facing, ~50-cm-high fault scarp (Figure 10), which forms a fault-parallel saddle landform on the hanging wall. At a larger scale, along the Golmeym Fault, two river valleys have incised in the western fault block discharging their sedimentary loads on the

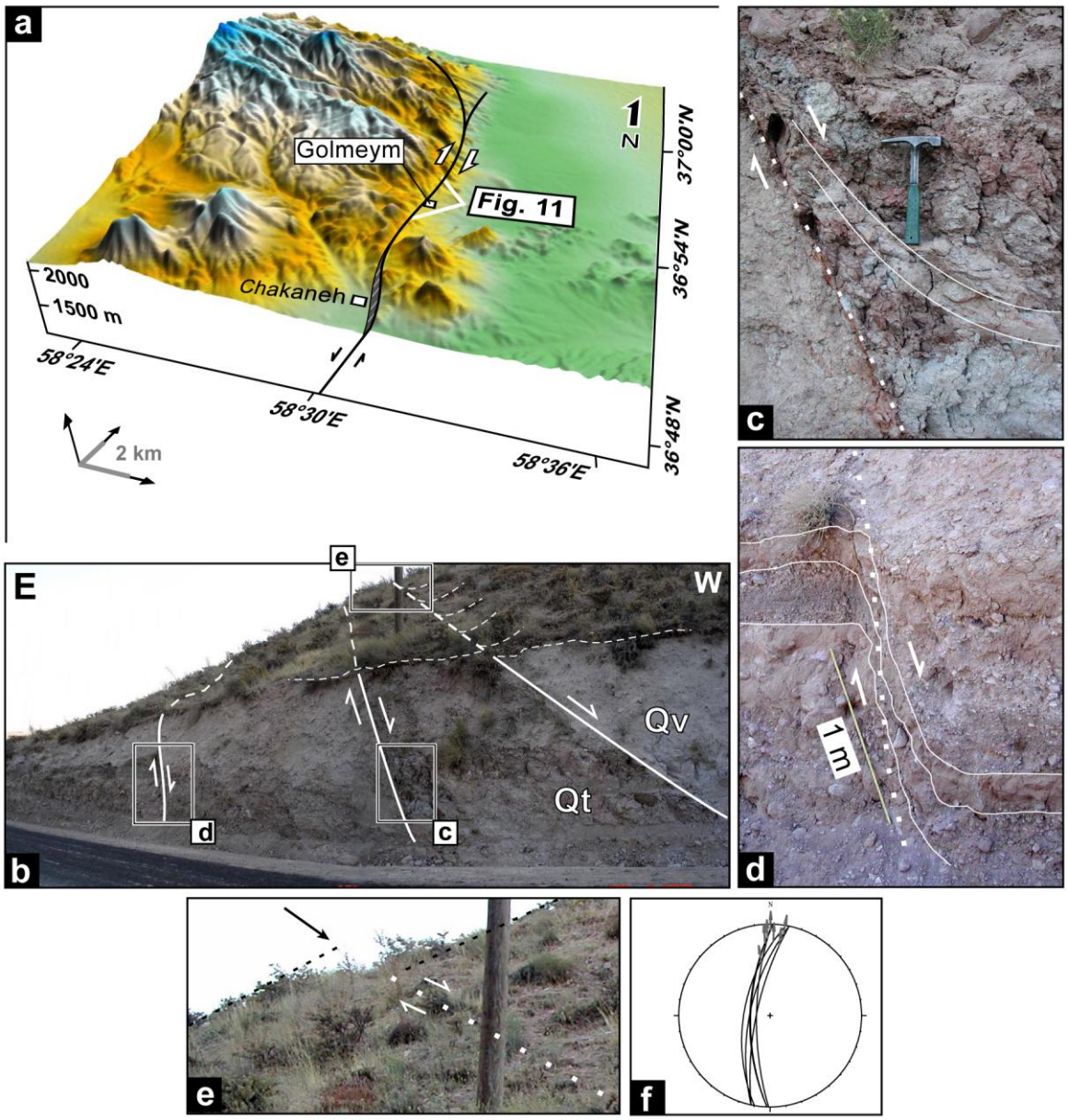


Figure 10. (a) 3D-view of the Golmeym Fault escarpment (based on SRTM digital topographic data) showing the topographic contrast between the Plio-Quaternary reliefs (western side) and the Quaternary alluvial plain (eastern side). (b) A cross-section of the Golmeym Fault thanks to a road-trench west of Golmeym village (see Figure 11 for location). Qv, Plio-Quaternary pyroclastic rocks; Qt, Quaternary alluvium. Within the fault zone, consisted of three fault splays, components of normal faulting are expressed by the fault zone architecture (c and d), and/or indicated by fault scarp morphology (e). (f) Major fault planes measured on the two eastern fault splays indicating the transtensional characteristics of the Golmeym fault in agreement with the geomorphic and structural features observed along the fault.

alluvial plain on the eastern side of the fault. Those valleys are currently subsided with respect to the corresponding alluvial surfaces at the eastern side (Figure 11). Such a geomorphic feature forms in the cases of pure strike-slip and/or extensional strike-slip faulting, which do not favor uplift in the western side of the fault. In other words, the initially uplifting block is now subsiding and sediment filled the stream bed behind the reversed fault scarp implying a

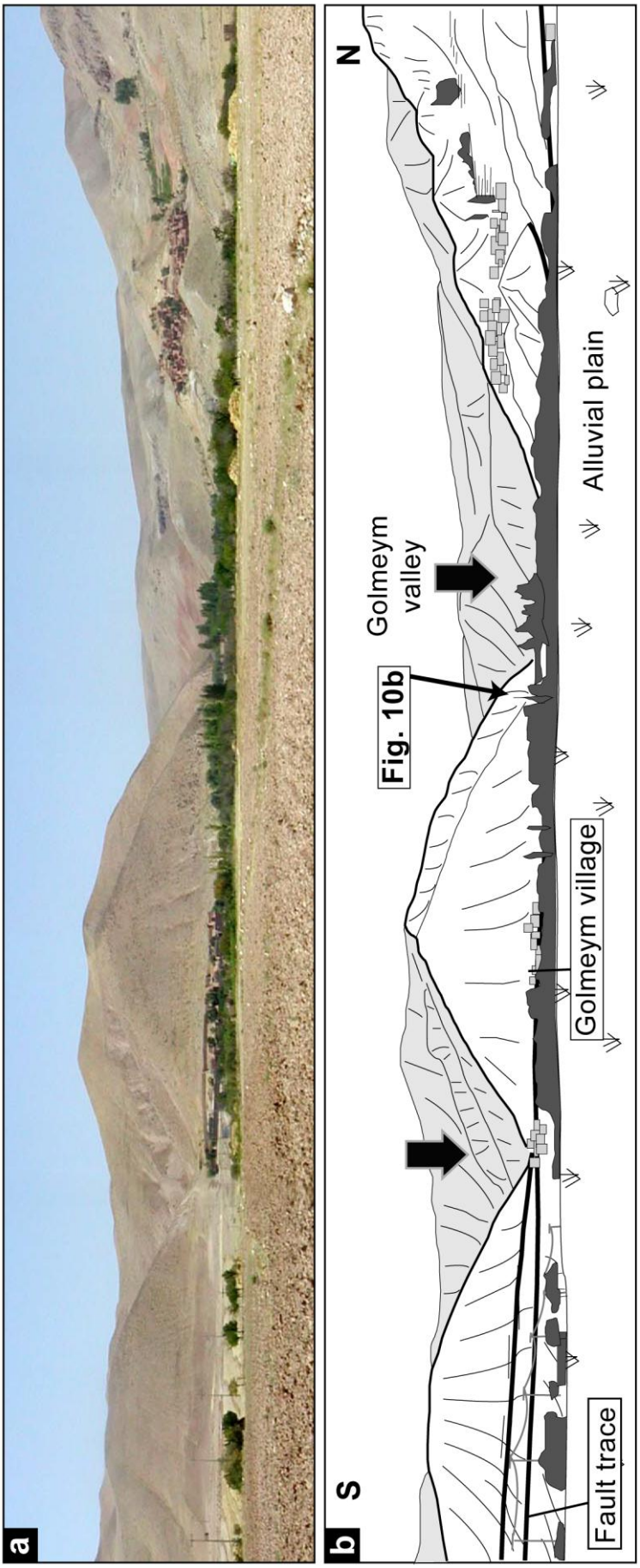


Figure 11. (a and b) Panoramic view of the Golmeym Fault escarpment taken from a distance of ~2 km, the photography location was marked on Figure 10a. Two subsided valleys along the fault are indicated by black arrows. Geomorphic level of the Golmeym river bed in the western side of the fault (hanging wall) is lower than its associated Quaternary alluvial surfaces in the eastern side (footwall).

normal faulting component along the West dipping Golmeym Fault. Combining these geological and geomorphic observations with the result of fault kinematic analysis one can conclude that the topographic contrast between the Plio-Quaternary reliefs and the late Quaternary piedmont along the Golmeym Fault is the geomorphic expression of older transpressional fault motions corresponding to the paleostress state (Figures 3 and 6). Subsequently, the fault escarpment was affected by the present-day transtensional strike-slip faulting due to the modern state of stress producing the younger geomorphic and structural features observed along the fault.

In summary, the structural and geomorphic examples presented above confirm that the changes in states of stress deduced from the inversions of fault kinematics data are representative for reliable Plio-Quaternary tectonic changes in northeast Iran.

## 6. The present-day state of stress deduced from inversion of focal mechanisms

Following the methodology exposed in section 3.2, we analyzed the present-day stress state in northeast Iran using the earthquake focal mechanisms (Table 2). In the first step of analysis, the entire region of northeast Iran was divided into three distinct structural domains, *i.e.*, Doruneh-Kuh Sorkh (northern part of Central Iran), Central-Western Kopeh Dagh, and Eastern Kopeh Dagh. These defined domains are characterized by different tectonic settings and/or structural patterns (Figure 12). Stress solutions computed for the Central-Western Kopeh Dagh and Eastern Kopeh Dagh are strike-slip and compressional, respectively, but with the same NNE trending direction of $\sigma_1$ axis for the both domains (Figure 12). Analyzing both data sets into a single data file, we obtained a well-constrained stress solution with a N022°E trending $\sigma_1$ axis representative for the regional state of stress acting throughout the Kopeh Dagh Mountains. This regionally significant solution indicates a transpressional stress regime consistent with both the active strike-slip and reverse faulting within the Kopeh Dagh Mountains. In such a regional stress regime both strike-slip and reverse faults having different but respective orientations have been reactivated with clear mechanical compatibilities (Figure 12). Conversely, the deviatoric stress solution computed for the Doruneh-Kuh Sorkh domain corresponds to a compressional tectonic regime with a N03°E trending $\sigma_1$ axis (Figure 12).

In summary, the inversion analysis of earthquake focal mechanisms that occurred in the last sixty years reveals that the present-day state of stress in the Kopeh Dagh is homogeneous,

Table 2. a. Earthquake source parameters used in the focal mechanism inversion.

| N | Date | Time | Lat. | Long. | Mb | Plane 1 | | | Plane 2 | | | Depth | R |
|---|---|---|---|---|---|---|---|---|---|---|---|---|---|
| | (yyyymmdd) | (hhmm) | (°N) | (°E) | | Azimuth | Dip | Rake | Azimuth | Dip | Rake | (km) | |
| 1 | 19481005 | 2012 | 37.78 | 58.41 | 7.3 | 99 | 5 | 80 | 289 | 85 | 91 | 5 | Mc |
| 2 | 19681115 | 0625 | 37.60 | 58.50 | 5.1 | 100 | 81 | -36 | 196 | 55 | -169 | 22 | M |
| 3 | 19690103 | 0316 | 37.13 | 57.90 | 5.6 | 132 | 60 | 95 | 322 | 30 | 81 | 11 | Mc |
| 4 | 19700101 | 1431 | 37.32 | 59.60 | 5.0 | 291 | 26 | 97 | 103 | 64 | 87 | 23 | M |
| 5 | 19700404 | 1058 | 36.99 | 59.47 | 4.9 | 73 | 68 | 15 | 337 | 76 | 157 | _ | M |
| 6 | 19700730 | 0052 | 37.85 | 55.92 | 6.4 | 293 | 56 | -150 | 185 | 66 | -38 | 11 | P |
| 7 | 19710214 | 1627 | 36.62 | 55.74 | 5.3 | 336 | 39 | 93 | 152 | 51 | 87 | 4 | P |
| 8 | 19710526 | 0241 | 35.51 | 58.22 | 5.4 | 57 | 42 | 23 | 309 | 75 | 130 | 26 | JM |
| 9 | 19721201 | 1139 | 35.45 | 57.92 | 5.4 | 156 | 65 | -176 | 64 | 87 | -25 | 8 | J |
| 10 | 19730517 | 1611 | 35.54 | 57.75 | 5.0 | 23 | 8 | 176 | 117 | 89 | 82 | 29 | M |
| 11 | 19730802 | 2028 | 37.32 | 56.60 | 4.9 | 297 | 10 | 86 | 121 | 80 | 91 | 34 | M |
| 12 | 19740307 | 1136 | 37.60 | 55.83 | 5,1 | 23 | 89 | -1 | 113 | 89 | -179 | 21 | JF |
| 13 | 19770809 | 2142 | 36.74 | 60.13 | 4.6 | 243 | 57 | 19 | 142 | 74 | 145 | 8 | M |
| 14 | 19790224 | 1356 | 37.22 | 56.66 | 4.7 | 278 | 41 | 56 | 140 | 57 | 116 | 33 | M |
| 15 | 19790308 | 2240 | 37.52 | 57.49 | 4.5 | 292 | 57 | -56 | 61 | 46 | -131 | 10 | M |
| 16 | 19791209 | 0912 | 35.15 | 56.87 | 5.6 | 325 | 36 | 99 | 133 | 54 | 83 | 9 | J |
| 17 | 19840323 | 2008 | 37.32 | 57.53 | 4.9 | 5 | 57 | -148 | 256 | 64 | -38 | _ | M |
| 18 | 19840706 | 0408 | 36.56 | 58.33 | 4.8 | 267 | 64 | 29 | 163 | 64 | 151 | 10 | M |
| 19 | 19851201 | 2031 | 37.63 | 56.62 | 4.6 | 281 | 54 | 69 | 134 | 41 | 116 | _ | M |
| 20 | 19870410 | 0643 | 37.21 | 57.70 | 5.0 | 256 | 62 | 60 | 127 | 40 | 133 | 6 | M |
| 21 | 19870705 | 0743 | 37.74 | 58.41 | 4.9 | 19 | 30 | -63 | 169 | 64 | -104 | 2 | M |
| 22 | 19870916 | 1606 | 37.44 | 57.20 | 4.6 | 284 | 38 | 65 | 135 | 56 | 108 | 33 | M |
| 23 | 19880311 | 0738 | 37.27 | 56.26 | 4.5 | 277 | 43 | 13 | 177 | 81 | 132 | 33 | M |
| 24 | 19880508 | 0650 | 35.33 | 55.94 | 4.7 | 219 | 87 | 4 | 129 | 86 | 177 | 53 | M |
| 25 | 19900818 | 0951 | 37.06 | 56.21 | 4.9 | 211 | 77 | -4 | 302 | 85 | -166 | 13 | M |
| 26 | 19921127 | 2109 | 37.36 | 59.77 | 5.1 | 166 | 68 | 172 | 259 | 82 | 22 | 24 | H |
| 27 | 19941214 | 2044 | 35.56 | 58.66 | 5.1 | 319 | 32 | 144 | 80 | 72 | 63 | 33 | H |
| 28 | 19960225 | 1614 | 35.65 | 57.35 | 4.8 | 82 | 77 | 10 | 350 | 80 | 166 | 33 | H |
| 29 | 19960225 | 1742 | 35.85 | 57.22 | 4.8 | 257 | 79 | 5 | 166 | 85 | 169 | 33 | H |
| 30 | 19970204 | 0954 | 37.99 | 57.54 | 5.3 | 78 | 64 | 15 | 342 | 77 | 153 | 15 | H |
| 31 | 19970204 | 1037 | 37.39 | 57.33 | 5.4 | 326 | 75 | 173 | 58 | 83 | 15 | 8 | J |
| 32 | 19970205 | 0753 | 37.84 | 57.58 | 5.2 | 187 | 78 | -178 | 97 | 89 | -12 | 15 | H |
| 33 | 19980804 | 1142 | 37.47 | 57.45 | 5.1 | 252 | 84 | -6 | 343 | 84 | -174 | 15 | H |
| 34 | 20000202 | 2258 | 35.46 | 58.19 | 5.1 | 83 | 43 | 79 | 278 | 48 | 100 | 27 | H |
| 35 | 20000822 | 1655 | 38.07 | 57.19 | 5.2 | 133 | 69 | 171 | 227 | 81 | 30 | 4 | J |
| 36 | 20030703 | 1459 | 35.66 | 60.84 | 5.2 | 316 | 30 | 109 | 114 | 62 | 79 | 30 | H |

b. Deviatoric stress tensors deduced from the inversion of focal mechanisms.

| Zone | $\sigma_1$ | | $\sigma_2$ | | $\sigma_3$ | | R | N | Rm |
|---|---|---|---|---|---|---|---|---|---|
| | Tr. | Pl. | Tr. | Pl. | Tr. | Pl. | | | |
| Zone 1 | 211 | 06 | 312 | 63 | 118 | 27 | 0.665 | 15 | S |
| Zone 2 | 197 | 01 | 287 | 01 | 092 | 89 | 0.680 | 5 | C |
| Zone 1 & 2 | 022 | 06 | 279 | 65 | 115 | 24 | 0.782 | 19 | S |
| Zone 3 | 003 | 07 | 272 | 09 | 129 | 78 | 0.585 | 8 | C |

[a] Focal mechanisms used for the fault kinematics inversion presented in Figure 11. All angles are in degrees. N, site number refers to Figure 11. The last column refers to the source of focal mechanism: J, *Jackson et al.* (2002); JF, *Jackson and Fitch* (1979); JM, *Jackson and McKenzie* (1984); H, Harvard catalogue (http://www.globalcmt.org/CMTsearch.html); M, *Mostriouk and Petrov* (1994); Mc, *McKenzie* (1972); N, *Nowroozi* (1972); P, *Priestly et al.* (1994).

[b] Deviatoric stress tensors deduced from the inversion of focal mechanisms for the boxed area in Figure 11. Tr. and Pl. are trend and plunge values of stress axes, respectively. For stress tensor parameters see the caption of Table 1.

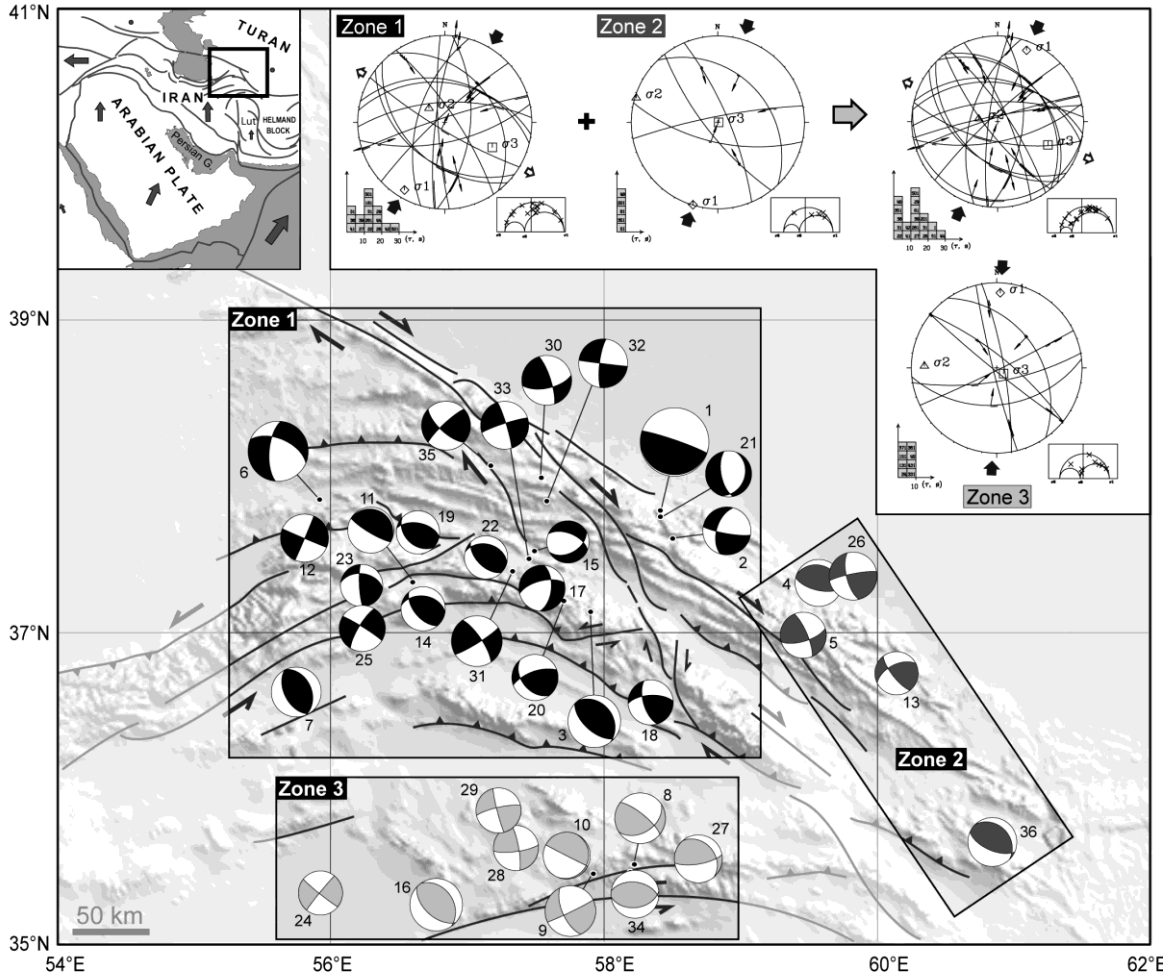


Figure 12. Simplified structural map of NE Iran; Earthquake focal mechanisms are presented as "beach balls". The inversion results deduced from the boxed focal solutions (Table 2) are shown in upper right stereoplots (Figure 2 for details). The boxed Mohr diagrams for stress solutions indicate the mechanical compatibility of the inverted data sets with corresponding stress tensors (*see Ritz and Taboada*, 1993). The trends of the major known faults are marked by solid lines, taken from Figure 1. Zone1, Central-Western Kopeh Dagh; Zone2, Eastern Kopeh Dagh; Zone3, Doruneh-Kuh Sorkh. Among the analyzed focal mechanisms, seven out of thirty 36 data (6, 7, 10, 12, 15, 21 and 25) were rejected from the calculation. Three of those solutions (10, 15, and 21 from *Mostriouk and Petrov* (1994)) show randomly arranged nodal planes with respect to the geometry of the inherited and active geological structures of the region. The other focal mechanisms are not consistent with a certain deviatoric stress tensor, but it is difficult to find whether those are the result of local kinematics instabilities or those are the solutions having greater uncertainties with respect to other data consistent with geological reality of the region.

consistent with a transpressional tectonic regime with a regional N023±5°E trending $\sigma_1$. This result is in agreement with the modern state of stress computed from the youngest fault kinematics data (section 4.1).

## 7. Summary and discussion

In this paper, we provided evidence for three distinct states of stress which have been responsible for the Plio-Quaternary deformations in northeast Iran. Change from one stress

state to another seems sharp enough so there is no solution halfway between two successive stress states (Figure 13). The temporal changes in the stress states clearly results from three distinct and successive changes in the Plio-Quaternary tectonic regimes (section 5). Conversely, there is no evidence for regionally significant spatial changes in each individual Plio-Quaternary stress fields (Figure 3). In other words, the stress states have been homogenous throughout the Kopeh Dagh and the adjacent deformation domains (Meshkan transfer zone and Allah Dagh-Binalud Mountains).

### 7.1. Temporal changes in the Plio-Quaternary stress states in NE Iran

Clear relative chronologies of crosscutting fault planes or fault striations as well as the well-known geological relationships between the tectonic regimes responsible for the successive slip episodes indicate the geological reality of the temporal stress changes discussed in this paper. The fault kinematics have been measured in Cretaceous to Quaternary deposits, but the slip evidence of pre-Pliocene tectonic regimes was eliminated in our data sets by the systematic geological data selection (section 3.3). This allowed us to analyze the Plio-Quaternary stress states not affected by pre-Pliocene tectonic regimes. However, it is difficult to constrain the absolute age for fault striations more precisely than being younger than the age of the rocks cut by the faults. The majority of the analyzed striations are observed on fault planes affecting deposits of ages ranging from Pliocene to late Quaternary. The youngest deposits affected by the paleostress state are Pleistocene in age implying that the three distinct temporal changes in the stress state occurred during the Quaternary. But, despite the recent attempts to date regional Quaternary surfaces and the last Quaternary volcanic activity in NE Iran (*Shabanian et al*., 2009a; 2009b), age data for the Quaternary deposits affected by the analyzed fault sets are not available. This precludes constraining absolute ages of the stress changes in northeast Iran.

At a larger regional scale, in the Alborz Mountains, such drastic changes have been reported by *Axen et al*. (2001), *Ritz et al*. (2006), and *Abbassi and Farbod* (2009). *Axen et al*. (2001) suggested that the present-day sinistral transpression on WNW trending faults in the Alborz probably began in Pliocene time, reversing motion on older dextral faults of the same strike. A stress change from a N trending to a NE trending compression was reported by *Ritz et al*. (2006) through geomorphic and paleoseismological investigations in the Central Alborz. This significant stress change is suggested to be Pleistocene (1 to 1.5 Ma) in age. On the other hand, at the southern flank of the Central Alborz (Tehran piedmont), *Abbassi and Farbod*

(2009) have shown that the fault pattern comprises two groups of normal faults (1) NW trending old normal faults affecting deposits older than the Middle Pleistocene, and (2) NE trending active normal faults, which affect Late Pleistocene deposits. Such a fault pattern could not be explained by a single stress state (*i.e.*, modern stress state) leading *Abbassi and Farbod* (2009) to conclude that a change in the state of stress occurred after deposition of the Middle Pleistocene deposits. The age relations described above indicate that there is no consensus of opinions about the timing of the changes in the state of stress in north and northeast Iran. However, in northeast Iran, what is clear is that the stress changes from the paleostress to the intermediate, and then to the modern stress states have occurred during the Quaternary.

### 7.2. Regional tectonic regimes

Figure 13 illustrates the relationship between R ratios and stress regimes (see section 3.5) for the modern, intermediate, and paleostress states. Such an analysis allowed us to characterize predominant tectonic regimes in NE Iran. It is noteworthy that only the A and B quality deviatoric stress solutions were analyzed in the LP diagrams of Figure 13.

When all paleostress solutions are considered, the diagram displays compressional to uniaxial compressional stress regimes with a slight tendency to a strike-slip stress regime (Figure 13). If only well-constrained solutions (A quality) are taken into account, the data clustered within the uniaxial compressional zone with vertical $\sigma_2$ or $\sigma_3$ axes. This clustering shows the transition from compressional to strike-slip stress regimes. The well-constrained stress tensors are representative for regional tectonic regimes (see *Ritz and Taboada*, 1993); therefore, the focalization of the R ratio in the uniaxial compressional zone (Figure 13) can be explained by a transpressional tectonic regime that favors such a stress regime transition. Further analysis of R values versus the direction of maximum stress axis ($\sigma_1$) reveals that almost all of the computed stress tensors, regardless of the corresponding stress regimes, represent a regionally significant N140±10°E trending $\sigma_1$ stress axis (Figure 13). This indicates that only one transpressional tectonic regime, coherent with a combination of reverse and strike-slip faulting, was responsible for deformation throughout the region.

The R ratio analysis of the modern state of stress shows that all stress tensors, whatever their quality (A or B), are sparsely distributed within three stress domains representative for strike-slip, compressional, and uniaxial-compressional tectonic regimes (Figure 13). All of these different tectonic regimes are characterized by a predominant N030±15°E trending σ1

(Figure 13) implying that the present-day fault motions, whatever their kinematics, are consistent with only one regionally significant stress state, throughout the Kopeh Dagh and Allah Dagh-Binalud deformation domains.

Interestingly, the number of unstable solutions of modern stress states is less than the paleostress state instabilities. This may indicate that the non-evident effect of tilting and/or rotation on the fault planes submitted to more than one tectonic regime cannot be completely ruled out despite the efforts that one may make to restore the evidently tilted or rotated data sets.

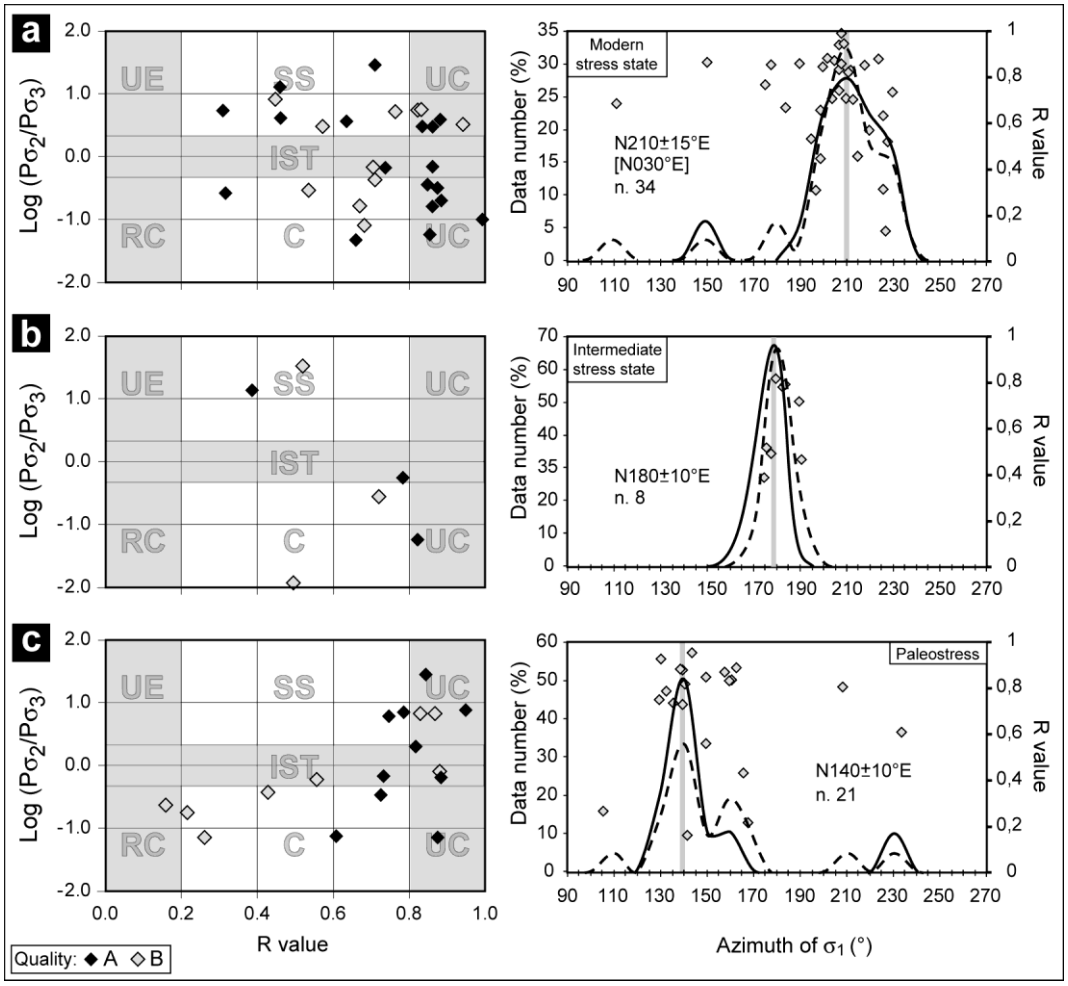


Figure 13. LP diagrams (left) showing the tectonic regimes predominated in the Kopeh Dagh and Binalud mountains corresponding to the modern stress (a), intermediate tress (b), and paleostress (c) states (Figure 2 for descriptions). Right diagrams are frequency histograms of $\sigma_1$ direction obtained from individual stress solutions corresponding to the modern stress (a), intermediate tress (b), and paleostress (c) states. All stress states are characterized by the nearly symmetric Normal curves. The predominant direction of the maximum horizontal stress axes is shown on each diagram. The frequency curve for all solutions, regardless their quality, is presented by dashed line. The frequency curve for only well-constrained solutions (A quality) is presented by solid line. For the intermediate and paleostress states (b and c), the frequency distribution curves of $\sigma_1$ direction for all stress solutions show a slight shift with respect to the curves from well-constrained stress tensors. Therefore, a significant weight was attributed to well-constrained stress solutions interpreting regional stress regimes.

### 7.3. Consistency of the inversion results with previous studies

The previous studies to understand states of stress in the Kopeh Dagh and surroundings were made by *Lyberis and Manby* (1999), and *Zamani et al.* (2007). The N trending compression presented by *Lyberis and Manby* (1999), for the northeastern boundary of the Kopeh Dagh with the Turan platform, was based on a kinematic analysis of sixteen fault data sets measured in the Mesozoic and Tertiary rocks. Unfortunately, the authors did not present any technical explanation (slip deviation angle, mechanical compatibility, etc.) by which one can examine the quality of the reported solutions. Nevertheless, considering the existence of at least two different slip directions on several parallel fault planes implies that apparently data separation was not performed by the authors. Therefore, the N trending maximum stress axis presented by *Lyberis and Manby* (1999) may be the result of kinematic analyses of mixed fault slip generations that belong to different states of stress. Such analyses can provide an average direction of the stress axes without any geological significance (see *Angelier*, 1984; *Carey-Gailhardis and Mercier*, 1987).

Recently, the present-day state of stress in northeast Iran was analyzed by *Zamani et al.* (2007) on the basis of systematic inversion of earthquake focal mechanisms. They used focal mechanisms of earthquakes (magnitudes between 4.5 and 7.3) located in at least three different tectonic domains (Eastern Alborz, Kopeh Dagh, central Iran), which are characterized by different structural patterns and geodynamic settings. *Zamani et al.* (2007) calculated an average stress regime indicating a major N32°E trending compression, and a secondary stress regime with a N172°E trending compression. The authors suggested that the "coexistent" NE and N trending compressions in the Western Kopet Dagh, Eastern Alborz and the northwestern Doruneh fault zone are consistent with the NE trending "structural grain" of the domains, while the absence of the N trending compression in the Eastern-Central Kopet Dagh, Binalud and northeastern Doruneh Fault zone is due to the structural grain perpendicular to NE trending relative plate motion. Examining the kinematical complexity presented by *Zamani et al.* (2007), we performed inversions of the same data set, but collected from their source articles (Table 2), avoiding the propagation of probable errors to our data set. Our inversion results (section 6) are not consistent with the results published by *Zamani et al.* (2007). In our paper, the inversion of earthquake focal mechanisms reveals a homogeneous and predominant strike-slip regime with the regional N023°±5°E trending σ1 representative for the present-day state of stress in the Kopeh Dagh domains (Figure 12). Furthermore, the automatic data separation performed by *Zamani et al.* (2007) did not respect difference either in structural domains or in fault mechanisms. In such a case, the computed coexistent stress

solutions are not geologically significant, and thus cannot be an argument for stress partitioning in northeast Iran as proposed by the authors. Also, our geological data and deduced results do not confirm coexistent stress states in northeast Iran. In fact, the data set used by *Zamani et al.* (2007) include focal mechanism data from at least two distinct deformation domains that are thus submitted to different present-day states of stress. Analyzing such data set, without considering geological characteristics of the deformation domains, can lead to mean deviatoric stresses that are not representative of the geological reality of the region (*Carey*, 1979).

### 7.4. Tectonic implications

Late Cenozoic faulting and the accompanying mode of deformations in northeast Iran has been discussed by *Tchalenko* (1975), *Lyberis and Manby* (1999), *Jackson et al.* (2002), *Hollingsworth et al.* (2006, 2008), *Shabanian et al.* (2009a, 2009b), and *Siame et al.* (2009). NE Iran, including the Kopeh Dagh and Allah Dagh-Binalud mountains, is involved in oblique convergence at the northeastern boundary of the Arabia-Eurasia collision. According to analysis of earthquake focal mechanisms and their slip vectors, *Jackson et al.* (2002) suggested that the oblique right-lateral shortening is, to some extent, achieved by separation (partitioning) of oblique convergence into its orthogonal strike-slip and reverse components on parallel faults in the Kopeh Dagh. The authors also expected that the strike-slip faulting within the range, which strikes NNW at an oblique angle to the belt, rotates anticlockwise about a vertical axis as the deformation progresses to eventually become parallel to the regional strike (see also *Jackson and McKenzie*, 1984; *Jackson et al.*, 1995; *Hollingsworth et al.*, 2006, 2008). Recently, quantitative geological and geomorphic investigations by *Shabanian et al.* (2009a, 2009b) indicated that the late Cenozoic active deformation in northeast Iran has principally been accommodated by simple strike-slip faulting focalized on few NNW-striking right-lateral fault systems with incomparable slip rates (see *Shabanian*, 2009). Such a mechanism translates central Iran northward relative to Eurasia. *Shabanian et al.* (2009b) showed that the old range-parallel boundaries of both the Kopeh Dagh and Binalud deformation domains were affected by the late Cenozoic strike-slip faulting forming a new tectonic configuration since the Pliocene. This structural rearrangement disagrees with the basic assumptions for the model-derived interpretations mentioned above, and subsequently, does not favor the strain partitioning and systematic anticlockwise block rotations in NE Iran.

According to our data and the deduced results, the present-day oblique convergence is taken up in northeast Iran by strike-slip faulting along NE trending left-lateral and NNW trending right-lateral strike-slip faults, as well as reverse to oblique-slip reverse faulting along NW trending faults characterized by relatively low-angle dip (less than 50°). This structural assemblage is involved in a mechanically compatible and homogeneous modern stress field. The reverse faulting mechanism is clearly observed along the southern boundary of the Allah Dagh-Binalud deformation domains (Figure 3). The majority of strike-slip faulting regimes are observed along the major strike-slip faults that obliquely dissect the Kopeh Dagh Mountains and cross the Allah Dagh-Binalud deformation domains through the Meshkan transfer zone. For all stress states (*i.e.*, paleostress, intermediate and modern stress states), the direction of $\sigma_1$ obtained from the inversions of reverse and strike-slip striae is spatially consistent through different tectonic domains in the area of study.

In this paper, the possible occurrence of strain partitioning was examined looking at the slip compatibility within a uniform regional stress field. Partitioning mechanisms have been previously described within subduction zones associated with oblique convergence. The relative plate motion along such convergent margins is partitioned into dip-slip displacements along the subduction plane and deformation within the overriding plate (*e.g.*, *Fitch*, 1972; *McCaffrey*, 1992; *Bellier and Sébrier*, 1995). The deformation in the overriding plate commonly corresponds to a shear component that is localized on strike-slip fault zones parallel to the trench. Similarly, partitioning was documented within intracontinental oblique convergence domains (*e.g.*, *Gaudemer et al.*, 1995; *Ward and Valensise*, 1996; *Authemayou et al.*, 2006), where deformation is taken up by parallel structures of which dip-slip thrusts and pure strike-slip faults accommodate the normal and lateral components of the convergence, respectively. In northeast Iran, the transpressional character of both the paleostress and modern stress regimes explains the compatibility between the observed reverse and strike-slip faulting. The homogeneity of the stress states does not agree with a partitioning between the faults in the Kopeh Dagh. The different fault motions, from pure dip-slip to pure strike-slip, are only due to the fault orientations with respect to the far-field stress pattern (horizontal stress directions at the regional scale), not due to partitioning (Figure 14). These remarkably homogeneous stress fields with spatially constant horizontal stress orientations indicate that systematic large-scale block rotations did not occur in the Kopeh Dagh and Allah Dagh-Binalud deformation domains during the Plio-Quaternary. Only local perturbations were observed in the direction of horizontal stress axes that could result from block rotations at the scale of the fault zones (*e.g.*, *Shabanian et al.*, 2009a). Most of the modern stress solutions

indicating strike-slip regime are aligned between the Binalud and the Kopeh Dagh Mountains, along the Chakaneh Fault system (section 4.1). This strengthens the existence of a continuous right-lateral strike-slip faulting from the Kopeh Dagh to the Binalud Mountains as proposed by *Shabanian et al.* (2009b).

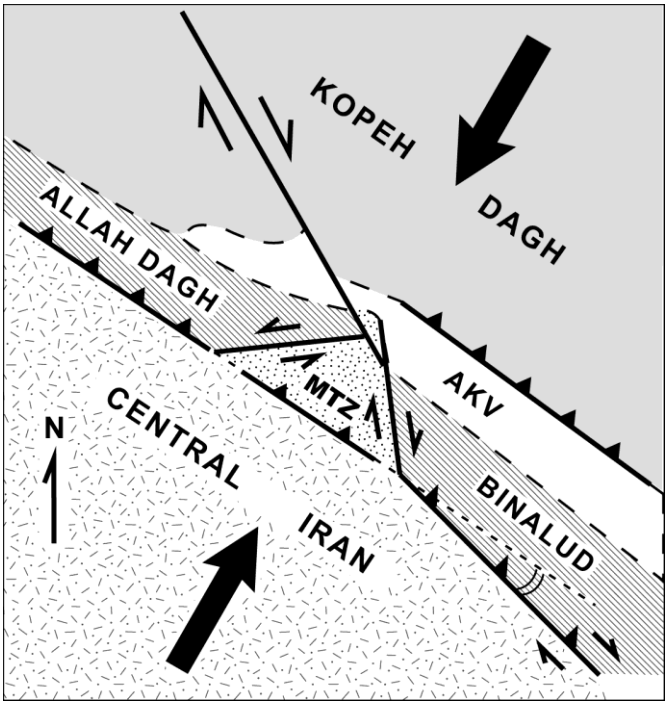


Figure 14. Schematic kinematic model of the Kopeh Dagh and Allah Dagh-Binalud deformation domains showing the major strike-slip and reverse (triangles indicate fault hanging walls) faults involved in the present-day NE trending transpressional stress regime. Dashed line is approximate boundary of the domains. The angular relationships between the structures and the $\sigma_1$ stress axis are respected. AKV, Atrak-Kashafrud Valley.

The regionally consistent σ1 direction (N30°E trending) for the present-day stress state in NE Iran does not correspond to the orientation of GPS-derived velocity vectors (Figure 1), but it agrees with the shortening axis given by the GPS measurements (*Masson et al.*, 2005; *Tavakoli*, 2007). It is worthy to note that the vectors represent the relative displacement between the western and eastern parts of the region, *i.e.*, Iran and Eurasia, respectively. This displacement is principally taken up on nearly-vertical strike-slip faults oblique to the convergence (*Shabanian*, 2009; *Shabanian et al.*, 2009a, 2009b). Therefore, it is not surprising that the relative motion of NE Iran relative to Eurasia is parallel to the NNW striking right-lateral faults. Because, major strike-slip faults slip under very low resolved shear stress (*e.g.*, *Mount and Suppe*, 1987; *Zoback et al.*, 1987), these faults can strike, and off course slip, in a direction that is not parallel to the relative motion of the blocks or plates they bound.

### 7.5. Dynamics of the stress changes in NE Iran

The stress changes from the paleostress state (NW trending $\sigma_1$) to the intermediate one (N trending $\sigma_1$), and then to the modern state of stress (NNE trending $\sigma_1$) in northeast Iran have been sharp and discontinuous, so there is no halfway stress solution between two successive stress states. These changes are expressed in inversion of the vertical faulting component along the strike-slip faults, and in conversion of thrusting into oblique-slip to strike-slip faulting (section 5). Such a major change in the Plio-Quaternary tectonic regime was also reported by *Ritz et al.* (2006) in the Alborz. There, the change from a compressional tectonic regime (with a N trending $\sigma_1$) to the present-day transpressional tectonic regime (with a NNE trending $\sigma_1$) has caused inversion of lateral movements (right- lateral to left-lateral) along the strike-slip faults in the Western Alborz, and inversion of the vertical component of the thrusting faults in the internal part of the range (*i.e.*, transtension in the internal domain of the range). *Ritz et al.* (2006) suggested that the northwestward motion of the South Caspian Basin to Eurasia and/or its clockwise rotation provoked the recent kinematical change in the Alborz. Considering the changes in fault kinematics in the Alborz (*e.g.*, *Abbassi and Farbod,* 2009; *Ritz et al*., 2006), as well as the present-day GPS-derived extension in the Talesh at the southwestern border of the Caspian Basin (*Masson et al.*, 2006), it seems that a Quaternary regional kinematic reorganization has occurred at the scale of the South Caspian Basin and its surrounding domains (*e.g.*, *Ritz et al.*, 2006). Explaining the dynamics of this reorganization, *Masson et al.* (2006) proposed a second tectonic force due to the northward subduction of the old remnant oceanic crust of the South Caspian Basin, in addition to the northward Arabian push. If one accepts this geodynamic model, the self-governing northwestward motion of the South Caspian Basin to Eurasia or more precisely, the change from indenter tectonics to slab driven tectonics may have significantly influenced the Plio-Quaternary stress field in northeast Iran. This drastic change in boundary forces can reduce the NW trending horizontal stress magnitude (at least within the Kopeh Dagh) transforming the paleostress state to the modern one, with a predominant NE trending compression more consistent with the direction of the Arabia-Eurasia convergence. A mechanism of similar nature has been proposed by *Bellier et al.* (1997) explaining the change in tectonic regime within the Anatolian domains in relation with the Arabia-Eurasia collision and Aegean subduction. But, it is difficult to adequately explain changes in the dynamics of the Arabia-Eurasia convergence taking into account the lack of knowledge of the late Cenozoic geodynamic history of the Arabia-Eurasia collision.

## 8. Conclusion

Our inversion analyses of fault kinematics data indicate drastic temporal changes in the Plio-Quaternary states of stress in NE Iran. The modern stress state, deduced from fault kinematics analyses, is in close agreement with the present-day state of stress given by the inversions of earthquake focal mechanisms. The paleostress field was characterized by a regional mean of N140±10°E trending horizontal compression ($\sigma_1$), and a transpressional tectonic regime. The modern state of stress shows two more distinct strike-slip and compressional tectonic regimes with a regional mean of N030±15°E trending horizontal $\sigma_1$ different from the paleostress $\sigma_1$ direction. The change from paleostress to modern stress states has occurred through an intermediate stress state characterized by a mean regional N trending $\sigma_1$. The Plio-Quaternary states of stress are regionally consistent throughout the Kopeh Dagh and Allah Dagh-Binalud deformation domains.

At the northeastern boundary of the Arabia-Eurasia collision, the present-day oblique convergence is taken up by the NE Iran structural assemblage involved in a mechanically compatible and homogeneous modern stress field. This implies that no strain and/or stress partitioning, as well as systematic block rotations have occurred in the Kopeh Dagh and Allah Dagh-Binalud deformation domains.

The Plio-Quaternary stress changes documented in this paper and the late Cenozoic (3-5 Ma) tectonic reorganization in NE Iran (*Shabanian et al.*, 2009a, 2009b) indicate that the rate and style of deformation in northeast Iran may have significantly changed during the Late Cenozoic. This fact should be seriously considered when extrapolating the present-day seismic and GPS-derived deformation rates over a long period of several millions years (*e.g.*, *Jackson et al.*, 1995; *Masson et al.*, 2007; *Hollingsworth et al.*, 2006, 2008).

## Acknowledgements

This work was funded by the INSU-CNRS (France) and the International Institute of Earthquake Engineering and Seismology (IIEES, Iran), supervised by D. Hatzfeld and M. Ghafouri Ashtiani. We thank M. Mokhtari and M. Zare (IIEES) for support and administrative assistance. Funding was provided by the Dyeti and PNRN programs (INSU-CNRS), and ACI FNS program (French Ministry of Research), within the above mentioned co-operative agreement. SPOT images were provided thanks to the ISIS program (©CNES 2004 to 2007, distribution SPOT images S.A.). E. Shabanian benefits of a Foreign Affair Ministry (Ministère des Affaires Etrangères) grant through French Embassy in Iran, and a complement support through the "Cotutelle de thèse" program (ACI du Ministère des Affaires Etrangères). We thank V. Grimault, Ch. Duhamel and the staff of the SCAC of the French Embassy in Tehran, for their support. We are grateful to Mark Quigley and an anonymous reviewer for helpful and constructive reviews. We are indebted to Nick Marriner (CEREGE - Aix en Provence) for comments and English language corrections. The General governments of Khorassan-e Razavi and Shomali provinces have efficiently helped us during three years.

**References**

Abbassi, M. R., and Y. Farbod (2009), Faulting and folding in quaternary deposits of Tehran's piedmont (Iran), *Journal of Asian Earth Sciences, 34*, 522–531, doi:10.1016/j.jseaes.2008.08.001.

Afshar Harb, A. (1979), The stratigraphy, tectonics and petroleum geology of the Kopet Dagh region, northeastern Iran, Ph.D. thesis, Petroleum Geology Section, Royal School of Mines, Imperial College of Science and Technology, London.

Alavi, M. (1992), Thrust tectonics of the Binalood region, NE Iran, *Tectonics, 11*(2), 360-370.

Angelier, J. (1979), Determination of the mean principal directions of stresses for a given fault population, *Tectonophysics 56*, 17-26.

Angelier, J. (1984), Tectonic analysis of fault slip data sets, *J. Geophys. Res, 89*(B7), 5835-5848.

Angelier, J. (1990), Inversion of field data in fault tectonics to obtain the regional stress-part II: A new rapid direct inversion method by analytical means, *Geophys. J. Int., 103*, 363-376.

Angelier, J., J. F. Dumont, H. Karamanderesi, A. Poisson, S. Simsek, and S. Uysal (1981), Analyses of fault mechanisms and expansion of southwestern Anatolia since the Late Miocene, *Tectonophysics, 75*, T1-T9.

Angelier J., and P. Mechler (1977), Sur une méthode graphique de recherche des contraintes principales également utilisable en tectonique et en séismologie: la méthode des dièdres droits, *Bull. Soc. Géol. France, 19*(6), 1309–1318.

Authemayou, C., D. Chardon, O. Bellier, Z. Malekzade, E. Shabanian, M. and Abbassi (2006), Late Cenozoic partitioning of oblique plate convergence in the Zagros fold-and-thrust belt (Iran), *Tectonics, 25*, TC3002, doi:10.1029/2005TCOO1860.

Axen, G. J., P. S. Lam, M. Grove, D. F. Stockli, and J. Hassanzadeh (2001), Exhumation of the west-central Alborz Mountains, Iran, Caspian subsidence, and collision-related tectonics, *Geology, 29*(6), 559–562.

Bellier, O., J. F. Dumont, M. Sébrier, and J. L. Mercier (1991), Geological constraints on the kinematics and fault-plane solution of the Quiches fault zone: reactivated during the 10 November 1946 Ancash earthquake, Northern Peru, *Bull. Seis. Soc. Am., 8*(2), 468-490.

Bellier, O., and M. L. Zoback (1995), Recent state of stress change in the Walker Lane zone, western Basin and Range province, United States, *Tectonics, 14*, 564–593.

Bellier, O., S. Över, A. Poisson, and J. Andrieux (1997), Recent temporal change in the stress state and modern stress field along North Anatolian Fault Zone (Turkey), *Geophys. J. Int., 131*, 61-86.

Bellier, O., and M. Sébrier (1995), Is the slip rate on the Great Sumatran fault accommodated by fore-arc stretching?, *Geophys. Res. Lett., 22*, 1969-1972.

Carey, E. (1979), Recherche des directions principales de contraintes associées au jeu d'une population de failles, *Rev. Geol. Dyn. Geogr. Phys., 21*, 57-66.

Carey, E., and B. Brunier (1974), Analyse théorique et numérique d'un modèle mécanique élémentaire appliqué à l'étude d'une population de failles, *C. R. Acad. Sci., Ser. D, 279*, 891-894.

Carey-Gailhardis, E., and J.-L. Mercier (1987), A numerical method for determining the state of stress using focal mechanism of earthquake populations: Application to Tibetan teleseisms and microseismicity of southern Peru, *Earth Planet. Sci. Lett., 82*, 165-179.

Carey-Gailhardis, E., and J.L. Mercier (1992), Regional state of stress, fault kinematics and adjustments of blocks in a fractured body of rocks: application to the microseismicity of the Rhine graben, *Journal of structural geology, 14*(8/9), 1007-1017.

Carey-Gailhardis, E., and P. Vergely (1992), Graphical analysis of fault kinematics and focal mechanisms of earthquakes in term of stress; the right dihedra method, use and pitfalls, *Annales Tectonics, VI*(1), 3-9.

Etchecopar, A. (1984), Etude des états de contraintes en tectonique cassante et simulation de deformations plastiques (approche mathématique), Thèse d'Etat, Université Montpellier II, France.

Fitch, T. J. (1972), Plate convergence, transcurrent faults and internal deformation adjacent to Southeast Asia and the western Pacific, *J. Geophys. Res., 77*, 4432–4460.

Gaudemer, Y., P. Tapponnier, B. Meyer, G. Peltzer, G. Shunmin, C. Zhitai, D. Huagung, and I. Cifuentes (1995), Partitioning of crustal slip between linked, active faults in the eastern Qilian Shan, and evidence for a major seismic gap, the ''Tianzhu Gap,'' on the western Haiyuan fault, Ganzu (China), *Geophys. J. Int., 120*, 599 – 645.

Hollingsworth, J., J. Jackson, R. Walker, M. R. Gheitanchi, and M. J. Bolourchi (2006), Strike-slip faulting, rotation and along-strike elongation in the Kopeh Dagh Mountains, NE Iran, *Geophys. J. Int., 166*, 1161-1177, doi:10.1111/j.1365-246X.2006.02983.x.

Hollingsworth, J., J. Jackson, R. Walker, and H. Nazari (2008), Extrusion tectonics and subduction in the eastern South Caspian region since 10 Ma, *Geology, 36*(10), 763–766, doi:10.1130/G25008A.1.

Homberg, C., J. C. Hu, J. Angelier, F. Bergerat, and O. Lacombe (1997), Characterization of stress perturbations near major fault zones: Insights from 2-D distinct-element numerical modelling and field studies (Jura mountains), *Journal of Structural Geology, 19*, 703-718.

Jackson, J. A., and T. J. Fitch (1979), Seismotectonic implications of relocated aftershock sequences in Iran and Turkey, *Geophys. J. R. astr. Soc., 57*, 209–229.

Jackson, J., and D. McKenzie (1984), Active tectonics of the Alpine-Himalayan Belt between western Turkey and Pakistan, *Geophys. J. R. astr. Soc., 77*(1), 185-264.

Jackson, J. A., A. J. Haines, and W. E. Holt (1995), The accommodation of Arabia–Eurasia plate convergence in Iran, *J. geophys. Res., 100*, 15,205-15,219.

Jackson, J., K. Priestley, M. Allen, and M. Berberian (2002), Active tectonics of the South Caspian Basin, *Geophys. J. Int., 148*, 214–245.

Lyberis, N., G. Manby, J.T. Poli, V. Kalugin, H. Yousouphocaev, and T. Ashirov (1998), Post-Triassic evolution of the southern margin of the Turan plate, *C. R. Acad. Sci., 326*, 137–143.

Lyberis, N., and G. Manby (1999), Oblique to orthogonal convergence across the Turan block in the post-Miocene, *Am. Assoc. Petrol. Geol. Bull., 83*(7), 1135-1160.

Masson, F., J. Chéry, D. Hatzfeld, J. Martinod, P. Vernant, F. Tavakoli, and M. Ghafory-Ashtiani (2005), Seismic versus aseismic deformation in Iran inferred from earthquakes and geodetic data, *Geophys. J. Int., 160*, 217-226, doi:10.1111/j.1365-246X.2004.02465.x.

Masson, F., Y. Djamour, S. Vangorp, J. Chéry, F. Tavakoli, M. Tatar and H. Nankali (2006), Extension in NW Iran inferred from GPS enlightens the behavior of the south Caspian basin, *Earth Planet. Sci. Lett., 252*, 180–188.

Masson, F., M. Anvari, Y. Djamour, A. Walpersdorf, F. Tavakoli, M. Daignières, H. Nankali, and S. Van Gorp (2007), Large-scale velocity field and strain tensor in Iran inferred from GPS measurements: new insight for the present-day deformation pattern within NE Iran, *Geophys. J. Int., 170*, 436-440, doi:10.1111/j.1365-246X.2007.03477.x.

McCaffrey, R. (1992), Oblique plate convergence, slip vectors, and fore arc deformation, *J. Geophys. Res., 97*, 8905-8915.

McClusky, S., R. Reilinger, S. Mahmoud, D. Ben Sari, and A. Tealeb (2003), GPS constraints on Africa (Nubia) and Arabia plate motions, *Geophys. J. Int., 155*(1), 126–138, doi:10.1046/j.1365-246X.2003.02023.x.

McKenzie, D. P. (1972), Active tectonics of the Mediterranean region, *Geophys. J. Int., 30*(2), 109–185, doi:10.1111/j.1365-246X.1972.tb02351.x.

McKenzie, D., and J. Jackson (1983), The relationship between strain rates, crustal thickening, paleomagnetism, finite strain, and fault movements within a deforming zone, *Earth planet. Sci. Lett., 65*, 182-202.

McKenzie, D., and J. Jackson (1986), A block model of distributed deformation by faulting, *J. Geol. Soc. London, 143*, 349-353.

Mercier, J. L., E. Carey-Gailhardis, and M. Sébrier (1991), Paleostress determinations from fault kinematics: application to the neotectonics of the Himalayan-Tibet and the central Andes, *Philos. Trans. R. Soc. London, Ser. A, 337*, 41-52.

Mostriouk, A. O., V. A. Petrov (1994), Catalogue of focal mechanisms of Earthquakes 1964–1990, *Materials of World Data Center B.*, pp. 87, Moscow (available at http://wwwbrk.adm.yar.ru/russian/l_512/stress/fps_cate.htm).

Mount, V. S., and J. Suppe (1987), State of stress near the San Andreas Fault: implications for wrench tectonics, *Geology, 15*, 1143-1146.

Nowroozi, A.A. (1972), Focal mechanisms of Earthquakes in Persia, Turkey, West Pakistan, and Afghanistan and plate tectonics of the Middle East, *Bull. Seismol. Soc. Am. 62*, 823–850.

Över, S., U. C. Ünlügenç and O. Bellier (2002), Quaternary stress regime change in the Hatay region (SE Turkey), *Geophys. J. Int. 148*, 649-662.

Priestley, K., C. Baker, and J. Jackson (1994), Implications of earthquake focal mechanism data for the active tectonics of the South Caspian Basin and surrounding regions, *Geophys. J. Int., 118*, 111–141.

Regard, V., O. Bellier, J.-C. Thomas, M. R. Abbassi, J. Mercier, E. Shabanian, K. Feghhi, and S. Soleymani (2004), The accommodation of Arabia-Eurasia convergence in the Zagros-Makran transfer zone, SE Iran: a transition between collision and subduction through a young deforming system, *Tectonics, 23*, TC4007, doi:10.1029/2003TC001599.

Reilinger, R., et al. (2006), GPS constraints on continental deformation in the Africa-Arabia-Eurasia continental collision zone and implications for the dynamics of plate interactions, *J. Geophys. Res., 111*, B05411, doi:10.1029/2005JB004051.

Ritz, J.-F., and A. Taboada (1993), Revolution stress ellipsoids in brittle tectonics resulting from an uncritical use of inverse methods, *Bulletin de la Societe Geologique de France, 164*(4), 519-531.

Ritz, J.-F., H. Nazari, A. Ghassemi, R. Salamati, A. Shafei, S. Solaymani, and P. Vernant (2006), Active transtension inside Central Alborz: A new insight into northern Iran–southern Caspian geodynamics, *Geology, 34*(6), 477–480, doi:10.1130/G22319.1.

Sella, G. F., T. H. Dixon, and A. Mao (2002), REVEL: A model for recent plate velocities from space Geodesy, *J. Geophys. Res., 107*(B4), 2081, doi:10.1029/2000JB000033.

Shabanian, E. (2009), Active tectonic study in northeast Iran: contribution of the Kopeh Dagh and Binalud mountains to the accommodation of the Arabia-Eurasia convergence, Ph.D. thesis, University of Paul Cézanne (Aix – Marseille III), France, Aix-en-Provence.

Shabanian, E., L. Siame, O. Bellier, L. Benedetti, and M. R. Abbassi (2009a), Quaternary slip rates along the northeastern boundary of the Arabia-Eurasia collision zone (Kopeh Dagh Mountains, Northeast Iran), *Geophys. J. Int.*, *178*, 1055-1077, doi: 10.1111/j.1365-246X.2009.04183.x.

Shabanian, E., O. Bellier, L. Siame, N. Arnaud, M. R. Abbassi, and J.-J. Cochemé (2009b), New tectonic configuration in NE Iran: active strike-slip faulting between the Kopeh Dagh and Binalud mountains, *Tectonics*, *28*, TC5002, doi: 10.1029/2008TC002444.

Siame, L. L., E. Shabanian, and O. Bellier (2009), Extrusion tectonics and subduction in the eastern South Caspian region since 10 Ma, *Geology*, (comment) in press.

Stöcklin, J. (1968), Structural history and tectonics of Iran: A review, *Am. Assoc. Petr. Geol. Bull., 52*(7), 1229–1258.

Tavakoli, F. (2007), Present-day kinematics of the Zagros and east of Iran faults, Ph.D. thesis, University of Joseph Fourier, France, Grenoble.

Tchalenko, J. S. (1975), Seismicity and structure of the Kopet Dagh (Iran, USSR), *Phil. Trans. R. Soc. Lond., Series A, 278* (1275), 1–28.

Vernant, P., F. Nilforoushan, D. Hatzfeld, M. R. Abbassi, C. Vigny, F. Masson, H. Nankali, J. Martinod, A. Ashtiani, R. Bayer, F. Tavakoli, and J. Chéry (2004), Present-day crustal deformation and plate kinematics in the Middle East constrained by GPS measurements in Iran and northern Oman, *Geophys. J. Int., 157*(1), 381–398, doi:10.1111/j.1365-246X.2004.02222.x.

Ward, S. N., and G. Valensise (1996), Progressive growth of San Clemente Island, California, by blind thrust faulting: Implications for fault slip partitioning in the California Continental Borderland, *Geophys. J. Int., 126*, 712-734.

Zamani, B., J. Angelier, and A. Zamani (2007), State of stress induced by plate convergence and stress partitioning in northeastern Iran, as indicated by focal mechanisms of earthquakes, *Journal of Geodynamics, 45*, 120–132, doi:10.1016/j.jog.2007.07.003.

Zoback, M. D., M. L. Zoback, V. S. Mount, J. Suppe, J. P. Eaton, J. H. Healy, D. Oppenheimer, P. Reasenberg, L. Jones, C. B. Raleigh, I. G. Wong, O. Scotti, and C. Wentworth (1987), New evidence on the state of stress on the San Andreas fault system, *Science, 238*, 1105-1111, doi: 10.1126/science.238.4830.1105.

Zoback, M. L. (1989), State of stress and modern deformation of the basin and range province, *J. Geophys. Res., 94*, 7105-7128.

# *Conclusion*

In this study, detailed quaternary fault mapping provides a new structural database, which has at least to impacts on active tectonics in northeast Iran. At first, 2-D geometry and structural pattern (significance) of pre-defined fault zones were revised and detailed. Secondly, several new-defined quaternary fault zone or fault systems are recognized and structurally characterized (*e.g.*, the Chakaneh and Farhadan fault systems). During this stage cumulative geological offsets were measured in at least four hundreds distinct points along minor and major faults distributed within the entire region, especially within the Kopeh Dagh Mountains. Moreover, cross-cutting relationships between different fault and fault systems were examined. Such a remote sensing data set allowed evaluating the structural significance of faults and examining distribution of late Cenozoic faulting in NE Iran. Using the result derived from this stage, the main framework of the detailed geological and geomorphic investigations was established.

In the Northeast, the Kopeh Dagh range is bounded by the Main Kopeh Dagh Fault system (MKDF) forming the northeast boundary between Iran and Turan platform. It is intersected by the post-Miocene Bakharden-Quchan Fault System (BQFS) constituted by active NNW-trending right-lateral strike-slip faults dissecting the Central-Eastern Kopeh

Dagh range (Fig. 1). This fault system extends between the MKDF to the North, and the Binalud range to the South. Based on the distribution of cumulative displacements along the different fault segments mapped within the BQFS the sum of total cumulative offsets across the Kopeh Dagh is estimated at about 35-40 km. This sum is accommodated along at least eleven distinct faults and is suggested representative for total strike-slip deformation in this part of the range due to the relative Arabia-Eurasia northward motion. Resolving the total strike-slip displacement value of 35-40 km on a regional average structural orientation representative of the BQFS (azimuth: N28°W, dip: 75°NE, rake: 10°) total ~34 km northward and ~16 km westward displacements can be derived for Central and Western Kopeh Dagh with respect to Eurasia. Anyway, about 80 per cent (30±2 km) of this motion (between central Iran and Eurasia) should be accommodated along the BQFS indicating that the BQFS can be considered as an intercontinental boundary between Iranian micro-plate and Eurasia. Within this regional fault system, the Quchan and Baghan faults are considered as the two principal structures along which, exhibiting maximum cumulative displacements of 15.5±0.5 and 9.8±0.2 km, respectively, our detailed morphotectonic investigations were conducted. Combined quantitative geomorphic and geometric analysis, as well as in situ-produced cosmogenic $^{36}$Cl dating of two alluvial fans offset by the Quchan and Baghan faults yielded the first geological estimate of the Late Quaternary slip rates of 4.3±0.6 mm/yr (Quchan Fault) and 2.8±1.0 mm/yr (Baghan Fault) averaged over two different time scales of 83±4 kyr and maximum 450±65 kyr, respectively (Fig. 1). Assuming that the slip rates have been constant during the life of the fault, onset of strike-slip motion was estimated on the Quchan and Baghan faults, applying the calculated Late Quaternary slip rates to maximum post-folding cumulative geological offsets along the faults. This yields the age of ~4 Ma for the initiation of strike-slip faulting within the Kopeh Dagh Mountains.

These new data and the obtained results indicate that a large portion (9±2 mm/yr) of the Arabia-Eurasia northward motion is accommodated by strike-slip faults within the Kopeh Dagh. Further south, the northward motion between Central Iran and western Afghanistan (part of Eurasia) is expressed as right-lateral shear on several major N-trending strike-slip fault systems on both sides of the Lut Block (*Tirrul et al.,* 1983*; Walker and Jackson,* 2004*; Meyer and Le Dortz,* 2007). Between the Lut Block and Eurasia, geodetic (GPS) measurements (*Vernant et al.,* 2004; *Tavakoli,* 2007) indicate a rate of 7±2 mm/yr for this right-lateral shear, which is comparable to the geological (this study) and geodetic (*Tavakoli,* 2007) strike-slip rates (9±2 mm/yr) in the Kopeh Dagh, mainly (7±2 mm/yr) localized along the Bakharden-Quchan Fault system. Considering these geologic and geodetic rates

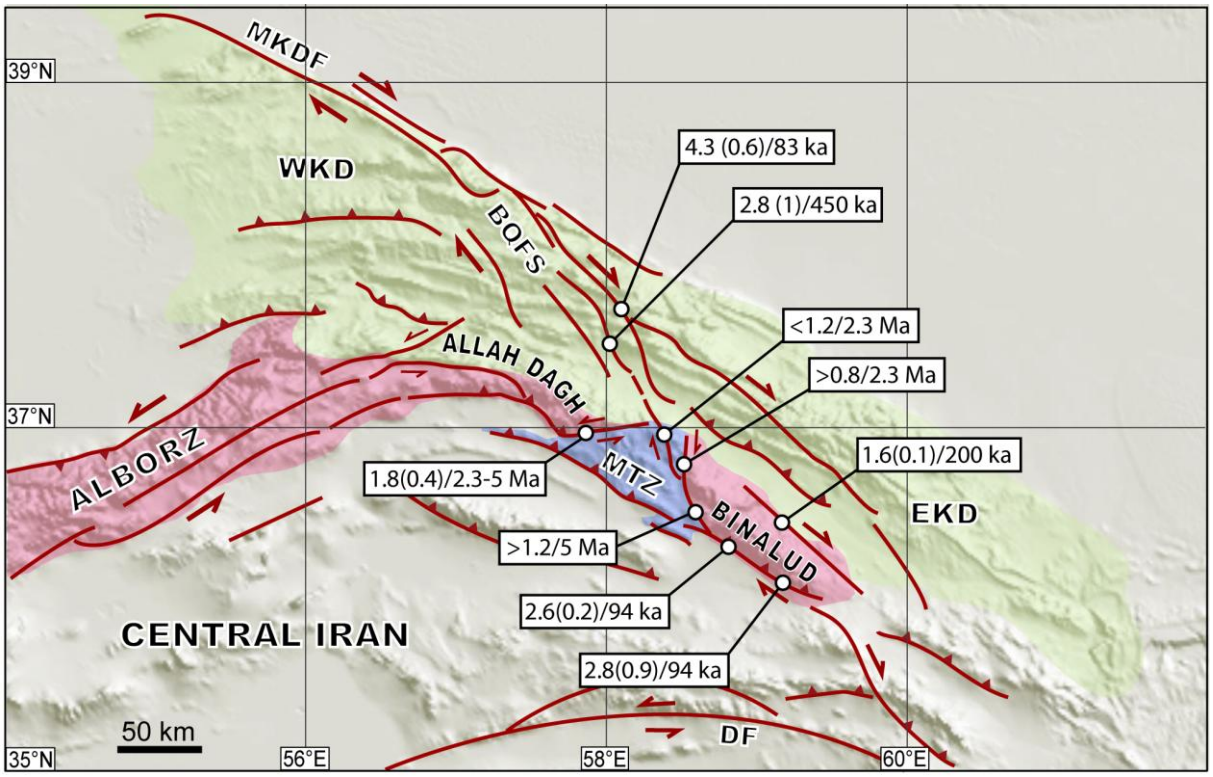


Figure 1. GTOPO30 topographic image showing the regional tectonic setting and major active faults of NE Iran. Abbreviations: MKDF, Main Kopeh Dagh Fault; BQFS, Bakharden-Quchan Fault System; DF, Doruneh Fault; MTZ, Meshkan Transfer Zone; EKD, Eastern Kopeh Dagh; WKD, western Kopeh Dagh. Circles indicate the sites in which offset geomorphic or geological markers were analyzed. Slip rates estimated at each site is indicated within white rectangles; from left to right: slip rate, uncertainty, age of the offset marker. Slip rates are marked by minimum or maximum signs, when age the offset marker is not constrained.

representative for the present-day tectonic deformation, the similar rates for the northward motion in northeast and eastern Iran imply that the relative Arabia-Eurasia northward motion is permanently transferred between eastern Iran faults (*e.g.*, Sistan Fault System) and the Bakharden-Quchan Fault system. Within this general context, the key question that needed to be answered was to know how is transferred to the north the deformation accommodated in eastern Iran between the Doruneh Fault and Kopeh Dagh Mountains. Therefore, to better understand the kinematics of deformation in northeast Iran the study was focused on the regions south of the Kopeh Dagh. As a discussion, the possibility of a structural linkage between the Kopeh Dagh and Binalud mountain ranges has already been evaluated in previous studies (*Tchalenko*, 1975; *Afshar Harb*, 1979; *Hollingsworth et al*., 2006). Despite the lack of clear structural linkage between the Kopeh Dagh and Binalud mountain ranges, the pioneer work by *Tchalenko* (1975) suggested a possible connection between the two deformation domains. Conversely, on the same basis, *Hollingsworth et al*. (2006) concluded that the strike-slip faulting within the Kopeh Dagh is not transferred southward beyond the

Atrak valley. Such interpretations have important impacts on geodynamic constrains in northeast Iran. For instance, accepting that strike-slip faulting die out at the southern boundary of the Kopeh Dagh, should follows by other assumptions such as rigidity of the southern deformation domains (*i.e*., the region between the Doruneh Fault and the Kopeh Dagh), and continuum kinematics of deformation processes, which seems more complicated than it is necessary (*e.g*., *McKenzie and Jackson*, 1986; *Hollingsworth et al*., 2006, 2008).

As the second step of this study, geomorphic and geological investigations were conducted in the region between the Kopeh Dagh and Binalud deformation domains to uncover this obscure segment of the northeast Iran puzzle. Active faulting investigation revealed that strike-slip deformation within the Kopeh Dagh is transferred southward through a new-defined deformation domain, *i.e*., the Meshkan transfer zone (MTZ). Our results demonstrate that at least 2 mm/yr (~25 per cent) of the northward motion between central Iran and Eurasia has been transferred southward through the MTZ (Fig. 1). This deformation is taken up by N-trending right-lateral strike slip faults extended between the Neyshabur fault system and the Kopeh Dagh faults. Analyzing cumulative displacements recorded by different ages offset geological markers the inception of strike-slip faulting has estimated at $\leq$5 Ma, more probably coeval with the time of the major tectonic reorganization in the Kopeh Dagh. These observations indicate that the strike-slip faulting within the Kopeh Dagh does not die out at the northern boundary of the Kopeh Dagh, and strongly supports the existence of a simple strike-slip faulting mechanism in the northeastern Arabia-Eurasia collision zone.

Investigation of the tectonic geomorphology of active faulting at both sides of the Binalud Mountains, northeast Iran, reveals the geomorphic and tectonic aspects of development of the mountain range produced by quaternary faulting. This investigation is conducted along seven individual fault segments belong to the Neyshabur and Mashhad fault systems. Three regional abandonment episodes of alluvial surfaces were dated at 5.3±1.1 kyr (Q1), 94±5 kyr (Q3), and 200±14 kyr (S3). The geomorphic reconstruction of both vertical and horizontal fault offsets postdating these surface abandonment episodes yielded individual slip rates for the late quaternary faulting along the two fault systems (Fig. 1). For the Neyshabur Fault System, the respective total horizontal and vertical slip rates of 2.7±0.8 mm/yr and 2.4±0.2 mm/yr are estimated reconstructing cumulative offsets recorded by the Q3 fan surfaces across the fault system. All together, these vertical and horizontal slip rates lead us to determine a total slip rate of 3.6±1.2 mm/yr for the late Quaternary deformation at the southwestern flank of the Binalud Mountains. Reconstructing the cumulative lateral offset recorded by the S3 surfaces, a Late Quaternary slip rate of 1.6±0.1 mm/yr is attributed to the

Mashhad Fault System. The distribution pattern of slip rates both sides of the Binalud reveals that Late Quaternary strike-slip faulting has been taken up by the Mashhad and Neyshabur Fault Systems at a long-term rate of ~4 mm/yr. This also implies a ~2.4 mm/yr long-term slip rate for vertical deformation which is uplifting the southwestern flank of the Binalud Mountains. All together, sum of both strike-slip and reverse components of faulting at both sides of the Binalud Mountains is account for about 5 mm/yr of total slip rate at both sides of the range. This in turn, is resolved to a northward slip rate of ~4.5 mm/yr, and a rate of ~2 mm/yr for the westward motion of Central Iran to the West relative to the Eastern Kopeh Dagh to the East. Combining our geological observations with geomorphic result deduced from quantitative hypsometric analyses of drainage basins nested in the Binalud mountains suggests that the locus of active deformation front is migrating southwestward along new reverse faults formed basin-ward.

In northeast Iran, the inversions of fault kinematics data revealed three distinct states of stress during the Plio-Quaternary (since ~5 Ma), whereas, each stress state has been spatially homogenous during corresponding activity time span. The paleostress regime is characterized by a regional transpressional tectonic regime with a mean N140±10°E-trending horizontal maximum stress axis (σ1). The younger state of stress ("modern" one) shows two distinct strike-slip and compressional tectonic regimes with a regional mean of N030±15°E-trending horizontal σ1. The change from the paleostress to modern stress states has been occurred through an intermediate stress field characterized by a mean regional N-trending σ1. These Quaternary stress analyses indicates that the present-day convergence is taken up by strike-slip faulting along NE-trending left-lateral and NNW-trending right-lateral strike-slip faults, as well as reverse to oblique-slip reverse faulting along NW-trending faults. This structural assemblage is involved in a mechanically compatible and homogeneous modern stress field. The reverse faulting mechanism is clearly observed along the southern boundary of the Allah Dagh-Binalud deformation domains. The majority of strike-slip faulting regimes are observed along the major strike-slip faults that obliquely dissect the Kopeh Dagh Mountains and cross the Allah Dagh-Binalud deformation domains through the Meshkan transfer zone. For all stress states (*i.e.*, paleostress, intermediate and modern stress states), the direction of σ1 obtained from the inversions of reverse and strike-slip striae is spatially consistent through different tectonic domains in the area of study. The transpressional character of both the paleostress and modern stress regimes explains the compatibility between the observed reverse and strike-slip faulting. The homogeneity of the stress states does not agree with a partitioning between the faults. The different fault motions, from pure dip-slip to pure strike-

slip, are only due to the fault orientations with respect to the far-field stress pattern (horizontal stress directions at the regional scale), not due to partitioning. These homogeneous stress fields with constant horizontal stress orientations indicate that systematic large-scale block rotations did not occur in the Kopeh Dagh and Allah Dagh-Binalud deformation domains during the Plio-Quaternary. Only local perturbations were observed in the direction of horizontal stress axes that could result from block rotations at the scale of the fault zones. Most of the modern stress solutions indicating strike-slip regime are aligned between the Binalud and the Kopeh Dagh Mountains, along the Chakaneh Fault system strengthening the existence of a continuous right-lateral strike-slip faulting from the Kopeh Dagh to the Binalud Mountains as deduced from morphotectonic investigations.

At a regional scale, all these new data and results provide fundamentally new constraints on the rate and distribution of the late quaternary deformation allowing proposing a new and consistent tectonic configuration for the northeastern Arabia-Eurasia collision zone (Fig. 2). The first kinematics model for northeast Iran was proposed by *McKenzie and Jackson* (1983, 1986). They claimed that continuum mechanisms can appropriately describe the instantaneous deformation in NE Iran. In this context the Kopeh Dagh was considered as an excellent example that exhibits the characteristic features of their 'pinned model' by distributed deformation. According to this model, the overall motion in the Kopeh Dagh is expressed by large blocks bounded by the through-going faults that rotate about two pivot points, one on each plate, that is, Eurasia in the North and Central Iran in the South. Strike-slip fault motions are accompanied by a component of thrust faulting. On the basis of the same model, *Jackson et al*. (2002) expected that the strike-slip faulting within the Kopeh Dagh, which strikes NNW at an oblique angle to the belt, rotates anticlockwise about a vertical axis as the deformation progresses to eventually become parallel to the regional strike (see also *Jackson and McKenzie*, 1984; *Jackson et al.*, 1995; *Hollingsworth et al.*, 2006, 2008). *Hollingsworth et al*. (2006) proposed a nearly similar block rotation model to explain the total right-lateral cumulative offset of 35-40 km along the Bakharden-Quchan Fault system as the apparent offsets due to anticlockwise rotation of fault-bounded blocks around vertical axes. According to this model, northward motion of Central Iran was thought to be accommodated between the Turan platform and Central Iran involving: (1) dominant thrust faulting at the southern boundaries of the Kopeh Dagh (north of the Atrak-Kashafrud valley), without significant strike-slip faulting, and (2) anticlockwise block rotation around a vertical axis within the Kopeh Dagh (see also *Jackson et al*., 2002). All the hypotheses mentioned above are based on the idealized continuum model proposed by *McKenzie and Jackson* (1983,

1986) to explain the relationship between finite strain and fault movements within a deforming zone submitted to the oblique convergence or divergence. The fundamental assumptions of such models are that (1) the deformation is uniformly distributed over the deforming zone, *i.e.*, the homogeneous deformation, and (2) the rigid boundaries of the deforming zone remain constant during the deformation process. In this view, the through-going strike-slip faults, oblique to the strike of the zone, are passive structures confined within the zone boundaries. Consequently, observed deformation on these faults is controlled by kinematic constraints associated with the finite deformation.

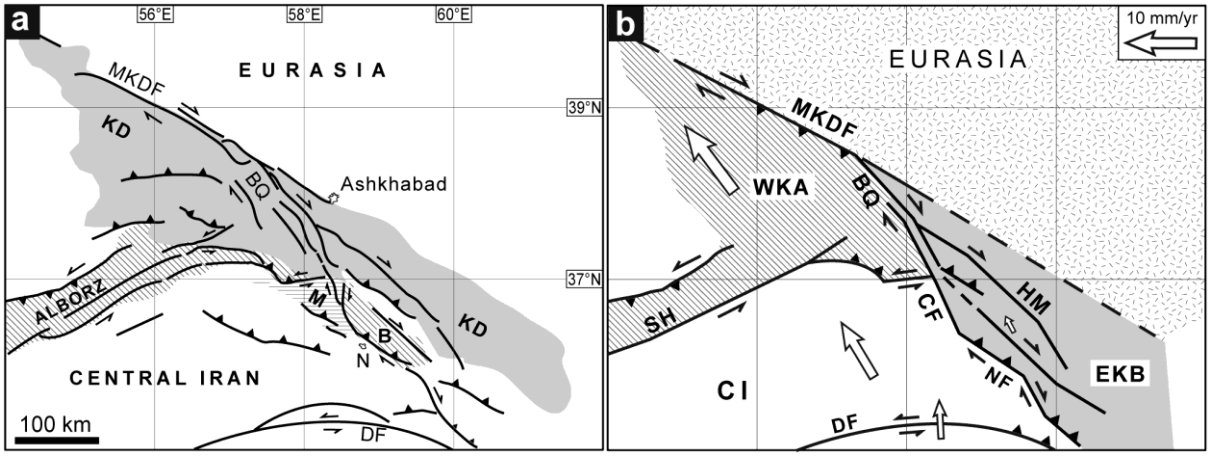


Figure 2. (a) Generalized active fault map together with the main tectonic domains of NE Iran. KD, Kopeh Dagh; MKDF, Main Kopeh Dagh Fault system; BQ, Bakharden-Quchan Fault System; M, Meshkan Transfer Zone; DF, Doruneh Fault; B, Binalud; N, Neyshabur. (b) Schematic kinematic model showing the new tectonic configuration in NE Iran based on the data and results presented in this study. WKA, Western Kopeh Dagh-Alborz tectonic domain; EKB, Eastern Kopeh Dagh-Binalud tectonic domain; SH, Shahrud fault system; HM, Hezar Masjed Fault system; CF, Chakaneh Fault System; NF, Neyshabur Fault System, CI, Central Iran. White arrows are GPS velocity vectors in a Eurasia-fixed reference frame (YAZT station - *Tavakoli*, 2007). The inactive NE margin of the Kopeh Dagh is marked by dashed line.

In the present study, the quantitative geological and geomorphic investigations provided the first geological constraints on the Late Cenozoic faulting in the Kopeh Dagh. Examining distribution of post-folding brittle deformation we shown that (1) the strike-slip brittle deformation is not uniformly distributed within the Kopeh Dagh, but it is focalized on a well-defined intracontinental strike-slip fault system (BQFS) which obliquely dissect the belt, and (2) there is no structural evidence supporting regional anticlockwise block rotation within the Central-Eastern Kopeh Dagh. We also show that a significant part (≥25 per cent) of the Late Cenozoic brittle deformation within the Kopeh Dagh is taken up by prominent strike-slip faulting through the MTZ being transferred to the Binalud Mountains. Moreover, the relative northward motion between Central Iran and Eurasia is taken up by right-lateral and oblique-

slip reverse faulting at both sides of the Binalud Mountains. Such a mechanism strongly favors a simple strike-slip faulting mechanism that translates the Central Iran northwards relative to the East (Fig. 2). Moreover, it implies that the original range-parallel boundaries of both the Kopeh Dagh and Binalud deformation domains was affected by the Late Cenozoic strike-slip faulting focalized on few NNW-trending faults (*i.e*., the Chakaneh Fault System). All together, the geological-derived results reveal that the distribution pattern of deformation is easily described as the focalized deformation along major block bounding strike-slip faults, where previous authors (*McKenzie and Jackson*, 1983, 1986; *Hollingsworth et al*., 2006, 2008) predict several rotating 'slats'. With the great benefit of quantitative geological observation we see their model as more complex than is necessary to explain the large-scale kinematics. However, our data and observation propose a simpler model in which Central Iran and the Western Kopeh Dagh are translated northward with respect to Eurasia by focalized intracontinental strike-slip faulting. It is noteworthy that, in an oblique convergence, an along-strike elongation of the deforming zones can occur due to the obliquity of the strike-slip faults with respect to the zone boundaries. Therefore, in the case of the Kopeh Dagh and Binalud, a NW elongation results from right-lateral fault motions along the NNW-trending strike-slip faults. Such a mechanism simply explains material translation in the Western Kopeh Dagh toward the South Caspian Basin, taken up by lateral motion on the Main Kopeh Dagh Fault and the Shahrud fault system. In summary, our data and deduced results do not support the fundamental assumptions for the popular hypothesis of distributed deformation proposed by *McKenzie and Jackson* (1983), and subsequently followed by *Jackson and McKenzie* (1984), *Jackson et al*. (1995), *Jackson et al*. (2002), and *Hollingsworth et al*. (2006, 2008).

The new tectonic configuration presented here is also consistent with the GPS-derived velocity field (*Tavakoli*, 2007) for northeast Iran. All the stations west of the right-lateral strike-slip fault systems (*i.e*., BQFS and Chakaneh Fault System) move Northwest with respect to YAZT station in the eastern side (Eurasia). Their relative overall motion is nearly parallel to the regional strike (NNW) of the fault systems. This suggests a clear NW-ward translation of the western side along the right-lateral strike-slip faults, which are considered as the present-day active boundary between Iran and Eurasia (Fig. 2). Since major strike-slip faults slip under very low resolved shear stress (*e.g*., *Mount and Suppe*, 1987; *Zoback et al*., 1987), these faults can slip in a direction that is not parallel to the relative motion of the microplates or plates they bound. In such a case, the GPS velocity field indicates a direction different from the both directions of convergence and maximum compressional stress axis ($\sigma_1$).

**References**

Afshar Harb, A. (1979), The stratigraphy, tectonics and petroleum geology of the Kopet Dagh region, northeastern Iran, Ph.D. thesis, Petroleum Geology Section, Royal School of

Hollingsworth, J., Jackson, J., Walker, R., Gheitanchi, M. R., and Bolourchi, M. J. (2006), Strike-slip faulting, rotation and along-strike elongation in the Kopeh Dagh Mountains, NE Iran, *Geophys. J. Int., 166*, 1161-1177, doi:10.1111/j.1365-246X.2006.02983.x.

Hollingsworth, J., Jackson, J., Walker, R., and Nazari, H. (2008), Extrusion tectonics and subduction in the eastern South Caspian region since 10 Ma, *Geology*, *36*(10), 763–766, doi:10.1130/G25008A.1.

Jackson, J. A., Haines, A. J., and Holt, W. E. (1995), The accommodation of Arabia–Eurasia plate convergence in Iran, *J. geophys. Res., 100*, 15,205-15,219.

Jackson, J., and McKenzie, D. (1984), Active tectonics of the Alpine-Himalayan Belt between western Turkey and Pakistan, *Geophys. J. R. astr. Soc., 77*(1), 185-264.

Jackson, J., Priestley, K., Allen, M., and Berberian, M. (2002), Active tectonics of the South Caspian Basin, *Geophys. J. Int., 148*, 214–245.

McKenzie, D., and Jackson, J. (1983), The relationship between strain rates, crustal thickening, paleomagnetism, finite strain, and fault movements within a deforming zone, *Earth planet. Sci. Lett., 65*, 182-202.

McKenzie, D., and Jackson, J. (1986), A block model of distributed deformation by faulting, *J. Geol. Soc. London, 143*, 349-353.

Meyer, B., and Le Dortz, K. (2007), Strike-slip kinematics in Central and Eastern Iran: Estimating fault slip-rates averaged over the Holocene, *Tectonics, 26*, TC5009, doi:10.1029/2006TC002073.

Mount, V. S., and Suppe, J. (1987), State of stress near the San Andreas Fault: implications for wrench tectonics, *Geology, 15*, 1143-1146.

Tavakoli, F. (2007), Present-day kinematics of the Zagros and east of Iran faults, Ph.D. thesis, University of Joseph Fourier, France, Grenoble.

Tchalenko, J. S. (1975), Seismicity and structure of the Kopet Dagh (Iran, USSR), *Phil. Trans. R. Soc. Lond., Series A, 278* (1275), 1–28.

Tirrul, R., Bell, I. R., Griffis, R. J., and Camp, V. E. (1983), The Sistan suture zone of eastern Iran, *Geol. Soc. Am. Bull., 94*, 134 – 150.

Vernant, P., et al. (2004), Present-day crustal deformation and plate kinematics in the Middle East constrained by GPS measurements in Iran and northern Oman, *Geophys. J. Int., 157*(1), 381–398, doi:10.1111/j.1365-246X.2004.02222.x.

Walker, R., and Jackson, J. (2004), Active tectonics and Late Cenozoic strain distribution in central and eastern Iran, *Tectonics, 23*, TC5010, doi:10.1029/2003TC001529.

Zoback, M. D., et al., (1987), New evidence on the state of stress on the San Andreas fault system, *Science, 238*, 1105-1111, doi: 10.1126/science.238.4830.1105.

# *Synthèse*

## Tectonique active du Nord-est de l'Iran et accommodation de la convergence entre l'Arabie et l'Eurasie: contribution des chaînes du Kopeh Dagh et du Binalud

### 1. Introduction

A l'échelle de la tectonique des plaques, la déformation de la lithosphère continentale se distribue généralement sur des zones de quelques centaines de kilomètres de large séparant des blocs relativement aséismiques. Cette caractéristique a conduit les géo-scientifiques à élaborer des modèles cinématiques théoriques extrêmes. D'un côté, il a été suggéré que les domaines de déformation active sont constitués de blocs ou microplaques rigides (sans déformation interne) séparés par des failles majeures où l'essentiel de la déformation se localise (*Avouac and Tapponnier*, 1993; *Peltzer and Saucier*, 1996; *Replumaz and Tapponnier*, 2003; *Ryerson et al*., 2006, *Thatcher*, 2007). D'un autre côté, il a aussi été proposé que la déformation soit uniformément répartie, permettant de traiter les continents comme des milieux visqueux se déformant de façon continue (*England and McKenzie*, 1982; *Vilotte et al*., 1982; *McKenzie and Jackson*, 1983; *England and Molnar*, 1997; *Flesch et al*., 2001). Selon cette dernière conception, les failles jouent un rôle relativement mineur et les glissements dans la couche supérieure cassante de la croûte se produisent sur d'innombrables failles dont les taux doivent être relativement identiques. Des articles de synthèse ont discuté les points forts et les limites de chacune de ces deux conceptions de la déformation continentale (*Molnar*, 1988; *England and Jackson*, 1989; *Gordon and Stein*, 1992; *Thatcher*, 1995; *Thatcher*, 2003). Toutefois, le plus important n'est pas finalement de savoir laquelle est correcte mais plutôt d'évaluer comment la déformation réellement observée peut être le plus simplement décrite par un modèle approprié (e.g., *Molnar*, 1988; *Thatcher*, 1995).

La géodynamique de l'Iran est un puzzle compliqué. Coincé entre les plaques Arabie et Eurasienne (Fig. 1), le plateau iranien est constitué d'un ensemble de domaines où les déformations s'expriment sous forme de chaînes de montagnes (Zagros, Alborz et Kopeh Dagh) ou le long de grandes zones décrochantes d'échelle lithosphérique (e.g., le system de faille de Sistan). La limite Nord de ce système de convergence de plaque est marquée par la faille majeure du Kopeh Dagh (MKDF) qui, longue d'environ 350 km, correspond à la frontière tectonique entre l'Iran et la plateforme de Turan. Dans ce contexte général, les chaînes de l'Alborz, du Kopeh Dagh et de l'Allah Dagh et du Binalud jouent un rôle majeur dans l'accommodation ou le transfert de la part de la convergence non prise en compte par les domaines méridionaux.

Ces dix dernières années, de nombreuses études morpho-structurales ont été conduites dans les chaînes du Zagros (*Authemayou et al*., 2005; *Authemayou et al*., 2006; *Authemayou et al*., 2009; *Bayer et al*., 2006; *Regard et al*., 2004; Regard et al., 2005; *Talebian and Jackson* 2004; *Walpersdorf et al*., 2006; *Yamini-Fard et al*., 2007; *Navabpour*, 2009), de l'Alborz (*Axen et al*., 2001; *Jackson et al*., 2002; *Masson et al*., 2006; *Ritz et al*., 2006), et en Iran Central (*Meyer and Le Dortz*, 2007), permettant de progresser considérablement dans la compréhension des processus de déformation active dans ces différentes régions. Au début de ce travail de thèse, le manque de données précises dans le Nord-est Iranien, tant en termes de distribution des déformations actives que de mesures quantitatives, contrastait fortement avec le reste de l'Iran. Les évolutions tectono-stratigraphiques des montagnes du Kopeh Dagh et du Binalud avaient été respectivement examinées par *Afshar Harb* (1979) et *Alavi* (1992). De même, il existait déjà quelques informations de premier ordre puisque la fracturation cénozoïque et le mode d'accommodation de celle-ci avaient été discutés par *Tchalenko* (1975) et *Lyberis and Manby* (1999).

Pourtant, le Nord-est de l'Iran, et plus particulièrement la région du Kopeh-Dagh, a toujours été considéré comme une région clef permettant de d'étayer la fiabilité géologique du modèle de déformation continue (*McKenzie and Jackson*, 1983, 1986; *Jackson and McKenzie*, 1984). Sur la base des données existantes telles que la sismicité instrumentale ou la cartographie régionale des failles, les déformations actives y étaient décrites comme dominées par des chevauchements de direction parallèle à des zones de déformations isolées, c'est-à-dire les chaînes du Kopeh Dagh et de l'Allah Dagh-Binalud, sans zones de décrochements significatifs (e.g., *Jackson and McKenzie*, 1984, *Berberian and Yeats*, 1999; *Hollingsworth et al*., 2006). Selon cette description, les décalages kilométriques cumulés le long des failles de direction NNW dans le Kopeh Dagh décrits par *Tchalenko* (1975) et *Afshar Harb* (1979)

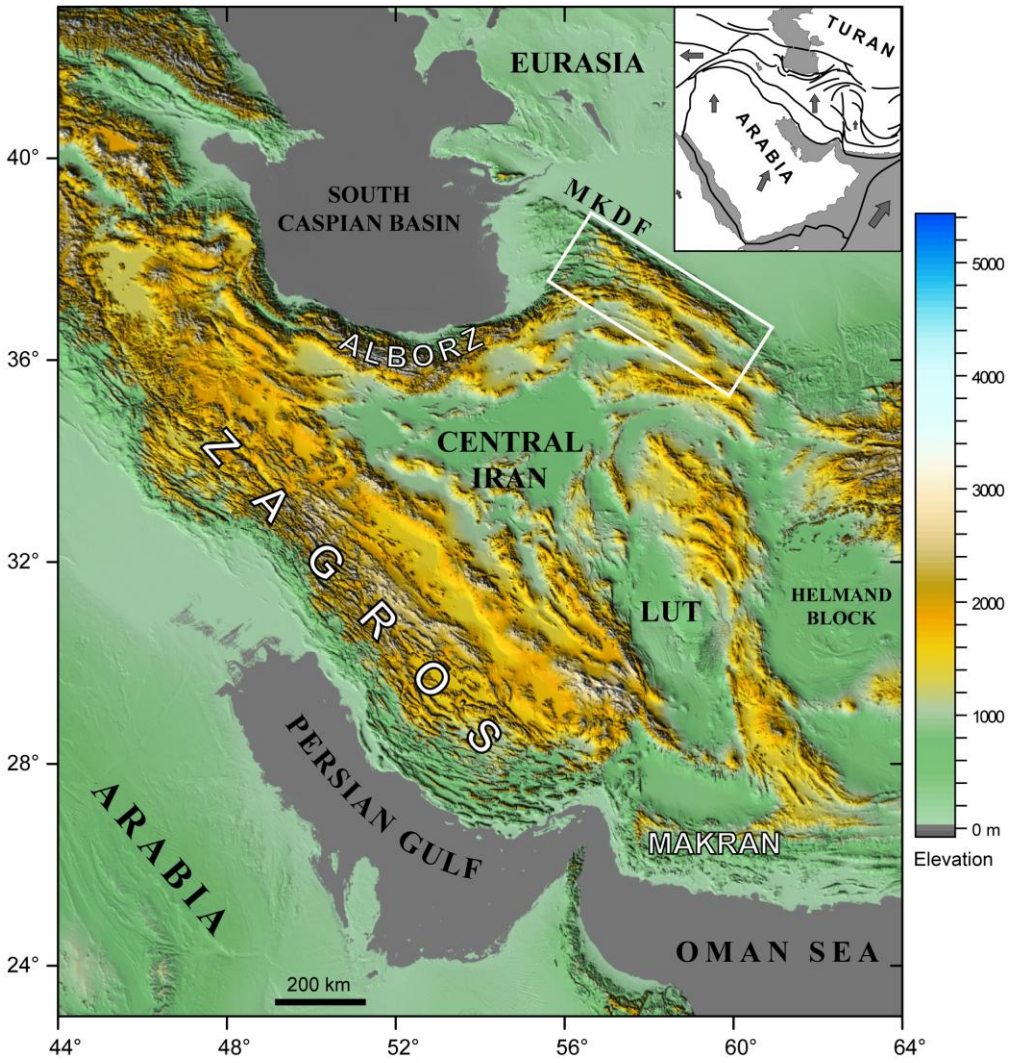


Figure 1. Image de la morphologie générale de l'Iran (topographie numérique, source GTOPO30) localisant les principaux domaines structuraux. Le rectangle blanc localise le secteur étudié et l'encart en haut à droite montre le contexte général de la collision entre les plaques Arabie et Eurasie. Les flèches grises indiquent les mouvements relatifs de ces deux plaques en différents secteurs (d'après *Reilinger et al.,* 2006).

étaient interprétés comme résultant d'un processus de déformation continue au cours duquel une rotation systématique de blocs autour d'axes verticaux conduit les failles décrochantes à devenir parallèles à la direction des chevauchements (*McKenzie and Jackson*, 1983, 1986; *Jackson and McKenzie*, 1984; *Jackson et al*., 2002; *Hollingsworth et al*., 2006). Cependant, en l'absence d'une cartographie détaillées des failles actives et de données suffisamment bien contraintes sur les vitesses de celles-ci, il était difficile d'accepter cette vision des choses et surtout de préciser le modèle le plus en mesure de décrire la cinématique de la déformation active dans le Nord-est Iranien. Malgré tous les efforts fournis lors des études précédentes, le Nord-est Iranien souffrait encore d'un manque de données structurales et cinématiques détaillées et précises et restait comme une zone d'ombre dans le puzzle compliqué de la

convergence oblique entre l'Arabie et l'Eurasie. Cet état de fait était d'autant plus inacceptable que cette région est la seconde de l'Iran en termes de populations et qu'elle a déjà souffert neuf séismes majeurs (M≥ 7) au cours des six derniers siècles (*Tchalenko*, 1975; *Ambraseys and Melville*, 1982; *Berberian and Yeats*, 1999; 2001).

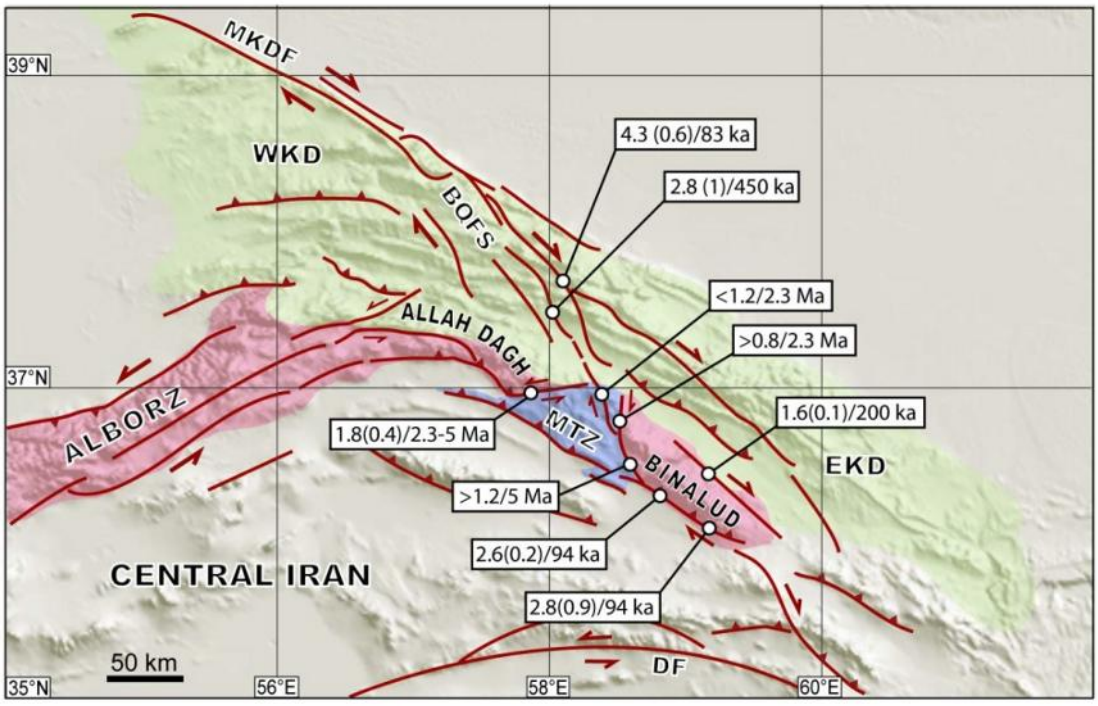


Figure 2. Image de la topographie du Nord-est Iranien (source GTOPO30) indiquant le contexte tectonique et les failles actives majeures. Abréviations: MKDF, Faille Majeure du Kopeh Dagh; BQFS, Système de Failles de Bakharden-Quchan; DF, Faille de Doruneh; MTZ, Zone de Transfert de Meshkan; EKD, Kopeh Dagh Oriental; WKD, Kopeh Dagh Occidental. Les cercles indiquent les sites où des décalages géologiques ou géomorphologiques ont été étudiés. Les rectangles blancs indiquent les vitesses de faille en chaque site étudié (de gauche à droite: valeur, incertitude, âge du marqueur géomorphologique).Pour les sites où l'âge du marqueur n'est qu'estimé, les valeurs de vitesse sont précédées par > ou <.

En s'intéressant aux régions montagneuses du Nord-est Iranien, ce travail de thèse a donc cherché à répondre à une question simple mais fondamentale: Comment est prise en compte la déformation issue de la convergence Arabie-Eurasie dans le Nord-est Iranien? Afin d'y répondre, il a fallu traiter les objectifs principaux suivants. Tout d'abord, il était nécessaire d'établir une cartographie des zones de failles actives qui soit suffisamment détaillée afin de pouvoir en établir la segmentation, leurs relations structurales et leurs possibles interactions. Une fois les principales failles actives identifiées et caractérisées, il était fondamental d'en déterminer les vitesses intégrées sur des échelles de temps de l'ordre de quelques dizaines de milliers d'années à plusieurs millions d'années. Par ailleurs, pour appréhender la cinématique des déformations récentes et actives, il était important de caractériser les états de contraintes responsables des déformations plio-quaternaires observées à l'échelle régionale et d'en

analyser la distribution. Ces différents objectifs scientifiques ont été poursuivis grâce à une combinaison pluridisciplinaire mêlant les approches de la géologie structurale, de la géomorphologie quantitative et de plusieurs méthodes de datation (datation radiométrique par Ar/Ar et nucléides cosmogéniques produits *in situ*). Le travail s'est organisé autour de plusieurs chantiers régionaux. Le premier chantier a concerné la distribution et la vitesse des déformations actives dans les montagnes du Kopeh Dagh (*Shabanian et al*., 2009a). Le second chantier s'est intéressé à l'existence d'une zone de transfert de la déformation depuis les montagnes du Kopeh Dagh vers le massif du Binalud au Sud (*Shabanian et al*., 2009b). Le troisième chantier a permis d'étudier la distribution et la vitesse des déformations actives sur les deux versants du Binalud (résultats non publiés). Enfin, le dernier chantier concernait la détermination des états de contrainte plio-quaternaires à l'échelle régionale dans les montagnes du Kopeh Dagh, de l'Allah Dagh et du Binalud (*Shabanian et al*., 2009c). Par ailleurs, nos investigations nous ont également permis d'écrire un commentaire à propos des modèles cinématiques en vogue pour cette région du monde (*Hollingsworth et al*., 2008; *Siame et al*., 2009).

## 2. Tectonique active dans les montagnes du Kopeh Dagh

Le premier chantier a concerné la distribution et la vitesse des déformations actives dans les montagnes du Kopeh Dagh (*Shabanian et al*., 2009a). Dans le Nord-est Iranien, la chaîne du Kopeh Dagh est bordée par le système de faille majeur du Kopeh Dagh (MKDF) qui forme la frontière tectonique majeure entre l'Iran et la plateforme de Turan (Eurasie). Ce système de failles lithosphériques est intersecté par le système de failles post-Miocène de Bakharden-Quchan (BQFS) qui est constitué par un ensemble de segments décrochants dextres actifs, d'orientation NNW-SSE et qui dissèque les chainons du Kopeh Dagh Central et Oriental (Fig. 2). Ce système de failles s'étend entre la MKDF au Nord et les Binalud au Sud.

En se basant sur la distribution régionale des déplacements cumulés le long des différents segments de failles, nous avons estimé un déplacement total de l'ordre de 35-40 km au travers de la chaîne du Kopeh Dagh. Ce déplacement total se distribue en fait sur au moins onze failles distinctes et nous avons proposé qu'il soit représentative de la déformation décrochante totale due à la convergence entre les plaques Arabie et Eurasie dans cette région de l'Iran. En projetant cette quantité de déformation sur une structure théorique représentative des failles du BQFS (azimut: N28°W, pendage: 75°NE, pitch: 10°), des déplacements d'environ 34 km vers le Nord et d'environ 16 km vers l'Ouest peuvent être estimés pour le Kopeh Dagh

Central et Occidental par rapport à l'Eurasie. Par ailleurs, nos résultats montrent qu'environ 80% de la quantité de déplacement entre l'Iran et l'Eurasie, soit 30±2 km, doivent être pris en compte par le BQFS, suggérant que ce système de failles peut être considéré comme une frontière intercontinentale majeure.

Au sein de ce système de failles, les failles de Quchan et de Baghan sont considérées comme les deux structures principales le long desquelles des décalages cumulés maximum de 15.5±0.5 km et de 9.8±0.2 km peuvent être respectivement mesurés. Le long des ces deux failles régionales, nous avons conduit des investigations morpho-tectoniques de détail alliant l'analyse géomorphologie et géométrique des marqueurs quaternaires décalés (cônes alluviaux) et des datations par la méthode du $^{36}$Cl cosmogénique produit in situ. Ces études de sites ont permis d'établir les premières estimations de vitesses de faille dans le Kopeh Dagh avec 4.3±0.6 mm/an (Faille de Quchan) et 2.8±1.0 mm/an (Faille de Baghan) intégrées sur des intervalles de temps 83±4 ka et un maximum de 450±65 ka. En faisant l'hypothèse que ces vitesses sont demeurées constantes depuis l'activation des failles de Quchan et de Baghan et en appliquant ces vitesses sur les décalages géologiques maximum mesurés le long de ces deux structures, permet de déterminer que l'initiation des déformations décrochantes qui dissèquent les chainons du Kopeh Dagh a débuté il y a environ 4 millions d'années.

### 3. Tectonique active dans la zone de transfert de Meshkan

Le second chantier s'est intéressé à l'existence d'une zone de transfert de la déformation depuis les montagnes du Kopeh Dagh vers celles du Binalud au Sud (*Shabanian et al.*, 2009b). La possibilité d'une connexion structurale entre les montagnes du Kopeh Dagh et celles du Binalud a été évaluée dans des études précédentes (*Tchalenko*, 1975; *Afshar Harb*, 1979; *Hollingsworth et al.*, 2006). Le travail précurseur de *Tchalenko* (1975) a suggéré une possible connexion entre les deux domaines de déformation. Cependant, à cause du manque de connaissance sur d'éventuelles failles de transfert, *Hollingsworth et al*. (2006) ont conclu que la déformation en décrochement dans le Kopeh Dagh n'est pas transférée vers le Sud au-delà de la Vallée d'Atrak. D'un autre côté, les mesures géodésiques réalisées à partir de positionnement GPS suggèrent des déplacements parallèles à la direction de la chaîne de l'ordre de 2 à 4 mm/an (*Masson et al.*, 2007; *Tavakoli*, 2007), ce qui implique que des déformations en décrochement significatives doivent être accommodées de part et d'autre du Binalud. Une telle configuration structurale ne pouvait pas être expliquée par l'état des connaissances dans le Nord-est Iranien.

Nos investigations ont révélé que la déformation en décrochement dans le Kopeh Dagh peut être transférée vers le Sud grâce à une série de structures tectoniques définissant un nouveau domaine de déformation : la zone de transfert de Meshkan (MTZ). Nos résultats démontrent qu'au moins 2 mm/an, soit près de 25% du déplacement relatif vers le Nord de la plaque Arabie par rapport à l'Eurasie, doivent être transférés au travers de la MTZ. Cette déformation est accommodée par des structures décrochantes dextres, d'orientation N-S, localisées entre le système de failles de Neyshabur (Sud du Binalud) et les failles du Kopeh Dagh. L'analyse des déplacements cumulés et enregistrés par des marqueurs géologiques montre que l'initiation de cette déformation en décrochement a débuté il y a environ 5 millions d'années, c'est-à-dire contemporaine de la réorganisation structurale majeure du Kopeh Dagh. Ces observations indiquent que les décrochement du Kopeh Dagh ne s'amortissent pas au niveau de la limite méridionale du Kopeh Dagh (*e.g., Hollingsworth et al*., 2006) et renforcent l'idée que des mécanismes simples de déformation en décrochement soient à l'œuvre dans la région nord-orientale de la collision entre les plaques Arabie et Eurasie.

## 4. Tectonique active le long des versants Nord et Sud du Massif du Binalud

Le troisième chantier a permis d'étudier la distribution et la vitesse des déformations actives sur les deux versants du Binalud (résultats non publiés). Sur les deux versants du massif du Binalud, nos investigations révèlent différents aspects de l'évolution du massif en termes de géomorphologie et de tectonique. Cette investigation a été conduite plus particulièrement le long de sept segments de failles individuels appartenant aux systèmes de Neyshabur (NFS), le long du versant Sud, et de Mashhad (MFS), le long du versant Nord. Grâce à la méthode de datation par âge d'exposition aux rayons cosmiques ($^{10}$Be produit *in situ*), trois périodes de fin d'aggradation alluviale ont pu être datées régionalement à 5.3±1.1 ka (Q1), 94±5 ka (Q3), et 200±14 ka ($S_3$). Ces différentes surfaces étant affectées par les failles de Neyshabur et de Mashhad, ce cadre chronologique permet de préciser les vitesses tectoniques associées. Pour le NSF, les vitesses moyennes de déplacement vertical (2.4±0.2 mm/an) et horizontal (2.7±0.8 mm/an) sont déterminées en reconstruisant les décalages cumulés enregistrés par la surface alluviale $Q_3$ (Fig. 2). Ces vitesses verticale et horizontale nous permettent de déterminer une vitesse tectonique totale de 3.6±1.2 mm/an, intégrée sur les derniers 100 ka le long du flanc Sud du Binalud. Pour le MFS, les

déplacements en décrochements cumulés par la surface $S_3$ donnent une vitesse tectonique moyenne de 1.6±0.1 mm/an et donc pour le versant Nord du Binalud (Fig. 2).

Le long des versants méridionaux et septentrionaux du Massif du Binalud, la distribution des quantités de décalages cumulés implique que (1) la déformation en décrochement a été prise en compte pendant le Pléistocène par les systèmes de failles de Neyshabur et de Mashhad à une vitesse long-terme d'environ 4 mm/an et (2) que la vitesse de soulèvement du flanc Sud du massif est d'environ 2.4 mm/an. Les composantes horizontale et verticale de déplacement le long des deux versants du massif impliquent également un mouvement vers le Nord à environ 4.5 mm/an et un mouvement vers l'Ouest à environ 2 mm/an de l'Iran Central à l'ouest par rapport au Kopeh Dagh Orientale à l'est. De plus, la combinaison de nos observations géologiques avec les résultats d'une analyse quantitative de l'hypsométrie des bassins versants qui drainent les deux versants du massif suggère que la localisation du front de déformation active migre vers le sud-ouest à mesure que de nouvelles failles sont créées vers le bassin.

## 5. Etats de contraintes pendant le Plio-Quaternaire dans le Nord-est Iranien

Dans le Nord-est Iranien, les analyses cinématiques réalisées pendant ce travail indiquent que la convergence est accommodée par du décrochement le long de structures senestres d'orientation NE-SW et dextres d'orientation NNW-SSE, ainsi que par des failles d'orientation E-W purement inverse ou à glissement oblique. Cet assemblage structural est impliqué dans un champ de contraintes actuel mécaniquement compatible et homogène. Le mécanisme en failles inverses est clairement observé le long de la limite méridionale des domaines de déformation de l'Allah Dagh et du Massif du Binalud. La majorité des régimes en décrochements sont observés le long des structures décrochantes majeures qui dissèquent les chaînons du Kopeh Dagh et traversent ceux de l'Allah Dagh au travers de la zone de transfert de Meshkan. Pour tous les états de contraintes (anciens, intermédiaires et modernes), la direction de la contrainte principale maximum ($\sigma_1$) obtenue à partir des inversions des populations de failles mesurées sur le terrain est spatialement cohérente au travers des différents domaines tectoniques de la zone d'étude. Le caractère transpressif des états de contraintes anciens (<5 Ma) et modernes explique la compatibilité entre la fracturation inverse et la fracturation décrochante. L'homogénéité des états de contraintes n'est par contre pas en faveur d'un quelconque partitionnement entre les failles. Les différents types de mouvements observés sur les failles ne résultent que de l'orientation des failles par rapport au champ de

contraintes à l'échelle régionale. Ces champs de contraintes homogènes avec une contrainte principale maximum horizontale d'orientation constante ($\sigma_1$) indiquent que des rotations de blocs systématiques ne peuvent avoir lieu dans le Kopeh Dagh, l'Allah Dagh et le Massif du Binalud pendant le Plio-Quaternaire. Des perturbations locales de ces directions ont été observées mais elles résultent de rotations de blocs à l'intérieur des zones de failles et non de ces zones elles-mêmes. La plupart des états de contraintes modernes qui ont été déterminés indiquent des régimes décrochants alignés entre le Massif du Binalud et les montagnes du Kopeh Dagh, le long de la Faille de Chakaneh, renforçant l'idée d'une continuité structurale en décrochement dextre entre ces deux domaines de déformation.

## 6. Discussion

A une échelle régionale, les données et résultats issus de ce travail doctoral fournissent des contraintes nouvelles et fondamentales sur les taux et la distribution des déformations quaternaires et permettent d'élaborer une proposition nouvelle de configuration tectonique pour la bordure Nord-orientale de la collision entre les plaques Arabie et Eurasie. Le premier modèle cinématique à être proposé pour cette région du monde est celui de *McKenzie and Jackson* (1983, 1986) où des mécanismes continus sont censés décrire de façon appropriée les déformations instantanées du Nord-est Iranien. Dans ce contexte, le Kopeh Dagh est vu comme un exemple parfait ayant les caractéristiques attendues, c'est-à-dire de grands blocs bordés par des failles recoupant à l'emporte-pièce la chaîne et pivotant autour de pivots, un sur chaque plaque tectonique. A partir d'un modèle similaire, *Jackson et al*. (2002) ont proposé que les failles décrochantes qui traversent le Kopeh Dagh avec une direction oblique à la chaîne pivotent de façon antihoraire autour d'axes verticaux jusqu'à devenir parallèles à la direction de la chaîne à mesure que la déformation progresse (voir aussi *Jackson and McKenzie*, 1984; *Jackson et al*., 1995). Par la suite, cette séduisante hypothèse est devenue une sorte de dogme pour expliquer la cinématique des déformations dans le Kopet Dagh. *Hollingsworth et al*. (2006) ont ainsi proposé un modèle de blocs en rotation pour expliquer les 35-40 km de décalage dextre total cumulé le long du système de failles de Bakharden-Quchan. Selon eux, le mouvement de l'Iran Central vers la plaque de Turan au Nord est accommodé (1) par des chevauchements dominants à la limite méridionale du Kopet Dagh (au nord des vallées de l'Atrak et de Kashafrud), sans mouvements décrochants significatifs, et (2) par des rotations antihoraires de blocs autour de pivots verticaux disséminés dans le Kopet Dagh. Tous les modèles cités précédemment sont dérivés sur celui du continuum de

déformation par *McKenzie and Jackson* (1983, 1986) et mettent en relation la déformation finie et les mouvements sur les failles dans une zone en déformation soumise à convergence oblique. Les hypothèses fondamentales de ces modèles sont que la déformation doit être répartie uniformément (déformation homogène) et que les frontières rigides des zones de déformation doivent rester constantes pendant la déformation. Selon ce point de vue, les failles décrochantes obliques sont donc des structures « passives » confinées aux limites de blocs. En conséquence, les déformations observées le long des ces failles sont contrôlées par des contraintes cinématiques associées à la déformation finie.

Dans le cadre de ce travail doctoral, les investigations géologiques et géomorphologiques ont donné les premières vraies contraintes sur la fracturation fini-Cénozoïque et Quaternaire dans le Kopeh Dagh et secteurs avoisinants. En examinant la distribution de la déformation postérieure aux plissements du Kopeh Dagh, nous avons montré que (1) la déformation cassante en décrochement n'est pas distribuée uniformément au sein de la chaîne, mais au contraire qu'elle est concentrée sur un système décrochant majeur (BQFS) qui la dissèquent obliquement, et (2) qu'il n'y a pas d'évidence structurale supportant une quelconque rotation antihoraire de blocs rigides dans le Kopet Dagh Central et Oriental (*Shabanian et al*., 2009a). Par ailleurs, nous montrons également qu'une part significative (≥25 pourcent) de la déformation cassante fini-Cénozoïque est accommodée dans le Kopeh Dagh par une zone de transfert tectonique, jamais décrite précédemment, et constituée par des structures décrochantes connectant les failles du Kopeh Dagh à celles qui bordent le sud du Massif du Binalud (*Shabanian et al*., 2009b). Par ailleurs, le mouvement relatif vers le Nord de l'Iran Central par rapport à l'Eurasie est pris en compte par des décrochements dextres et des failles inverses à glissement oblique localisés de part et d'autres du Massif du Binalud. De telles observations privilégient fortement un mécanisme simple de décrochements régionaux qui translatent l'Iran Central vers le Nord par rapport à l'Iran Oriental (Fig. 3). Dans un tel contexte, les frontières originales du Kopeh Dagh et du Massif du Binalud ont été affectées par de la déformation décrochante fini-Cénozoïque localisée sur quelques structures d'orientation NNW-SSE (comme le système de failles de Chakaneh).

Pris dans leur ensemble, les résultats de ce travail doctoral révèlent que la distribution régionale des déformations peut facilement être décrite comme étant concentrée sur certaines structures majeures là où les auteurs précédents (*McKenzie and Jackson*, 1983, 1986; *Hollingsworth et al*., 2006; *Hollingsworth et al*., 2008) prédisaient des rotations de blocs. A la lueur de nos investigations, les modèles précédents semblent en fait plus compliqués que nécessaire pour expliquer la cinématique régionale du Nord-est Iranien. En fait, nos données

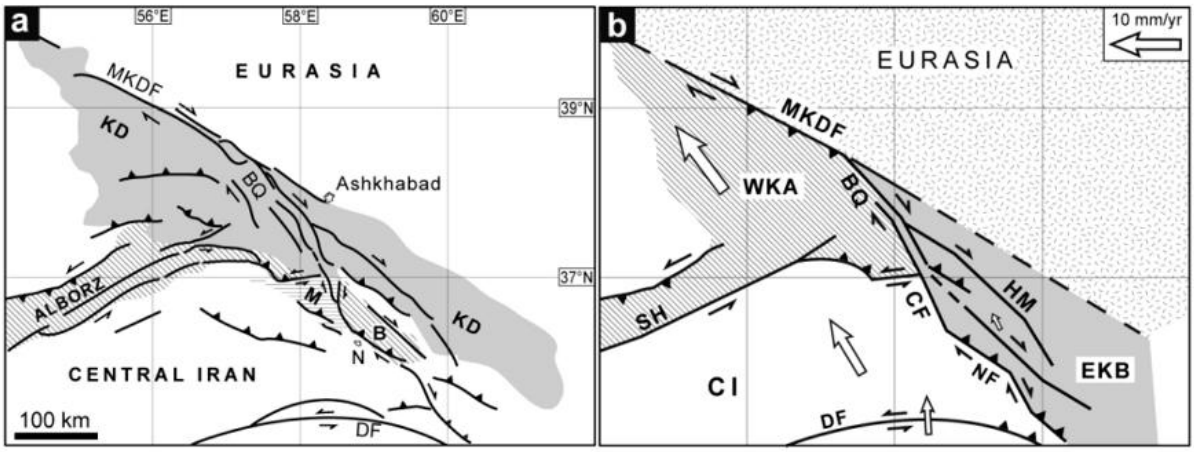


Figure 3. (a) Carte simplifiée des failles actives et domaines tectoniques principaux du Nord-est Iranien. Abréviations: KD, Kopeh Dagh; MKDF, Faille Majeure du Kopeh Dagh; BQ, Faille de Bakharden-Quchan; M, Zone de Transfert de Meshkan; DF, Faille de Doruneh; B, Massif du Binalud; N, Neyshabur. (b) Modèle cinématique schématique montrant la nouvelle configuration tectonique du Nord-est Iranien sur la base des données, résultats et interprétations de cette étude. Abréviations: WKA, Kopeh Dagh Occidental-Alborz; EKD, Kopeh Dagh Oriental-Massif du Binalud; SH, Système de Faille de Shahrud; HM, Système de Failles de Hezar Masjed; CF, Faille de Chakaneh; NF, Faille de Neyshabur; CI, Iran Central. Les flèches blanches correspondent aux vecteurs de vitesse GPS déterminés dans le système de référence « Eurasie fixe » (Station de YAZT - *Tavakoli*, 2007). La marge Nord-orientale inactive du Kopeh Dagh est indiquée par une ligne en pointillés.

et observations suggèrent un modèle beaucoup plus simple dans lequel l'Iran Central et le Kopeh Dagh Occidental sont translatés vers le Nord par rapport à l'Eurasie selon de grands décrochements intracontinentaux (Fig. 3). Il est notable que dans le cadre d'une convergence oblique comme celle de l'Arabie par rapport à l'Eurasie, une élongation longitudinale des zones de déformation puisse avoir lieu du fait même de l'obliquité des failles décrochantes par rapport à la direction des limites de ces domaines. Dans le cas du Kopeh Dagh et du Binalud, une élongation NW-SE résulte des déplacements dextres le long de structures décrochantes d'orientation NNW-SSE. Un tel mécanisme explique simplement la translation de matière dans le Kopeh Dagh Occidental vers le bassin de la Mer Caspienne Méridionale, accommodée par des déplacements latéraux localisés sur la MKDF et le système de failles de Shahrud (Fig. 3). En conclusion, nos données et les interprétations qui en résultent ne permettent pas d'étayer les hypothèses fondamentales attenantes à l'hypothèse de déformation distribuée propose par *McKenzie and Jackson* (1983) et ensuite relayée par *Jackson and McKenzie* (1984), *Jackson et al*. (1995), *Jackson et al*. (2002), et *Hollingsworth et al*. (2006, 2008).

La nouvelle configuration tectonique proposée dans ce travail est aussi cohérente avec le champ de vitesse dérivé des données géodésiques GPS pour le Nord-est Iranien (*Tavakoli*,

2007). Toutes les stations situées à l'Ouest des systèmes de failles dextres (BQFS et Faille de Chakaneh) se déplacent vers le Nord-ouest par rapport à la station YAZT située à l'Est sur la plaque Eurasienne. Leur déplacement est presque parallèle à la direction régionale (NNW-SSE) des systèmes de failles. Cela suggère clairement une translation vers le Nord-ouest du côté occidental le long de failles décrochantes dextres qui peuvent donc être considérées comme la limite de plaque actuelle entre l'Iran et l'Eurasie (Fig. 3).

**Références bibliographiques issues du travail doctoral**

Shabanian, E., Siame, L.L., Bellier, O., Abbassi, M., Benedetti, L. (2009a), Quaternary slip rates along the northeastern boundary of the Arabia-Eurasia collision zone (Kopeh Dagh Mountains, Northeast Iran), *Geophys. J. Int., 178,* 1055-1077, doi:10.1111/j.1365-246X.2009.04183.x.

Shabanian, E., Bellier, O., Siame, L.L., Abbassi, M., Ghassemi, H., Arnaud, N., Cochemé, J.J. (2009b), New tectonic configuration in NE Iran: active strike-slip faulting between the Kopeh Dagh and Binalud mountains. *Tectonics, 28,* TC5002, doi:10.1029/2008TC002444.

Shabanian, E., Bellier, O., Abbassi, M., Siame, L.L., Farbod, Y. (2009c), Plio-Quaternary stress states in NE Iran: Kopeh Dagh and Allah Dagh-Binalud mountains, *Tectonophysics, sous presse,* doi:10.1016/j.tecto.2009.10.022.

Siame, L.L., Shabanian, E., Bellier, O. (2009), Comment to "Extrusion tectonics and subduction in the eastern South Caspian region since 10 Ma" by Hollingsworth et al. (2008). *Geology, sous presse*.

**Autres références bibliographiques**

Afshar Harb, A. (1979), The stratigraphy, tectonics and petroleum geology of the Kopet Dagh region, northeastern Iran, Ph.D. thesis, Petroleum Geology Section, Royal School of Mines, Imperial College of Science and Technology, London.

Alavi, M. (1992), Thrust tectonics of the Binalood region, NE Iran, *Tectonics, 11*(2), 360-370.

Ambraseys, N., and Melville, C. (1982), *A History of Persian Earthquakes*, Cambridge University Press, Cambridge, UK.

Authemayou, C., Bellier, O., Chardon, D., Benedetti, L., Malekzade, Z., Claude, C., Angeletti, B., Shabanian, E., and Abbassi, M. R. (2009), Quaternary slip-rates of the Kazerun and the Main Recent Faults: active strike-slip partitioning in the Zagros fold-and-thrust belt, *Geophys. J. Int., 178,* 524-540, doi: 10.1111/j.1365-246X.2009.04191.x.

Authemayou, C., Bellier, O., Chardon, D., Malekzade, Z. and Abbassi, M. (2005), Role of the Kazerun fault system in active deformation of the Zagros fold and-thrust belt (Iran), *C. R. Geosci., 337,* 539–545.

Authemayou, C., Chardon, D., Bellier, O., Malekzade, Z., Shabanian, E., and Abbassi, M. (2006), Late Cenozoic partitioning of oblique plate convergence in the Zagros fold-and-thrust belt (Iran), *Tectonics, 25,* TC3002, doi:10.1029/2005TCOO1860.

Avouac, J.-P., and Tapponnier P., (1993), Kinematic model of active deformation in central Asia, *Geophys. Res. Lett., 20*, 895-898.

Axen, G. J., Lam, P. S., Grove, M., Stockli, D. F., and Hassanzadeh J. (2001), Exhumation of the west-central Alborz Mountains, Iran, Caspian subsidence, and collision-related tectonics, *Geology, 29*(6), 559–562.

Bayer, R., Chéry, J., Tatar, M., Vernant, Ph., Abbassi, M., Masson, F., Nilforoushan, F., Doerflinger, E., Regard, V., and Bellier, O. (2006), Active deformation in Zagros-Makran transition zone inferred from GPS measurements, *Geophys. J. Int., 165*(1), 373–381. doi:10.1111/j.1365-246X.2006.02879.x.

Berberian, M., and Yeats, R. (1999), Patterns of historical earthquake rupture in the Iranian Plateau, *Bull. Seism. Soc. Am., 89*, 120–139.

Berberian, M., and Yeats, R. (2001), Contribution of archaeological data to studies of earthquake history in the Iranian Plateau, *J. Structural Geology, 23*, 563-584.

England, P. C., and Jackson, J. A. (1989), Active deformation of the continents, *Annu. Rev. Earth Planet. Sci., 17*, 197-226

England, P., and McKenzie, D. (1982), A thin viscous sheet for continental deformation, *Geophys. J.R. Astron. Soc., 70*, 295-321.

England, P., and Molnar, P. (1997), Active deformation of Asia: From kinematics to dynamics, *Science, 278*, 647-650.

Flesch, L. M., Haines, A. J., and Holt, W. E. (2001), Dynamics of the India-Eurasia collision zone, *J. Geophys. Res., 106*, 16,435-16,460.

Gordon, R. G., and Stein, S. (1992), Global tectonics and space geodesy, *Science, 256*, 333-342.

Hollingsworth, J., Jackson, J., Walker, R., and Nazari, H. (2008), Extrusion tectonics and subduction in the eastern South Caspian region since 10 Ma, *Geology, 36*(10), 763–766, doi:10.1130/G25008A.1.

Hollingsworth, J., Jackson, J., Walker, R., Gheitanchi, M. R., and Bolourchi, M. J. (2006), Strike-slip faulting, rotation and along-strike elongation in the Kopeh Dagh Mountains, NE Iran, *Geophys. J. Int., 166*, 1161-1177, doi:10.1111/j.1365-246X.2006.02983.x.

Jackson, J., and McKenzie, D. (1984), Active tectonics of the Alpine-Himalayan Belt between western Turkey and Pakistan, *Geophys. J. R. astr. Soc., 77*(1), 185-264.

Jackson, J., Priestley, K., Allen, M., and Berberian, M. (2002), Active tectonics of the South Caspian Basin, *Geophys. J. Int., 148*, 214–245.

Lyberis, N., and Manby, G. (1999), Oblique to orthogonal convergence across the Turan block in the post-Miocene, *Am. Assoc. Petrol. Geol. Bull., 83*(7), 1135-1160.

Masson, F., Anvari, M., Djamour, Y., Walpersdorf, A., Tavakoli, F., Daignières, M., Nankali, H., and Van Gorp, S. (2007), Large-scale velocity field and strain tensor in Iran inferred from GPS measurements: new insight for the present-day deformation pattern within NE Iran, *Geophys. J. Int., 170*, 436–440. doi:10.1111/j.1365-246X.2007.03477.x.

Masson, F., Djamour, Y., Vangorp, S., Chéry, J., Tavakoli, F., Tatar M., and Nankali, H. (2006), Extension in NW Iran inferred from GPS enlightens the behavior of the south Caspian basin, *Earth Planet. Sci. Lett., 252*, 180–188.

McKenzie, D., and Jackson, J. (1983), The relationship between strain rates, crustal thickening, paleomagnetism, finite strain, and fault movements within a deforming zone, *Earth planet. Sci. Lett., 65*, 182-202.

McKenzie, D., and Jackson, J. (1986), A block model of distributed deformation by faulting, *J. Geol. Soc. London, 143*, 349-353.

Meyer, B., and Le Dortz, K. (2007), Strike-slip kinematics in Central and Eastern Iran: Estimating fault slip-rates averaged over the Holocene, *Tectonics, 26*, TC5009, doi:10.1029/2006TC002073.

Molnar, P. (1988), Continental tectonics in the aftermath of plate tectonics, *Nature, 335*, 131-137.

Navabpour, P. (2009), Brittle tectonics and palaeostress reconstructions in the Zagros: passive palaeo-margin and continental collision, Ph.D. thesis, University of Nice-Sophia Antipolis, France.

Peltzer, G., and Saucier, F. (1996), Present-day kinematics of Asia derived from geologic fault rates, *J. Geophys. Res., 101*, 27,943-27,956.

Regard, V., Bellier, O., Thomas, J.-C., Abbassi, M. R., Mercier, J., Shabanian, E., Feghhi, K., and Soleymani, S. (2004), The accommodation of Arabia-Eurasia convergence in the Zagros-Makran transfer zone, SE Iran: a transition between collision and subduction through a young deforming system, *Tectonics, 23*, TC4007, doi:10.1029/2003TC001599.

Regard, V., Bellier, O., Thomas, J.-C., Bourlès, D., Bonnet, S., Abbassi, M. R., Braucher, R., Mercier, J., Shabanian, E., Soleymani, S., and Feghhi, K. (2005), Cumulative right-lateral fault slip rate across the Zagros–Makran transfer zone: role of the Minab–Zendan fault system in accommodating Arabia–Eurasia convergence in southeast Iran, *Geophys. J. Int., 162*, 177–203, doi:10.1111/j.1365-246X.2005.02558.x.

Reilinger, R., et al. (2006), GPS constraints on continental deformation in the Africa-Arabia-Eurasia continental collision zone and implications for the dynamics of plate interactions, *J. Geophys. Res., 111*, B05411, doi:10.1029/2005JB004051.

Replumaz, A., and Tapponnier, P. (2003), Reconstruction of the deformed collision zone between India and Asia by backward motion of lithospheric blocks, *J. Geophys. Res., 108*(B6), 2285, doi:10.1029/2001JB000661.

Ritz, J.-F., Nazari, H., Ghassemi, A., Salamati, R., Shafei, A., Solaymani, S., and Vernant, P. (2006), Active transtension inside Central Alborz: A new insight into northern Iran–southern Caspian geodynamics, *Geology, 34*(6), 477–480, doi:10.1130/G22319.1.

Ryerson, F. J., et al. (2006), Applications of morphochronology to the active tectonics of Tibet, *Spec. Pap. Geol. Soc., 415*.

Talebian, M. and Jackson, J. (2004), A reappraisal of earthquake focal mechanisms and active shortening in the Zagros mountains of Iran, *Geophys. J. Int., 156*(3), 506–526.

Tavakoli, F. (2007), Present-day kinematics of the Zagros and east of Iran faults, Ph.D. thesis, University of Joseph Fourier, France, Grenoble.

Tchalenko, J. S. (1975), Seismicity and structure of the Kopet Dagh (Iran, USSR), *Phil. Trans. R. Soc. Lond., Series A, 278* (1275), 1–28.

Thatcher, W. (1995), Microplate versus continuum descriptions of active tectonic deformation, *J. Geophys. Res., 100*, 3885-3894.

Thatcher, W. (2003), GPS constraints on the kinematics of continental deformation, *Int. Geol. Rev., 45*, 191-212.

Thatcher, W. (2007), Microplate model for the present-day deformation of Tibet, *J. Geophys. Res., 112*, B01401, doi:10.1029/2005JB004244.

Vilotte, J. P., Daignieres, M., and Madariaga, R. (1982), Numerical modeling of intraplate deformation: Simple mechanical models of continental collision, *J. Geophys. Res., 87*, 10,709-10,728.

Walpersdorf, A., Hatzfeld, D., Nankali, H., Tavakoli, F., Nilforoushan, F., Tatar, M., Vernant, P., Chéry, J., and Masson, F. (2006), Difference in the GPS deformation pattern of North and Central Zagros (Iran), *Geophys. J. Int., 167*(3), 1077-1088. doi:10.1111/j.1365-246X.2006.03147.x.

Yamini-Fard, F., Hatzfeld, D., Farahbod, A.M., Paul, A., and Mokhtari, M. (2007), The diffuse transition between the Zagros continental collision and the Makran oceanic subduction (Iran): microearthquake seismicity and crustal structure, *Geophys. J. Int., 170*(1), 182–194.

# *References*


1. Afshar Harb, A. (1979), The stratigraphy, tectonics and petroleum geology of the Kopet Dagh region, northeastern Iran, Ph.D. thesis, Petroleum Geology Section, Royal School of Mines, Imperial College of Science and Technology, London.
2. Afshar Harb, A. (1982), Geological quadrangle map of Iran no. K3 (Darreh Gaz sheet), scale 1:250 000, Geological Survey of Iran.
3. Afshar Harb, A., Bolourchi, M., and Mehr Parto, M. (1987), Geological quadrangle map of Iran no. J5 (Bojnurd sheet), scale 1:250 000, Geological Survey of Iran.
4. Afshar Harb, A., Soheili, B. M., and Valeh, C. N. (1980), Geological quadrangle map of Iran no. I3 (Kuh-e Kurkhud sheet), scale 1:250 000, Geological Survey of Iran.
5. Aghanabati, A. (1986), Geological quadrangle map of Iran, Mashhad sheet, scale 1:250,000, Geol. Survey of Iran, Tehran.
6. Alavi, M. (1992), Thrust tectonics of the Binalood region, NE Iran, *Tectonics, 11*(2), 360-370.
7. Allen, M. B., Jones, S., Ismail-Zadeh, A., Simmons, M., and Anderson, L. (2002), Onset of subduction as the cause of rapid Pliocene-Quaternary subsidence in the South Caspian Basin, *Geology, 30*(9), 775-778, doi:10.1130/0091-7613(2002)030<0775.
8. Allen, M., Jackson, J., and Walker, R. (2004), Late Cenozoic reorganization of the Arabia-Eurasia collision and the comparison of short-term and long-term deformation rates, *Tectonics, 23*, TC2008, doi:10.1029/2003TC00153.
9. Allen, M. B., Blanc, E. J.-P., Walker, R., Jackson, J., Talebian, M., and Ghassemi, M. R. (2006), Contrasting styles of convergence in the Arabia-Eurasia collision: Why escape tectonics does not occur in Iran, in Postcollisional tectonics and magmatism in the Mediterranean region and Asia, pp. 579–589, ed. Dilek, Y. & Pavlides, S., *Geol. Soc. Am. Special Paper, 409*. doi:10.1130/2006.2409(26).
10. Ambraseys, N., and Melville, C. (1982), *A History of Persian Earthquakes*, Cambridge University Press, Cambridge, UK.
11. Amini, B., and Khan-Nazer, N. H. (2000), Geological map of Iran, Series 7563 (Mashkan sheet), scale 1:100 000, Geological Survey of Iran, Tehran.
12. Amurskiy, G. I. (1971), The deep structure of the Kopetdagh, Geotectonics, 1, 34-40. (Engl. Transl.).
13. Angelier, J. (1979), Determination of the mean principal directions of stresses for a given fault population, *Tectonophysics 56*, 17-26.
14. Angelier, J. (1984), Tectonic analysis of fault slip data sets, *J. Geophys. Res, 89*(B7), 5835-5848.
15. Angelier, J. (1990), Inversion of field data in fault tectonics to obtain the regional stress-part II: A new rapid direct inversion method by analytical means, *Geophys. J. Int., 103*, 363-376.

16. Angelier, J., Dumont, J. F., Karamanderesi, H., Poisson, A., Simsek, S., and Uysal, S. (1981), Analyses of fault mechanisms and expansion of southwestern Anatolia since the Late Miocene, *Tectonophysics, 75*, T1-T9.

17. Authemayou, C., Bellier, O., Chardon, D., Malekzade, Z. and Abbassi, M. (2005), Role of the Kazerun fault system in active deformation of the Zagros fold and-thrust belt (Iran), *C. R. Geosci., 337*, 539–545.

18. Authemayou, C., Chardon, D., Bellier, O., Malekzade, Z., Shabanian, E., and Abbassi, M. (2006), Late Cenozoic partitioning of oblique plate convergence in the Zagros fold-and-thrust belt (Iran), *Tectonics, 25*, TC3002, doi:10.1029/2005TCOO1860.

19. Authemayou, C., Bellier, O., Chardon, D., Benedetti, L., Malekzade, Z., Claude, C., Angeletti, B., Shabanian, E., and Abbassi, M. R. (2009), Quaternary slip-rates of the Kazerun and the Main Recent Faults: active strike-slip partitioning in the Zagros fold-and-thrust belt, *Geophys. J. Int., 178*, 524-540, doi:10.1111/j.1365-246X.2009.04191.x.

20. Avouac, J.-P., and Tapponnier P., (1993), Kinematic model of active deformation in central Asia, *Geophys. Res. Lett., 20*, 895-898.

21. Axen, G. J., Lam, P. S., Grove, M., Stockli, D. F., and Hassanzadeh J. (2001), Exhumation of the west-central Alborz Mountains, Iran, Caspian subsidence, and collision-related tectonics, *Geology, 29*(6), 559–562.

22. Bayer, R., Chéry, J., Tatar, M., Vernant, Ph., Abbassi, M., Masson, F., Nilforoushan, F., Doerflinger, E., Regard, V., and Bellier, O. (2006), Active deformation in Zagros-Makran transition zone inferred from GPS measurements, *Geophys. J. Int., 165*(1), 373–381. doi:10.1111/j.1365-246X.2006.02879.x.

23. Bellier, O., and Zoback, M. L. (1995), Recent state of stress change in the Walker Lane zone, western Basin and Range province, United States, *Tectonics, 14*, 564–593.

24. Bellier, O., Dumont, J. F., Sébrier, M., and Mercier, J. L. (1991), Geological constraints on the kinematics and fault-plane solution of the Quiches fault zone: reactivated during the 10 November 1946 Ancash earthquake, Northern Peru, *Bull. Seis. Soc. Am., 8*(2), 468-490.

25. Bellier, O., Över, S., Poisson, A., and Andrieux, J. (1997), Recent temporal change in the stress state and modern stress field along North Anatolian Fault Zone (Turkey), *Geophys. J. Int., 131*, 61-86.

26. Berberian, M., and Yeats, R. (1999), Patterns of historical earthquake rupture in the Iranian Plateau, *Bull. Seism. Soc. Am., 89*, 120–139.

27. Berberian, M., and Yeats, R. (2001), Contribution of archaeological data to studies of earthquake history in the Iranian Plateau, *J. Structural Geology, 23*, 563-584.

28. Bierman, P. R., 1994. Using *in situ* produced cosmogenic isotopes to estimate rates of landscape evolution: A review from the geomorphic perspective, *J. Geophys. Res., 99*(B7), 13885-13896.

29. Bierman, P. R., Gillespie, A. R., Caffee, M. W., and Elmore, D. (1995), Estimating erosion rates and exposure ages with $^{36}$Cl produced by neutron activation, *Geochimica Cosmochimica Acta, 59*, 3779–3798.

30. Bozkurt, E. (2001), Neotectonics of Turkey – A synthesis, *Geodinamica Acta, 14*(1), 3-30. doi:10.1016/S0985-3111(01)01066-X.

31. Bullard, T. F., and Lettis, W. R. (1993), Quaternary fold deformation associated with blind thrust faulting, Los Angeles basin: California, *Journal of Geophysical Research, 98*, p. 8349–8369.

32. Carey, E. (1979), Recherche des directions principales de contraintes associées au jeu d'une population de failles, *Rev. Geol. Dyn. Geogr. Phys., 21*, 57-66.

33. Carey, E., and Brunier, B. (1974), Analyse théorique et numérique d'un modèle mécanique élémentaire appliqué à l'étude d'une population de failles, *C. R. Acad. Sci., Ser. D, 279*, 891-894.

34. Carey-Gailhardis, E., and Mercier, J.-L. (1987), A numerical method for determining the state of stress using focal mechanism of earthquake populations: Application to Tibetan teleseisms and microseismicity of southern Peru, *Earth Planet. Sci. Lett., 82*, 165-179.

35. Carey-Gailhardis, E., and Mercier, J. L. (1992), Regional state of stress, fault kinematics and adjustments of blocks in a fractured body of rocks: application to the microseismicity of the Rhine graben, *Journal of structural geology, 14*(8/9), 1007-1017.

36. Carey-Gailhardis, E., and Vergely, P. (1992), Graphical analysis of fault kinematics and focal mechanisms of earthquakes in term of stress; the right dihedra method, use and pitfalls, *Annales Tectonics, VI*(1), 3-9.

37. Copley, A. and Jackson, J. (2006), Active tectonics of the Turkish-Iranian Plateau, *Tectonics, 25*, TC6006, doi:10.1029/2005TC001906.

38. Daëron, M., Benedetti, L., Tapponnier, P., Sursock, A. and Finkel, R. C. (2004), Constraints on the post ~25-ka slip rate of the Yammoûneh fault (Lebanon) using in situ cosmogenic $^{36}$Cl dating of offset limestone-clast fans, *Earth Planet. Sci. Lett., 227*, 105-119.

39. Davis, D., Suppe, J., and Dahlen, F. (1983), Mechanics of Fold-and-Thrust Belts and Accretionary Wedges, *J. Geophys. Res., 88*(B2), 1153-1172.

40. Deino, A. and Potts, R. (1992), Age-probability spectra from examination of single-crystal $^{40}$Ar/$^{39}$Ar dating results: Examples from Olorgesailie, Southern Kenya Rift, *Quaternary International, 13/14*, 47-53.

41. Devlin, W., Cogswell, J., Gaskins, G., Isaksen, G., Pitcher, D., Puls, D., Stanley, K. and Wall, G. (1999), South Caspian Basin: Young, cool, and full of promise, *GSA Today, 9*(7), 1-9.

42. Dixon, T. H, Norabuena, E., and Hotaling, L. (2003), Paleoseismology and Global Positioning System: Earthquake cycle effects and geodetic versus geologic fault slip rates in the Eastern California shear zone, *Geology, 31*, 55-58.

43. England, P. C., and Jackson, J. A. (1989), Active deformation of the continents, *Annu. Rev. Earth Planet. Sci., 17*, 197-226

44. England, P., and McKenzie, D. (1982), A thin viscous sheet for continental deformation, *Geophys. J.R. Astron. Soc., 70*, 295-321.

45. England, P., and Molnar, P. (1997), Active deformation of Asia: From kinematics to dynamics, *Science, 278*, 647-650.

46. Etchecopar, A. (1984), Etude des états de contraintes en tectonique cassante et simulation de deformations plastiques (approche mathématique), Thèse d'Etat, Université Montpellier II, France.

47. Faccenna, C., Bellier, O., Martinod, J., Piromallo, C., and Regard, V. (2006), Slab detachment beneath eastern Anatolia: A possible cause for the formation of the North Anatolian fault, *Earth Planet. Sci. Lett., 242*, 85-97.

48. Fleck, R. J., Sutter, J. F., and Elliot, D. H. (1977), Interpretation of discordant $^{40}Ar/^{39}Ar$ age spectra of Mesozoic tholeiites from Antarctica, *Geochim. Cosmochim. Acta, 41*, 15-32.

49. Flesch, L. M., Haines, A. J., and Holt, W. E. (2001), Dynamics of the India-Eurasia collision zone, *J. Geophys. Res., 106*, 16,435-16,460.

50. Friedrich, A. M., Wernicke, B. P., Niemi, N. A., Bennett, R. A. and Davis J. L. (2003), Comparison of geodetic and geologic data from the Wasatch region, Utah, and implications for the spectral character of Earth deformation at periods of 10 to 10 million years, *J. Geophys. Res., 108*(B4), 2199. doi:10.1029/2001JB000682.

51. Ghaemi, F., Ghaemi, F., and Hosseini, K. (1999), Geological map of Iran, *Series 7766 (Neyshabur sheet), scale 1:100 000*, Geological Survey of Iran, Tehran.

52. Gordon, R. G., and Stein, S. (1992), Global tectonics and space geodesy, *Science, 256*, 333-342.

53. Gosse, J. C., and Phillips, F. M. (2001), Terrestrial in situ cosmogenic nuclides: theory and application, *Quat. Sci. Rev., 20*, 1475-1560.

54. Hempton, M. R. (1987), Constraints on Arabian plate motion and extensional history of the Red Sea, *Tectonics, 6*(6), 687-705, doi:10.1029/TC006i006p00687.

55. Hessami, K., Nilforoushan, F., and Talbot, C. (2006), Active deformation within the Zagros Mountains deduced from GPS measurements, *J. Geol. Soc. Lond., 163*, 143–148.

56. Hollingsworth, J., Jackson, J., Walker, R., Gheitanchi, M. R., and Bolourchi, M. J. (2006), Strike-slip faulting, rotation and along-strike elongation in the Kopeh Dagh Mountains, NE Iran, *Geophys. J. Int., 166*, 1161-1177, doi:10.1111/j.1365-246X.2006.02983.x.

57. Hollingsworth, J., Jackson, J., Alarcón, J. E., Bommer, J. J., and Bolourchi, M. J. (2007), The 4th February 1997 Bojnurd (Garmkhan) earthquake in NE Iran: field, teleseismic, and strong-motion evidence for rupture directivity effects on a strike-slip fault, *Journal of Earthquake Engineering, 11*, 193–214.

58. Hollingsworth, J., Jackson, J., Walker, R., and Nazari, H. (2008), Extrusion tectonics and subduction in the eastern South Caspian region since 10 Ma, *Geology, 36*(10), 763–766, doi:10.1130/G25008A.1.

59. Homberg, C., Hu, J. C., Angelier, J., Bergerat, F., and Lacombe, O. (1997), Characterization of stress perturbations near major fault zones: Insights from 2-D

distinct-element numerical modelling and field studies (Jura mountains), *Journal of Structural Geology, 19*, 703-718.

60. Horton, R. E. (1945), Erosional development of streams and their drainage basins: hydrophysical approach to quantitative morphology, *Geol. Soc. Am., Bull., 56*(3), 275-370.
61. Huber, H. (1977), Geological map of Iran Sheet no. 3, North East Iran, scale: 1:1 000 000, National Iranian Oil Company.
62. Jackson, J. A., and Fitch, T. J. (1979), Seismotectonic implications of relocated aftershock sequences in Iran and Turkey, *Geophys. J. R. astr. Soc., 57*, 209–229.
63. Jackson, J. A., Haines, A. J., and Holt, W. E. (1995), The accommodation of Arabia–Eurasia plate convergence in Iran, *J. geophys. Res., 100*, 15,205-15,219.
64. Jackson, J., and McKenzie, D. (1984), Active tectonics of the Alpine-Himalayan Belt between western Turkey and Pakistan, *Geophys. J. R. astr. Soc., 77*(1), 185-264.
65. Jackson, J., Priestley, K., Allen, M., and Berberian, M. (2002), Active tectonics of the South Caspian Basin, *Geophys. J. Int., 148*, 214–245.
66. Keller, E. A. and Pinter, N. (1996), Active Tectonics, Earthquakes, Uplift and Landscape, Prentice Hall, Upper Saddle River, 338 p.
67. Keller, E. A., Seaver, D. B., Laduzinsky, D. L., Johnson, D. L. and Ku, T. L. (2000), Tectonic geomorphology of active folding over buried reverse faults: San Emigdio Mountain front, southern San Joaquin Valley, California, *Geol. Soc. Am. Bull., 112*(1), 86–97.
68. Koçyigit, A., Yilmaz, A., Adamia, S., and Kuloshvili, S. (2001), Neotectonics of East Anatolian Plateau (Turkey) and Lesser Caucasus: implication for transition from thrusting to strike-slip faulting, *Geodinamica Acta, 14*(1), 177-195, doi:10.1016/S0985-3111(00)01064-0.
69. Livnat, A., Lifshitz, A., and Flexer, A. (1987), The tectonic style of the southern Arava Rift margins, Israel: alternating stress fields in wrench-rifting processes, *Tectonophysics, 141*(1-3), 151-168. doi:10.1016/0040-1951(87)90182-X.
70. Lowell, T. V. (1995), The application of radiocarbon age estimates to the dating of glacial sequences: an example from the Miami sublobe, Ohio, USA, *Quaternary Science Reviews, 14*, 85– 99.
71. Lyberis, N., and Manby, G. (1999), Oblique to orthogonal convergence across the Turan block in the post-Miocene, *Am. Assoc. Petrol. Geol. Bull., 83*(7), 1135-1160.
72. Lyberis, N., Manby, G., Poli, J.T., Kalugin, V., Yousouphocaev, H., and Ashirov, T. (1998), Post-Triassic evolution of the southern margin of the Turan plate, *C. R. Acad. Sci., 326*, 137–143.
73. Maggi, M., Jackson, J., McKenzie, D. and Priestley, K. (2000), Earthquake focal depths, effective elastic thickness, and the strength of the continental lithosphere, *Geology, 28*(6), 495–498.

74. Majidi, B. (1978), Etude petrostructurale de la région de Mashhad, Iran: Les problèmes des métamorphites, serpentinites, et granitoïdes hercyniens, Thèse de doctorat, l'Université Scientifique et Médicale de Grenoble, France, 274 p.

75. Masson, F., Chéry, J., Hatzfeld, D., Martinod, J., Vernant, P., Tavakoli, F., and Ghafory-Ashtiani, M. (2005), Seismic versus aseismic deformation in Iran inferred from earthquakes and geodetic data, *Geophys. J. Int., 160*, 217-226, doi:10.1111/j.1365-246X.2004.02465.x.

76. Masson, F., Djamour, Y., Vangorp, S., Chéry, J., Tavakoli, F., Tatar M., and Nankali, H. (2006), Extension in NW Iran inferred from GPS enlightens the behavior of the south Caspian basin, *Earth Planet. Sci. Lett., 252*, 180–188.

77. Masson, F., Anvari, M., Djamour, Y., Walpersdorf, A., Tavakoli, F., Daignières, M., Nankali, H., and Van Gorp, S. (2007), Large-scale velocity field and strain tensor in Iran inferred from GPS measurements: new insight for the present-day deformation pattern within NE Iran, *Geophys. J. Int., 170*, 436–440. doi:10.1111/j.1365-246X.2007.03477.x.

78. McClusky, S., Reilinger, R., Mahmoud, S., Ben Sari, D,. and Tealeb, A. (2003), GPS constraints on Africa (Nubia) and Arabia plate motions, *Geophys. J. Int., 155*(1), 126–138, doi:10.1046/j.1365-246X.2003.02023.x.

79. McDonald, E. V. (1994), The relative influence of climatic change, desert dust, and lithological control on soil-geomorphic processes and hydrology of calcic soils formed on Quaternary alluvial-fan deposits in the Mojave Desert, California, PhD thesis, Univ. of New Mexico, Albuquerque.

80. McFadden, L. D., McDonald, E. V., Wells, S. G., Anderson, K., Quade, J., and Forman, S. L. (1998), The vesicular layer and carbonate collars of desert soils and pavements: formation, age and relation to climate change, *Geomorphology, 24*, 101–145.

81. McKenzie, D. P. (1972), Active tectonics of the Mediterranean region, *Geophys. J. Int., 30*(2), 109–185, doi:10.1111/j.1365-246X.1972.tb02351.x.

82. McKenzie, D., and Jackson, J. (1983), The relationship between strain rates, crustal thickening, paleomagnetism, finite strain, and fault movements within a deforming zone, *Earth planet. Sci. Lett., 65*, 182-202.

83. McKenzie, D., and Jackson, J. (1986), A block model of distributed deformation by faulting, *J. Geol. Soc. London, 143*, 349-353.

84. McQuarrie, N., Stock, J. M., Verdel, C., and Wernicke, B. P. (2003), Cenozoic evolution of Neotethys and implications for the causes of plate motions, *Geophys. Res. Lett., 30*(20), 2036, doi:10.1029/2003GL017992.

85. Merchel, S., Arnold, M., Aumaître, G., Benedetti, L., Bourlès, D. L., Braucher, R., Alfimov, Freeman, V., S.P.H.T., Steier, P., and Wallner, A. (2008), Towards more precise 10Be and 36Cl data from measurements at the 10−14 level: Influence of sample preparation, Nuclear Instruments and Methods in Physics Research Section B, *Beam Interactions with Materials and Atoms, 266*(22), 4921-4926.

86. Mercier, J. L., Carey-Gailhardis, E., and Sébrier, M. (1991), Paleostress determinations from fault kinematics: application to the neotectonics of the Himalayan-Tibet and the central Andes, *Philos. Trans. R. Soc. London, Ser. A, 337*, 41-52.

87. Meyer, B., and Le Dortz, K. (2007), Strike-slip kinematics in Central and Eastern Iran: Estimating fault slip-rates averaged over the Holocene, *Tectonics, 26*, TC5009, doi:10.1029/2006TC002073.

88. Molnar, P. (1988), Continental tectonics in the aftermath of plate tectonics, *Nature, 335*, 131-137.

89. Mostriouk, A. O., Petrov, V. A. (1994), Catalogue of focal mechanisms of Earthquakes 1964–1990, *Materials of World Data Center B.*, pp. 87, Moscow (available at http://wwwbrk.adm.yar.ru/russian/l_512/stress/fps_cate.htm).

90. Mount, V. S., and Suppe, J. (1987), State of stress near the San Andreas Fault: implications for wrench tectonics, *Geology, 15*, 1143-1146.

91. Namson, J., and Davis, T. L. (1988), Seismically active fold and thrust belt in the San Joaquin Valley, central California: *Geological Society of America Bulletin, 100*, 257-273.

92. Navabpour, P. (2009), Brittle tectonics and palaeostress reconstructions in the Zagros: passive palaeo-margin and continental collision, Ph.D. thesis, University of Nice-Sophia Antipolis, France.

93. Nishiizumi K., Imamura M., Caffee M. W., Southon J. R., Finkel R. C., and McAninch J. (2007), Absolute calibration of 10Be AMS standards, *Nuclear Instruments and Methods in Physics Research, B258*, 403-413.

94. Nowroozi, A. A. (1972), Focal mechanisms of Earthquakes in Persia, Turkey, West Pakistan, and Afghanistan and plate tectonics of the Middle East, *Bull. Seismol. Soc. Am. 62*, 823–850.

95. Nyst, M., and Thatcher, W. (2004), New constraints on the active tectonic deformation of the Aegean, *J. Geophys. Res., 109*, B11406, doi:10.1029/2003JB002830.

96. Över, S., Ünlügenç U. C., and Bellier, O. (2002), Quaternary stress regime change in the Hatay region (SE Turkey), *Geophys. J. Int. 148*, 649-662.

97. Peltzer, G., and Saucier, F. (1996), Present-day kinematics of Asia derived from geologic fault rates, *J. Geophys. Res., 101*, 27,943-27,956.

98. Phillips, F. M., Zreda, M. G., Gosse, J. C., Klein, J., Evenson, E. B., Hall, R. D., Chadwick, O. A., and Sharma, P. (1997), Cosmogenic $^{36}$Cl and $^{10}$Be ages of Quaternary glacial and fluvial deposits of the Wind River Range, Wyoming, *Geol. Soc. Am. Bull., 109*(11), 1453–1463.

99. Phillips, F. M., Zreda, M. G., Flinsch, M. R., Elmore, D. and Sharma, P. (1996), A reevaluation of cosmogenic $^{36}$Cl production rates in terrestrial rocks, *Geophys. Res. Letters, 23*, 949–952.

100. Priestley, K., Baker, C., and Jackson, J. (1994), Implications of earthquake focal mechanism data for the active tectonics of the South Caspian Basin and surrounding regions, *Geophys. J. Int., 118*, 111–141.

101. Regard, V., Bellier, O., Thomas, J.-C., Abbassi, M. R., Mercier, J., Shabanian, E., Feghhi, K., and Soleymani, S. (2004), The accommodation of Arabia-Eurasia convergence in the Zagros-Makran transfer zone, SE Iran: a transition between collision and subduction through a young deforming system, *Tectonics, 23*, TC4007, doi:10.1029/2003TC001599.

102. Regard, V., Bellier, O., Thomas, J.-C., Bourlès, D., Bonnet, S., Abbassi, M. R., Braucher, R., Mercier, J., Shabanian, E., Soleymani, S., and Feghhi, K. (2005), Cumulative right-lateral fault slip rate across the Zagros–Makran transfer zone: role of the Minab–Zendan fault system in accommodating Arabia–Eurasia convergence in southeast Iran, *Geophys. J. Int., 162*, 177–203, doi:10.1111/j.1365-246X.2005.02558.x.

103. Regard, V., Bellier, O., Braucher, R., Gasse, F., Bourlès, D., Mercier, J., Thomas, J.-C., Abbassi, M.R., Shabanian, E. & Soleymani, S. (2006), $^{10}$Be dating of alluvial deposits from Southeastern Iran (the Hormoz Strait area), *Palaeogeography, Palaeoclimatology, Palaeoecology, 242*(1-2), 36–53. doi:10.1016/j.palaeo.2006.05.012.

104. Reilinger, R., et al. (2006), GPS constraints on continental deformation in the Africa-Arabia-Eurasia continental collision zone and implications for the dynamics of plate interactions, *J. Geophys. Res., 111*, B05411, doi:10.1029/2005JB004051.

105. Renne, P. R., Swisher, C. C., Deino, A. L., Karner, D. B., Owens, T., and Depaolo, D. J. (1998), Intercalibration of Standards, absolute ages and uncertainties in $^{40}$Ar/$^{39}$Ar dating, *Chemical Geology, 145*,117–152.

106. Replumaz, A., and Tapponnier, P. (2003), Reconstruction of the deformed collision zone between India and Asia by backward motion of lithospheric blocks, *J. Geophys. Res., 108*(B6), 2285, doi:10.1029/2001JB000661.

107. Ritz, J.-F., and Taboada, A. (1993), Revolution stress ellipsoids in brittle tectonics resulting from an uncritical use of inverse methods, *Bulletin de la Societe Geologique de France, 164*(4), 519-531.

108. Ritz, J. F., Brown, E. T., Bourlès, D., Philip, H., Schlupp, A., Raisbeck, G. M., Yiou, F., and Enkhtuvshin, B. (1995), Slip rates along active faults estimated with cosmic-ray–exposure dates: Application to the Bogd fault, Gobi-Altaï, Mongolia, *Geology, 23*(11), 1019-1022.

109. Ritz, J.-F., Nazari, H., Ghassemi, A., Salamati, R., Shafei, A., Solaymani, S., and Vernant, P. (2006), Active transtension inside Central Alborz: A new insight into northern Iran–southern Caspian geodynamics, *Geology, 34*(6), 477–480, doi:10.1130/G22319.1.

110. Roddick, J. C., Cliff, R. A., and Rex, D. C. (1980), The evolution of excess argon in alpine biotites, *Earth and Planetary Sciences Letters, 48*, 185-208.

111. Ron, H., Freund, R., Garfunkel, Z., and Nur, A. (1984), Block-rotation by strike–slip faulting: structural and paleomagnetic evidence, *J. Geophys. Res., 89*(B7), 6256-6270.

112. Ryerson, F. J., et al. (2006), Applications of morphochronology to the active tectonics of Tibet, *Spec. Pap. Geol. Soc., 415*.

113. Sahandi, M. R. (1993), Geological quadrangle map of Iran, No. J-4 (Sabzevar sheet), scale 1:250 000, Geological Survey of Iran, Tehran.

114. Schimmelpfennig, I., Benedetti, L., Finkel, R., Pik, R., Blard, P.H., Bourlès, D., Burnard, P., and Williams, A. (2009), Sources of in-situ $^{36}$Cl in basaltic rocks. Implications for calibration of production rates, *Quaternary Geochronology*, in press, xxxx doi:10.1016/j.quageo.2009.06.003.

115. Schwartz D. P., and Coppersmith, K. J. (1984), Fault behavior and characteristic earthquakes: Examples from the Wasatch and San Andreas Fault zones. *J. Geophys. Res.*, *89*, 5681-5698.

116. Sella, G. F., Dixon, T. H., and Mao, A. (2002), REVEL: A model for recent plate velocities from space Geodesy, J. Geophys. Res., 107(B4), 2081. doi:10.1029/2000JB000033.

117. Shabanian, E., Siame, L., Bellier, O., Benedetti, L., and Abbassi, M. R. (2009a), Quaternary slip-rates along the north-eastern boundary of the Arabia-Eurasia collision zone (Kopeh Dagh Mountains, North-East Iran), *Geophys. J. Int.*, *178*, 1055-1077, doi:10.1111/j.1365-246X.2009.04183.x.

118. Shabanian, E., Bellier, O., Siame, L., Arnaud, N., Abbassi, M. R., and Cochemé, J.-J. (2009b), New tectonic configuration in NE Iran: active strike-slip faulting between the Kopeh Dagh and Binalud mountains, *Tectonics*, *28*, TC5002, doi:10.1029/2008TC002444.

119. Siame, L. L., Shabanian, E., and Bellier, O. (2009), Extrusion tectonics and subduction in the eastern South Caspian region since 10 Ma, *Comment, Geology*, in press.

120. Stöcklin, J. (1968), Structural history and tectonics of Iran: A review, *Am. Assoc. Petr. Geol. Bull.*, *52*(7), 1229–1258.

121. Stone, J. O. H. (2000), Air pressure and cosmogenic isotope production, *J. Geophys. Res.*, *105*(B10), 23753-23759.

122. Stone, J. O. H., Allan, G. L., Fifield, L. K., and Cresswell, R. G. (1996), Cosmogenic chlorine-36 from calcium spallation, *Geochimica et Cosmochimica Acta*, *60*(4), 679-692.

123. Stone, J. O. H., Evans, J. M., Fifield, L. K., Allan, G. L., and Cresswell, R. G. (1998), Cosmogenic chlorine-36 production in calcite by muons, *Geochimica et Cosmochimica Acta*, *62*(3), 433-454.

124. Storti, F., Holdsworth, R. E., and Salvini, F. (2003), Intra plate strike-slip deformation belts, in *Intra plate strike-slip deformation belts*, edited by F. Storti et al., *Geological society, London*, Special publications, 210, pp. 1-14.

125. Strahler, A. N. (1952), Hypsometric (area-altitude) analysis of erosional topology, *Geological Society of America Bulletin*, *63*(11), 1117–1142.

126. Talebian, M., and Jackson, J. (2002), Offset on the Main Recent Fault of NW Iran and implications for the late Cenozoic tectonics of the Arabia–Eurasia collision zone, *Geophys. J. Int.*, *150*, 422-439.

127. Talebian, M. and Jackson, J. (2004), A reappraisal of earthquake focal mechanisms and active shortening in the Zagros mountains of Iran, *Geophys. J. Int.*, *156*(3), 506–526.

128. Tapponnier, P., Frederick , J. R., Van der Woerd, J., Mériaux, A. S., and Lasserre, C. (2001), Long-term slip rates and characteristic slip: keys to active fault behaviour and earthquake hazard, *C. R. Acad. Sci. Ser. II, 333*(9), 483–494.

129. Tavakoli, F. (2007), Present-day kinematics of the Zagros and east of Iran faults, Ph.D. thesis, University of Joseph Fourier, France, Grenoble.

130. Taylor, J. R. (1997), An Introduction to Error Analysis, The Study of Uncertainties in Physical Measurements, 2nd ed., University Science Books, Sausalito, CA.

131. Tchalenko, J. S. (1975), Seismicity and structure of the Kopet Dagh (Iran, USSR), *Phil. Trans. R. Soc. Lond., Series A, 278* (1275), 1–28.

132. Tchalenko, J. S., Braud, J., and Berberian, M. (1974), Discovery of three earthquake faults in Iran, *Nature, 248*, 661-663.

133. Thatcher, W. (1995), Microplate versus continuum descriptions of active tectonic deformation, *J. Geophys. Res., 100*, 3885-3894.

134. Thatcher, W. (2003), GPS constraints on the kinematics of continental deformation, *Int. Geol. Rev., 45*, 191-212.

135. Thatcher, W. (2007), Microplate model for the present-day deformation of Tibet, *J. Geophys. Res., 112*, B01401, doi:10.1029/2005JB004244.

136. Tirrul, R., Bell, I. R., Griffis, R. J., and Camp, V. E. (1983), The Sistan suture zone of eastern Iran, *Geol. Soc. Am. Bull., 94*, 134-150.

137. Trifonov, V. (1978), Late Quaternary tectonic movements of western and central Asia, *Geol. Soc. Am. Bull., 89*, 1059-1072.

138. Troeh, F. R. (1965), landform equations fitted to contour maps, *American Journal of Science, 263*, 616-627.

139. Vernant, P., et al. (2004), Present-day crustal deformation and plate kinematics in the Middle East constrained by GPS measurements in Iran and northern Oman, *Geophys. J. Int., 157*(1), 381–398, doi:10.1111/j.1365-246X.2004.02222.x.

140. Vilotte, J. P., Daignieres, M., and Madariaga, R. (1982), Numerical modeling of intraplate deformation: Simple mechanical models of continental collision, *J. Geophys. Res., 87*, 10,709-10,728.

141. Walker, R., and Jackson, J. (2004), Active tectonics and Late Cenozoic strain distribution in central and eastern Iran, *Tectonics, 23*, TC5010, doi:10.1029/2003TC001529.

142. Walpersdorf, A., Hatzfeld, D., Nankali, H., Tavakoli, F., Nilforoushan, F., Tatar, M., Vernant, P., Chéry, J., and Masson, F. (2006), Difference in the GPS deformation pattern of North and Central Zagros (Iran), *Geophys. J. Int., 167*(3), 1077-1088. doi:10.1111/j.1365-246X.2006.03147.x.

143. Wells, S. G., McFadden, L. D., Dohrenwend, J. C., Turrin, B. D., and Mahrer, K. D. (1985), Late Cenozoic landscape evolution of lava flow surfaces of the Cima volcanic field, Mojave Desert, California, *Geol. Soc. Am. Bull., 96*, 1518–1529.

144. Wells, S. G., McFadden, L. D., and Dohrenwend, J. C. (1987), Influence of Late Quaternary climatic changes on geomorphic and pedogenic processes on a desert piedmont, eastern Mojave Desert, California, *Quaternary Res.*, *27*, 130–146.

145. Wells, S. G., McFadden, L. D., Poths, J., and Olinger, C. T. (1995), Cosmogenic $^{3}$He exposure dating of stone pavements: implications for landscape evolution in deserts, *Geology, 23*, 613–616.

146. Westaway, R. (1994), Present-day kinematics of the Middle East and eastern Mediterranean, *J. Geophys. Res.*, *99*(B6), 12071-12090.

147. Yamini-Fard, F., Hatzfeld, D., Farahbod, A.M., Paul, A., and Mokhtari, M. (2007), The diffuse transition between the Zagros continental collision and the Makran oceanic subduction (Iran): microearthquake seismicity and crustal structure, *Geophys. J. Int.*, *170*(1), 182–194.

148. Yeats, R. S. (1986), Active faults related to folding, in Active Tectonics, Washington, D.C., National Academy Press, 63-79.

149. York, D. (1969), Least-square fitting of a straight line with correlated errors, *Earth and Planetary Sciences Letters, 5*, 320-324.

150. Zamani, B., Angelier, J., and Zamani, A. (2007), State of stress induced by plate convergence and stress partitioning in northeastern Iran, as indicated by focal mechanisms of earthquakes, *Journal of Geodynamics, 45*, 120–132, doi:10.1016/j.jog.2007.07.003.

151. Zoback, M. L. (1989), State of stress and modern deformation of the basin and range province, *J. Geophys. Res., 94*, 7105-7128.

152. Zoback, M. D., et al., (1987), New evidence on the state of stress on the San Andreas fault system, *Science, 238*, 1105-1111, doi: 10.1126/science.238.4830.1105.

153. Zoback, M. D., and Townend J., (2001), Implications of hydrostatic pore pressures and high crustal strength for the deformation of intraplate lithosphere, *Tectonophysics, 336*, 19-30.

154. Zreda, M. G., Phillips, F. M., and Elmore, D. (1994), Cosmogenic $^{36}$Cl accumulation in unstable landforms, 2. Simulations and measurements on eroding moraines, Water *Resources Research, 30*, 3127–3136.

# *Appendix*

## Extrusion tectonics and subduction in the eastern South Caspian region since 10 Ma: comment*

Lionel L. Siame[1], Esmaeil Shabanian[1,2], Olivier Bellier[1]

[1]*CEREGE (Centre Européen de Recherche et d'Enseignement des Géosciences de l'Environnement), U.M.R. 6635 (CNRS-INSU, Université Aix-Marseille), B.P.80, Plateau de l'Arbois, 13545, Aix-en-Provence cedex 4, France*

[2]*International Institute of Earthquake Engineering and Seismology (IIEES), BP 19395-3913 Tehran, Iran*

**ABSTRACT**

*Hollingsworth et al*. (2008) proposed a "new" kinematic model for the complicated tectonic pattern in the eastern South Caspian Sea region. Our comment is focused on the Ashkhabad Fault and the Kopeh Dagh Mountains, examining the data and hypothesis used by the authors to support their model. Along the Ashkhabad Fault, *Hollingsworth et al*. (2008) presented 10 m of right-lateral displacement recorded by a river bank and a line of irrigation system. In this area, the well-expressed fault trace (Fig. 1A) is not consistent with that proposed by the authors (their Fig. 2B). Moreover, there is no clear evidence of right-lateral displacements where the fault traces intersect either other river banks or erosional gullies (Fig. 1A). Accepting this particular line of irrigation as representative for right-lateral fault offset, it should be noted that the offset is on the order of 14 m, and not 10 m. Noteworthy, irrigation lines can be right-laterally or left-laterally (Fig. 1B) offset along the fault (ranging from 1 to 20 m; *e.g.*, *Trifonov*, 1978). Assuming that the 14 m right-lateral offset is representative for, and taking into account that the first irrigation lines were constructed not later than the 5th century B.C. (*Trifonov*, 1978), yields a maximum slip rate of 5.6 mm/yr for this part of the fault, which in turn decreases the proposed strike-slip faulting inception age to ~6 My.

* *Publisher: GSA/Journal: Geology, Article ID: G25701C*

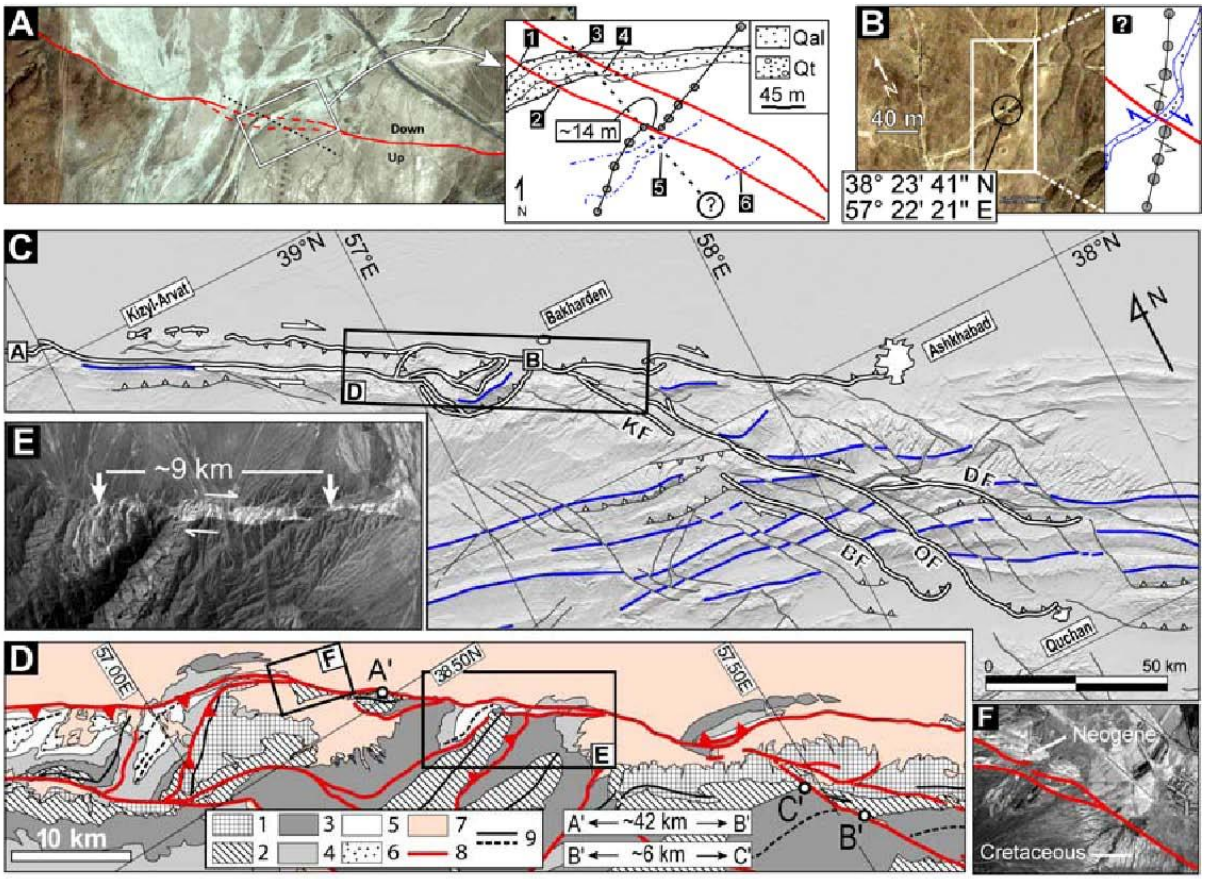


Figure 1. A: Quickbird image (GoogleEarth) centered on the Kazandzhik Fault, showing the fault-related morphology and possible fault traces. Inset shows a simplified morphotectonic map focused on the area investigated by *Hollingsworth et al*. (2008). Points 1–6 are intersection points of the fault traces with geomorphic features (1–4: river banks; 5–6: erosional gullies). The fault traces from our mapping (red lines) are compared to that proposed by *Hollingsworth et al*. (2008, black dotted line). B: Quickbird image (GoogleEarth) showing an apparent left-lateral offset in an irrigation line. C: Simplified structural map of the Kopeh Dagh based on SPOT5 images showing the major faults (white solid lines, simplified after *Shabanian et al*., 2009) and the fold axes (blue lines). D: Structural map of the north-central Kopeh Dagh showing the Ashkhabad Fault based on SPOT5 images. Keys: Cretaceous, 1, Tirgan limestone; 2, Sarcheshmeh marl; 3, Sanganeh shale and marl; 4. Aitamir sandstone and shale; 5, Miocene marl, 6, Pliocene conglomerate; 7, Quaternary deposits; 8, Main fault, 9, Fold axes (continuous lines are anticline axes). E: SPOT5 image of the 9-km-long, right-lateral offset cumulated by a syncline developed within Neogene deposits. F: SPOT5 image extract showing that the Ashkhabad Fault trace clearly runs between the Cretaceous and Neogene deposits.

Along the Ashkhabad Fault, the authors reconstructed a cumulative offset of 35 km using Cretaceous and Neogene deposits. Even if one accepts the reliability of this offset, it should be at minimum 42 km (Fig. 1D). Following the authors' map, the NW termination of the Ashkhabad Fault runs with a NW-trending yielding the Neogene deposits to belong to the southern block. However, a detailed geomorphic analysis using satellite SPOT imagery (with a pixel resolution of 2.5 m) convinced us that the Ashkhabad Fault clearly runs with a WSW-trending just North of the Cretaceous formations (Fig. 1F), yielding the Neogene deposits to

belong to the northern block. In fact, the Neogene deposits are always located on the northern side of the fault. At the NE termination of the fault, the Cretaceous units belong to a well-preserved syncline that shows a maximum right-lateral offset of ~6 km (Fig. 1D). Following our observations, the measurable post-Neogene offset along the same segment of the fault is ~9 km, indicated by an offset syncline (Fig. 1E).

The proposed geodynamic interpretation relies largely on rigid block rotations in the Kopeh Dagh (Fig. 1 and Fig. 5 in *Hollingsworth et al*., 2008) that cannot be confirmed by the regional fold axes pattern (Fig. 1C). Indeed, the post-folding, brittle deformation pattern favors a simple strike-slip faulting mechanism within the Kopeh Dagh. More important is the 10 My age for the inception of the deformation associated with the westward motion of the South-Caspian basin. This value strongly relies (1) on the observations discussed in this comment, and (2) on the audacious hypothesis that the instantaneous GPS rates remained constant throughout the late Cenozoic. However, given the concerns we highlight on the Ashkhabad Fault and the Kopeh Dagh, one should be cautious about the validity of the data set presented by the authors before accepting that their model clarifies the active tectonics of this complicated region.

**References**

Hollingsworth, J., Jackson, J., Walker, R., and Nazari, H. (2008), Extrusion tectonics and subduction in the eastern South Caspian region since 10 Ma, *Geology, 36*(10), 763-766, doi:10.1130/G25008A.1.

Shabanian, E., Siame, L.L., Bellier, O., Benedetti, L., and Abbassi, M.R. (2009), Quaternary slip-rates along the northeastern boundary of the Arabia-Eurasia collision zone (Kopeh Dagh Mountains, Northeast Iran), *Geophys. J. Int., 178*, 1055-1077, doi:10.1111/j.1365-246X.2009.04183.x.

Trifonov, V. (1978), Late Quaternary tectonic movements of western and central Asia: Geological Society of America Bulletin, 89, 1059-1072, doi:10.1130/0016-7606(1978)89<1059:LQTMOW>2.0.CO;2.

# Active tectonic study in northeast Iran: contribution of the Kopeh Dagh and Binalud mountains to the accommodation of the Arabia-Eurasia convergence


## Abstract

This study focuses on the Plio-Quaternary faulting in northeast Iran including the Kopeh Dagh and Allah Dagh-Binalud mountains. A combined approach of detailed geological mapping, morphotectonic and fault kinematic analyses, as well as radiometric ($^{40}Ar/^{39}Ar$) and *in situ*-produced exposure dating ($^{36}Cl$ and $^{10}Be$) allowed us to characterize the active tectonic configuration of the northeastern Arabia-Eurasia collision zone. Along the Kopeh Dagh fault systems, a total strike-slip rate of 9±2 mm/yr is estimated. This is resolved to northward and westward slip rates of ~8 and ~4 mm/yr, respectively, for the western Kopeh Dagh relative to Eurasia. This strike-slip deformation is partly (~25 per cent) transferred southward through the "new-defined" Meshkan transfer zone. At the southwestern and northeastern sides of the Binalud, slip rates of 3.6±1.2 and 1.6±0.1 mm/yr are estimated, respectively. Our geologically determined long-term slip rates for both strike-slip (~4 mm/yr) and reverse (~2.4 mm/yr) components of faulting account for about 5 mm/yr of total slip rate at both sides of the range. This is resolved to a northward motion rate of ~4.5 mm/yr, and a rate of ~2 mm/yr for the westward motion of Central Iran relative to the eastern Kopeh Dagh. Quaternary stress analyses indicates that the different fault motions, from pure dip-slip to pure strike-slip, are only due to the fault orientations with respect to the far-field stress pattern, not due to partitioning. Altogether, these new data allow proposing a new tectonic configuration in which central Iran and the western Kopeh Dagh are translated northwestward relative to Eurasia due to intracontinental strike-slip faulting localized on distinct fault systems with unlike slip rates.



***Discipline*:** Géosciences de l'Environnement (géologie, tectonique active et géodynamique)

***Keywords**: Morphotectonics; stress state; continental deformation; in situ-produced exposure dating.*



**Laboratoire: C**entre **E**uropéen de **R**echerche et d'**E**nseignement en **G**éosciences de l'**E**nvironnement (CEREGE), UMR6635 CNRS - Université Aix-Marseille III

Europôle Méditerranéen de l'Arbois, 13545 Aix-en-Provence Cedex 4